$$\frac{1}{Fv(a)}\frac{d(Fv(a))}{da}=\frac{1}{Et(a)}\frac{d(Et(a))}{da}$$

Soil Retaining Structures

DEVELOPMENT OF MODELS FOR STRUCTURAL ANALYSIS

K.J.Bakker

SOIL RETAINING STRUCTURES
DEVELOPMENT OF MODELS FOR STRUCTURAL ANALYSIS

SOIL RETAINING STRUCTURES

Development of models for structural analysis

KLAAS JAN BAKKER

Delft University of Technology, Netherlands
Rijkswaterstaat, Utrecht, Netherlands

A.A. BALKEMA / ROTTERDAM / BROOKFIELD / 2000

Published by
A.A. Balkema, P.O. Box 1675, 3000 BR Rotterdam, Netherlands
Fax: +31.10.4135947; E-mail: balkema@balkema.nl; Internet site: http://www.balkema.nl

A.A. Balkema Publishers, Old Post Road, Brookfield, VT 05036-9704, USA
Fax: 802.276.3837; E-mail: info@ashgate.com

ISBN 90 5809 321 2

Printed in the Netherlands

Contents

6 FLEXIBLE RETAINING WALLS

7 BORED TUNNELS IN SOFT SOIL

8 CONCLUSIONS AND RECOMMENDATIONS

CHAPTER 1

Introduction

1.1 PRELIMINARY

This thesis describes a part of the work that I have been involved with while working at the Dutch Public Works department, after graduation from Delft University of Technology. The work has mainly been focussed on the development of models for the structural analysis of soil retaining structures. One of the objectives that has been taken, to describe this work in a coherent framework, is the proposition that structural analysis is an essential step to be taken in the design process for a civil engineering product. This assumption enables the view that structural analysis is not only meant to secure the structural safety, but also to optimise the civil engineering product.

The initial phase of this research was carried out when I was working in the Hydraulic Engineering section of the Road and Hydraulic engineering division. This research was concerned with soil-water-structure interaction including erosion control, filter stability and revetment design. The research on soil-water-structure interaction is described in the chapter on blockrevetments, i.e. a revetments function is to keep the soil particles together, against wave attack and erosion. Here the typification soil retaining structure is used if the structure's function is to maintain a soil slope that is steeper than the natural angle of repose. The research related to filter stability is not included in this thesis.

After leaving the Road and Hydraulic Engineering division for the Structural Engineering division the core of the work was changed to soil mechanics and foundation engineering, i.e. sheet pile retaining walls and tunnelling. These projects were, among others, the CUR sheet piling handbook, and the monitoring of the Second Heinenoord tunnel.

During that period I was also involved with the development of the computer code PLAXIS. The development and implementation of structural elements in this computer code, which was initially developed for the analysis of soil behaviour only, has improved the practical benefit of this computer code.

In order to relate the analytical work to the practical purposes they are needed for, the application of this analytical work into design is described. Design offers the perspective needed to give structural analysis a frame of reference. Besides analysis, creativity is required to generate alternatives. For design purposes, analysis and creativity are linked by the optimisation process. The proposition of

an alternative (a creative effort), may not be considered as a design without a thorough analysis. Analysis is required to differentiate between the alternative designs that have been proposed. Structural analyses, together with creativity and optimisation techniques, are the key tools for the design process.

1.2 SOIL RETAINING STRUCTURES

Soil retaining structures are components to be used to construct systems in the National infrastructure, such as water defences, water-control, and transport & traffic.

If we focus on the design of such components, inevitably we are confronted with aspects of the design of the systems, especially when the functional aspects of these components have to be considered. With this consideration, the similarities in the design approach for a system and in the design approach for a component, become visible. If the view is taken that the only difference between the design of a system and the design of a component is a difference in the level of abstraction, it becomes clear that the main objective for a design process is optimisation of the benefit of an investment decision.

If optimisation is the main objective for a design process it becomes clear that besides creativity, analysis is needed to deliver the quantitative information for comparison and decision making. From this observation it is realised that at least two abilities of a human's brain are needed for design; on the one hand we need the power of synthesis; the creativity to consider all the available data, and to develop those alternatives that have the least discrepancy with the demands. On the other hand we need analysis, which offers the power to verify whether each design alternative satisfies the design specification. There is a general reasoning that the power of analytical theories goes beyond verification only. The creation of design alternatives within a frame of solutions that have been tried out, exceeds the limitations related to testing an alternative. This aspect of analysis cannot be classified as creative in the true sense, however. For true creativity, other parts of the human brain are necessary than those that are used for analysis.

Here the use of the term synthesis is not limited to the definition according to the dialectic process. Synthesis is also used in a meaning that is more associated with induction. In comparison to that, analysis is used more in association with deduction. In scientific developments one might recognise a drive to change inductive design processes and to transform these into more deductive, analytic ones. The advantage of the latter is apparent, because deductive processes are much more easily automated. We have to consider, however, that there is a limit to the inversion of design into deductive processes, because this inversion can only be performed for solved problems. With which it is meant that the main parameters of the solution have to be clear and solved; the design must be fairly well defined, so that it only needs to be modified for a specific situation. The deductive approach lacks performance if an innovative solution is required. For

this purpose the creative power of induction is needed.

We need the power of analysis to construct *safe* and *optimised* innovative solutions.

1.3 THE TOOLS FOR ANALYSIS

Mathematics is an essential means of formulating an analysis. Mathematics is not a science in the true sense such as physics. Physics is a true science in the sense that there is a real world, in which we can perform tests to verify the concepts we develop to describe the observations we make. We try to generalise these observations in such a way that we only need a minimum of basic assumptions to describe reality.

Mathematics is the abstract language to transfer ideas; 'images' of reality (Proposition 2.1 according to Wittgenstein (1922); "Bilder der Tatsachen"). Mathematics in that sense is a subset of language; the most concise form of language. Mathematics makes images transportable. The tests within mathematics are logical tests, not physical.

The base components of language are; 1) consensus of opinion, and 2) logic. The latter, logic, is partly a-priori (Frege, see Kenny (1995)) and partly empirical. The distinction is hard to make; it has long been thought that Euclidean geometry was a priori. Later on it became clear that this was a misconception.

The touchstone of the 'value' of a formulation is verification or falsification; a one error leads to a rejection of the formulation. A thousand satisfactory outcomes do not constitute a proof.

1.4 THE OBJECTIVE OF THIS STUDY

The main objective in this study is the development of models for structural analysis. This objective is pursued for soil retaining structures. For this purpose structural analysis needs an objective frame of reference. One might ask what the criteria are to decide whether a design is adequate. As the designs we develop are essentially models of the structures to be constructed, the next question would be what the demands are on the structural models that are applied for the analysis of a design.

The demands on structural models and the process that is being used in order to test feasible models for structural analysis are the main object of this thesis.

One of the first questions coming forward if looking into this topic is, what the relation is between the functional demands posed upon a design and the structural demands posed upon the structure when dimensioning an alternative structure type.

As the application of finite element analysis to integrate different design

aspects in one concept is a joint aspect for all the applications being considered, the principles being used to develop such models are looked upon in more detail. One of these principles is the mathematical formulation of groundwater flow. Groundwater flow is analysed taking into account that it is not an energy neutral physical process, energy is dissipated during the process; i.e. potential and kinematics energy is transformed into heat.

If one puts models of a higher hierarchy into practice, due to the increased number of parameters of the model, the solution space of the model increases. Therefore it is not self-evident that the bandwidth in solutions, and the discrepancy with respect to prototype measurements becomes smaller. One of the sub-targets in this study is the establishing of insight into the question whether marginal benefits of development are not surpassed by the marginal costs.

1.5 THE APPROACH TAKEN AND THE CONTENT OF THIS THESIS

The approach taken in this study is quite practical, and contains the development and validation of models for structural analysis, preferably with prototype measurements. This approach is taken for three different types of soil retaining structures; i.e. block revetments, sheet pile walls, and bored tunnels. Secondary to the main objective of the study, objectives related to the structure types are being pursued too. Conclusions related to the different structure types are formulated within the subsequent chapters dedicated to these types.

In the chapter 2, 3 and 4, the main principles for this study are described. In chapter 1 with respect to designing. In chapter 3 with respect to the development of models for analysis and in chapter 4 with respect to the principles being used to derive mechanical models.

Subsequently in the chapters; 5, 6 and 7, three examples are given of developments of models for structural analysis that may be used for structural designing of soil retaining structures. In chapter 5 on block revetments. In chapter 6 on flexible retaining walls and in chapter 7 on bored tunnels in soft soil.

Finally in chapter 8, conclusions are drawn. Where in the chapters 5, 6 and 7 conclusions are drawn related to the development of models for specific structure types, here in chapter 8, conclusions are drawn with respect to the development of models and its application on a generic level.

CHAPTER 2

Design methodology

2.1 INTRODUCTION

Where design is mentioned in this thesis, the emphasis will be on the structural design of soil retaining structures. In practice this usually means the analysis of stresses, strains, deformations and stability of a particular civil engineering structure. Design may also have a wider scope. If the functional requirements in a design specification have to be taken into account, this wider perspective is necessary. In this chapter, this wider perspective of design will be considered. Structural design will then be recognised as a partial contribution to the design process of a structure.

The development of models for the structural design of several types of soil retaining structure is the topic of the chapters 5, 6 and 7. Models for structural analysis are necessary to test the design for the necessary requirements it has to meet. A strategy for the development of such models will be discussed, and illustrated by a number of examples. In chapter 3, an attempt will be made to formulate a coherent view on the development of such models; from crude models to more refined models; from empirical to more analytic methods involving 2D and 3D continuum models.

From the point of view of the scientist, the developer of models, there is an urge to push technology, to promote the use of new methods and models for engineering practice. A practical engineer however might take another view. When he chooses for a model, he weights the advantages against the disadvantages. Practice will therefore require well-established models, which are easy to handle. The gap that appears to exist between science and practice is a long-standing one.

To gain a better understanding of the value which is related to the closing of this gap, an attempt will be made to describe a rational approach that implicitly solves this problem. Within the process of a design, the structural design may be recognised as only one of the stages of development of an object, the development stage where the structure is being conceived and optimised. Subsequent stages of development for an object design are concerned with narrowing down that part of the solution space which is being varied, in the optimisation process.

In this chapter an attempt will be made to widen the perspective of what is meant by the word *design*. The word design is a homonym, which means that the word may reflect different meanings to different persons, or depending on the context in which the word is used. Sometimes with 'the design' the object itself is being referred. This type of meaning is not intended here, as the view is taken that designing is the activity which is necessary to develop an object. The design is the conceptual model being conceived in the designing process. The design is the concept of the object being generated, and not the object itself. The activity of designing may have several aspects. The activity will not only be discussed as a process, the subsequent execution of development stages; not only as a creative effort to develop alternatives, which meet the requirement (the skill), but also as the activity where the result of a civil engineering activity is being optimised.

For the latter view, in this chapter, the *economic perspective* is taken and its implications are discussed.

2.2 THE COMMON DESIGN APPROACH

Because there is no single meaning for the term design; the interpretation of what design is depends on the background of the person. One may justly ask,

> *'What is (structural) design ?'*

In his teaching, Polak (1993) states that he sees designing as

> *'A thinking pattern', taking the following steps;*
> - *posing the problem statement*, and *collecting information, related to the question 'What is the problem ?'*
> - *development of alternatives* and *testing of alternatives for the requirements, related to the question, 'How do we have to solve the problem ?'*
> - *description of the solution which has been chosen.'*

De Ridder (1994) alternatively answers the question with:

> *' Initiated by the problem declaration of an independent party, (step 1 in the process), mostly by way of the same process, (successive stepping) searching for the (optimum) solution.'*

In addition to Polak, De Ridder emphazises three things;

1. *who is taking the initiative (the problem owner ?).*
2. *the process character, and*
3. *the optimisation.*

The emphasis on design as a process is shared with a number of writers on the subject. Wijnen in 'Projectmanagement' (1988) formulates his view with respect to the management of a process (here being interpreted as the process to generate a design) as:

1. *decisions to be taken about alternative schemes or parts being undertaken in successive steps*
2. *an integral control on time, cost, quality, information and organisation.*

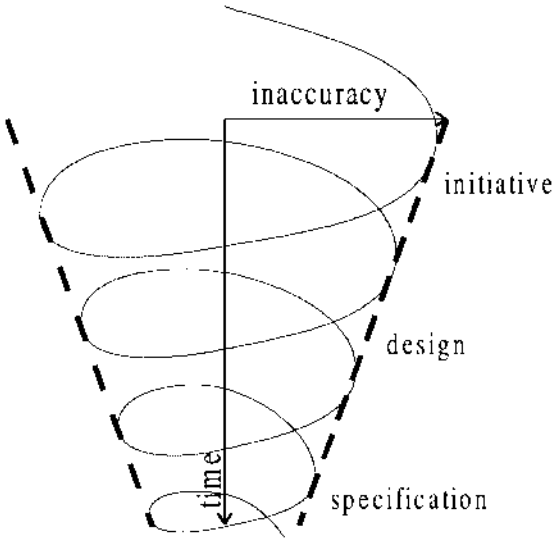

Figure 2.1 Cyclic behaviour of a design process

Here it is proposed to give some recognition to the fact that: 'Design is also a skill', a contemplative art, of generating alternatives (solutions) which meet the requirements. This aspect is recognized by Polak, but not strongly emphasised. It is hidden in the step of creating alternatives.

Without the generation of alternatives, within the context of civil engineering, one cannot speak of a design process. It would merely be creative effort only. The latter might be acceptable within the bounds of artistic design, but not for a civil engineering design. One of the characteristic aspects being recognised is that design is a recursive process. In a civil engineering design process it is often observed that the designer has to go back to earlier points of departure, i.e. a number of times, premises have to be evaluated and sometimes changed to derive alternatives for the final design, to meet all internal and external requirements.

Within this process, the accuracy of the final design increases, and the uncertainties about value and cost of the final design become smaller, see Fig. 2.1

Within a process step, alternatives are put in order of preference; with respect to their performance; their ability to meet the requirements (for the lowest cost). The value of an alternative is weighted in relation to the cost. The alternative with the highest profit is chosen, assuming that there is sufficient budget for such a choice. Here with profit, the difference between value and cost is meant. As the scope within each design step is changing from general to more specific and detailed, each decision is determinate for the main direction in which following steps to the final solution are taken.

Following De Ridder (1994) it is proposed to give more emphasis to optimisation too.

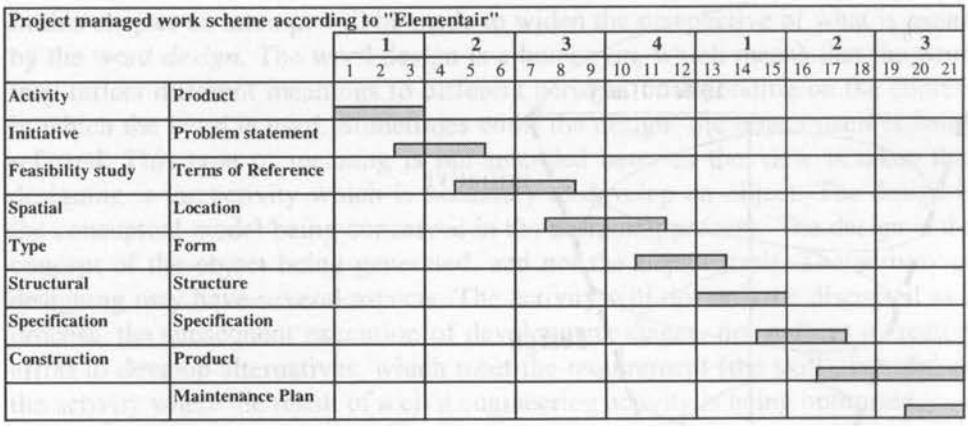

Figure 2.2 Planning scheme according to the Project based work method

Summing up, design may be seen as:

- *a process (developing in time)*
- *requiring skill (for the creation of alternatives)*
- *optimisation (of a future object)*

In the next paragraphs the aspects recognised above will be discussed in more detail

2.2.1 *Designing as a process*

The *Elementair* system (which the Structural Engineering Division of Rijkswaterstaat has introduced in 1994), is an example of the process character of design. This system was introduced to meet the requirements of quality assurance according to ISO 9001. The acquisition of a Quality Assurance certificate has been a trend in the last decade in the Netherlands to improve uniformity in working processes, and to enhance the effectiveness of an organisation. *Elementair* may be regarded as a slightly adapted version of the project based work scheme according to Wijnen (1984). In *Elementair*, rigid phasing, has been traded in for a more flexible scheme, see Fig. 2.2, where at some points, successive steps are executed in parallel.

The objective being pursued to execute subsequent design steps partially in parallel is (probably) a stronger grip on the control of time. One has to realise however that this advantage of better time control is traded for loosening of information control. Consequently a risk with respect to the control of the design is accepted; traded in for a better grasp of the time control.

In the system *Elementair* there is a strong emphasis on the process. Control of the technical quality is only taken into account implicitly. Presumably, it is assumed that if there is a well-defined specification of the result and a strong control of the process, in combination with a strict *minimisation of cost* for the alternatives, this

should provide a product of high quality. The principle that minimising the cost is the leading argument in the design process is not explicitly mentioned, but what else is, if a project-manager has to work within a (too limited) budget ?

The project managed approach demands the formulation of a *program of requirements,* the *premises* and *boundary conditions* for a phase prior to the execution of it. Thus far, however, it is not clear how this program of requirements should be related to the results of preceding steps. Especially for those cases that the preceding step is not formally finished yet, while the requirements and premises for the next step are being formulated. This might lead to inconsistencies; in general it is not clear if all the necessary information is available or what essential information might be lacking, at the start of the next design step.

2.2.2 *Designing as a skill*

The development of creativity, i.e. the ability to produce alternatives that meet requirements, is one of the main objectives of a civil engineering education. The skill to find alternatives that fulfil and satisfy the required functions, based on analysis of the structure's functions and knowledge of subsystems and components.

The actions that might be recognised as being executed in this process, in a successive way are:

- *The collection of information*
- *Analysis of the structures functions*
- *distinguishing subsystems in the structural functioning*
- *database solutions of subsystems of structural functions*
- *brainstorming (optional)*
- *deductive power,*
- *composing of alternatives*
- *checking the integrity of an alternative*
- *ranking alternatives*
- *choosing the favourable alternative*

For a lot of civil engineering structures (structure-types), a large number of alternatives are available. In this case the creative effort diminishes to some sort of standard algorithm, where the most favourable alternative is taken from the shelf, given a rub, analysed and materialised for the boundary conditions required, and then applied.

Within this procedure, the alternative is being tested on its ability to satisfy standard requirements such as;

1. *Functions*
2. *Forces, the structure has to sustain*

For the latter, the structure is being put to the test on:

- *stability*
- *stiffness*
- *strength*
- *et cetera*

In most situations, standard procedures will suffice for this.

The use of comparison, the search for similarity with physical processes that have been analysed and solved in the past, might help to enhance creative skills.

Development of alternatives

After alternative solutions have been put to the tests with respect to their structural behaviour, and after the differences with respect to their structural behaviour have been taken away, the alternatives are to be classified with respect to their fitness for purpose and cost.

In the classical process of development of alternatives, to reduce the complexity, the following aspects are *not* taken into account here:

- *construction aspects (only implicitly)*
- *maintenance*
- *external cost/benefit*

If the choice of an alternative within this limited frame of reference is dominated by direct cost, only a local optimum in the solution space can be found. As soon as it is recognised that the final result is being damaged by neglecting the earlier mentioned aspects, the next question is, which aspects are worth considering in the optimisation process ?

With respect to external benefits, or external cost, such as mentioned above, one might think of cost and benefits that do not fall to the party which is commissioning the project, but to a third party, see Field (1994).

With respect to civil engineering structures, or infrastructure one might think of:

- *Life cycle cost, such as:*
  - *Maintenance and control,*
  - *Demolition and or replacement (if possible)*
  - *Energy demand*
- *Environmental issues,*
  - *Land use*
  - *Impact on the landscape*
  - *Ecology*
  - *Barrier*
  - *Noise*

If the cost or the benefits have a distribution in time, as might be the case if the benefits or the cost are related to the complete life cycle of an object, they can be discounted.

With respect to the design of an object in the national infrastructure one might think that all cost and benefits fall to the same party; the citizens. However, for that situation the Government Budget might be a hindrance, because different items might be financed by different articles in the budget system, or different layers of government. Such a situation is surely the case for the budget for the development of infrastructure, and the budget for control and maintenance of the same infrastructure. The result of this situation is that in the evaluation of alternatives, when deciding between alternative solutions, this is not based on an overall, i.e. an integral, summing up of the cost and benefit of the alternative solutions. Integral evaluation is not excluded, but an increasingly more difficult task, which in practice is often not performed.

2.2.3 *Designing as an optimisation exercise*

The last aspect of design to be considered in this section is the development of knowledge; i.e. relevant information. Among others, De Ridder, (1994) makes a reference to the fact that there is a parallel between the development of a design, and the methodology of scientific development. With respect to this he quotes Popper (1959), who states that:

> *Tentative Solutions; TS_i are being generated based on available knowledge. Depending on the friction between the ability to full-fill the demands on the tentative solution, TS_i will be taken in consideration or rejected (in terms of Popper falsified).*

In the case of scientific development there is no consensus about an objective standard to measure progress. For the case of a design for a civil engineering object, it is common practice to express the relevant issues in financial terms to obtain an objective measure for the effort of creating the object and of the value being created by it. The attribution of value to an alternative is not a trivial act. In practice it is easier to establish the cost of a design than the value. In section 2.4 the optimisation will be discussed. In the next section the cost components of a civil engineering design will be discussed.

2.3 COST COMPONENTS

Before discussing the optimisation from an economic point of view, here in this section in addition to what was mentioned to this subject in section 2.2.2, some supplementary considerations will be given about the cost components in the optimisation function. In section 2.4 the optimisation itself will be discussed in more detail

According to Stuip (1980) for the design of a CE structure, the following cost components can be distinguished:

Direct investment cost

- *Acquisition of land, material*
- *Design cost*
- *Construction cost*
- *Quality assurance; (staff and testing equipment)*
- *External cost, (not directly coupled with the primary function)*

Indirect investment cost:

I Design and manufacturing
I.1 Research
I.2 Adjustments
I.3 Adjustments and alterations
I.4 Loss of income
II Failure after completion of the work
II.1 Cleaning up and reconstruction
II.2 Research
II.3 Damage to 3rd parties
II.4 Loss of income
II.5 Nuisance
II.6 Pollution
II.7 Temporary recovering works

According to Van der Toorn (1994), this list of cost should be extended to include:

III Control and Maintenance
III.1 Control
III.2 Maintenance
III.2.1 Inspection
III.2.2 Repair
IV Demolition
IV.1) Demolition and/or reconstruction

In practice the item-list of external cost components ends here. At the time of formulation of this list, within the public works department, environmental aspects such as land use, or damage to scarce natural values were not yet considered to be external cost. However if a more rigorous optimisation based on economic premises were adopted, the choice not to include environmental issues could be regarded as in contradiction with fundamental premises of economic theory.

J.S. Mill (1862) postulated economy as

'Scarcity of the means to satisfy needs with respect to these needs'

Although environment, and natural beauty used to be looked upon as a free commodity, the diminishing availability of these, especially in the industrialized

countries, (within the reach of its citizens), would suggest that these issues should be included in a design evaluation, if applicable.

In practice the situation has evolved in that direction, as society requires technology to consider environmental issues. For the situation that an additional investment is asked to mitigate for environmental impact, the environmental benefits have to be evaluated in relation to the related cost. If a cheap environmentally friendly solution is available then a problem does not exist. If the environmentally friendly solution increases cost however, a conflicting situation might arise.

For example; in the case of energy consumption, how much more investment is justified to reduce the demand on energy ? In short, what is the marginal value of an energy reduction of one amount ?

Or for a different situation; if a project has to be developed within the limits of a fixed budget; how much of the performance (as a part of the direct benefit; the value of the project) may be exchanged for a better environmental result ?

Among others Hueting (1974), and Field (1994) discussed this topic. Hueting states that environment fulfils a function, and that actions against environment lead to functional loss. Functional losses would, according to his theory, have to be weighed in the primary profit function as an extra term with respect to cost.

Hueting distinguishes:

- *Compensation;* *(cost of an alternative function)*
- *Elimination;* *(cost to restore the function)*
- *Direct Financial loss;* *(Loss of fortune or income due to functional loss)*

Where Hueting states that the cost can be estimated by the amount of money which would be needed to restore a function. Hueting's approach can be classified as a *restoration approach*.

Field (1994) on the other hand although recognising the cost components as formulated by Hueting, emphasises the fact that these are *external cost*. Restoration of the lost functions on the other hand would have to be classified as external benefits. Field brings in the theory of marginal cost-benefit analysis, and states that the cost to consider has to be related to the level that society is prepared to pay for the restoration of functional loss. If no one is prepared to pay for a functional repair, than it is not feasible to account for the functional loss. The danger lies in the fact that maybe no one is prepared to pay, because consequences are not yet known. In more general terms both *external cost* and *external benefits* should be taken into account to derive an integral weighting of the alternatives.

Here it is proposed to extend the list of indirect cost according to

V Environmental issues
V.1 Compensation
V.2 Elimination
V.3 Direct financial loss

2.4 THE ECONOMIC APPROACH TO DESIGNING

2.4.1 *The optimisation function*

In the preceding paragraphs, the question was raised how an optimum solution could be derived. In section 2.3 different aspects related to the design of a structure have been put forward. Here in this section it will be tried to describe a frame of reference for the evaluation of all these aspects in a coherent framework.

In practice, one of the approaches often taken is the formulation of functional and operational demands in a program of requirements, and additional to that minimisation of the cost related to the fulfilment of these requirements is demanded. This approach assumes that the result; i.e. the *quality of the achievement*, here denoted as Q, cannot be damaged in the design process, if the program of requirements is being formulated strict enough. Which would mean that $\frac{\partial Q}{\partial a}=0$, where a, represents the independent variable in the space of solutions. The disadvantage of this approach, however, is that external benefits and external cost will not be taken in consideration.

The emphasis on the result to be derived, the structure, in combination with the task to limit the cost related to this as much as possible, generally leads to a situation that the questions such as

> *'what is the purpose of this structure?'*
> *'why is this project undertaken ?'*
> *'why is this project undertaken now ? why not 10 years earlier, or 10 years later ?'*

For members of a classical design team is sometimes difficult to answer.

> *'Why do you work on the design for a bridge at that site ? Well,...er, the principal has asked for the design of a bridge !!!'*

On the one hand one might say, why bother the structural analyst with things he does not need to know ? On the other hand, not having the scope of the effort in view, the structural analyst might decide for an unfavourable alternative, if looked upon from a higher level of abstraction, because the structural analyst cannot oversee the whole scope of the project.

If the optimisation of a civil engineering structure is judged from an economic view, where the task is to optimise the value created, and to minimise the effort (the cost) involved, a more clear view comes forward. Then it will be clear that the investment has to be considered with respect to opportunity cost too; the capital involved, could be invested alternatively creating greater value.

> *Leading in a design process according to an economic view, should be the optimisation of the profit. On the one hand by the choice of the subject; the nature of the investment, the 'type' of achievement, by the choice of requirements for this achievement; 'functional requirements'*

and 'operational requirements'. On the other hand by minimising the cost related to realise this achievement.

In economic textbooks, it is often a premises that the 'social desirable' optimum solution is being found for that situation, where the *marginal willingness to pay* for an additional amount of product is equal to the *marginal cost* related to it. In terms of the number of units to produce, (in terms of the textbooks), this would mean that the consumer buys that number of units product, till his satisfaction has decreased so far, that an equilibrium has been arrived with his willingness to pay for the last unit.

In terms of civil infrastructure, or real estate, where transactions are mostly made one unit at a time, the willingness to pay for one financial unit extra, for the condition that the value of the item being purchased is at least *worth* one financial unit extra, might be considered.

For that situation, the profit of the investment has a maximum. In economic

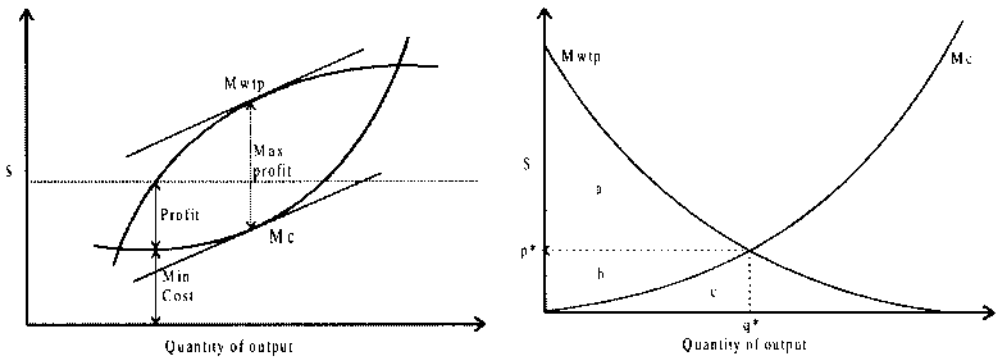

Figure 2.3 a) Value and cost optimisation b) Optimisation of Marginal value and marginal cost

textbooks this is often illustrated with a figure similar to Fig. 2.3b, where the curve of declining added value intersects with the curve of increasing added cost, for an additional amount of product(ion). In addition in Fig. 2.3a it is shown how for this situation, the profit has a maximum. In Fig. 2.3a one can recognise that the gradient of both curves is parallel for the point where the optimum is reached. In terms of the marginal value and cost this means both become equal. The latter on the other hand is easier to recognise in Fig. 2.3b. For both figures the number of units of product is on the horizontal axis and value, i.e. money is on the vertical axis. In terms of civil engineering structures, one might read the horizontal axis as the alternatives, being ordered on size or on additional functions.

From a mathematical point of view, the aforementioned balancing of marginal value (marginal willingness to pay), and marginal cost can also be understood as the optimising of profit. Where the profit is defined as the difference between

value and cost;

$$Fp(a) = Fv(a) - Et(a) \tag{2.1}$$

Where:

$Fp(a)$	=	*the profit as a function within the solution space*
$Fv(a)$	=	*the (functional) value; or in other words the Achievement*
$Et(a)$	=	*the total cost, the expenditures (including interest)*
a	=	*the 'space of solutions'*

The formulation given in equation 2.1 is unfortunately not objective. The profit is expressed in value; money. To derive an objective measure, where opportunity cost is being also considered, one has to adopt the *Relative profit*.

$$\mathrm{R(a)} = \frac{Profit}{Cost} = \frac{Fv(a)}{Et(a)} - 1 \tag{2.2}$$

The next question is, which optimum to pursue; profit or relative-profit, This choice is not trivial, the outcome is only equal for the situation that value and cost balance, as will be shown. Here after De Ridder (1994) it is proposed to choose for an optimum relative-profit, because the amount of investment is better taken in consideration.

An optimum solution for the relative-profit can be found for that alternative that satisfies the equation

$$\frac{d(R(a))}{da} = \frac{1}{Et(a)}\frac{d(Fv(a))}{da} - \frac{Fv(a)}{Et^2(a)}\frac{d(Et(a))}{da} = 0 \tag{2.3}$$

or

$$Et(a)\frac{d(Fv(a))}{da} = Fv(a)\frac{d(Et(a))}{da} \tag{2.4}$$

or

$$\frac{1}{Fv(a)}\frac{d(Fv(a))}{da} = \frac{1}{Et(a)}\frac{d(Et(a))}{da} \tag{2.5}$$

If the value of the design is equal to its cost, equation 2.5 simplifies to give

$$\frac{d(Fv(a))}{da} = \frac{d(Et(a))}{da} \tag{2.6}$$

In which the marginal value and marginal cost approach of economic theory can be recognised, as this is the same solution as would be found optimising equation 2.1.

With this result, the problem seems to be solved formally. It has to be considered however, that a rigorous optimising of the profit might be subject to

diverging opinions, because this would ask for an explicit evaluation of the achievement $F_i(a)$. For a lot of situations it is difficult to reach consensus on the value of alternatives. In practice, large deviations might be observed between parties when alternatives are being valued. Therefore this approach is often avoided and left to the political process.

Another aspect to be considered is that the exact solution of equation 2.5 and 2.6 demands that value and cost functions have to be continuous, and continuous differentiable. The satisfaction of the demand of continuity and continuity of gradients, presumably can only be fulfilled within the bounds of a product-type; a single type of structure, such as a bridge, if a water crossing is considered. In the initiative phase of a design project however, the alternatives might vary between several product-types. As well as a bridge, a ferry or a tunnel might be considered. The consequence of this, and the alternative approach taken in practice, is illustrated in Fig. 2.4, where subsequent profit functions for several product types are sketched.

The approach taken in practice, for the argument of feasibility, is that a sort of total benefit-cost analysis is being adopted. For that approach, the total benefit and cost of alternatives is being put in a relevant order. Subsequently the alternative for which there is consensus that the highest profit is being derived is adopted. This approach is typical for the initial phase of large infrastructure projects, where policy is evaluated and environmental impact analysis is performed on either location or proposed route. Total benefits, are 'weighted', often under application of multi-criteria procedures, including cost and displayed to the (political) decision making forum.

The procedure is illustrated in Fig. 2.4, where imaginary profit functions are drawn for four alternatives; A, B, C and D. External values and cost might differ

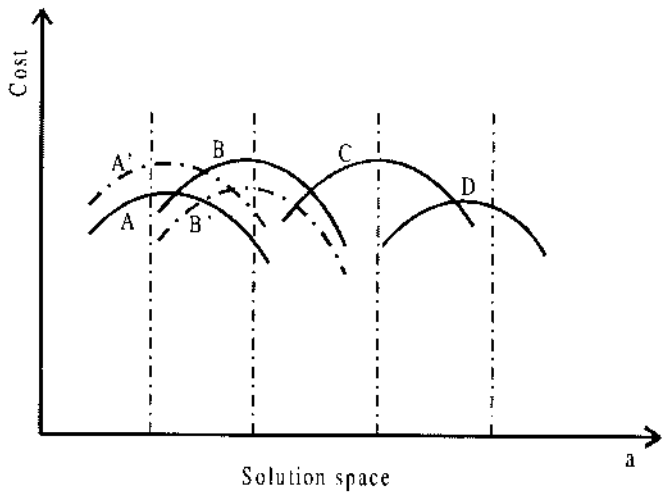

Figure 2.4 Total profit functions

per alternative, as is illustrated by the dashed lines for alternatives A' and B'. How the profit functions are being weighted in the initial phase is illustrated by the vertical dot-dash line (not yet on the optimum per product-type). The intersection marked with the large dot, with the profit function is the profit weighed in the initiative phase.
The fact that this procedure does not guarantee an optimum solution is caused by the following facts:

- As this approach is a type of implicit total benefit-cost evaluation, the alternatives regarded do not necessarily fulfil the demand for marginal benefit-cost balancing. For slight differences in Profit between alternatives the decision for one or the other alternative might be different, if alternatives are locally optimised; the alternative is not necessarily intersected at its local optimum.
- In practice only direct benefits and cost are weighed; external cost and external benefits are not necessarily taken into account. The external profit might be different for alternatives, which might influence the choice for one or the other alternative too. In Fig. 2.4 this is illustrated, where the preference for alternative B over A, is being overthrown if external profit is considered, illustrated by the preference for A' over B'

This direct method of applying alternative solutions has the practical merit of being a feasible approach. Especially for the functional phase and for the choice of a location or the track of a project this procedure seems to be next best. The consensus about the procedure overthrows the theoretical objections. Perhaps that should be given merit too.

For the subsequent stages of design, where the *form* and the *dimensions* of a structure are established, it is often presumed that the benefit, the value of the achievement, is not influenced by the choice for one, or the other alternative. Here the assumption that the '*terms of reference*' stand guarantee for the value of the project is more explicit. For that situation the profit function equation 2.1 may be reformulated to give:

$$Fp(a) = Constant - Et(a) \tag{2.7}$$

The optimum profit is than derived by minimising cost only. Reformulated the profit will read as:

$$Fp(a) = -Et(a) \text{ or } Fp^{*} = Et(a) \tag{2.8}$$

The inaccuracy introduced by this assumption, is that there is a chance that a number of relevant components of the (functional) value, such as; environmental functions, or loss of these, or hindrance, are not being formulated in the terms of reference, and not constant for different design alternatives.

This problem is more prominent if the alternatives are not indifferent with respect to functional behaviour.

Another aspect to be considered, is the influence of management. If the project-management is not performed adequately, the principal for the project, who has commissioned the work, and is paying for its outcome, may not have adequate control on the evolving results. If there is a lack of budget the designer might be tempted to reduce the functional requirements in order to bring the project within the budget.

The rigorous achievement of a marginal benefit cost analysis however, in practice, is unlikely to be feasible. The origin of this difficulty is that value and cost are difficult to describe in explicit functions. This shortcoming is most important in the initial phase of a design where crucial questions with respect to benefit and cost are the main topic of consideration.

The choice for an approach for the optimisation in a design step is often implicitly made. Observing practice the following optimisation approaches are applied:

- *Total Benefit-cost evaluation*
- *Marginal Benefit-cost evaluation*
- *Minimisation of cost*

In the next paragraph it will be tried to discus some aspects which influence the choice for an optimisation, evaluation approach.

2.4.2 *Staged execution of the design process*

As explained in section 2.2.1. practical design may be thought of as a process. According to a more or less fixed number of development steps, with as a final result a specification of the object, the relevant information about the civil engineering product to be established is being developed. Sometimes within the bounds of project-management this process is being extended, including the construction of the work itself. As mentioned too in section 2.2.1, the steps taken in the subsequent design phases may be regarded as a step-wise optimisation.

In each phase a sub-optimisation is performed for that part of the solution space relevant to that phase, other aspects being considered as fixed. Especially in the functional phase and in the phase that the track of a connection, or the location of a structure, is being determined, it is of the utmost importance to do the proper variations because for those phases decisions such as the product-type are made, determining large parts of the benefit of the investment; the value and the cost. The decision for a bridge or a tunnel; or if the work is related to a geo-technical problem, an embankment or a sheet-pile wall.

In terms of the profit, for a favourable situation, the cost function, in mathematical terms may be established continuous, and continuous differentiable. The question arises however, whether the benefits, the value which is related to the functions to be installed, can be derived explicitly too.

In hydraulic engineering, the crossing of watercourse is a typical example.

Depending on functional demands, local situation, and boundary conditions, such as

- *width of the water*
- *traffic density*
- *required shipping height*
- *depth of the water*

Quite different civil engineering product types might come forward as a solution.

Product-types such as

- *an alternative land route; traffic diversion*
- *a ferry*
- *a bridge*
  - *opening bridge*
  - *pillared bridge*
  - *arch-bridge*
  - *cable stay bridge*
  - *suspension bridge*
- *a tunnel*
  - *submerged tunnel*
  - *bored tunnel*
  - *NATM tunnel*

Depending on the local situation and functional requirements all of these product-types might yield an optimum solution, for one situation or another.

As mentioned previously it may be unpractical to optimise all benefits and cost, to balance these explicitly, in each step of the design process. For this situation, a step-wise sub-optimisation is more practical. A stepwise sub-optimisation presumes that

$$\min\left(\sum_{i=1}^{n} Fp_i^{**}(a)\right) = \sum_{i=1}^{n} \min\left(Fp_i^{**}(a)\right) \tag{2.9}$$

Equation 2.9 however is only true (or by approximation), for a linear system. If the assumption of linearity is true, the step-wise sub-optimisation will lead to an optimum, whatever the sequence. It was presumed earlier that for that situation the solution space has to be continuous and continuously differentiable. In that case step-wise variation may be performed according

$$\frac{d(Fv(a))}{da_i}\Delta a_i = \frac{d(Et(a))}{da_i}\Delta a_i \tag{2.10}$$

If it is feasible to do independent variations Δa_i, convergence in the direction of the optimum will be approached too.

In practice it is very difficult to do independent variations, as the feasible alternatives in solution space are mostly not continuous and continuously differentiable.

2.4.3 *Time related aspects of a civil engineering project*

In the step-wise approach of a solution for a civil engineering design, in the functional design, but also in the spatial structural design phase, where type and size of the structure will be distinguished, topics related to the Life Cycle of an object may come forward. For that situation life cycle analysis, (in short LCA) is used. The LCA approach contains

- *distinguishing of cost components*
- *pricing of the cost in the present*
- *discounting for cost, depending for the point of time the cost have to be beard*

Which means that equation 2.1 has to be integrated over the life span of the structure

$$Cv(Fp(a)) = \int_{t=0}^{t=l} \frac{\partial Fv(a)}{\partial t} dt - \int_{t=0}^{t=l} \frac{\partial Et(a)}{\partial t} dt \tag{2.11}$$

Where Cv stands for the Cash value and l is the estimated service life span of the structure under consideration. In practice, it is often hard to formulate what the time derivatives are. Besides that, it is common economic practice to estimate value and cost in the future on another scale as in the present. Therefore in most situations the equation 2.11 is summed up incrementally on a yearly basis, and discounted for cost lying in future years, considering a rate of interest r, according to:

$$Cv(Fp(a)) = \sum_{i=1}^{i=l} \frac{Fv_i(a)}{(1+r)^i} - \sum_{i=1}^{i=l} \frac{Et_i(a)}{(1+r)^i} \tag{2.12}$$

2.4.4 *Optimisation of an engineering structure*

In practice, equation 2.5 (or 2.6) is not analysed rigorously and consistently. The determination of the height of sea dikes in the Netherlands however is an elegant example of how it can be done. In this case the solution of a safety level for the design of dike height is solved taking a variant form of equation 2.5, where the profit is optimised and found. The description of the approach taken is given by Vrouwenvelder & Vrijling (1982). The base taken for this approach is the balance of marginal benefits and cost.

Within the bounds taken for this problem it is not practical to acquire the functional value of such a structure explicitly. Therefore for the sea dike problem the functional value is taken into account implicitly, by adding the risk related to the (temporary) loss of function of the system to the cost. The argument for such

an approach is that it is presumed that the polder whose sea defence has to be strengthened is an existing polder. In other words, variations with respect to the size of the polder, which might influence the functional value, are not feasible.

For that situation the profit may be expresses as

$$Fp^{*}(a) = Et(a) + R(a) \tag{2.13}$$

Where $R(a)$ stands for the risk taken with this situation.

This leads to an evaluation based on marginal values of cost and benefit, in which it is established for what level of investment an extra monetary unit of investment leads to a reduction of the risk, which value is just equal to the cost of that extra monetary unit.

$$\min(Fp^{*}(a)) \Rightarrow \frac{\partial(Et(a))}{\partial a} = -\frac{\partial(R(a))}{\partial a} \tag{2.14}$$

That is, as the risk is defined as $R(a) = P_f(x > x_{cr}|a) * W(x > x_{cr})$, , i.e. the probability of failure $P_f(x > x_{cr}|a)$ times the estimated damage in case of a failure $W(x > x_{cr})$.The optimum solution is found than for:

$$\frac{\partial(Et(a))}{\partial a} = \frac{-\partial\left(P_f(x > x_{cr}|a)\right)}{\partial a} * W(x > x_{cr}) \tag{2.15}$$

In principal $P_f(x > x_{cr}|a)$ can be solved for this. It should be noted that $\frac{\partial\left(P_f(x > x_{cr}|a)\right)}{\partial a}$ is the probability density function. The balance between this, and the gradient in cost is determinant for the dike-height. If the functions Et(a) and $P_f(x > x_{cr}|a$ and the damage due to the exceptional occasion, $W(x > x_{cr})$ are known as a function of the solution space, then the optimum dike-height can be established.

Depending on local conditions, as in the example of the water crossing, the solution of the equations may lead to different solutions. Therefore in practice there is a tradition to solve this problem for the *probability of failure*. The application for a tangible situation does depend on the type of function for the frequency of exceeding. If that is an extreme value distribution, direct integration of the equations is possible, and being looked up in a table. In a more general form the integration reads:

$$P_f(x > x_{cr}|a) = -\int_{a_{opt}}^{\infty} \frac{1}{W(x > x_{cr})} \frac{\partial(Et(a))}{\partial a} da \tag{2.16}$$

The solution can be found by integrating the gradients in cost over the cost of the unfavourable exceptional occasion.

The approach illustrated in this example can be generalised for the majority of the civil engineering structures, i.e. for the structural design part the optimisation being taken is:

'Balancing marginal risk with marginal cost'

2.4.5 *Limit state analysis*

The example given in the previous section, the prevention of sea-dike failure, is an example of Limit state analysis. Limit states are defined as those unfavourable states of a structure, which are related to large damages or major dis-functioning.

In general two main classes of Limit states are recognised:

- *Ultimate limit states (ULS)*
- *Serviceability limit states (SLS)*

Ultimate limit states are those unfavourable limit states, where the damage is invoked at a more distinct point in time. Examples of Ultimate limit states are, collapse e.g. the development of a structural mechanism or flooding.

Serviceability limit states may be recognises as those unfavourable limit states, where the related damage is the summation of partial damages in time, contributing to a total loss when summed up over the life cycle of a structure. Serviceability limit states are mainly related to dis-functioning of the structure.

Sometimes the difference between ULS or SLS is hard to distinguish. Subsequent partial collapse of a structural element, leading to loss of function can either be classified as ULS for the structural element or as SLS for the structure. Important in this is that for a type of structure, the Limit states are distinguished, and that criteria are developed to limit these unfavourable states up to an allowable probability of occurrence. To balance the cost of prevention with the risk related to the limit state.

The establishment of Limit states is enhanced by fault-finding techniques, such as the development of fault trees. Based on the fault trees, balancing marginal cost and marginal benefit of a solution, allowable probabilities of occurrence can be established. The application of probability techniques makes it possible to establish partial factors, e.g. for load or strength or other determinate parameters. See among others, Vrouwenvelder & Vrijling (1982)

2.4.6 *The normative approach to additional demands.*

Sometimes a normative approach for environmental issues is proposed. The intention for such an approach is the introduction of proper legislation that should be met. This intention is derived taking a parallel to the procedure that has been used for the demands which have to be laid upon structures to comply to structural requirements. Such an approach could than be used as a procedure to solve and handle additional requirements for a civil engineering design. Referring to the way that standards have been set for the structural design. With a standardised approach the designer would be shielded for a personal evaluation.

It is unclear however, whether in the short term this would lead to an optimum solution, as contrary to structural design, there is a lack of a database of relevant knowledge. In addition to that, standards have to be agreed upon in a more or less centralised way. To achieve this, a number of solved cases, either analytical or semi-analytical, would have to be available to create a frame of reference.

Besides that, it has to be considered that according to a procedure for standardisation, optimised solutions can only be approached on a general level. The most desirable alternative can only be approached approximately. This is because standards can only be set at an averaged level, for a class of problems, optimal for a product type. For structural design, experience has been obtained using this type of approach. For the most common structural types, such as buildings and houses, there is a general level of agreement about the procedure. The chance for an undesirable solution is thought to be sufficiently small.

In contradistinction to design for new infrastructure, the situation for maintenance of structures, which is sometimes regarded as one of the later steps in the Life cycle of infrastructure, is such that the normative approach is not feasible too. The diversity of structure types and the absence of a generally agreed frame of reference to evaluate alternative strategies lead to an unmanageable number of variables and potential solutions. With this a generalised approach with standards is difficult to apply.

There is a tendency to think that Life Cycle Analysis, optimising the profit for a complete life cycle would offer interesting opportunities.

With respect to environmental issues the most favourable approach remains unclear.

The most promising alternatives are

- *Expressing all aspects in terms of money*
- *Multi-criteria*
- *Broad debate, (political forum)*

For the larger nationally discussed infrastructure projects, the latter alternative might appear to be efficient. The true marginal value is then established by political discussion. For the smaller projects this approach would lead to a process which is not manageable; the marginal cost of the procedure would not balance with the marginal value created by this effort. In this case multi- criteria approaches might be used to give a solution.

In principal expressing all aspects in terms of money is thought to be the most objective approach. A draw back for a rigorous adoption of a remunerative approach is that it is often difficult to derive agreement on the value of certain items.

It seems that Oscar Wild once has stated that

> *' Everybody knows what is the cost of things, ... But nobody knows the value !! '*

2.5 ORGANISATION; PARALLEL EXECUTION

'The problem of the collective brain'

The description thus far implicitly assumes that all the relevant information that is generated all through the design process, and which is necessary as a source for further development, is instantaneously available for all contributing parties. The organisation is thought to operate like a single person with a collective brain. In practice the organisation is composed of discrete persons, and is far from this idealised model. The organisation comprises of discrete persons that actively have to communicate with each other to share the information. To facilitate this sharing, the information has to be converted to transportable media, such as reports, notes, letters, faxes and emails. This converted information is exchanged at discrete time intervals.

If the object being developed is particularly important, the organisation might be subdivided into several parts. For that situation the interval of information exchange might be as limited as a design step. This might lead to the unfavourable situation that subsequent design work is based on information agreed at time (i-1), and applied at time (i), and subsequently has to be reconsidered at time (i+1), because the technical requirements cannot be met by one of the design teams. The other design teams, will not be eager to do their work all over again, (on whose account ? who carries this risk ?). If they were no part in the source of the problem, and it is not their responsibility, why should they make a sacrifice to help solve the problem ? Quickly the opinion might be expressed that the party or person who has encountered the problem has to solve the problem too (whatever the cost ?), instead of requiring other parties to carry out additional work.

The building that is too heavy, and cannot be placed on the foundation which has been designed for a much lighter building is a classical example.

- *Should the building designer reduce the weight of the building ?*
- *Should the geo-technical designer responsible for the foundation produce a new design?*

To begin with, both parties will start by claiming that the other party has a problem.

Learning from past experiences, a tendency might be triggered to exchange conservative values of relevant information, instead of mean values. One design team might propose an upper bound value, of which he or she is certain that their team can meet it, whereas other teams might interpret this value as a lower bound value. Unwillingly this might lead to an uncontrolled and unwanted combination of necessary and unnecessary partial safety factors, which together make the design too expensive for its purpose.

For a characteristic hydraulic structure, such as a shipping lock, in the structural phase of a design, boundaries for interchange of information might occur between:

- *Soil mechanics advisor*
- *Foundation specialist*
- *Concrete designer*
- *Hydraulic engineer*
- *Steel structure advisor*
- *Mechanical Engineer*

Similar boundaries of interchange of information might arise if the spatial and the structural design are partly performed in parallel. Generally with respect to information control it is recommended to limit the number of boundaries for information exchange. However, If there is a strong demand to process within a very limited time schedule, parallel execution cannot always be excluded.

In the project managed work scheme according to Wijnen (1984), five control parameters are recognised; to begin with the trio, time, cost and quality, and subsequently the duo; organisation and information.

In the first trio, the benefit-cost aspects may be recognised, whereas within that frame quality is a weak parameter to control. The latter is awkward as the benefit of a project is related to this parameter. Maybe quality is a too abstract formulation for the control of the benefit of an investment.

In the latter duo, the problem of sharing information and of decision making is controlled. If it is recognised that optimisation is an important issue for design, the necessity to give a strong emphasis on organisation would not be necessary. The problem of sharing information however would deserve much more attention and would give a more direct link to the way in which an organisation to carry out the design is selected.

2.5.1 *Automating as an objective means of sharing information*

With respect to the communication problem, in a time that automating and the development of an IT infrastructure in offices is strongly developing, these developments can also be used to solve the problem of sharing information. If all the relevant information related to the development of an object could be stored in a central database, which is available for all the project partners, the communication problem would be strongly diminished. However, a requirement for success in such an approach would be that it is a structured database, where all the information is stored only once in an objective way. The advantage of such a development would be increased, if the various design analyses took their input directly from the data in this database. The availability of coupling-interfaces, between this structured database and application software to perform sub-optimisations such as discussed in the preceding paragraphs, would be necessary.

The CUR/LWI development program is a step in this direction. In practice, this technology is not yet operational, as most of the necessary application software is not yet available.

Although this type of working is not available in its completeness, small steps in the direction of a work procedure like this might be taken, and taken advantage of.

Especially if we focus on structural analysis, and within that frame on the main subject in this thesis, geo-technical analysis, the application of one spatial mechanical model to analyse

- *deformations*
- *stability*
- *dynamics*
- *time depended behaviour*

For successive steps in the staged construction of a civil engineering work, is an example of a successful approach for this problem.

Seen from the more broad perspective of integral design this example is only a small step. For the advancement geo-technical engineering however, this development is an important step.

Where formerly for each point of evaluation it was necessary to apply a different model:

• *stability;*	*Slip surface analysis (according to Bishop)*
• *stress distribution,*	*Boussinesq, solar of Newmark etc.*
• *deformations*	*Empirical; e.g. settlement trough proposed by Peck*
• *structural analysis*	*Subgrade reaction models (Hetenyi)*

For each aspect a different model is needed to test whether requirements related to this aspect can be met. Quite often in this process, inconsistencies with respect to the use of parameters in the models cause a difficulty. Sometimes more than one parameter is used for what essentially is one property, e.g. the Young's modulus E_{50}, the shear modulus G_{50}, the compression modulus according to the Oedometer test E_{oed}, m_v, or related to stiffness, the consolidation coefficient.

To add to these difficulties, sometimes completely different parameters are denoted by the same character, e.g. k for spring modulus, as well as k for the Darcy permeability of soils or for the subgrade reaction modulus.

With the introduction of Finite Element analysis, material behaviour based on continuum mechanics is introduced. Besides that, Finite Element analysis can be used to analyse most of the aforementioned aspects within the framework of one spatial model. With this, the difficulties in interpreting the relevant input parameters and in communicating information about these is strongly diminished.

2.6 SUMMARY

In this chapter, different aspects related to the design of civil engineering works have been discussed. Designing is not only seen from the perspective of the design process, or as a creative effort. Designing is also discussed from the perspective of optimisation by employing the economic approach.

In the latter perspective the interaction between creativity, (the skill to generate alternatives which meet requirements), and the evaluation of alternatives, leads to a systematic approach in which alternatives are ordered according to their merit.

Observed from the economic perspective, the common approach, which is applied in the initial phase of a project, can be classified as a total benefit-cost analysis. Whereas in subsequent design stages, the evaluation of alternatives shifts to marginal benefit-cost analysis in the functional-Spatial design phase, where the type of structure is determined. Finally in the structural design phase the optimisation usually is limited to optimising the solution with respect to cost.

Among structural designers, those who explicitly realise that the evaluation of alternatives is being performed according to these procedures form a minority. This lack of appreciation is enhanced by the common practice of introducing partial safety factors, conforming to the standard requirements for structural design, the 'Bouwbesluit' and the 'TGB'. The introduction of partial safety factors masks the way that alternatives are being evaluated.

As a common shared view on how an objective approach for an optimisation process would have to look like is lacking, there is no strong hold on the way the optimisation process is applied in practice. Especially for the design of public works, society would benefit from the choice for a marginal benefit-cost analysis.

Based on the assumption that structural design is essentially a form of cost minimisation, two aspects have to be named which might influence the choice of models to be used in structural design. Aspects which need a more refined evaluation before a final position with respect to the use of models, is being taken,

- *Model uncertainty*
- *Cost of analysis*

In the following chapters, both aspects will play a role in the evaluation of the development of models.

CHAPTER 3

Development of models for structural analysis

3.1 INTRODUCTION

In chapter 2, structural design has been discussed in general terms. What we have seen is that the design process is composed of a creative effort, where feasible alternatives are brought forward, and analytical effort, where the alternatives are optimised. The second aspect of structural design that we have seen is that in the optimisation step a balance is sought between the value of the function being created, and the investment.

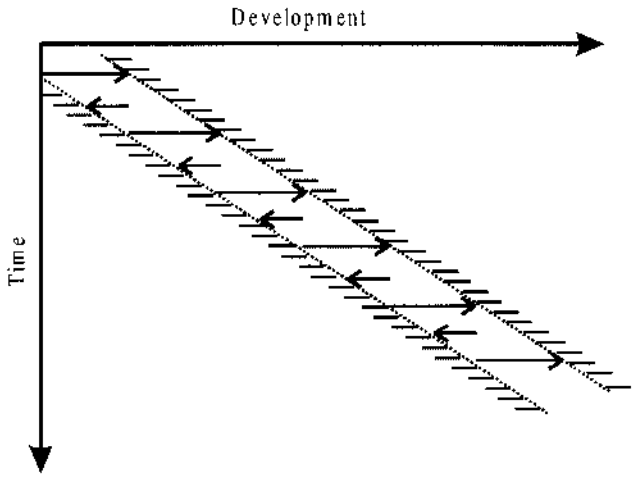

Figure 3.1 Design; two steps forward, creating an alternative, one step backward evaluating its performance.

For structures, where the risk of structural failure, i.e. collapse, always plays an important roll, it has to be remembered that the risk of failure is implicitly included in the cost. This risk might dominate above other value components if not taken into account properly. Therefore it is a common acknowledged fact that structural analysis is an important part of the design. The evaluation of the ultimate limit state is therefore mandatory.

Another important consideration in the optimisation is that if the structure is not able to sustain its structural integrity in a proper way during its lifetime,

(although not failing), the functions it has to fulfil might not be guaranteed. The serviceability of the structure is then at risk.

After the creative step taken first, inevitably, a second step follows where the feasible alternatives are put to the test, and optimised with respect to their performance and cost. Metaphorically, one might say that the creation of a design alternative takes us two steps forward, see Fig. 3.1, whereas subsequently the optimisation and evaluation of the alternative takes us back one step.

The two steps forward is strongly related to the human capability to synthesise a solution, based on a thorough knowledge of all the demands and the resources available. This synthesis is related to our intuition to what is feasible. The backward step is much more analytic and relies on deductive processes and understanding of behaviour. Although we have been put back one step, on the whole the design has made progress.

Structural analysis has to be placed in the context of the backward step; putting design alternatives to the test. That is, analysing whether the behaviour of the structure satisfies the relevant criteria.

3.2 STRUCTURAL ANALYSIS

Here the adjective 'structural' is used if the analysis is related to a coherent mechanical system. Though a dike or an embankment is a structure according to this definition, here in this study, the description 'structural' is mainly used in the context, where a soil body is combined with a structure, not being a soil body, such as a building on top of the soil, or a structure build up of steel or concrete, on top, or in the soil, such as a sheet pile wall. As there is a large difference in the length scale of a structural element and a soil particle, and related to that a large difference in strength and stiffness, soil retaining structures often show a mechanical behaviour which is distinctly different to that of a soil body, such as a dike or an embankment.

Common acknowledged aspects for the evaluation of a structure in its limit states are:

- *Strength*
- *Stiffness*
- *Stability*

These aspects relate to the behaviour of a structure both in the ultimate limit state, and for the serviceability limit state.

In order to test a feasible structure for its limit state conditions, models are used. The time when a structure was built and then verified by a loading test, i.e. a predefined overloading of the prototype, has now passed. Therefore, modern structural analysis relies on models.

Since the introduction of computers in the second half of the 20th century, the development of numerical models has been strongly enhanced. For structural analysis, and also for groundwater-flow, the development of numerical models

based on finite element techniques has strongly enhanced the use of these models. The development and tailoring of such for practical purposes is the main topic of this thesis.

3.3 SOURCES FOR MODEL DEVELOPMENT

3.3.1 *Limit state analysis*

Structural models have to be able to describe the limit states for structures, i.e. the ultimate limit state, and if possible be able to describe behaviour to evaluate the serviceability limit state(s). To begin developing structural models a certain amount of knowledge about the modes of failure is needed. A behavioural model that is unable to describe failure modes is a weak model.

Examples of models based on the description of a single mechanism are

- *Bishop's slip circle analysis for the stability of sloping surfaces*
- *Prandtl's theory of bearing capacity*
- *Brinch Hansen's empirical model for bearing capacity*
- *Blum's theory for sheet pile walls*

Knowledge about failure modes directly or indirectly comes from observations. Case histories describing real failures, for example, are an important source. Laboratory tests on samples or on structural parts may also develop insight into the way that a structure might behave. Based on that, mechanical concepts might be used to evaluate the probability of a feasible mode of failure.

Both direct observations as well as mechanical concepts might be a source for model development.

3.3.2 *Development space*

In addition to observations only, which are a primary source for knowledge about limit states, another source for model development would be the evaluation of models, used and applied in practice, in combination with observations related to these structures. If these observations relate to failures they even have a higher value. Back-analysis of case histories might give us another source.

If one would recognise the existence of a mathematical domain, to develop models to describe structural behaviour, such a development space might be spanned on a finite number of parameters. If there would be an insight where in this development space, the models show an inability to describe observed behaviour, further model development could be directed on this part of the development space.

In this context it is important to have a view on models developed in the past and also on the shortcomings of subsequent models. If a hierarchy, a classification of grades of performance of models, was apparent between subsequent models, this might help to distinguish promising further developments.

The parameters being used as a base for a model are decisive for the model

space that comes forward from a model. The addition of additional parameters expands the solution space. Contrary to the arbitrary use of parameters, from a physical point of view a specific hierarchy in the use of parameters is also possible. Based on this the development space for model developments, creating a sequential hierarchy between models along the following lines of model extension, might be recognised:

1.	*static*
2.	*cyclic*
3.	*dynamic*
a.	*discrete*
b.	*continuum*
A.	*elastic*
B.	*elastic plastic*
C.	*elastic visco-plastic*
D.	*visco-elastic visco-plastic*
i	*one dimensional*
ii	*plane strain/plane stress*
iii	*axi-symmetric*
iv	*three dimensional*
B.1	*Coulomb friction*
B.2	*Mohr Coulomb strength*
B.3	*Tresca*
B.4	*Von Mises*
B.5	*Cam-Clay model*
B.6	*Friction hardening model*
Δ.	*one phase model*
Φ.	*uncoupled two phase; (groundwater flow - stress analysis)*
Γ	*coupled two phase; (consolidation analysis)*
ϑ	*three phase*

Each line of extension might be regarded as an axis in a multi dimensional development space. A coordinate in this development space would characterize a model type.

If weighting would be assigned to each axis in the development space, an explicit hierarchy would become apparent between models. As the weighting assigned to an axis is arbitrary, the only hierarchy recognized is that between models, (which have a similar co-ordinate) only differing on one development axis. To develop an opinion to decide for promising development directions, the evaluation of subsequent models, and observed discrepancy of these models with observations is valuable, taking into account the position of a model with respect to its position in the development space.

Within this concept of a development space, development might proceed by making new combinations, where feasible new models move further away from

the origin in this development space. Theoretically this process might proceed up to the point that the space is filled up with models, then the process halts until a new development axis is recognised.

If one chooses a careful position for observation of the models, a certain hierarchy between the models may be recognised. If one validates models of subsequent hierarchy, a diminishing error between observations and model should be observed. Although it must be recognised that the absolute error of a model will not necessarily become smaller when a model is refined. A complex model will only give a better prediction if all the parameters are correctly estimated.

The additional parameters in a complex model may introduce additional uncertainty that counteracts the improved accuracy of the model.

3.3.3 *Verification*

An important step to be taken when developing a new model is verification. Verification in practice means making a comparison with previous models. For these previous models, which are assumed to be lower in hierarchy and therefore simpler, it is assumed that there are a sufficient number of commonly accepted solutions.

Verification is a logical test.

The following models for verification are available

- *Analytical solutions, often elastic solutions*
- *Upper bound solutions applying plasticity theory*
- *Lower bound solutions, equilibrium solutions*
- *Hierarchical models of lower order*

For a specific case, one or more of these models may be used to compare with the new model. For an elastic analysis, the new model should provide a close match. If the material model is used to model associated flow plasticity, then it should provide a solution that is between the upper and lower bound solutions. For non-associative material behaviour, the new model should provide a close match with models of lower hierarchy, for the case that new parameters are assigned neutral values. The new model should be able to exhibit the behaviour of the preceding models in the hierarchy.

3.3.4 *Validation*

The final stage in the development of a model is validation. The term 'validation' describes the effort to establish insight into the capability of a model to describe prototype behaviour. This means that a different type of comparison is made, not with other models, but with observations. The following observations might be used for this purpose:

- *Empirical relations (implicit observations)*

- *Physical model tests; e.g. 1D lab tests; centrifuge tests*
- *Prototype tests;*
  - *Prediction/evaluation*
  - *Back-analysis*

Empirical relations are judged here as a form of condensed observations and therefore applicable for validation. Laboratory tests might be used for testing the integrity of important components of a model. Essentially in laboratory tests relatively homogeneous processes are tested, for which the model needs to be able to describe observed behaviour.

Finally prototype measurements, and preferably in combination with a set up where the model is used for predictions, make it possible to do real validation. Where a back-analysis gives an impression about the integrity of a model, the combination prediction versus measurement; evaluation gives a view on the practical value of a model; the power to use the model for design purposes.

If a model is used to investigate the variations of the parameters, the comparison of the results with the measurements might give an impression about the model accuracy. Though this variation implicitly includes the uncertainty of the parameters, the band-with in model outcome gives an impression of the stability of the model. If this band-with is large, it means that a small variation, or uncertainty, in a parameter means a large shift in the outcome. If a parameter is difficult to establish, and the model is sensitive for such a parameter, this would mean that the model is unfit for design purposes, though the model might still be useful for back-analyses purposes.

3.4 THE MERIT OF A MODEL

The merit of a model consists of several components. Good agreement with observations in a back-analysis is the first one. If a model is able to predict tests with a high accuracy, such a model becomes useful for design purposes.

Another aspect is the cost of the development of a model. The specification of a model is developed much faster than that the model is formulated, tested for integrity, verified, and validated. Furthermore if the model will be used by a larger group of users, the cost related to making the model accessible to others must be considered. Efforts related to user-friendliness and education; seminars and workshops needed for the transfer of information to prospective users have to be considered. If the model has to be maintained for a long period, cost related to maintenance of the model and also updates involving adjustments and corrections have to be considered. If the model is a numerical model, the source code has to be maintained and kept up with new releases of compilers and operating systems.

If there is a necessity for a model, such as if the proposed structure cannot be designed and realised within a low enough probability of failure without the accurate model (e.g. rocket to the moon, storm surge barrier), the aforementioned cost are relatively small in comparison to the investment in the main project.

Without a necessity for a model or if the investment is not small in comparison to the main project, the economic evaluation such as discussed in chapter 2 has to be taken into account again.

3.4.1 *Finite element analysis*

The development of numerical models; e.g. finite element analysis, based on continuum mechanics, enables the development of a consistent concept for a unified approach for structural models; i.e. one single concept for all types of structures.

One of the main features of the finite element method is that it is general enough to produce failure mechanisms that have not been included as such in the model, but are incorporated on a deeper level, by using a general field of deformations.

The advantages of such an approach are:

- Unification of model developments. The effort being put in model development for different criteria is less. Developments are not primarily aimed at one application or criteria to evaluate.
- Education. The structural analyst only has to know one type of model
- Maintenance of source code

In this thesis a secondary aim is to evaluate the power of the finite element method to cope with different types of engineering problem. One of the crucial questions then is whether the consistency of the finite element method is more reliable than the implicit strength of empirical models. Empirical models implicitly include aspects such as 3D, dynamics, creep, ageing, which have to be included in finite element analysis in an explicit way.

In the cases treated in chapter 5, 6 and 7, the composition of the finite element method to adjust to a number of practical problems is analysed and evaluated.

3.5 DEVELOPMENT STRATEGY

The development strategy followed in this thesis is related to the development of finite element techniques for practical purposes in civil engineering; i.e. soil retaining structures.

The strategy is composed of the following steps, see Fig. 3.2

1. *Knowledge of the mechanisms and modes of failure.*
2. *Knowledge of the hierarchy of existing models for structural analysis.*
3. *Insight into the inaccuracy of existing models.*
4. *Proposing new models, within the framework of finite element techniques.*
5. *Verification of the models, comparing the results with models of lower hierarchy.*
6. *Making predictions with the new model.*
7. *Performing tests.*
8. *Validation of the model eveluating the new model with respect to the tests results.*

3.6 CONCLUDING REMARKS

In this chapter, a strategy to develop models for structural analysis is discussed. The application domain for developments is mainly aimed at soil retaining structures. Structural analysis is discussed in the context of design of structures. Design of structures is considered as being composed of a creative effort producing feasible alternatives, followed by an analytic effort, where the alternatives are being put to the test and optimised.

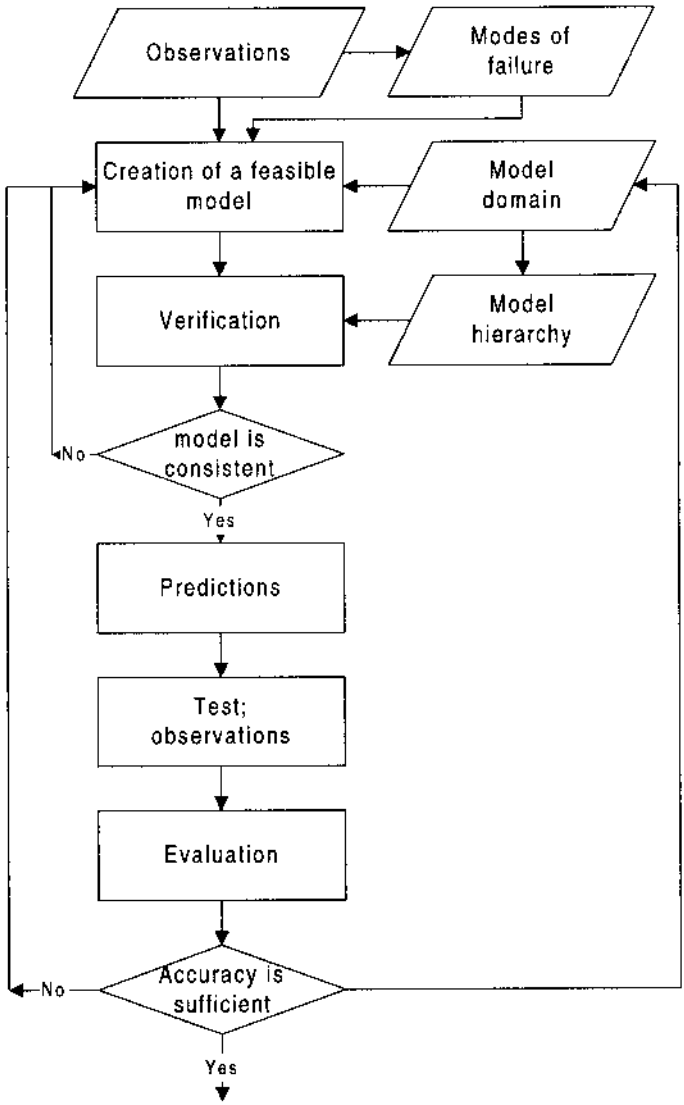

Figure 3.2 Scheme for the development of models for structural analysis

Structural analysis is an important part of the optimisation of a structure. Without knowledge (using models) of the behaviour of a structure, the optimisation merely would become an arbitrary extrapolation, which would be a high-risk process. The sources for the development of models for structural analysis are discussed. The merit of finite element analysis, as a development domain for models for structural analysis was discussed. Finally the development strategy is summarised.

CHAPTER 4

Soil mechanics and groundwater flow

4.1 INTRODUCTION

Thus far in the first three chapters the main focus is on methodology, the methodology to optimise the design for a civil engineering structure, and on a different level the methodology to develop models for structural analysis. The latter will be looked upon in more detail in the second part of this study, i.e. in the chapters 5, 6 and 7. In these chapters, the development of models for three different types of civil engineering structures will be studied and evaluated. In between these distinctly different parts of this thesis, here in chapter 4, a crossover is being made between the part that is related to methodology and the part that is related to technology. In this chapter a review is given of the main principles that are being used in the development of models for structural analysis, i.e. for the approach mainly taken in this study applying the method of finite elements. Apart from the review, two items that are not being found in the textbooks will be focussed on. The first is that for large volume strains higher order terms should be taken in consideration. The second is, that groundwater flow may be analysed applying the principle of virtual work.

In this chapter, the main principles of soil mechanics, i.e. continuity of particles, groundwater and stress will be discussed. When the structural design of a soil retaining structure is considered, i.e. the analysis of stresses and strains, this is mostly aimed at the analysis of strength and stability of the structure and in some cases this includes the analysis of stiffness and displacements. In this thesis it is generally assumed that soil particles are small with respect to the scale of the problems analysed and therefore soil is analysed using continuum mechanics.

The main principles for soil mechanics are:

- *conservation of mass of the components (solids and water)*
- *conservation of momentum*
- *constitutive relations*

These principles will be discussed in a coherent frame of reference; i.e. the balance equations needed to develop mechanical models for analysis will be derived using the same line of reasoning.

Since the strong formulation of stress equilibrium and or the storage equation (which will be discussed in paragraph 4.2, involves differential equations that

cannot be integrated directly, (to give a linear system of algebraic equations), an alternative scheme related to physical aspects is discussed. The approach taken, both for stress analysis as well as for groundwater flow is the principle of virtual work. This approach was chosen, in order not to lose a relationship between the numerical schemes and the physical background of the problems analysed. Moreover, it will be shown that groundwater flow, in a weak formulation, can be handled by the principle of virtual work.

With respect to groundwater flow, and in relation to equilibrium of stresses, consideration will be given to the effects of groundwater flow in a static analysis of ground deformations, and stability analysis.

Finally the elementary derivation of the partial differential equation for elasto-plastic constitutive behaviour of soil, i.e. the Mohr-Coulomb criterion, is reproduced.

4.2 THE STORAGE EQUATION

To begin with the balance equations for a soil mass will be evaluated, i.e. conservation of mass for both pore-water and soil particles. A continuum approach to derive equations will be used.

Conservation of soil mass

For the soil particles this requires

$$\frac{D\left((1-n)\rho_p\right)}{Dt} = \frac{\partial(1-n)\rho_p}{\partial t} + \frac{\partial\left((1-n)\rho_p v_i\right)}{\partial x_i} = 0 \tag{4.1}$$

Where ρ_p is the density of the soil particles, n is the porosity (the relative pore volume), v_i is the velocity vector of the soil, and x_i is the position vector of a material point, the spatial co-ordinates. As a first assumption we assume that soil particles are incompressible, so ρ_p is a constant and we can divide equation 4.1. by ρ_p to obtain

$$\frac{\partial n}{\partial t} - \frac{\partial\left((1-n)v_i\right)}{\partial x_i} = 0 \tag{4.2}$$

or subsequently if we apply differentiation by parts:

$$\frac{\partial n}{\partial t} - (1-n)\frac{\partial(v_i)}{\partial x_i} - v_i\frac{\partial(1-n)}{\partial x_i} = 0 \tag{4.3}$$

which can be rearranged to give:

$$\frac{Dn}{Dt} - (1-n)\frac{\partial v_i}{\partial x_i} = 0 \tag{4.4}$$

where $\frac{Dn}{Dt}$ is the material derivative defined by $\frac{Dn}{Dt}=\frac{\partial n}{\partial t}+v_i\frac{\partial n}{\partial x_i}$

Conservation of pore-water

Secondly we demand conservation of mass for the pore-water

$$\frac{Dn\rho_w}{Dt}=\frac{\partial n\rho_w}{\partial t}+\frac{\partial n\rho_w w_i}{\partial x_i}=0 \tag{4.5}$$

where ρ_w is the density of the pore-water and w_i is the velocity of the pore-water. After Verruijt (1969), we will introduce the hydraulic discharge as the difference between pore-water velocity, and the velocity of the soil particles, taking into account the porosity: $q_i=n(w_i-v_i)$

Substituting this in equation 4.5 gives:

$$\frac{\partial n\rho_w}{\partial t}+\frac{\partial(\rho_w q_i)}{\partial x_i}+\frac{\partial n\rho_w v_i}{\partial x_i}=0$$

or

$$\frac{\partial n\rho_w}{\partial t}+\frac{\partial(\rho_w q_i)}{\partial x_i}+v_i\frac{\partial n\rho_w}{\partial x_i}+(n\rho_w)\frac{\partial v_i}{\partial x_i}=0$$

or

$$\frac{Dn\rho_w}{Dt}+\frac{\partial(\rho_w q_i)}{\partial x_i}+(n\rho_w)\frac{\partial v_i}{\partial x_i}=0$$

or

$$n\frac{D\rho_w}{Dt}+\rho_w\frac{Dn}{Dt}+\frac{\partial(\rho_w q_i)}{\partial x_i}+(n\rho_w)\frac{\partial v_i}{\partial x_i}=0 \tag{4.6}$$

Substitution of equation 4.4 in equation 4.6 will give

$$n\frac{D\rho_w}{Dt}+(1-n)\rho_w\frac{\partial v_i}{\partial x_i}+\frac{\partial(\rho_w q_i)}{\partial x_i}+(n\rho_w)\frac{\partial v_i}{\partial x_i}=0$$

or

$$n\frac{D\rho_w}{Dt}+\rho_w\frac{\partial v_i}{\partial x_i}+\frac{\partial(\rho_w q_i)}{\partial x_i}=0 \tag{4.7}$$

In contradistinction to the assumption that soil particles are incompressible, it is assumed that pore-water is indeed compressible. Comparing the strains observed in soil with the Young's modulus of e.g. silica (for sand), in a tri-axial cell, it is observed that the stress levels and therefore the strain levels in the particle are

low. Therefore the conclusion is drawn that the main cause of deformations such as observed during soil loading has to be attributed to rearrangement of particles. Though pure water is essentially incompressible too, in practice the volumetric deformation has to be accounted for the presence of air bubbles. This matter was dealt with in more detail by Barends (1980) and Teunissen (1982). Only when the overpressure takes a value of about three times the atmospheric pressure, the compressibility of the pore-water reduces to a small value. This lies beyond the pressure encountered in normal civil engineering practice.

As an intermediate step we will look into the character of the divergence term $\frac{\partial v_i}{\partial x_i}$. Here it should be realised that the soil velocity is defined as

$$v_i = \frac{D x_i}{Dt} = \frac{\partial x_i(X_R, t)}{\partial t} \tag{4.8}$$

where X_r is a reference frame of co-ordinates so that:

$$\frac{D x_i}{Dt} = \frac{\partial x_i}{\partial t} + \frac{\partial x_i}{\partial X_i}\frac{\partial X_i}{\partial t} \tag{4.9}$$

If we recognise that $\frac{\partial X_i}{\partial t} = 0$, because we assume that the frame of reference does not change in time, this gives:

$$\frac{D x_i}{Dt} = \frac{\partial x_i}{\partial t} \tag{4.10}$$

and therefore

$$\frac{\partial v_i}{\partial x_i} = \frac{\partial^2 x_i}{\partial X_i \partial t} \tag{4.11}$$

According to this derivation it seems as if it does not matter whether the volumetric strain; $\frac{\partial v_i}{\partial x_i}$, is calculated based on small deformations or on large deformations. With respect to small or large deformations such a conclusion is valid. The conclusion with respect to small or large strains however must be different, as will be shown.

Considering the volumetric strain based on a kinematics perspective, the volumetric strain would be:

$$\varepsilon_v = \frac{\partial x_i}{\partial X_i} + \left[\frac{\partial x_i \partial x_j}{\partial X_i \partial X_j} + \frac{\partial x_i \partial x_j \partial x_k}{\partial X_i \partial X_j \partial X_k}\right] \tag{4.12}$$

If we ignore all terms of higher order (the terms within the brackets), a simple relation between the deformations and the volume strain is found

$$\varepsilon_v \approx \frac{\partial x_i}{\partial X_i} \tag{4.13}$$

For which by time differentiation the volume strain rate can be found

$$\frac{D\varepsilon_v}{Dt} = \frac{D\dfrac{\partial x_i}{\partial X_i}}{Dt} \tag{4.14}$$

Applying equation 4.10 and changing the order of integration, it becomes clear that for small strains, the total derivative may be exchanged by the partial derivative, even for large deformations:

$$\frac{D\varepsilon_v}{Dt} \approx \frac{\partial^2 x}{\partial X \partial t} + \frac{\partial^2 y}{\partial Y \partial t} + \frac{\partial^2 z}{\partial Z \partial t} \approx \frac{\partial \varepsilon_v}{\partial t} \tag{4.15}$$

Thus, for a small strain rate:

$$\frac{D\varepsilon_v}{Dt} \approx \frac{\partial v_i}{\partial x_i} \tag{4.16}$$

If we combine this with equation 4.7 we arrive at:

$$\frac{\partial(\rho_w q_i)}{\partial x_i} + n\frac{D(\rho_w)}{Dt} + \rho_w \frac{D\varepsilon_v}{Dt} = 0 \tag{4.17}$$

Furthermore, after Barends (1980), a relation between density, and pore-pressure will be used according to

$$\rho_w = \rho_w^0 \exp(\beta(p - p_0)) \tag{4.18}$$

and therefore:

$$d\rho_w = \rho_w^0 \exp(\beta(p - p_0))\beta\, dp = \beta \cdot \rho_w dp \tag{4.19}$$

Which gives:

$$\frac{D\rho_w}{Dt} = \rho_w \beta \cdot \frac{Dp}{Dt} \tag{4.20}$$

This equation may be used to derive the storage equaion in which grain compressibility is neglected and volumetric strains are small. For that conditions, the storage equation reads as:

$$\frac{\partial(\rho_w q_i)}{\partial x_i} + \rho_w \frac{D\varepsilon_v}{Dt} + n\rho_w \beta' \frac{Dp}{Dt} = 0 \tag{4.21}$$

Which can be rewritten in terms of partial derivatives, considering equation 4.16, as:

$$\frac{\partial(\rho_w q_i)}{\partial x_i} + \rho_w \frac{\partial \varepsilon_v}{\partial t} + n\rho_w \beta' \left[\frac{\partial p}{\partial t} + v_i \frac{\partial p}{\partial x_i} \right] = 0 \tag{4.22}$$

The last term in the brackets $v_i \frac{\partial p}{\partial x_i}$ can be recognised as the convection term due to large displacements (for small strains).

For most practical problems the velocity of the soil skeleton is very small. Convection terms may therefore be treated as terms of higher order and neglected. Equation 4.22 may then be simplified for the case of small deformations according to:

$$\frac{\partial(\rho_w q_i)}{\partial x_i} + \rho_w \frac{\partial \varepsilon_v}{\partial t} + n\rho_w \beta' \left(\frac{\partial p}{\partial t} \right) = 0 \tag{4.23}$$

If the gradient in the pore-water density is small, this simplifies even further according to:

$$\frac{\partial q_i}{\partial x_i} + \frac{\partial \varepsilon_v}{\partial t} + n\beta' \left(\frac{\partial p}{\partial t} \right) = 0 \tag{4.24}$$

which is recognised as the storage equation in the form described by Verruijt (1969)

4.3 GROUND-WATER FLOW AND DEFORMATION INTERACTION

Equilibrium of stresses within a continuum requires that

$$\frac{\partial \sigma_{ij}}{\partial x_i} + \rho f_j = 0 \tag{4.25}$$

Where σ_{ij} is the Cauchy stress tensor, ρ is the soil density, and f_j is the distributed force per unit of soil mass. According to Terzaghi's principle of effective stresses, see Terzaghi (1948), we divide the total stresses into an effective part denoted with a dash ($'$) and a pore-water pressure

$$\sigma_{ij} = \sigma'_{ij} + p\,\delta_{ij} \tag{4.26}$$

Where δ is the Kronecker delta, for which $\delta_{ij} = 0$ if $i \neq j$ and $\delta_{ij} = 1$ if $i = j$. The decomposition of the soil stresses into effective stresses, and pore-water pressure,

and the subsequent assumption that the soil deformation is governed by the effective stresses only, indicates the important role of groundwater in deformation analysis.

The effect of this role is more clearly displayed if we assume a simple relation for the strength of soil, e.g. the Coulomb relation for the shear strength.

$$\tau_{cr} = \sigma' \tan\varphi + c \tag{4.27}$$

Where τ_{cr} is the critical shear strength, σ' is the effective normal stress, and c is the cohesion of the soil and φ is the effective soil friction angle.

Since the effective stress is the total stress minus the pore-water pressure; $\sigma'_{ij}=\sigma_{ij}-p\delta_{ij}$, and since the total stress σ_{ij} is often dominated by the overburden pressure, for drained soil, the absolute value of the pore-water pressure indirectly influences the shear strength of the soil.

To calculate the deformations of the soil we have to combine the equilibrium equations with the constitutive behaviour of the soil. Here to begin with, we will not focus on the constitutive behaviour, but on the equilibrium equation. Written out using Terzaghi's principle of effective stresses this reads:

$$\frac{\partial \sigma'_{ij}}{\partial x_j} + \frac{\partial p}{\partial x_i} + \rho f_i = 0 \tag{4.28}$$

The pore-water pressure gradient appears in the equations of equilibrium for the soil mass. For a full understanding of the effects that are associated with this, the relation between the pore-water pressure and the groundwater head will be considered.

If the groundwater head, Φ, is related to the pore-water pressure according to

$$\Phi = z + \int \frac{dp}{\gamma_w} \tag{4.29}$$

Where γ_w is the unit weight of the groundwater; i.e. $\gamma_w = \rho_w g$, and z is the geometric height, with reference to a system of co-ordinates; the z axis is upwards.

This means that $p = (\Phi - z)\gamma_w$, and therefore:

$$\frac{\partial p}{\partial x_i} = \gamma_w \left(\frac{\partial \Phi}{\partial x_i} - \frac{\partial z}{\partial x_i} \right) \tag{4.30}$$

If the groundwater condition is only described by a water table, assuming a hydrostatic pressure below the water table, then the gradient in groundwater head in the z direction is often neglected, see Dupuit (1863). For cases where this vertical groundwater head gradient is small, with respect to unity, this is acceptable. For many sea dike and river embankment problems, this assumption

is valid. If we look at groundwater flow under a sheet pile wall in sand, however, the seepage might create large vertical gradients.

Consider for example, a deep excavation where there is a danger of collapse at the base of the excavation when there is high pore-water pressure in deeper sand layers. In this case such an assumption is clearly not valid. For the common semi-empirical models often used in practice, this aspect has to be considered explicitly. For the continuum mechanics based finite element models, this feature of behaviour is included implicitly.

4.4 EQUILIBRIUM OF STRESSES; I.E. VIRTUAL WORK

Consider a stress field, and let $\sigma_{ij}(x,y)$ be the equilibrium field of the Cauchy stress tensor in plane strain. Equilibrium being governed by the equilibrium equation 4.25, which means that in the body of a continuum V it is demanded that

$$in\ V \quad \frac{\partial \sigma_{ij}}{\partial x_i} + \rho f_j = 0 \tag{4.31}$$

Where on a boundary with a stress boundary condition, denoted as S_1, an equilibrium boundary condition for the stresses is given according to:

$$on\ S_1: \quad \sigma_{ij} n_i = t_j \tag{4.32}$$

Whereas on a boundary where the boundary condition is determined by displacements, denoted as S_2 a kinematics boundary condition for the displacements is given according to:

$$on\ S_2: \quad u_j = g_j \tag{4.33}$$

The solution for these equations is sought, such that an admissible deformation field u_j is assumed which satisfies equation 4.33. Subsequently a perturbed deformation distribution $u_j + \delta u_j$ is assumed. The deformation field u_j and the perturbed deformation field $u_j + \delta u_j$ are not necessarily correlated to the stress-field σ_{ij}. This perturbed deformation field is subjected to the condition that $\delta u_j|_{S2} = 0$. That is, the variation becomes zero for those parts of the domain where a boundary condition is imposed upon the solution. If we now form the scalar product of (the vector) δu_j with the left-hand side of equation 4.31 and integrate over the field, we obtain

$$\int_V \left(\frac{\partial (\sigma_{ij})}{\partial x_i} \delta u_j + \rho f_j \delta u_j \right) dv = 0 \tag{4.34}$$

Applying integration by parts on the first term we obtain:

$$\int_V \frac{\partial(\sigma_{ij})}{\partial x_i}\delta u_j\,dv = \int_V \frac{\partial(\sigma_{ij}\delta u_j)}{\partial x_i}dv - \int_V \sigma_{ij}\frac{\partial \delta u_j}{\partial x_i}dv \tag{4.35}$$

where the first term can be transformed into a boundary integral according to the divergence theorem

$$\int_V \frac{\partial \sigma_{ij}}{\partial x_i}\delta u_j\,dv = \oint_S (\sigma_{ij}\delta u_j)\cdot n_i\,ds - \frac{1}{2}\int_V \sigma_{ij}\left(\delta\frac{\partial \delta u_j}{\partial x_i} + \delta\frac{\partial \delta u_i}{\partial x_j}\right)dv \tag{4.36}$$

Where:

$$\delta\varepsilon_{ij} = \frac{1}{2}\left(\delta\frac{\partial \delta u_i}{\partial x_j} + \delta\frac{\partial \delta u_j}{\partial x_i}\right) \tag{4.37}$$

The boundary integral can be simplified due to the assumption that δu_j is necessarily 0 on S_2, which gives that:

$$\int_V \frac{\partial \sigma_{ij}}{\partial x_i}\delta u_j\,dv = \oint_{S_1} (\sigma_{ij}\delta u_j)\cdot n_i\,ds - \int_V \sigma_{ij}\delta\varepsilon_{ji}\,dv \tag{4.38}$$

Substituting this in equation 4.34 and making use of equation 4.32 gives the equation of virtual work:

$$\int_V [\sigma_{ij}\delta\varepsilon_{ij} - \rho f_j \delta u_j]\,dv = \oint_{S_1} t_j \delta u_j\,ds \tag{4.39}$$

4.5 CONTINUITY OF PORE-WATER

The strong formulation of the storage equation, 4.24, i.e. the groundwater flow equation, cannot be integrated directly to give a linear system of algebraic equations, as required for numerical analysis. As this drawback also applies for equilibrium of stresses, in practice for elastic systems, the principle of minimum potential energy is preferred above direct integration of the stress equilibrium equations, for the development of numerical analysis. For systems dissipating energy, the equation of virtual work is used.

For groundwater flow, which is also an energy dissipating system, a water particle moving along a streamline follows the negative gradient of the energy potential. The principle of virtual displacements is therefore not applicable. For practical purposes the mathematical principle of Galerkin is often applied, which gives the same equations as when applying Hamilton's principle, see the next section. It will be shown in the next section that groundwater flow, both for

steady and transient flow, may be analysed according to the principle of virtual work in the same way as for stress analysis.

4.5.1 *Hamilton's principle for groundwater flow*

Consider a groundwater particle moving in a field of groundwater flow, and let $p(x,y)$ be the vector of groundwater pressure. According to the storage equation for small deformations, the continuity of groundwater flow in the body of a continuum V is determined by, see equation 4.24:

$$in\,V \quad \frac{\partial q_i}{\partial x_i} + \frac{\partial \varepsilon_v}{\partial t} + n\beta' \left(\frac{\partial p}{\partial t} \right) = 0 \tag{4.40}$$

For the boundary where a continuity boundary is demanded, denoted as S_1 a continuity boundary condition for the discharges is demanded according to:

$$on \quad S_1: \quad q_i \cdot n_i = g \tag{4.41}$$

for the boundary where a condition with respect to the groundwater head is imposed, denoted as S_2 a boundary condition for the pressure according to:

$$on \quad S_2: \quad p = f \tag{4.42}$$

The solution for this equation is sought for in such a way that an admissible pressure p is assumed which satisfies equation 4.42.

Consider a pressure distribution $p + \delta p$ where δp is and arbitrary function of x, y, z and t, except for the fact that $\delta p = 0$ on S_2, i.e. the variation becomes zero for that part of the field where a pressure boundary condition is applied. If we subsequently form the scalar product of (the vector) δp with the left-hand side of equation 4.40 and integrate over the field, we obtain:

$$\int_V \left[\frac{\partial q_i}{\partial x_i} \delta p + \left(\frac{\partial \varepsilon_v}{\partial t} + n\beta' \left(\frac{\partial p}{\partial t} \right) \right) \delta p \right] dv = 0 \tag{4.43}$$

Applying integration by parts on the first term we obtain:

$$\int_V \frac{\partial q_i}{\partial x_i} \delta p\, dv = \int_V \frac{\partial (q_i \delta p)}{\partial x_i} dv - \int_V q_i \frac{\partial \delta p}{\partial x_i} dv \tag{4.44}$$

The first term can be transformed into a boundary integral according to the divergence theorem:

$$\int_V \frac{\partial q_i}{\partial x_i} \delta p\, dv = \oint_S (q_i \delta p) \cdot n_i\, ds - \int_V q \frac{\partial \delta p}{\partial x_i} dv \tag{4.45}$$

The boundary integral vanishes for S_2, due to the assumed properties of δp, Hence Equation 4.45 can be rewritten to give

$$\int_V \left[q_i \frac{\partial \delta p}{\partial x_i} - \left(\frac{\partial \varepsilon_v}{\partial t} + n\beta' \left(\frac{\partial p}{\partial t} \right) \right) \delta p \right] dv = \oint_{S_1} (g\, \delta p) ds \tag{4.46}$$

In similarity with equation 4.39, and recognising that the product $\oint q\, p\, ds$ has the dimension [*m*/sec * *N* = *Nm*/sec], i.e. work per unit of time, the right hand side of equation 4.46 may be recognised as the virtual work (per unit of time) of the discharge on boundary S_1. In addition to that, the volume integral may be recognised as the virtual work in the soil mass.

If groundwater flow is being considered as such, i.e. if the storage part of equation 4.46 is of minor importance, this equation can be rewritten in terms of the groundwater head only, applying equation 4.30, which gives:

$$\int_V q_i \frac{\partial \delta \Phi}{\partial x_i} dv = \oint_{S_1} (g\, \delta \Phi) ds \tag{4.47}$$

It may be recognised with this, that continuity in groundwater flow in a weak formulation can be modelled following the same line of reasoning as for structural mechanics, i.e. by applying the principle of virtual work.

4.6 SOIL BEHAVIOUR AND CONSTITUTIVE MODELLING

For the modelling of soil behaviour several options such as perfect plasticity, isotropic hardening, Hard-soil model and Cam-Clay, are feasible. In this section, for clarity purposes, only one of the simplest options for perfect plasticity is discussed, as for retaining walls, the marginal benefit of stepping from subgrade reaction models up to 2D elasto-plastic analysis is greater than any other subsequent step.

The equations for elasto-plasticity are derived by assuming that the total strain rate is the sum of an elastic part and a plastic part, i.e.

$$\dot{\boldsymbol{\varepsilon}} = \dot{\boldsymbol{\varepsilon}}^e + \dot{\boldsymbol{\varepsilon}}^p = \mathbf{D}^{-1}\dot{\boldsymbol{\sigma}} + \dot{\boldsymbol{\varepsilon}}^p \tag{4.48}$$

The matrix $\mathbf{D}$ denotes an elasticity matrix which for plane deformations with $\dot{\boldsymbol{\varepsilon}}^e_{zz} = 0$, is derived using Hooke's law to give:

$$\mathbf{D}^{-1} = \frac{1}{2G} \begin{bmatrix} 1-\nu & -\nu & 0 \\ -\nu & 1-\nu & 0 \\ 0 & 0 & 2 \end{bmatrix} \tag{4.49}$$

where:

G = *elastic shear modulus*
ν = *Poisson's ratio*

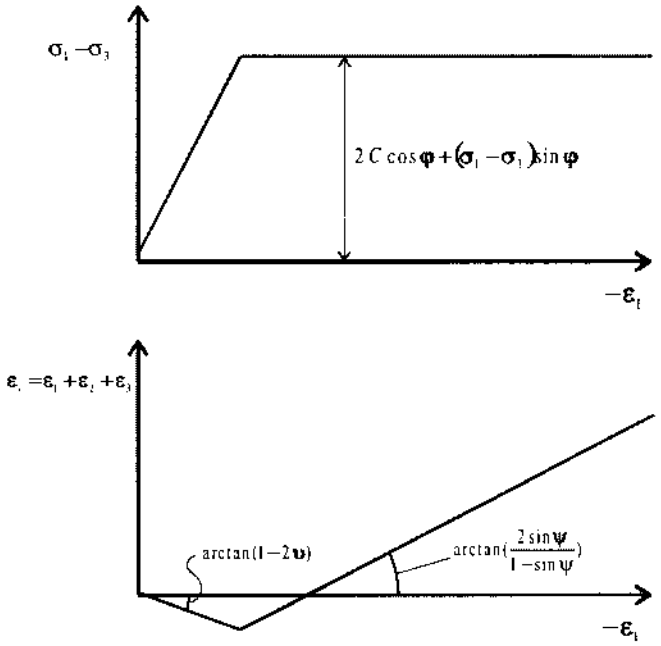

Figure 4.1 Characteristic soil behaviour according to the elasto-plastic modelling of Mohr-Coulomb constitutive behaviour.

Plastic strains are derived from a plastic potential function g according to

$$\dot{\varepsilon}^p = \lambda \frac{\partial g}{\partial \sigma} \tag{4.50}$$

under the assumption that for plastic straining, the stresses lie on a yield surface f i.e. that for the development of plastic strains it is demanded that the yield function $f = 0$.

The yield function f such as used in the main parts of the analyses in this thesis are defined according to the Mohr-Coulomb criterion:

$$f = \frac{\sigma_1 - \sigma_3}{2} - \frac{\sigma_1 + \sigma_3}{2}\sin\varphi - c\cos\varphi \tag{4.51}$$

The plastic potential function g is similar in form to the yield function:

$$g = \frac{\sigma_1 - \sigma_3}{2} - \frac{\sigma_1 + \sigma_3}{2}\sin\psi \tag{4.52}$$

The value of f is zero, and remains zero during plastic deformations; $f(\sigma) = 0$ and $\dot{f}(\sigma) = 0$

Partially differentiating f, and combining this with equation 4.48 gives:

$$\dot{f} = \frac{\partial f}{\partial \sigma}^T \dot{\sigma} = \frac{\partial f}{\partial \sigma}^T \left(\mathbf{D}\dot{\varepsilon}^e - \lambda \mathbf{D} \frac{\partial g}{\partial \sigma} \right) = 0 \tag{4.53}$$

From which λ can be solved to give

$$\lambda = \frac{\frac{\partial f}{\partial \sigma}^T \mathbf{D}\dot{\varepsilon}}{d} \tag{4.54}$$

Where

$$d = \frac{\partial f}{\partial \sigma}^T \mathbf{D} \frac{\partial g}{\partial \sigma} \tag{4.55}$$

The plastic flow is non-associated, as the angle of dilation, ψ, is generally much smaller than the friction angle φ (see, for example Smith (1982)). If both φ and ψ are taken as genuine constants, then d, can be simplified to give the auxiliary constant:

$$\frac{\partial f}{\partial \sigma}^T \mathbf{D} \frac{\partial g}{\partial \sigma} = d = G\left(1 + \frac{\sin\varphi \sin\psi}{1 - 2\nu}\right) \tag{4.56}$$

Combining this result with equation 4.48, the following incremental differential equation is derived:

$$\mathbf{D}\dot{\varepsilon} = \dot{\sigma} + \frac{\frac{\partial f}{\partial \sigma}^T \mathbf{D}\dot{\varepsilon}}{d} \mathbf{D} \frac{\partial g}{\partial \sigma} \tag{4.57}$$

If this equation is integrated over a 'time'-step, where the simplified notation is used that $\Delta\sigma = \int_{t-\Delta t}^{t} \dot{\sigma} dt$, and $\Delta\varepsilon = \int_{t-\Delta t}^{t} \dot{\varepsilon}\, dt$, then an incremental stress strain relation can be derived according to:

$$\mathbf{D}\Delta\varepsilon = \Delta\sigma + \frac{\mathbf{D}\frac{\partial g}{\partial \sigma}}{d} \int_{t=0}^{t=t} \frac{\partial f}{\partial \sigma}^T \mathbf{D}\dot{\varepsilon}\, dt \tag{4.58}$$

Where it is estimated that the integrand part is approximately $\frac{\partial f}{\partial \sigma}^T D\dot{\varepsilon} \approx \dot{f}(\sigma)$.

The integrated equation therefore becomes:

$$\mathbf{D}\Delta\varepsilon = \Delta\sigma + \frac{\mathbf{D}\frac{\partial g}{\partial \sigma}}{d} \left\{ f(\sigma^t) - f(\sigma^o) \right\} \tag{4.59}$$

If we recognise, that for plastic straining, $f(\boldsymbol{\sigma}^0) = 0$ this can be simplified to give a relatively simple incremental stress strain relation for elasto-plastic deformations:

$$\mathbf{D}\Delta\boldsymbol{\varepsilon} = \Delta\boldsymbol{\sigma} + \frac{f(\boldsymbol{\sigma}^t)}{d}\mathbf{D}\frac{\partial g}{\partial \boldsymbol{\sigma}} \tag{4.60}$$

In elasto-plastic analysis the finite increments $\Delta\boldsymbol{\sigma}$ and $\Delta\boldsymbol{\varepsilon}$ are used rather than the rates $\dot{\boldsymbol{\sigma}}$ and $\dot{\boldsymbol{\varepsilon}}$. Similarly we use $\Delta \boldsymbol{u}$ for the nodal displacement increments and $\Delta \boldsymbol{q}$ for the force increments.

4.7 FINITE ELEMENT IMPLEMENTATION

The implementation of basic equilibrium equations into the framework of finite Elements is illustrated for the equations of equilibrium of stresses, (see de Borst & Vermeer (1984)):

$$\int_V \delta\boldsymbol{\varepsilon}^T \boldsymbol{\sigma} - \delta u^T \rho \mathbf{f}\, dv = \oint_{S_2} \delta u^T t\, ds \tag{4.61}$$

Where here $\boldsymbol{t}$ is used here to denote the tractions on the boundary, according to: $t_i = \sigma_{ij} \bullet n_j$. In order to proceed, the relation between stresses and strains has to be formulated. Here the equations as described in paragraph 4.6, for the elasto-plastic version of the Mohr-Coulomb constitutive equations are adopted, according to equation 4.60

$$\Delta\boldsymbol{\sigma} = \mathbf{D}\Delta\boldsymbol{\varepsilon} - \frac{f(\boldsymbol{\sigma}^t)}{d}\mathbf{D}\frac{\partial g}{\partial \boldsymbol{\sigma}} \tag{4.62}$$

Applying the assumption that $\boldsymbol{\sigma} = \boldsymbol{\sigma}^0 + \Delta\boldsymbol{\sigma}$, and substituting equation 4.62 into equation 4.61 we arrive at:

$$\int_V \delta\boldsymbol{\varepsilon}^T \mathbf{D}\boldsymbol{\varepsilon}\, dv - \int_V \delta u^T \rho f\, dv = -\int_V \delta\boldsymbol{\varepsilon}^T \boldsymbol{\sigma}^0 dv + \oint_{S_2} \delta u^T t\, ds + \int_V \delta\boldsymbol{\varepsilon} \frac{f\left(\boldsymbol{\sigma}^t\right)}{d}\mathbf{D}\frac{\partial g}{\partial \boldsymbol{\sigma}} dv \tag{4.63}$$

To proceed with the discretisation, a set of interpolation functions is adopted for a finite set of sub-domains, (or finite elements), according to

$$\mathbf{u}(x, y) = \mathbf{N}^T \mathbf{a} \tag{4.64}$$

Where $\boldsymbol{u}$ is the continuous deformation field: $u = \left(u_x, u_y\right)^T$, and $\mathbf{a}$ denotes the nodal displacements at discrete points. The matrix $\boldsymbol{N}$ is a set of interpolation functions.

The relation between displacements and strains is given by

$$\boldsymbol{\varepsilon} = \mathbf{L}\mathbf{u} \tag{4.65}$$

Where **L** is the operator matrix

$$\mathbf{L} = \begin{bmatrix} \dfrac{\partial}{\partial x} & 0 \\ 0 & \dfrac{\partial}{\partial y} \\ \dfrac{\partial}{\partial y} & \dfrac{\partial}{\partial x} \end{bmatrix} \tag{4.66}$$

Taking **B** = **LN** and substituting equation 4.64 and equation 4.65 into equation 4.63 gives

$$\delta a^T \left\{ \int_v \mathbf{B}^T \mathbf{D}\mathbf{B}\,\Delta\mathbf{a}\,dv - \int_v \mathbf{N}^T \boldsymbol{\rho}\,\mathbf{f}\,dv + \int_v \mathbf{B}^T \boldsymbol{\sigma}^0 dv - \oint_{s_2} \mathbf{N}^T \mathbf{t}\,ds - \int \mathbf{B}^T \frac{f(\boldsymbol{\sigma}^t)}{d} \mathbf{D} \frac{\partial g}{\partial \boldsymbol{\sigma}} dv \right\} = 0 \tag{4.67}$$

As this equation must hold for any virtual displacement δa, we obtain

$$\int_V \mathbf{B}^T \mathbf{D}\mathbf{B}\,\Delta\mathbf{a}\,dv = -\int_V \mathbf{B}^T \boldsymbol{\sigma}^0 dv + \int_V \mathbf{N}^T \boldsymbol{\rho}\mathbf{f}\,dv + \oint_{S_2} \mathbf{N}^T \mathbf{t}\,ds + \int_V \mathbf{B}^T \frac{f(\boldsymbol{\sigma}^t)}{d} \mathbf{D} \frac{\partial g}{\partial \boldsymbol{\sigma}} dv \tag{4.68}$$

One of the interpolation schemes used in the finite element code PLAXIS is based on a fifteen-noded triangular element employing a fourth order polynomial displacement interpolation.

To integrate equation 4.68, according to the scheme developed for iso-parametric elements, such as the 15 noded elements of Fig 4.2, attention should be paid to the fact that for the interpolation of co-ordinates and functions, local co-ordinates; ξ, and η are used.

$$x(\xi,\eta) = \sum_{i=1}^{n} h_i(\xi,\eta) x_i \tag{4.69}$$

Which means that the Interpolation functions $\mathbf{H}^T = f(\xi,\eta)$, are a function of local co-ordinates, ξ and η.

The derivatives $\partial/\partial x_i$ are required to formulate the matrix **B**, where in practice it is the derivatives $\partial/\partial\xi$ that are available. Using the chain rule of differentiation

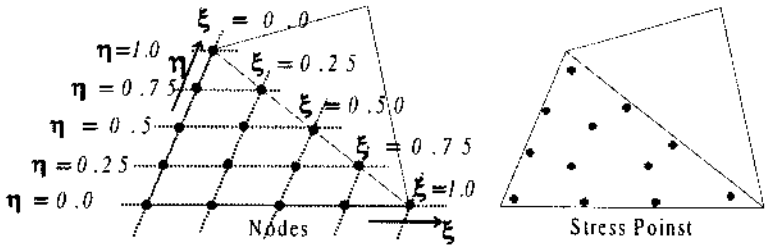

Figure 4.2 Fifteen noded triangular elements. Left: nodal points, Right: the calculation points.

however we have

$$\begin{bmatrix} \frac{\partial}{\partial \xi} \\ \frac{\partial}{\partial \eta} \end{bmatrix} = \begin{bmatrix} \frac{\partial x}{\partial \xi} & \frac{\partial y}{\partial \xi} \\ \frac{\partial x}{\partial \eta} & \frac{\partial y}{\partial \eta} \end{bmatrix} \begin{bmatrix} \frac{\partial}{\partial x} \\ \frac{\partial}{\partial y} \end{bmatrix} \tag{4.70}$$

Or, in matrix notation:

$$\frac{\partial}{\partial \xi_i} = \mathbf{J} \frac{\partial}{\partial x_i} \tag{4.71}$$

Where **J** is the Jacobean matrix relating the global co-ordinate derivatives to the local co-ordinate derivatives. The Jacobean matrix can easily be found, using the interpolation functions

$\mathbf{H}^T = f(\xi, \eta)$. The required relation for $\frac{\partial}{\partial x_i}$, can then be found according to

$$\frac{\partial}{\partial x} = \mathbf{J}^{-1} \frac{\partial}{\partial \xi} \tag{4.72}$$

For the linear interpolation, being used for the triangular elements with straight boundary edges, the inverse Jacobean may be obtained analytically. The **B** matrix can than be obtained by applying a modified version of the operator **L**, given by

$$\mathbf{L}^* = \begin{bmatrix} \frac{\partial}{\partial \xi} & 0 \\ 0 & \frac{\partial}{\partial \eta} \\ \frac{\partial}{\partial \eta} & \frac{\partial}{\partial \xi} \end{bmatrix} \tag{4.73}$$

The **B** matrix can then be found from the equation:

$$\mathbf{B}=\mathbf{J}^{-1}\mathbf{L}^{*}\mathbf{N} \tag{4.74}$$

Similar approaches are needed to deal with integration's over the element when those are required. Those integrals may be evaluated using the substitution illustrated below.

$$\int_V ( )\,dxdy=\int_V ( )\det\mathbf{J}\,d\xi d\eta \tag{4.75}$$

For boundary integration, the appropriate boundary interpolation functions have to be used, and the appropriate Jacobean of the line interpolation function needs to be applied.

In practice these integrals are mostly performed numerically, by applying Gauss's, or Newton-Cotes integration rules, (see among other textbooks Bathe (1982)).

Finally, when all aspects have been considered, the matrix equation for a loading step may be written as:

$$\mathbf{A}\Delta\mathbf{a} = \mathbf{q}_i+\Delta\mathbf{p} \tag{4.76}$$

Where **A** is the elastic stiffness matrix and Δp is a pseudo load vector

$$\mathbf{A}=\int_V \mathbf{B}^T\mathbf{D}\mathbf{B}\,dv \tag{4.77}$$

$$\mathbf{q}_1 = -\int_V \mathbf{B}^T\boldsymbol{\sigma}^0\,dv \tag{4.78}$$

$$\mathbf{q}_2=\int_V \mathbf{N}^T\rho\mathbf{f}\,dv \tag{4.79}$$

$$\mathbf{q}_3 = \oint_{S_2} \mathbf{N}^T\mathbf{t}\,ds \tag{4.80}$$

$$\Delta\mathbf{p}=\int_V \mathbf{B}^T\left(\frac{f(\boldsymbol{\sigma}^t)}{d}\mathbf{D}\frac{\partial g}{\partial\boldsymbol{\sigma}}\right)dV \tag{4.81}$$

This procedure may be classified as an elastic stiffness approach or, alternatively, as a modified Newton-Raphson scheme or the Initial-stress method. This method is adopted here, because for the simple Mohr-Coulomb law with a non-associated flow rule; it has proven to deliver an efficient scheme.

4.8 SUMMARY AND CONCLUDING REMARKS

Some elementary principles of the mechanics of soils have been discussed. The storage equation is discussed within the framework of large displacements. Continuity in groundwater flow is discussed within the framework of variations. For small displacements it is shown that continuity in groundwater flow can be conceived in a similar framework as used for equilibrium of stresses, with the principle of virtual work.

Finally, some aspects of the numerical modelling of elasto-plastic soil using the Mohr Coulomb failure criterion is discussed.

CHAPTER 5

Block revetments

5.1 INTRODUCTION

In this chapter the stability of block revetments under wave attack, on dikes or embankments is discussed. Revetments of placed blocks or block mattresses are often used to protect soil against erosion. The waves may be caused by shipping activity in canals, or by wind action on river dikes, dikes of larger lakes and sea dikes.

In the Netherlands, there is little natural stone and therefore the available material has been used efficiently. It was soon realised by our ancestors that the stability of regularly placed blocks is much better than if the stone was placed in a random fashion. It was realised further that placing a block with its largest dimension perpendicular to the slope further increased the stability. Placing blocks from early days has been a personal skill, executed by hand power, see Fig 5.1. The block weight in this construction method was 20 - 50 kg, which was the maximum that could be placed by hand.

Based on these principles an empirical revetment design emerged which could withstand a wave height of up to 1 - 2 m. The development of this design was based on trial and error. Empirical knowledge was the driving force for

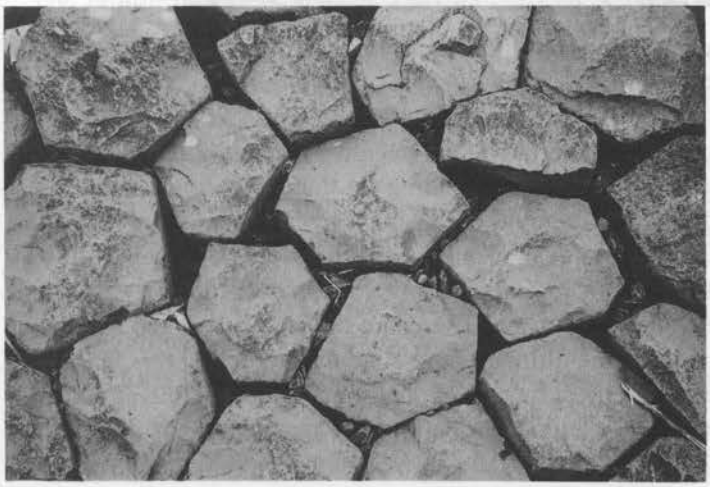

Figure 5.1 Block revetment of basalt collumns

development. The structure type finally coming forward with the largest capacity was a cover of pitched stone, often of basaltic columns closely put together, with lengths of the column of up to 50 cm where the attack was strongest.

The main construction method, see Fig. 5.2, consisted of placing mattresses of straw on top of a clay cover on the dike. A bricklayer was then placed on top of the straw mattresses, the brick layer being combined with broken stone material. On top of this the basaltic columns were placed. The broken stone material between the brick material and the columns was used to adjust for differences in length between the basaltic columns.

This empirically developed revetment type ensures stability for normal conditions. Since the execution of the Delta plan, the water defence system for

Figure 5.2 Construction of a block revetment on the Afsluitdijk, near Kornwerderzand (1927), © municipality of Wieringen

the Southwestern part of the Netherlands, the design philosophy has adjusted to evaluation of the ultimate limit state. Depending on the design philosophy for a dike, the revetment might be thought of as decisive for the stability in the ultimate limit state. The leading design philosophy for dike revetments follows the argument that if the revetment fails, an erosion process is likely to cause failure of the dike after a period of time. Therefore the stability of the revetment is considered to be crucial for the ultimate limit state of the dike. If this reasoning is extrapolated into the requirement that revetments should be capable of resisting wave attack caused by storms with a probability of occurrence of $P_f \approx 10^{-4}$ a problem arises, because the available data do not extend to this level of wave attack. Therefore, to evaluate revetments up to their limit state, models are

needed to describe the revetment behaviour.

To achieve this requirement much effort has been spent in the derivation of an adequate design model for block revetments. To develop such models, adequate insight into the limit states of a revetment is needed. Several modes of failure are identified, including uplift, sliding, and the stability of sub-layers.

In this chapter, generally accepted modes of failure are described in section 5.2. In section 5.3, the groundwater mechanical aspects that determine the transfer function between wave pressure on top of a revetment, and the uplift pressure underneath a revetment are described.

In section 5.4 an evaluation is given of the partial stability contribution associated with restricted inflow of water into the cavity created by an unstable single block. This partial stability contribution is evaluated for the case of a revetment under oblique wave loading.

In section 5.5 a method of analysis for the stability against sliding of revetments is described. As an example, the failure of block mattresses at the test site near Lelystad is discussed in section 5.6, taking into consideration the necessary stability requirements.

Final conclusions regarding block revetments are given in 5.7.

Parts of this chapter have been published earlier by Bakker (1988) and Bakker (1989), The contents of both papers have been ordered anew to avoid an irregular composition of theory and analysis.

5.2 THE STABILITY OF BLOCK REVETMENTS

To evaluate the stability of block revetments against wave attack, knowledge about the pressures above and below the blocks is needed. This requires an analysis of groundwater flow as well as geotechnical stability.

The failure mechanisms to be considered in designing flexible revetments on banks and dams are:

1. *uplifting of blocks,*
2. *sliding of the revetment*
3. *instability of layers underneath the blocks, e.g. filters or the subsoil*

Until the last decade, design of revetments was based on local experience or the results of model experiments. Since then, design has shifted to the application of theoretical models.

5.2.1 *Stability against uplift*

The basis for the evaluation of the stability of stones in a blocks revetment is:

1. *Hydraulic loading*, resulting in a pressure difference above and below the blocks. The pressure difference:

$$\rho_w g \Delta(\Phi) = f(\rho_w g H_s) \tag{5.1}$$

is a function of the wave height (H_s). This pressure difference is often the main active loading on a revetment, where:

$\Delta(\Phi)$	=	difference in pressure head below and above the blocks [m]
ρ_w	=	density of water [kg/m^3]
g	=	acceleration of gravity [m/sec]
H_s	=	the significant wave height [m]

2. *Strength components* such as
Block weight:

$$\Delta_w \rho_w g D \cos\alpha \tag{5.2}$$

which is related to the component of the weight due to gravity of the block, perpendicular to the plane of the revetment, see Fig. 5.4, where:

Δ_w	=	relative density ratio of the submerged block $\Delta_w = \frac{\rho_b - \rho_w}{\rho_w}$ [-]
D	=	block thickness (perpendicular to the revetment) [m]
α	=	inclination angle of the revetment with respect to the horizontal axis [°]

A partial stability factor, Γ_{u0}, is calculated as the ratio between block weight and pressure difference according to:

$$\Gamma_{u0} = \frac{\Delta_w \rho_w g D \cos\alpha}{\rho_w g \Delta(\Phi)} = \frac{\Delta_w D \cos\alpha}{\Delta(\Phi)} \tag{5.3}$$

The difference in pressure over the revetment is often a direct function of the wave height, e.g. $\Delta(\Phi) \approx (0.2 - 0.6)\, H_b$. In practice therefore a common type of characterisation for the strength of a revetment is the ratio $H/(\Delta D)$, the inverse of equation 5.3. Practical values of $H/(\Delta D)$ range between 2 and 4.

This equation may be further enhanced by, including the influence of the slope inclination, and the wave steepness, characterised by the parameter ξ. As the resulting design rule is strongly empirical, a number of effects might be included implicitly in this relation, for which the quantification needs attention. Effects such as in the next three sub-contributions to strength, 2.1 to 2.3.

2.1 *Interlocking, or friction.* Due to friction between blocks, a resistance is activated which leads to an increase in pressure difference needed to destabilise a block. If the block is not interlocked, a partial contribution Γ_{u1} may be calculated analytically as:

$$\Gamma_{u1} = \frac{\rho_w \Delta_w g D \sin\alpha \tan\varphi}{\Delta_w \rho_w g D \cos\alpha} = \tan\alpha \tan\varphi \tag{5.4}$$

This might be regarded as an additional component added to the force applied by gravity. In this relation the lateral force is assumed to be governed only by

the gravity component of the block. For this situation the relative contribution of Γ_{u1} is small, $0.05 < \Gamma_{u1} <= 0.10$..

For most revetments in practice the cover layer behaves as a plate with plate bending and shear force distribution. In this situation, interlock of the blocks might increase the lateral forces. Frissen (1996) and Gerresen (1997) have completed research on this topic. Due to uncertainty in the parameters governing plate bending and interlocking there is reluctance to adopt high values for the contribution of interlock. In practice any revetment of substance proves to exhibit loose blocks when inspected on this.

Another reluctance to adopt friction as a dominant parameter determining the stability is the knowledge that at a certain point of loading the revetment as a layer becomes unstable for larger areas, giving rise to rearrangement of particles in layers underneath. If this situation develops, the integrity of the revetment will become undermined in the long run.

2.2 *Inertia forces*. The block has to be accelerated in order to initiate movement. If it is assumed that the block is accelerated for up to half the wave period and if failure is assumed if the block displaces for 0.1 D, than the inertia force can be approximated, as

$$f_2 \approx \rho_p D \cdot \frac{0.1D}{0.5T_p} = \frac{0.2\rho_p D^2}{T_p} \tag{5.5}$$

Where ρ_p is the block density, and T_p is the wave period. Based on this, a partial stability contribution, Γ_{u2}, scaled with respect to the block weight, can be derived as:

$$\Gamma_{u2} = \frac{\dfrac{0.2\rho_p D^2}{T_p}}{\rho_w \Delta_w g D \cos\alpha} = \frac{0.2\rho_p D}{T_p \rho_w \Delta_w g \cos\alpha} \tag{5.6}$$

The relative contribution of Γ_{u2} is minor, (see for example Klein Breteler (1995)), and will not be discussed in further detail.

2.3 *Restricted inflow of pore-water* to the cavity that will develop if a block of the cover layer is 'lifted' due to a pressure difference which exceeds the effective block weight (i.e. $\Gamma_0 < 1.0$). The restricted inflow of water is a function of the pressure field above the cover layer, the permeability of the cover layer, and the permeability of the subsoil (the filter). If the velocity of an unstable moving block is known, the pressure drop can be calculated. This pressure drop, divided by effective block weight, may be expressed as an additional partial stability factor. Γ_{u3}.

Where Γ_{u3} is calculated as:

$$\Gamma_{u3} = \frac{\Delta(P)}{\Delta_w \rho_w g D \cos\alpha} = \frac{\Delta\left(\frac{P}{\rho_w g}\right)}{\Delta_w D \cos\alpha} \tag{5.7}$$

The derivation of Γ_{u3} will not be described in more detail because this is a complex issue. An evaluation of the acceptability of considering $\Gamma_{u3} > 0$ is described in section 5.4.

The assessment of potential uplift, assuming that the partial contributions are independent, is made by assuming addition of the partial contributions. Based on this, a total stability ratio is calculated, according to:

$$\Gamma_u = \Gamma_{u0}\left(1 + \Gamma_{u1} + \Gamma_{u2} + \Gamma_{u3}\right) \tag{5.8}$$

The revetment is considered to be stable against uplift for $\Gamma_u \geq 1.0$.

The method proposed here deviates from that described by Klein Breteler (1995). The advantage of the formulation described here is that all partial stability factors Γ_i are dimensionless and have a clear physical meaning. There might however be doubts about the validity of calculating a partial contribution with respect to restricted inflow; this aspect of the method is discussed in section 5.4

5.2.2 *Stability, against sliding of the revetment*

The danger of sliding exists as soon as a pressure head difference above and below, causes a considerable reduction of the friction between the cover layer and the subsoil. For an evaluation it is therefore necessary to know the groundwater head of the pore-water in the filter underneath the revetment. It is also necessary to consider some aspects of the analysis of the revetment against uplift as well. Other important phenomena such as the stability of the filter layer underneath the cover layer will not be considered here, because these are beyond the scope of this study. Stability factors with respect to sliding will be described in section 5.5.

5.2.3 *Geotechnical stability under wave impact.*

Sliding instability is associated with a shallow failure mechanism at the interface between cover layer and the first sub-layer. Other failure mechanisms associated with deeper slip surfaces however, cannot be ignored. It is assumed here, without proof that, for a water level drawdown or for a retraction of the wave during wave attack, that shallow sliding is the dominant mechanism for a revetment on a filter. For wave impact however, which might be regarded, as a strip-load on the revetment, geotechnical instability may not be disregarded. However the analysis of this phenomenon lies beyond the scope of this study.

5.3 GROUNDWATER FLOW THROUGH REVETMENTS

5.3.1 *Introduction*

As indicated in section 5.2.1 the pressure head difference acting on a block caused by the hydraulic loading has an important influence on the stability of the block against uplift, as well as on the stability against sliding of the cover layer. As a next step, the calculation of the groundwater head distribution will be described. To begin with an analytical formulation for the groundwater head in the filter is described. The results of this analysis are compared with a 2D Finite Element formulation. This finite element analysis includes the derivation of the groundwater table. It is based on a formulation within a fixed mesh, in order to simplify future developments of coupling groundwater flow with deformation analysis.

The derivation is based on a non-linear relation between groundwater head, and saturation. Saturation and permeability are assumed to be strongly correlated. The constitutive behaviour is formulated, taking into account the non-linear character of the groundwater flow in coarse grained filter materials, caused by turbulence. For the determination of the seepage surface, a method updating the groundwater head boundary conditions was used. This method consists of tracking whether for a particular subset of nodes the calculated groundwater head does not exceeds the height of that node. If this is the case the boundary condition to the numerical formulation are adapted to a fixed groundwater head. However, if in a subsequent iteration the groundwater discharge is negative, (meaning water flowing into the domain) the boundary condition is changed the other way round.

In section 5.3.4 the computer code is applied to model turbulent groundwater flow in a filter layer underneath a revetment under wave attack. The constant matrix scheme enables the calculation of turbulent flow without changes to the iterative procedure. The analysis presented here was used to verify the linearisation method for a semi-empirical design formula for the calculation of uplift pressures. The secant formulation, combined with a simple analytic solution based on a one-dimensional model of the flow in the filter layer, was compared with the FEM results for the maximum uplift pressures on a cover layer.

5.3.2 *Analytical formulation*

Modelling of the Flow: Starting from the principle of continuity, assuming that for the characteristic situation the flow may be analysed according to a scheme of static flow and assuming that the flow through the revetment and the filter layer is linear, the following differential equation for the groundwater flow problem may be derived (see Fig. 5.3).

$$\frac{dq_y}{dy} + \frac{k'(\Phi - \Phi_u)}{D} = 0 \tag{5.9}$$

In this formula Φ is the groundwater head in the filter layer, Φ_u is the pressure head on the outward side of the revetment, q is the specific discharge in the filter, k' is the linearised revetment permeability parameter, $\frac{d()}{dy}$ is the derivative in y direction and D is the cover layer thickness.

For linear flow in the filter the Darcy formula can be used:

$$q_y = -kb\frac{d\Phi}{dy} \tag{5.10}$$

Where b is the thickness of the filter layer.

Combining the equations 5.9 and 5.10 gives:

$$\frac{d^2\Phi}{dy^2} - \frac{k'}{bDk}\Phi = -\frac{k'}{bDk}\Phi_u \tag{5.11}$$

An important parameter for this differential equation, the leakage length, can be recognised as:

$$\Lambda = \sqrt{\frac{kbD}{k'}} \tag{5.12}$$

Equation 5.11 may be rewritten to give:

$$\frac{d^2\Phi}{dy^2} - \frac{\Phi}{\Lambda^2} = -\frac{\Phi_u}{\Lambda^2} \tag{5.13}$$

Equation 5.13, can be reformulated to include the vertical co-ordinate with respect to gravity. This is achieved by using the kinematics relation between the second derivative of y, and the second derivative of z, which gives:

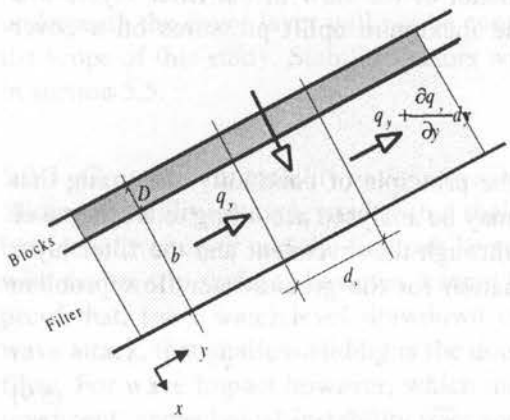

$$q_x = \frac{k'(\Phi - \Phi_u)}{D}$$

$$q_y = -k\,b\,\frac{d\,\Phi}{d\,y}$$

Figure 5.3 Scheme of the flow through and under the revetment

$$\frac{d^2\Phi}{dy^2} = \sin^2\alpha \frac{d^2\Phi}{dz^2} \tag{5.14}$$

If an alternative parameter, the leakage height λ, is introduced, where:

$$\lambda = \Lambda \sin\alpha \tag{5.15}$$

than equation 5.6 may be reformulated to give:

$$\frac{d^2\Phi}{dz^2} - \frac{\Phi}{\lambda^2} = -\frac{\Phi_u}{\lambda^2} \tag{5.16}$$

The derivation of a solution to this equation is discussed in section 5.3.2

Modelling the wave boundary condition

The groundwater head distribution, in the filter, can be derived if the pressure head distribution on top of the revetment is known by applying equation 5.16. For this boundary condition, the pressure head distribution on top of the revetment, registrations of wave pressures such as obtained by the Delft Hydraulics laboratory in the Delta flume in De Voorst (The Netherlands), can be used.

With these measurements it is possible to obtain the pressure differences in time over the revetment at any place, by using the numerical model STEENZET/1 Bezuijen (1987). From analysis and evaluation of results obtained from this model, it is found to be possible to apply a simpler model where only the most critical situation in time is needed.

The main characteristic to the simple evaluation model is that a time-averaged rise in the water table can be assumed in combination with the distribution of water pressures on a characteristic point in the time domain. The rise in the level of the water table in the filter is denoted by a rise Z_l above the Rundown point. Measurements indicate that $0.9\,H_b < Z_l \leq H_b$.

For the groundwater flow, according to Wolsink (1985), a static scheme of a breaking wave, modelled as in Fig. 5.10, is characteristic for the groundwater flow conditions.

For this scheme, four parameters are needed:

- *a maximum head above rundown point* H_b,
- *a breaker angle* β,
- *rundown* R_d
- *the rise in water table in the filter* Z_l

For the application of this model we have to translate the wave information on deep water, the incoming wave height H_i and the incoming wave period T_p, to values of H_b and β as defined previously.

Here the work of Banach (see Klein Breteler et al. 1988) can be used. Banach performed a regression analysis on wave pressure registrations, obtained on a 1:3 slope in the Delta flume, and also on scale model measurements in the Schelde

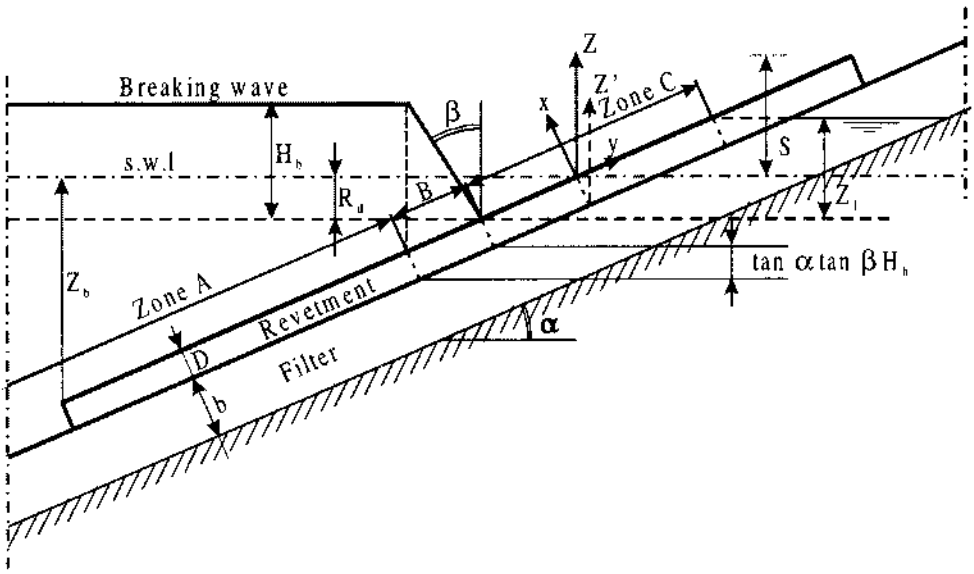

Figure 5.4 Wave scheme according to Wolsink

flume for 1:2, 1:3 and 1:4 slopes. He derived relationships between the incoming wave information, H_i and T_p, the water depth d, and the parameters H_b and β required here. Rundown values R_d where taken from laboratory tests such as presented by (Klein Breteler et al. 1995).
The water level depression in a canal due to a passing ship may be modelled by taking $H_b = 0.0$ and a breaker angle $\beta = 90^{o}$.

Solution of the differential Equation
For the wave boundary condition such as described in this section, the groundwater head distribution was solved by Wolsink (1985). The solution of Wolsink is repeated here because it will be used as a partial contribution to the problem of sliding stability. The derivation of sliding instability is described in more detail in section 5.5.

Because of the different boundary conditions on top of the revetment, three zones can be identified (see also Fig. 5.4): the zone below the point where $\Phi_u = H_b$, the zone between this point and the rundown point and the zone between the rundown point and the water table in the filter.
The solutions in these three zones, are:

1. for $z < -H_b \tan\alpha \tan\beta - R_d$, see Fig. 5.4, zone *A*:

$$\Delta(\Phi) = C_4 \exp(\frac{z + R_d}{\lambda}) \tag{5.17}$$

2. for $-H_b \tan\alpha \tan\beta - R_d \le z < -R_d$ see Fig. 5.4, zone *B*:

$$\Delta(\Phi) = C_3 \exp(\frac{z + R_d)}{\lambda}) + C_1 \exp(-\frac{z + R_d}{\lambda}) \tag{5.18}$$

3. for $-R_d <= z < z_1 - R_d$, see Fig. 5.4, zone C:

$$\Delta(\Phi) = C_5 \exp(\frac{z + R_d}{\lambda}) + C_2 \exp(\frac{-(z + R_d)}{\lambda}) \tag{5.19}$$

In these equations $\Delta(\Phi)$ is the head difference between the groundwater head in the filter under the cover layer and the pressure head on top of the revetment perpendicular to the slope. The coefficients C_1 to C_5 are:

$$C_1 = -\frac{\lambda \exp(-\tan\alpha \tan\beta \frac{H_b}{\lambda})}{2 \tan\alpha \tan\beta} \tag{5.20}$$

$$C_2 = -\frac{\lambda (1 - \exp(-\tan\alpha \tan\beta \frac{H_b}{\lambda})}{2 \tan\alpha \tan\beta + \lambda/2} \tag{5.21}$$

$$C_3 = -C_1 + C_2 (1 - \exp(-Z_1/\lambda)) \tag{5.22}$$

$$C_4 = C_3 + C_1 \exp(2 \tan\alpha \tan\beta \frac{H_b}{\lambda}) \tag{5.23}$$

$$C_5 = -C_2 \exp(-2 Z_1/\lambda) \tag{5.24}$$

The z-axis is taken vertical, as shown in Fig. 5.4, where $z = 0$ corresponds to the still-water level. It was decided that the solution is solved directly in terms of the pressure head differences, as for the evaluation of the stability against sliding this is the quantity of main interest. The maximum pressure head difference can be obtained at breaker point $(z = -R_d)$ on the boundary between zone 2 and zone 3.

The solution for this maximum pressure difference is:

$$\max(\Delta\Phi) = \frac{\lambda}{2}(1 + \frac{1 - \exp(-\tan\alpha \tan\beta \frac{H_b}{\lambda})}{\tan\alpha \tan\beta})(1 - \exp(-2Z_1/\lambda) \tag{5.25}$$

A graphical presentation of equation 5.25 is given in Fig. 5.5, for $Z_1 = H_b$ and $\tan(\alpha) = 1/3$.

A long leakage height and a small value of β will result in high uplift pressures.

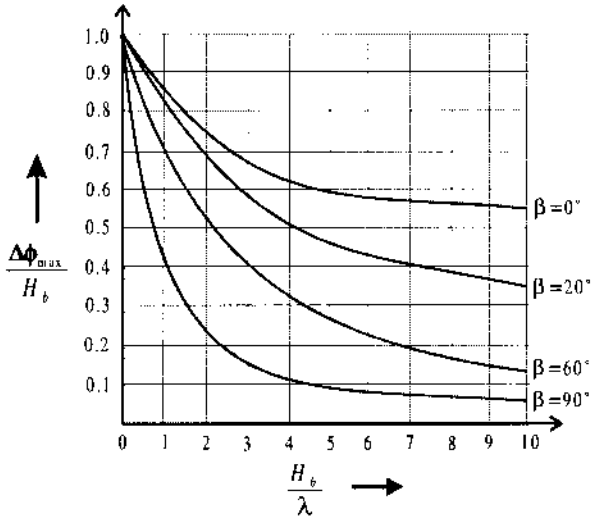

Figure 5.5 Graphical presentation of the maximum relative head-differences, as a function of the relative wave-height for $Z_1 = H_b$ and tan(α) = 1/3

Equation 5.25 can also be presented in terms of the leakage length and this gives:

$$\max(\Delta\Phi) = \frac{\Lambda \sin\alpha}{2}\left(1 + \frac{1 - \exp\left(-\tan\beta \frac{H_b}{\Lambda\cos\alpha}\right)}{\tan\alpha\tan\beta}\right)\left(1 - \exp\left(\frac{-2Z_1}{\Lambda\sin\alpha}\right)\right) \qquad (5.26)$$

This analytical solution is convenient for use in practice. Without much effort, uplift stability can be evaluated. The reliability of this solution was validated experimentally on large scale in the Delta Flume of Delft Hydraulics, see Bezuijen et al. (1987). This validation confirmed that there is a reasonable agreement between measurement and analytical model. The only drawback to the application of equation 5.26, is that the cover layer permeability *k'* is difficult to determine.

Another required verification is the way the flow of the groundwater in the filter is linearised. More details about this linearisation are discussed in section 5.3.4

5.3.3 *Numerical, 2D formulation and constitutive behaviour*

Theory; the problem of formulating the boundary value problem for the groundwater flow is solved, by assuming the continuity equation in the form:

$$\frac{\partial q_i}{\partial x_i} = 0 \qquad (5.27)$$

Where q_i is the vector of groundwater discharges: [q_x, q_y].

To solve the problem of a groundwater table in a fixed mesh, the following extended constitutive relation is applied:

$$q_i = K^r K_{ij} \frac{\partial \Phi}{\partial x_i} \tag{5.28}$$

where K_{ij} is the permeability matrix:

$$\begin{bmatrix} K_{xx} & K_{xy} \\ K_{yx} & K_{yy} \end{bmatrix} \tag{5.29}$$

or, for isotropic flow:

$$\begin{bmatrix} K & 0 \\ 0 & K \end{bmatrix} \tag{5.30}$$

The parameter K^r in equation 5.28 is a scalar called the 'relative permeability' that can take values $0.0 < K^r \leq 1.0$. The relation between relative permeability and water pressure P is shown in Fig. 5.6

Substituting equation 5.28 into equation 5.27 gives:

$$\frac{\partial \left(- K^r K_{ij} \dfrac{\partial \Phi}{\partial x_j} \right)}{\partial x_i} = 0 \tag{5.31}$$

This differential equation may be reformulated according to the principle of virtual work, as discussed in section 4.5.1, or alternatively by applying Galerkin's scheme, to derive a functional. Minimising this functional we arrive at a system of equations for nodal points:

$$\mathbf{KP}^t \mathbf{\Phi} = \mathbf{Q} \tag{5.32}$$

Where:

$$\mathbf{KP}^t = \int_V \mathbf{B}^T K^r \mathbf{KB}\, dV \tag{5.33}$$

and

$$\mathbf{Q} = - \int_S \mathbf{H}^T q_s\, dS \tag{5.34}$$

The superscript ^{t} on the matrix **KP** means that in the permeability law the tangent is used. By adopting the approach described by Desai (1983), this equation can be solved, in an iterative way by updating the constitutive model and recalculating $\mathbf{K}^r$ until the solution converges (see also Bathe 1979). An alternative way to formulate this process is:

$$\mathbf{KP}^t \mathbf{\Phi} = \mathbf{KP} \mathbf{\Phi} + \mathbf{KP}^t \mathbf{\Phi} - \mathbf{KP} \mathbf{\Phi} = \mathbf{KP} \mathbf{\Phi} - \int_V \mathbf{B}^T (1 - K^r) \mathbf{KB} dV\, \mathbf{\Phi} \tag{5.35}$$

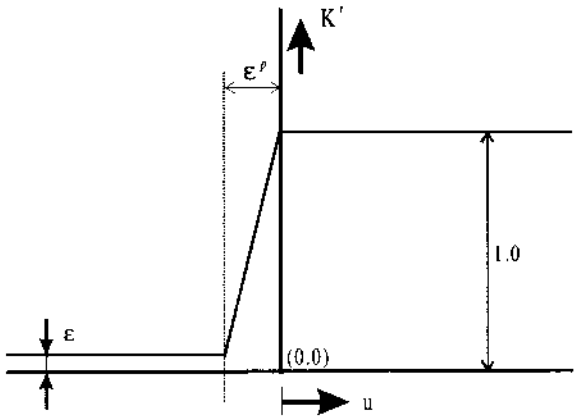

Figure 5.6 Pressure permeability relationship

Where **KP** is the matrix which would be derived for the condition of full saturation. The last integral in equation 5.35 can be recognised as the part of the system matrix that was originally attributed to the non-saturated part of the mesh, $\mathbf{KP}^{U}$. Substituting this in equation 5.35 gives

$$\mathbf{KP\Phi} = \mathbf{Q} + \mathbf{KP}^{u}\mathbf{\Phi} \tag{5.36}$$

Solving this equation incrementally gives:

$$\mathbf{KP}\delta\mathbf{\Phi}^{k+1} = \mathbf{Q} - \mathbf{KP}\mathbf{\Phi}^{k} + \mathbf{KP}^{u}\mathbf{\Phi}^{k} \tag{5.37}$$

If we note that $\mathbf{KP} - \mathbf{KP}^{u} = \mathbf{KP}^{t}$, then this formula can be simplified to give:

$$\mathbf{KP}\delta\mathbf{\Phi}^{k+1} = \mathbf{Q} - \mathbf{KP}^{t}\mathbf{\Phi}^{k} \tag{5.38}$$

For the iterative solution, only one vector, $\mathbf{KP}^{t}\mathbf{\Phi}^{k}$ has to be calculated for each iteration.

If we evaluate the vector **Q**, we may recognise that this vector has to be derived only once. Either the vector is determined due to the fact that a discharge boundary conditions is given, or a groundwater head boundary condition is given. In the latter situation the contribution to **Q** is derived only once too, taking this condition into account adapting the system of equations for that.

For each iteration, we only have to calculate:

$$\mathbf{KP}^{t}\mathbf{\Phi}^{k} = \int_{V} \mathbf{B}^{T} \mathbf{K}^{r} \mathbf{KB}\mathbf{\Phi}^{k}\, dV = -\int_{V} \mathbf{B}^{T} q^{k}\, dV \tag{5.39}$$

Firstly we calculate q_e^k, that is, the discharge based on the initial permeability at the integration points. Then q^k is derived by multiplication of q_e^k with $\mathbf{K}^{r}$

Turbulent flow within the bounds of numerical analysis

The iterative numerical formulation presented here permits the calculation of turbulent flow. Turbulence reduces the intrinsic permeability with an increase of the filter-velocity and the intrinsic permeability is written as a product of a relative permeability, K^r, and an initial laminar part of the intrinsic permeability. The permeability relation used is according to Forchheimer, see Den Adel (1986), with a laminar part, which is proportional to the filter velocity and a turbulent part which is quadratic with the hydraulic gradient

$$|i| = Aq + B|q|^2 \tag{5.40}$$

Where i is the hydraulic gradient of the potential head, and q is the groundwater discharge along a streamline. The coefficients A and B can be derived from permeability test results, or if direct tests are not available, empirical formulae can be used to derive A and B from the grain-size distribution as will be discussed later in section 5.3.4. Equation 5.40 can be inverted to give:

$$|q| = \frac{(-A + \sqrt{(A^2 + 4B|i|)})}{2B} \tag{5.41}$$

Then use of a secant permeability, K^s for $|q|/|i|$ gives:

$$K^s = \frac{-A + \sqrt{A^2 + 4B|i|}}{2B|i|} \tag{5.42}$$

If we define K^r *as* K^s/K^i, where K^i is the initial permeability, and take into account that for small values of the filter-velocity the quadratic part in the turbulent permeability relation vanishes, the initial permeability is found as: $K^i = 1/A$. For isotropic flow the relative permeability is given by:

$$K^r = \frac{2}{1 + \sqrt{1 + \frac{4B|i|}{A^2}}} \tag{5.43}$$

To verify the scheme as proposed in this section, a Newton-Raphson approach was used. For this approach it is not sufficient to calculate the secant of the permeability because the tangent to the permeability is also needed. The relative permeability with respect to the tangent permeability, defined as $K^{rt} = K^t/K^i$, is given by:

$$K^{rt} = \frac{1}{\sqrt{1 + \frac{4B|i|}{A}}} \tag{5.44}$$

5.3.4 *Turbulent flow through revetments*

For the analysis of the stability of block revetments, as discussed in section 5.2, the pressure head difference over the cover-layer, is an important parameter. Turbulent flow is of importance when modelling the flow through revetments because the filter material is mostly coarse. When a filter layer is present, the effects of elastic storage or consolidation are only minor and can in practice be neglected. Because the effects of changes to the water table on the maximum uplift pressures are also small, the problem was solved according to the solution for stationary flow. For the outward boundary conditions of the flow problem, the wave pressure distribution on top of the revetment is transformed and reformulated in terms of a groundwater head.

Linearisation of the groundwater flow

The analytic solution predicts that the maximum downward hydraulic gradient in the filter layer is equal to the slope angle. The maximum upward hydraulic gradient, however, is dominated by the breaker angle β damped by the cover layer, and is of the same order as α. Thus a linearisation around $i = \alpha$ is practical. To verify whether this linearisation should be secant or tangent, and to check the accuracy of adopting a one-dimensional solution, a true turbulent two-dimensional analysis was performed. For this evaluation an, imaginary revetment on a coarse filter layer of pebbles, $Df_{15} = 8$ mm was analysed. The dimensions of the problem are related to the tests that have been done in the Delta flume of Delft Hydraulics. The relatively thick filter layer is based on the thickness used in practice for mine stone filter layers underneath a revetment.

A comparison is made between two-dimensional and one-dimensional

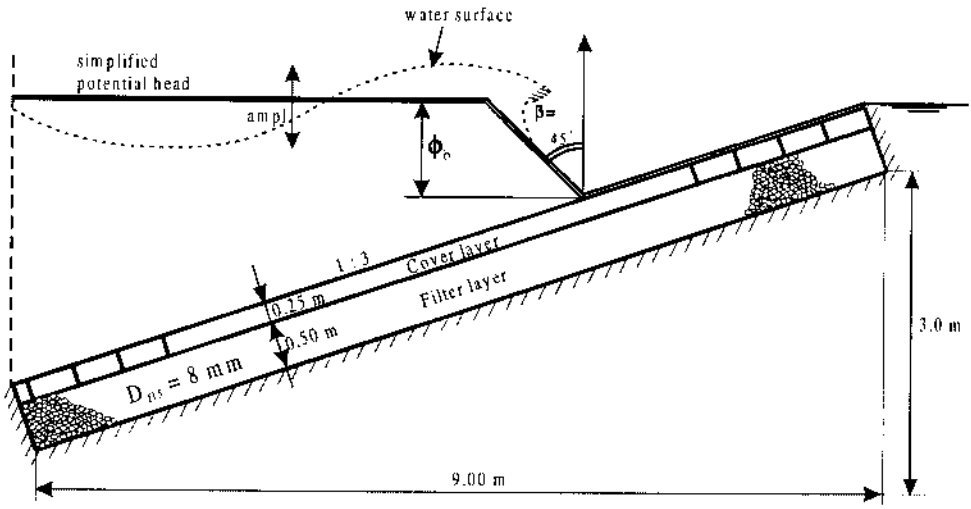

Figure 5.7 Flow through a revetment. Dimensions of the tests in the Delta Flume of Delft Hydraulics

linearised calculations. In this example the assumption of a coarse filter is needed to guarantee turbulence. An argument in favour of a tangent linearisation is that the pressure difference over the cover layer is governed by the divergence in discharge in the filter layer. As this divergence would lead to a change in permeability in the filter layer this means an accurate description of this change is needed. An argument in favour of a secant linearisation is that continuity should not be violated.

Numerical analysis

To study this topic, the results of the linearised analytic solution are compared with a 2D numerical analysis. The structure chosen for analysis is based on the dimensions of the Delta Flume of Delft Hydraulics, with a slope of 1 : 3, a breaker height, $\Phi_b = 1.0\ m.$ and a breaker angle of $\beta = 45^{\circ}$ as shown in Fig. 5.7. A revetment of blocks with a thickness of 0.25 m on a filter layer with a thickness of 0.50 m and a porosity of n=0.4 was chosen. For the analytical solution (equation 5.26), the height of the water table $Z_l = \Phi_b = 1.0\ m.$ is assumed. For the determination of the turbulent permeability the empirical relations for the Forchheimer coefficients A, and B in equation 5.40 where used:

$$A = 160\frac{\nu(1-n)^2}{g\,n^3 D_{15}^2} \qquad (5.45) \qquad \text{and,} \qquad B = \frac{2.2}{g\,n^2 D_{15}} \qquad (5.46)$$

The permeability of the cover layer is chosen to provide a realistic range of the leakage length, $0.3\ m. < \Lambda < 1.2\ m.$ For reasons of simplicity, the permeability of the cover layer is assumed to be linear so $B' = 0$.

The iterative solution technique as described in section 5.3.3 was verified with a true Newton-Raphson approach in which the system matrix was updated every iteration. The results of this numerical verification were in very close agreement with those presented in Table 5.1, and therefore not displayed here.

As can be observed in Table 5.1, both the secant linearised calculations (2-D and 1-D) are in good agreement with the 2-D turbulent calculation. The tangent

Table 5.1 Maximum potential head difference over the revetment as a function of the linearised cover layer permeability k'

					ΔΦ			
					Numerical 2-D	Numerical 2-D	Analytical 1-D	Analytical 1-D
	k'	A'	$\Lambda^{tangent}$	Λ^{secant}	turbulent	secant	secant	tangent
	m/s	s/m	m	m	m	m	m	m
1	$8.21*10^{-2}$	12.19	0.32	0.42	0.241	0.250	0.252	0.195
2	$2.05*10^{-2}$	48.78	0.63	0.85	0.421	0.402	0.420	0.343
3	$9.11*10^{-2}$	109.77	0.95	1.27	0.538	0.499	0.538	0.451

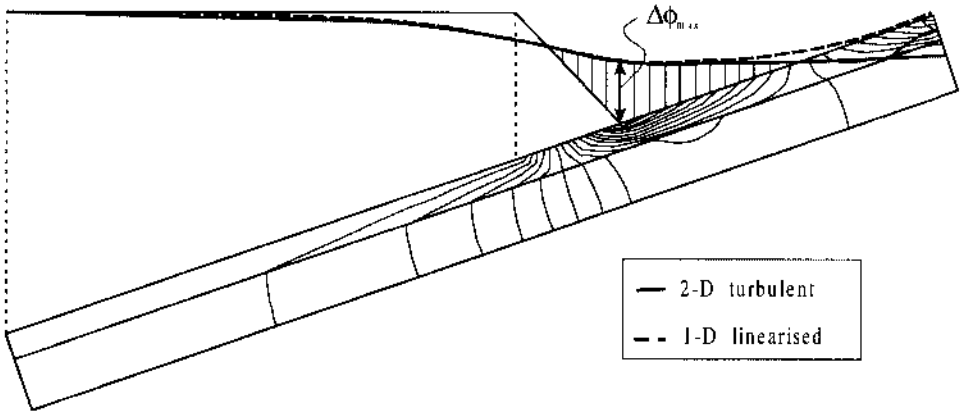

Figure 5.8 Contour lines of the groundwater head and the Pressure head difference distribution, as calculated for $\Lambda = 0.95$

linearised calculation however predicts too small values for the pressure head difference. Fig. 5.8 gives the potential head difference distributions calculated for solution 3 of Table 5.1. The groundwater head distribution in the filter layer is given as contour lines. The agreement between the analytical and the numerical solution is very close, except above the breaker-point, but for uplift this is of minor importance. This difference is ascribed to the approximate modelling of the water table in the two-dimensional analysis.

Recalculation of the analytic solution compensating for this aspect, assuming the calculated water table in the two-dimensional analysis, that is for $Z_l = 0.57$ gives an improved agreement with the linearised two-dimensional analysis. Even the maximum pressure head difference drops to 0.506 which, though it is less than in the 2-D turbulent calculation, is in better agreement with the result of the 2-D linearised calculation (0.499)

Conclusions regarding the modelling of turbulent flow in revetments

A computer code for the calculation of stationary non-linear groundwater flow was developed and tested using an initial system matrix scheme (modified Newton-Raphson). The calculation of a groundwater table in a fixed mesh, including the calculation of a seepage surface was accomplished. The advantage of implicitly solving the water table in this scheme of analysis does not comes forward in this example, where other aspects such as turbulence are more important. Though essentially it is not necessary to assemble the system matrix once again because new boundary conditions have to be considered, the matrix has to be decomposed every time that boundary conditions change. This disadvantage might be taken away, incorporating seepage interface elements, see Aubry (1988).

This numerical scheme was adapted to model turbulent flow. A simplified

approach, for the calculation of potential head differences to evaluate the stability of block revetments was compared with the results of a two-dimensional turbulent calculation. It was concluded that this simplification is valid for the calculation of the maximum uplift pressure. A secant linearisation of the permeability relation according to equation 5.42 assuming that $|i| \cong \alpha$ leads to adequate results for the calculation of uplift pressures.

5.4 OBLIQUE WAVE IMPACT, AND STABILITY

5.4.1 *Introduction*

In the study on oblique wave attack on block revetments by Stive (1986) the outward wave loading on the revetments was modelled using linear wave theory and evaluated by a comparison with perpendicular wave loading. Based on this study it was concluded that for the characteristic loading of a revetment, oblique waves give a reduced loading situation. For the wave height and the wave steepness, there is no reason to doubt this conclusion.

However, to think that oblique waves therefore are less dangerous than perpendicular wave loading is unsafe. That depends on the criteria to design the blocks with respect to block movements.

It is considered here, that as soil-loading interaction in the subsoil might influence the ultimate limit state of blocks in the Delta flume, this interaction might not be active under oblique wave loading. Therefore, the conclusion that oblique wave impact may be disregarded is not valid. On the contrary, it will be argued that oblique wave loading undermines the assumption that the restricted flow of water under a block contributes to the uplift stability.

Although this assumption would be valid for perpendicular wave loading for a 2D plane-strain situation, for the 3D case of oblique wave loading, there is no restriction for water flowing in from underneath adjacent blocks that were uplifted and then quickly returned to their original position.

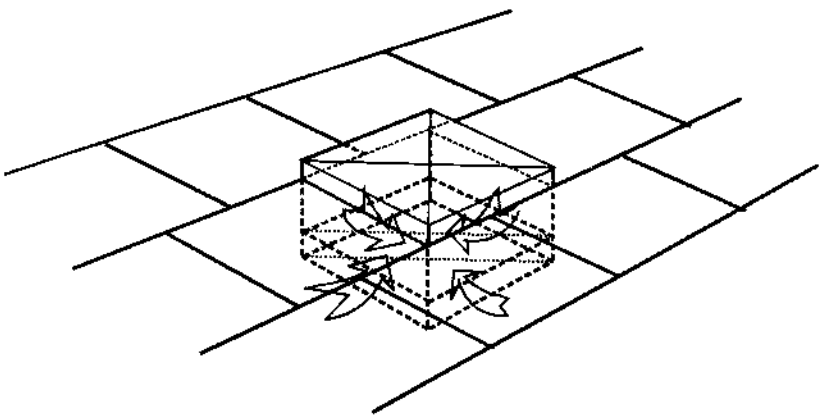

Figure 5.9 Groundwater flowing towards the cavity created by a moving block

5.4.2 *Oblique wave impact and criteria against uplift*

In the derivation of Γ_{u3}, as discussed in section 5.2.1, it is implicitly assumed that the inflow of water into the cavity created due to the displacement of an unstable block is only possible from the subsoil. Direct inflow of water from a cavity under adjacent blocks is not considered, as this situation is not feasible for a revetment with perpendicular wave loading.

For perpendicular wave loading, where the permeability of the revetment parallel to the cover layer is low $k_{//}^{top} < k_{\perp}^{top}$, this assumption might be considered valid. When the stability of blocks from tests such as in the large Delta-flume of Delft Hydraulics have to be evaluated, this aspect has to be taken into account.

For oblique wave loading on top of the revetment, the assumption that inflow of water is restricted to inflow from outside the subsoil has to be questioned. For this situation assume a co-ordinate system which moves along the revetment with the same speed, as the point of critical wave action is moving sideways. Two or more blocks in a row might be in such a related combination of displacement that some blocks might be pushed in the revetment by the incoming wave and other blocks may be just lifted out of the revetment by the retreating former wave, see Fig. 5.11.

Such a row of moving blocks have been observed, where it was appeared similar to the keys of a piano touched upon each other in a row; the 'pianola effect'. Another description might be; a train of moving blocks along a revetment just in front of the wave impact, see Fig. 5.10. This situation is characterised by a system of 'communicating' vessels. The water 'stored' underneath the one block is pushed into the cavity that is forming under another block. For this situation no additional inflow of water from the subsoil is needed. A slight additional inflow of water onto this storage volume might lead to an increase of the displacement of the moving blocks, and therefore to failure.

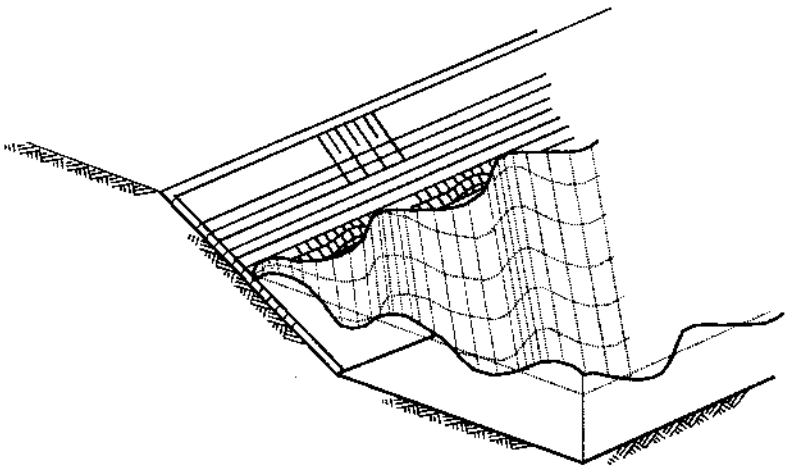

Figure 5.10 Train of moving blocks in combination with oblique wave loading

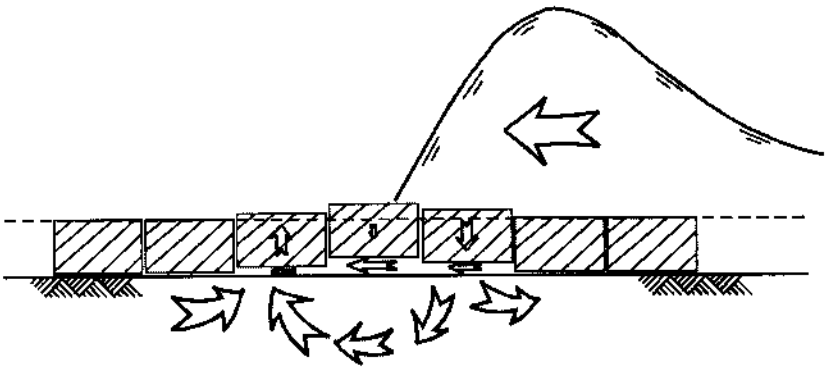

Figure 5.11 Communicating vessels of water, underneath a 'train' of unstable (uplifting) blocks

An additional aspect to be considered is the fact that the filter bed underneath a moving block might be fluidised due to high local groundwater gradients perpendicular to the subsoil interface. This leads to an increase in permeability for water flowing into the cavity. Alternatively this fluidisation might be cease, causing the water to flow less easily into the subsoil. This effect might contribute to an increasing volume of water within the system of communicating vessels.

Due to the adverse transport of water flowing between cavities underneath blocks, additional strength due to restricted inflow of water to a cavity formed by an uplifted block is not obtained.

For practical purposes, oblique wave action may not be ignored if the design philosophy allows displacement of blocks.

5.5 STABILITY AGAINST SLIDING OF FLEXIBLE REVETMENTS

In this section a method for the evaluation of the stability against sliding is formulated. In contrast to uplifting where the stability of a single block is evaluated, here the structure as a whole is regarded.

It must be understood that a local sliding criterion does not suffice because a local criterion would always result in the requirement that the normal stress between blocks and subsoil would be higher than a limit value; $\sigma_n > p_{cr}$. The normal situation for the design of blocks against uplift however, is that $\sigma_n = 0$.

It is observed that revetments are stable due to interlocking, even when the local criterion is violated. A more refined approach is therefore required.

In this section, the stability against sliding is considered in global terms, which makes it possible to account for additional strength. Formulae are presented for a revetment placed on a filter layer.

5.5.1 *Introduction*

The literature on sliding of revetments is generally focused on local criteria for relatively impermeable top layers. Using these criteria, much thicker blocks, or less steep banks, would be designed than are actually used in practice. To overcome this gap between theory and practice a global sliding criterion has been developed. Using the pressure difference distribution, such as discussed in section 5.3.2, the revetment is divided into zones which are potentially stable against sliding, zones which are potentially unstable against sliding, and zones which are potentially unstable against uplifting.

Assuming that the groundwater head distribution in the filter is given by the analytical solutions of section 5.3.2 the revetment is divided into stable and unstable zones. The stability of the revetment or the required strength of a toe structure or an anchorage may be evaluated by comparing the net resulting axial force in the unstable zones with the net resulting resistance to sliding in the stable zones.

As described by De Groot (1988), one of the basic assumptions underlying this concept is the recognition of three transfer functions. The transfer function from wave characteristics to pressure distribution along the slope surface, such as discussed in section 5.3.2. The transfer function from this pressure distribution to the loading on the elements of the revetment, (see sections 5.3.2 and the transfer function from the hydraulic load to the response of the structure, (see the sections 5.5.3, 5.5.4 and 5.5.5).

5.5.2 *Revetment on a filter layer*

Her in this section the attention is focussed on the evaluation of the stability against sliding of revetments which are built of loose blocks or block mattresses placed on a filter layer.

The flow in the filter layer is assumed to be parallel to the slope, and thus the linearized relations for the groundwater head distribution, as described in section 5.3.2. are assumed to be adequate. This assumption is valid if the permeability of the filter layer is large in comparison to the permeability of the subsoil. Only in the top layer, the revetment itself, is flow assumed to be perpendicular to the slope. The flow in the filter can in practice be linear or turbulent.

To derive a practical analytical solution, a linear relation for the permeability is used. When the flow in the filter is turbulent, and therefore non-linear, a secant formulation of the turbulent permeability relation as formulated by Forchheimer (see Den Adel (1987), will be used. The derivation and validation of the secant permeability has been discussed in section 5.3.4

5.5.3 *Stability criteria for sliding*

When evaluating the stability of revetments, two important stability criteria are recognised: equilibrium of forces perpendicular to the slope (uplifting of the

revetment) and equilibrium of forces parallel to the slope (sliding of the revetment). In this section attention is focused on the latter criterion.

First, the local stability criteria for the revetment will be described. To derive a limit shear stress between revetment and filter or subsoil the Coulomb yield condition will be adopted with neglect of any cohesion:

$$\tau_{cr} = \sigma_n \tan\varphi \tag{5.47}$$

Here τ_{cr} is the critical shear stress, σ_n is the normal stress, and φ is the friction angle.

For the net weight of the revetment above the breaker point, the component of the weight parallel to the slope has to be calculated using the dry weight of the revetment. For the component of the net weight of the revetment perpendicular to the slope the submerged weight has to be used. This in contrast to the revetment below the breaker point for which the submerged weight has to be considered for both components.

For the zone above the water table the dry weight has to be taken. For a small transition zone where the blocks are partly above and partly below the water table an average value of the weight has to be considered (see Fig. 5.12).
Accordingly the following limits for local stability against sliding are arrived at:

1. *For the zone between the breaker point and the water table*:

$$\{\Delta_w D\cos\alpha - \Delta(\Phi)\}\tan\varphi < (\Delta_w + 1)D\sin\alpha$$

or

$$\Delta(\Phi) < D\{\Delta_w \cos\alpha - \frac{(\Delta_w + 1)\sin\alpha}{\tan\varphi}\} \tag{5.48}$$

2. *Under the breaker point*

$$\{\Delta_w D\cos\alpha - \Delta(\Phi)\}\tan\varphi < \Delta_w D\sin\alpha$$

or

$$\Delta(\Phi) < \Delta_w D\{\cos\alpha - \frac{\sin\alpha}{\tan\varphi}\} \tag{5.49}$$

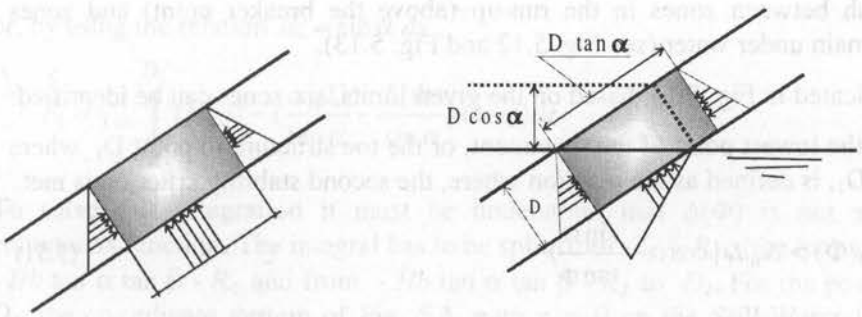

Figure 5.12 Water pressures for the revetment above the breaker point

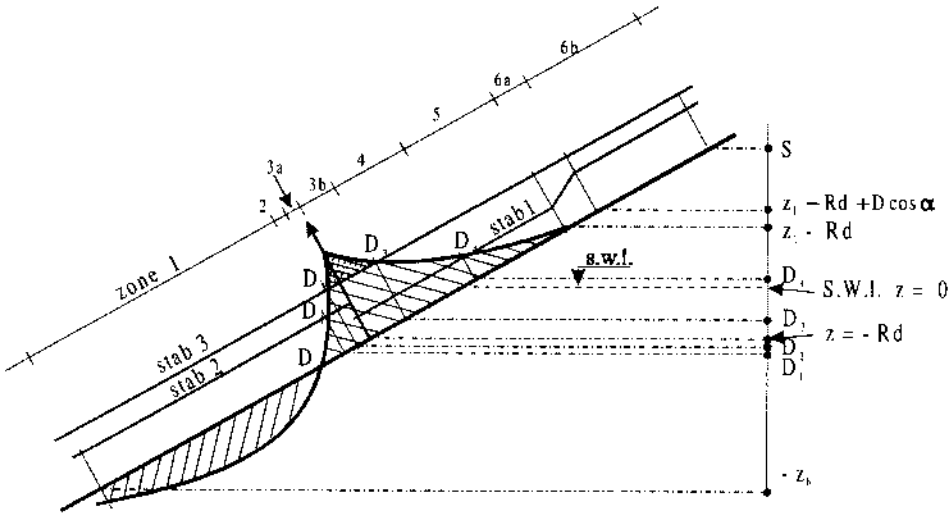

Figure 5.13 Characteristic pressure difference distribution, up and down the point of lowest wave rundown, (see also Fig. 5.8)

3. *For the limit against uplifting, both under and above the breaker point.*

$$\Delta(\Phi) = \Delta_w D \cos\alpha \tag{5.50}$$

Zones are distinguished where the resulting force parallel to the revetment is smaller than the critical shear force, and zones where this resulting force is larger than the critical shear force. The first zone will be qualified as potentially stable and the second as potentially unstable. In the stable zone there is a reserve in strength. In the potentially unstable zone equilibrium can only be reached when there is a possibility of redistribution, introducing normal forces in the revetment. This is a normal condition for placed block revetments or block mattresses.

Subsequently the potentially unstable zones have to be divided into zones where the pressure difference for the revetment is smaller than the submerged weight of the revetment (which means that there is still mobilisation of shear stresses) and zones where no additional shear stresses can be mobilised, because the block is potentially unstable against uplifting. To proceed, we have to distinguish between zones in the run-up (above the breaker point) and zones which remain under water (see Fig. 5.12 and Fig. 5.13).

As indicated in Fig. 5.13, based on the given limits, six zones can be identified:

1. From the lowest point of the revetment, or the toe structure to point D_1, where point D_1, is defined as the position where, the second stability criterion is met:

$$\Delta(\Phi) > \Delta_w D\{\cos\alpha - \frac{\sin\alpha}{\tan\varphi}\} \tag{5.51}$$

The potential shear stress will be bigger than the critical shear stress. The resultant force parallel to the slope for this zone is positive. This is a zone with a potential reserve of strength.

2 From point D_1, to point D_2 , where point D_2 is defined as the *lowest* position where the criterion is met that the pressure difference is higher than the uplift limit, so:

$$\Delta(\Phi) = \Delta_w D \cos\alpha \tag{5.52}$$

3. From point D_2 to point D_3 , where point D_3, is defined as the *highest* position where the criterion is met that pressure difference is higher than the uplift limit, according to equation 5.52.
4. From point D_3, to point D_4 , where point D_4, is defined as the position where the first stability criterion is met:

$$\Delta(\Phi) < D\{\Delta_w \cos\alpha - \frac{(\Delta_w + 1)\sin\alpha}{\tan\varphi}\} \tag{5.53}$$

5. From point D_4, to $z = Z_l - R_d$, where the latter point is the water table in the filter.

6_a. From $z = Z_l - R_d$ to $Z = Z_l - R_d + D \cos\alpha$; the transition zone.

6_b. From $z = Z_l - R_d + D \cos\alpha$, to the top of the revetment.

The resulting force parallel to the slope for each zone can be obtained by integrating the stresses within each zone. Here, the following simplifying expression is used:

$$\int_{z_i}^{z_j} \exp(z/\lambda)\,dz = \lambda\{\exp(z_j/\lambda) - \exp(z_i/\lambda)\} \tag{5.54}$$

For zone 1 this gives:

$$F_1 = \gamma_w \int_{-Z_b}^{D_1} \{\Delta_w D \sin\alpha - (\Delta_w D \cos\alpha - \Delta(\Phi))\tan\varphi\}dy \tag{5.55}$$

or, by using the relation $dz = \sin\alpha\, dy$,

$$F_1 = \gamma_w \int_{-Z_b}^{D_1} \{\Delta_w D - (\frac{\Delta_w D}{\tan\alpha} - \frac{\Delta(\Phi)}{\sin\alpha})\tan\varphi\}dz \tag{5.56}$$

To solve this integration it must be understood that $\Delta(\Phi)$ is not a single continuous function. The integral has to be split from $-Z_b + R_d$, (the toe) to $- Hb \tan\alpha \tan\beta - R_d$ and from $- Hb \tan\alpha \tan\beta - R_d$ to D_1. For the position of D_1, the co-ordinate system of Fig. 5.4, with $z = 0$ on the Still-Water Level is

maintained, where Z_b the position of the toe of the revetment and S the top of the revetment are fixed.

Finally after some mathematical manipulation, we reach solutions for the six zones:

$$F_1 = \gamma_w[\Delta_w D(1 - \tan\varphi/\tan\alpha)(D_1 + Z_b) + \lambda(\tan\varphi/\sin\alpha)\{C_4[\exp(-\tan\alpha\tan\beta\, H_b/\lambda) - \exp(-\frac{(Z_b - R_d)}{\lambda})] + C_3[\exp(\frac{(D_1 + R_d)}{\lambda}) - \exp(-\frac{\tan\alpha\tan\beta H_b}{\lambda})] - C_1[\exp(-\frac{D_1 + R_d}{\lambda}) - \exp(\tan\alpha\tan\beta H_b/\lambda)]\}] \quad (5.57)$$

$$F_2 = \gamma_w\{\Delta_w D(1 - \tan\varphi/\tan\alpha)(D_2 - D_1) + \lambda(\tan\varphi/\sin\alpha) \{C_3[\exp(\frac{(D_2 + R_d)}{\lambda}) - \exp(\frac{D_1 + R_d}{\lambda})] - C_1[\exp(-\frac{D_2 + R_d}{\lambda}) - \exp(-\frac{D_1 + R_d}{\lambda})]\}\} \quad (5.58)$$

$$F_3(a) = \gamma_w \Delta_w D(-R_d - D_2) \quad (5.59)$$

$$F_3(b) = \gamma_w(\Delta_w + 1)D(D_3 + R_d) \quad (5.60)$$

$$F_4 = \gamma_w\{\Delta_w D(\Delta_w + 1 - \tan\varphi/\tan\alpha)(D_4 - D_3) + \lambda(\tan\varphi/\sin\alpha) \{C_5[\exp(\frac{(D_4 + R_d)}{\lambda}) - \exp(\frac{D_3 + R_d}{\lambda})] - C_2[\exp(-\frac{D_4 + R_d}{\lambda}) - \exp(-\frac{D_3 + R_d}{\lambda})]\}\} \quad (5.61)$$

$$F_5 = \gamma_w\{D(\Delta_w + 1 - \Delta_w \tan\varphi/\tan\alpha)(Z_1 - R_d - D_4) + \lambda(\tan\varphi/\sin\alpha) \{C_5[\exp(\frac{Z_1}{\lambda}) - \exp(\frac{D_4 + R_d}{\lambda})] - C_2[\exp(-\frac{Z_1}{\lambda}) - \exp(-\frac{D_4 + R_d}{\lambda})]\}\} \quad (5.62)$$

$$F_{6a} = \gamma_w(\Delta_w + 1/2)D(1 - \tan\varphi/\tan\alpha)(D\cos\alpha) \quad (5.63)$$

$$F_{6b} = \gamma_w(\Delta_w + 1)D(1 - \tan\varphi/\tan\alpha)(S - Z_1 + R_d - D\cos\alpha) \quad (5.64)$$

To complete the model, the co-ordinates of D_1 to D_4 have to be obtained. For the positions of D_1 and D_2, if relevant, it is known that the co-ordinates can be found between $-Hb \tan\alpha \tan\beta - R_d < z < -R_d$

The position of the points D_1 and D_2, such as indicated in Fig. 5.13, can be obtained combining the equations for the pressure head difference with the criteria for uplift, which gives the equations 5.65 and 5.66, written down for zone 2 of the solution.

$$\Delta_w D\{\cos\alpha - \sin\alpha/\tan\varphi\} = C_3\exp((D_1 + R_d)/\lambda) + C_1\exp(-(D_1 + R_d)/\lambda) \quad (5.65)$$

and

$$\Delta_w D\cos\alpha = C_3 \exp(\frac{D_2 + R_d}{\lambda}) + C_1 \exp-(\frac{D_2 + R_d}{\lambda}) \tag{5.66}$$

In a similar way the position of the points D_3 and D_4, can be found in zone 3 solving equation 5.67:

$$\Delta_w D\cos\alpha = C_5 \exp(\frac{D_3 + R_d}{\lambda}) + C_2 \exp-(\frac{D_3 + R_d}{\lambda}) \tag{5.67}$$

and equation 5.68:

$$D\{\Delta_w \cos\alpha - (\Delta_w + 1)\frac{\sin\alpha}{\tan\varphi}\} = C_5 \exp(\frac{D_4 + R_d}{\lambda}) + C_2 \exp-(\frac{D_4 + R_d}{\lambda}) \tag{5.68}$$

However, to evaluate whether the points D_1, D_2, D_3, and D_4 have a physical meaning we have to distinguish 4 classes of stability as described below.

Stab = 1:

$$\max(\Delta(\Phi)) < D\{\Delta_w \cos\alpha - (\Delta_w + 1)\frac{\sin\alpha}{\tan\varphi} \tag{5.69}$$

For this class, the pressure difference is smaller than the pressure that corrsponds with the lowest stability criterion for sliding. The points D_1 D_2, D_3, and D_4 have no physical meaning. Mathematically they can be taken at the breaker point $Z = -Rd$.

Stab=2;

$$D\{\Delta_w \cos\alpha - (\Delta_w + 1)\frac{\sin\alpha}{\tan\varphi}\} < \max(\Delta(\Phi)) < \Delta_w D\{\cos\alpha - \frac{\sin\alpha}{\tan\varphi}\} \tag{5.70}$$

In the zone above the breaker point, the sliding limit is reached. D_4 has to be calculated, D_1, D_2 and D_3 have no physical meaning and are taken at the breaker point.

Stab=3:

$$\Delta_w D\{\cos\alpha - \frac{\sin\alpha}{\tan\varphi}\} < \max(\Delta(\Phi)) < \Delta_w D\cos\alpha \tag{5.71}$$

Both above and below the breaker point, the sliding limits are reached. The points D_2 and D_3, have no physical meaning and are taken at the breaker point. D_1 and D_4 have to be calculated.

Stab=4:

$$\Delta_w D\cos < \max(\Delta(\Phi)) \tag{5.72}$$

Even the uplift limit is reached, so in a limited zone no shear stress can be activated. All boundaries D_1 to D_4 have to be calculated.

The analytical calculation of D_1, to D_4 is not performed easy. For practical purposes, a numerical approach, e.g. Regula-Falsi is suggested.

5.5.4 *Stability of the revetment*

As a result of the integrations described in the preceding section, F_1, F_2, $F_6\,(a)$ and $F_6\,(b)$ will be negative, as these are the zones with a reserve of strength. F_2, $F_3(a)$, $F_3(b)$ and F_4 will be positive or zero, depending on the stability classification. The values of these last integrations indicate the axial force in the revetment that is needed to prevent these parts of the revetment from sliding.

Individual blocks

For a revetment constructed of an assembly of individual blocks, without cables or a connecting geotextile, the unstable zone has to be balanced by the reserves of strength in zone 1 force F_1. If there is not enough reserve of strength in zone 1, the difference has to be supported by a sufficiently strong toe structure.

When there is not a special toe structure, the stability factor against sliding may be defined as:

$$\Gamma_{S1} = \frac{abs(F_1)}{(F_2 + F_3 + F_4)} \tag{5.73}$$

If there is no special designed toe structure, Γ_{S1} must be larger than 1. How much larger can be estimated using probabilistic analysis.

Mattresses

If there are connecting cables or geotextiles, which make it possible to transmit a tension force to the higher zones on the slope, reserves of strength in zones 5 and 6 can be mobilized. Another stability factor Γ_{S2} can be defined according to:

$$\Gamma_{S2} = \frac{\left|(F_5) + F_6\right|}{(F_2 + F_3 + F_4)} \tag{5.74}$$

As is the case with Γ_{S1}, Γ_{S2}, must be larger than 1.

Anchorages or toe structures

If both Γ_{s1} and Γ_{s2} are less than 1, an additional support such as a toe structure or, for a mattress, an anchorage structure has to be designed.

The characteristic load at a toe structure in case of placed blocks can be calculated from:

$$F_{toe} = F_1 + F_2 + F_3 + F_4 \tag{5.75}$$

For a block mattress the load at the anchorage is:

$$F_{anch} = F_2 + F_3 + F_4 + F_5 + F_6 \tag{5.76}$$

5.5.5 *Examples*

To demonstrate the character of this model, graphs are presented for the required revetment dimension for two types of hydraulic loading.

1. For a rapid water level depression, a wave loading considered characteristic for the wave loading due to a ship is a canal.
2. For a standing wave front with a breaker angle $\beta = 45°$, a situation considered to be characteristic for the loading due to wind waves.

For the analysis, revetment with an upward slope of 1 to 3 was assumed. A revetment thickness of 0.2 m was assumed, with a dimensionless block weight Δ_w of 1.2 and a friction angle between revetment and filter of $\varphi = 25°$.

Ship wave

A rapid water level depression of 1.0 m with the assumption that the water table in the filter stays on the same height ($Z_f = 1.0$ m) was chosen, as an example of a severe wave due to shipping in a canal. The results of the calculation are given in Fig. 5.14. The depth Z_b (for the case of placed blocks) or the height S (for a block mattress) required to give equilibrium is given as a function of the leakage height. For this condition, the depth Z_b required to make equilibrium is large in comparison to the height S. To compare cost, it must be realised that if

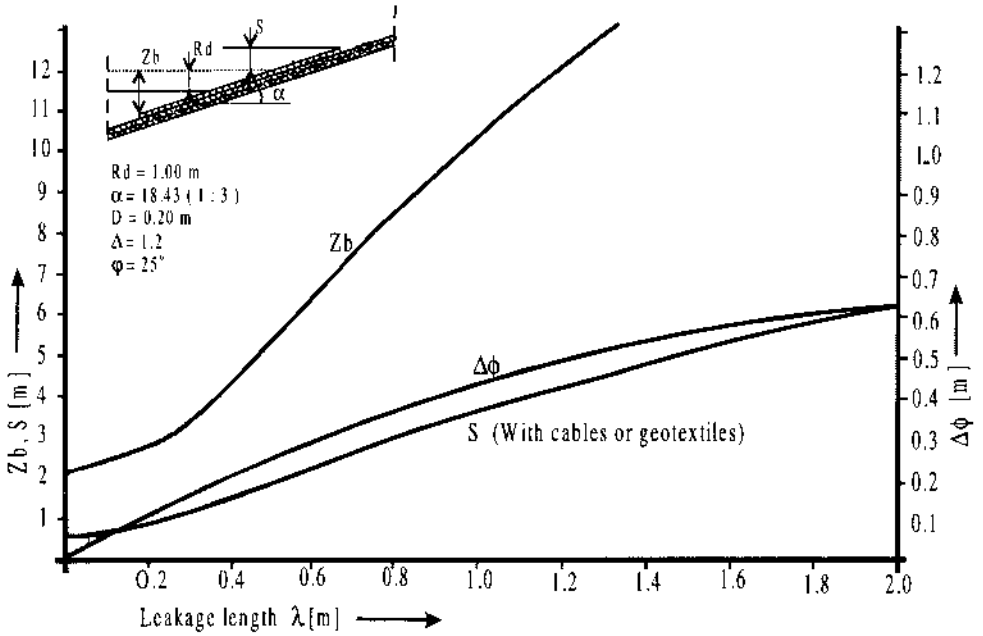

Figure 5.14 Revetment extent needed to guarantee stability for sliding of a revetment, loaded by a rapid water level depression, assuming equilibrium without toe structures or anchorages

equilibrium is achieved by making the height S large enough, expenses have to be made for geotextiles or cables used to transfer the loading to zones higher up. Construction of revetments of loose blocks deep under mean water level, on the other hand, is usually not feasible. This explains why for revetments on banks of shipping canals, shallow toe structures or block mattresses with anchorages, are often used.

Breaking wave

The second hydraulic loading condition, intended to represent a breaking wind wave, was modelled using the Banach formulae and the Wolsink model. The characteristic wave condition, a static wave front height H_b of 1.0 m, combined with a breaker angle of 45° and a rundown of half H_b was assumed.

The results of this analysis is given in Fig. 5.15. Comparing the results with those obtained for the water level depression, we do not observe a significant difference between the height required to maintain equilibrium, Z_b and S. The reason for this is that the wave pressure H_b applies a compensating pressure on the revetment below the breaker point. Though the differences in pressure head on the top layer are higher, smaller Z_b and S values are found, because the unstable zones are smaller than for a water level depression.

Notice the large depth Z_b, or height S (measured vertically), needed in both

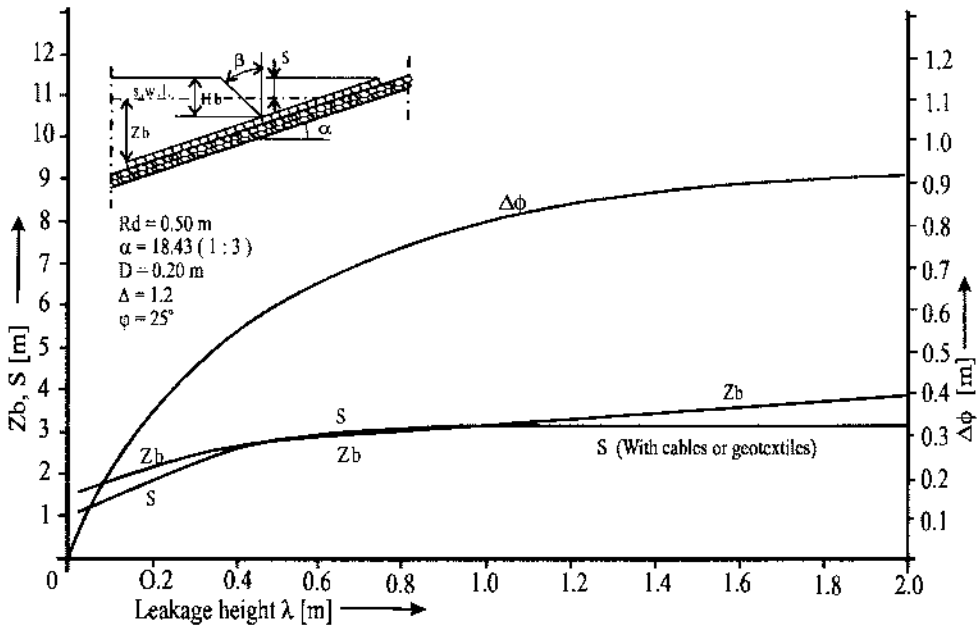

Figure 5.15 Revetment extent needed to guarantee stability for sliding of a revetment, loaded by a breaking wave, assuming equilibrium without toe structures or anchorages

cases to guarantee stability. In practice these are often not available, which means that toe structures, or in case of block mattresses, anchorages are needed.

5.5.6 *Concluding remarks*

Toe constructions and/or anchorages are often necessary. Without these, a large extent of the cover layer might be needed to guarantee equilibrium for sliding.

Notice that the friction angle between blocks and filter or subsoil might be smaller than the angle of internal friction of the material underneath the cover layer. A safe estimate for this interface friction might be $\delta = \frac{2}{3}\varphi$.

When the friction between blocks and a geotextile is necessary to guarantee stability, it is advised to perform some simple shearing tests.

For relatively thin revetments, the stability for buckling should be considered too.

5.6 FIELD STUDY OF BLOCK-MATTRESSES

In the autumn of 1986 soon after installation damage to the block mattresses at the test site on the 'Houtribdijk' near Lelystad was observed, see Hernandez, (1989), just south of the ship locks at the IJsselmeer side. In a storm of intermediate level, the local wave conditions were sufficiently severe, that the block mattresses where loaded above their strength and, as a consequence were severely damaged see Fig. 5.16

Figure 5.16 Damaged block mattresses at the test site near Lelystad at the IJsselmeer dike. Notice the fissure between the upper and the middle mattress, where the middle mattress has moved downward.

Table 5.2 Dimensions of the block-matresses at the Test-site Lelystad

	S mm	*B* mm	*L* mm	*D* mm
V.O.B	25	375	310	150
Armorflex	20	300	340	150
Beto	20	400	320	170
Asam	15	300	380	170

Where:

S = dimension of the crevices between the blocks
B = block length
L = block width
D = block thickness

At the test site, several types of block mattresses where placed, see Table 5.2 Because it was a test site, the revetments where constructed with a minimal factor of safety, as it was feared that otherwise the relevant behaviour of the structure would not show itself. The analysis afterwards was complicated by the fact that the instrumentation for wave registration was not operational at the time of the damage.

The case was studied by Hernandez (1989) with respect to

- *Uplifting of the revetment*
- *Sliding stability*
- *Soil instability (including liquefaction)*

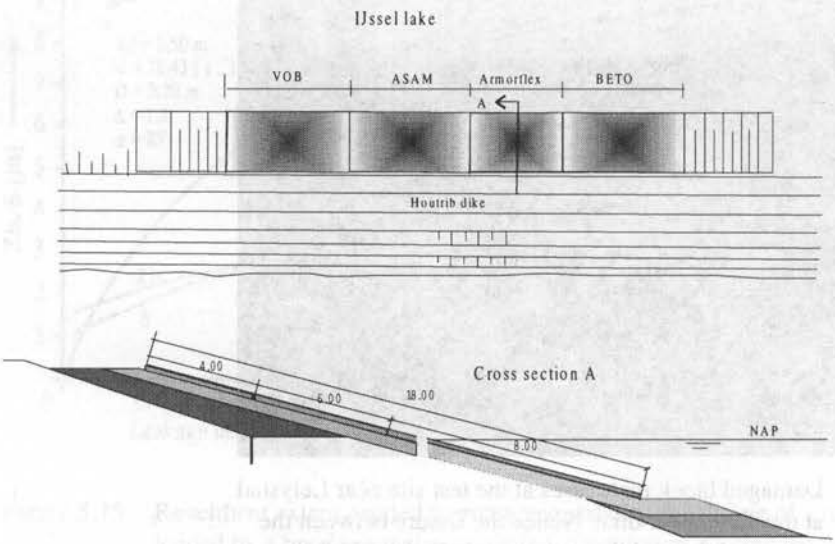

Figure 5.17 Block-mattresses at the test site near Lelystad

Table 5.3 Position of the matrasses on the slope

Section nr.	*Length m*	*Height with respect to N.A.P.*
1	4	+ 2.5 - +1.5
2	6	+ 1.5 - N.A.P.
3	8	NAP - - 2.0

For the evaluation of sliding stability, the theory as described in section 5.5 was applied.

Hydraulic conditions: According to Hernandez, after back analysis and evaluation, and taking into consideration wave registrations at the 'Urker-Hoek', the wave height varied between $1m < H_s < 2m$.. For the analysis it was assumed that the most probable significant wave height was $H_s \approx 1.6\ m.$ in combination with a water level rise due to wind of 1.0 m. The estimated wave period was $T_p \approx$ 5 s.

Materials and geometry: Considering that the characteristic grain-size of the filter-material is $8\ mm. < D_{f15} < 20\ mm.$, the leakage height λ was estimated to be $0.1\ m < \lambda < 0.13\ m.$

The revetment was built on a slope of 1 : 4, and consisted of 3 sections with a variable length (4, 6 and 8 m, as indicated in Fig. 5.17).

Uplifting: Based on the analytical model, see 5.3.2., using the Wolsink boundary condition for wave loading, and the estimated leakage heights, it was concluded, that the V.O.B. and Beto mattresses would be stable up to the maximum wave height of 2.0 m, the Armorflex mattresses up to a wave height of 1.9 m and the ASAM mattresses up to a wave height of 1.6 m. Therefore uplifting was not regarded as a dominant mechanism which could explain the damage.

All mattresses where classified in the stability class 4 as defined as section 5.5.3, for wave heights above 1.4 m, (which means that the blocks where partially depending on friction or restricted inflow of water for there reliance of stability). For some parts of the mattress the uplift pressure was above the block weight. As uplift is not the main topic of this section the details of the analysis are not elaborated further.

Uplift alone could not be identified as the main cause of failure. Further attention was therefore given to sliding stability.

Sliding: The mattresses where placed above each other on the embankment, and the connections between the adjacent mattresses were improvised. The extra length of the steel wires within the mattress where knotted around blocks of adjacent mattresses but not in such a way that significant deformations where prevented. As can be observed in Fig. 5.16, the middle mattress was displaced

Table 5.4 Parameters, revetment Lelystad

Parameters (see also Fig. 5.11)		*Mean value* μ	*Standard deviation* σ
Breaker height	*HB*	1.5 m	0.25 m
Breaker angle	β	40°	1°
Leakage length	λ	0.12 m	0.01 m
friction angle (adhesion)	δ	21°	1°
Dimensionless submerged weight	Δ	1.2	-
Slope angle	α	14.036 ° (1 : 4)	-
Block thickness	*D*	0.15 m	-
Revetment downwards	*Zb*	1.0 m	-
Revetment stretch upwards	*S*	1.0 m	-
Water table in filter	*Z1*	0.85 Hb	-
Rundown	*Rd*	0.4 Hb	-

downward on the slope for distances of between 0.1 and 0.2 m. Therefore the stability of the middle mattress was evaluated for the parameters shown in Table 5.4. (the variance σ^2 is added for the statistical analysis). Next the calculation of the design point, the combination of parameters with the highest probability of failure, will be described.

Using the mean value of Table 5.4 for the parameters, the stability factor against sliding for the mattress is calculated as a Γ_2 of 0.38, assuming that compressive forces cannot be transferred. This indicates that the wave loading exceeds the capacity for sliding of the structure.

To derive more insight into the extent of the overloading an AFDA (Approximate Full Distribution Analysis, see Vrouwenvelder & Vrijling (1982)) calculation was made, where the design point is calculated by updating the characteristic values, in such a way that the lowest Probability index, β (or safety level) is calculated.

Applying the updated level II method, the design point is calculated using the parameters of Table 5.4 and accounting for the standard deviation. The results of this analysis are shown in Table 5.5.

The results show that a breaker height, Hb, of 1.12 m, in combination with the other parameters, gives the most likely combination of instability. From this result it is concluded that because the observed wave-front height is significantly higher, that sliding is likely to be a dominant mechanism in the observed instability.

Table 5.5 Lelystad, sliding of revetment (lelystd1.dta); Design point

Date: 11/ 6/1997 Time: 14/5/3.9

Iteration 6. Difference Beta with former iteration 1.0E-0009

Beta = 1.938

Prob. Failure = 2.6E-0002

BTF = 1.863E-0009

Variable	Distr.	A	B	C	Mean vall (μ)	St.dev(σ)	Startvalue
Hb	N	1.500E+0000	2.500E-0001	2.000E-0001	1.500E+0000	2.500E-0001	1.000E+0000
Beta	N	4.000E+0001	1.000E+0000	0.000E+0000	4.000E+0001	1.000E+0000	4.000E+0001
Lambda	N	1.200E-0001	2.000E-0002	0.000E+0000	1.200E-0001	2.000E-0002	1.200E-0001
Phi	N	2.100E+0001	1.000E+0000	0.000E+0000	2.100E+0001	1.000E+0000	2.000E+0001

Variable	Design point	$\frac{\partial Z}{\partial X_i} X_i$	$\frac{\partial Z}{\partial X_i}$	$\frac{\partial Z}{\partial X_i}\sigma_{X_i}$	$\left\{\frac{\partial Z}{\partial X_i}\sigma_{X_i}\right\}^2$	α^2
Hb	1.1257830	1542.4628343	1370.1245189	342.5311297	117327.5748258	0.596
Beta	40.0247043	-226.2647776	-5.6531280	-5.6531280	31.9578565	0.000
Lambda	0.1068502	803.8078778	7522.7580965	150.4551619	22636.7557511	0.115
Phi	22.0410395	-5250.6825767	- 238.2230014	-238.2230014	56750.1983774	0.288
				---------- --------- +		
				196746.4868107		

σ(Z) = 443.5611; μ(Z) = 859.7862

Number iterations = 6 Calculation Time =11969.999969 ms

5.7 CONCLUDING REMARKS

Although in recent years more attention has been focussed on interaction between blocks, the analysis of stresses in the cover layer, and its influence on the strength of the cover layer, needs more attention. The influence of block arrangement on the stresses in the cover layer, and a proper arrangement to enhance the pre-stress in the layer might contribute to the overall capacity of the revetment to withstand wave action. Blocks arranged in rows along an embankment might be less advantageous. If the block arrangement would be based on rows that are arranged perpendicular to the embankment, there is less chance on blocks without interlock, because the normal force caused by blocks higher on the slope would be more directly subjected to lower blocks.

The development of a numerical model for the analysis of groundwater flow in coarse materials was described. The model includes the capability to calculate the water table within the mesh, using a crude model for the interface between

saturated and unsaturated zones. The model was verified making calculations both with a Newton-Raphson as well as with a Modified Newton-Raphson iterative scheme. The results were compared with more simple semi-empirical analytical solutions. A sufficient agreement was found to adopt the numerical implementation.

The attribution of strength due to undrained behaviour of a revetment, i.e. the restricted inflow of water in cavities that are created when a block is uplifted due to a positive pressure difference under and above a block, is not safe for the situation of oblique wave loading. Since oblique wave loading is a natural condition for most revetments it must be considered unsafe to account for the undrained strength of revetments. The validation of models with experiments in the Delta-flume has to be accounted for this effect.

A model for the evaluation of sliding stability of a cover layer for an embankment loaded by waves was developed. The model is composed of empirical sub-models that have been validated by experiments. The overall behaviour of the model was evaluated in a back analysis of measurements and observations of the Test-site near Lelystad. It is advised to develop appropriate partial safety factors to be used for the application of the model for design purposes.

The analysis of the test site at Lelystad, has shown that although, the apparent strength against uplifting was sufficient, the overall strength of the revetment was not sufficient. If the uplift pressure exceeds the block weight, the local capacity against sliding is exceeded too. Therefore the revetment has to be evaluated as a structure. Toe structures and/or anchorages should get proper attention and should be evaluated as structural elements, giving attention to the forces acting on these elements.

The situation that a cover layer is designed for uplift pressures, higher than its self weight must continue to be viewed with suspicion, as this implies that there are large hydraulic gradients perpendicular to the slope in the under-layers.

Considering the deformed surface of the revetments at Lelystad after the overloading, and noting that the cover layer was considered stable for uplifting, the substantial change in the contours of the cover layer surface can only be explained by severe instability of the under-layers. If the sliding had been the only mechanism, the mattress would only have shifted down the slope.

CHAPTER 6

Flexible retaining walls

6.1 INTRODUCTION

This chapter describes the development of models for the analysis of flexible retaining walls, as completed by the author.

Since the work of Blum (1932), the analysis of this type of structure has been based on a relatively simple, but powerful, concept. This concept consists of an equilibrium analysis of the structure combined with a plasticity analysis to estimate the horizontal stresses in the soil. The effectiveness of this approach is indicated by the fact that it has been in use successfully for over 60 years, only with minor adaptations to the method.

A drawback of the method developed by Blum is that it does not enable the analysis of multi-anchored systems, or staged construction, without the need for additional assumptions. A second drawback is that the uncoupling between the deformations and the equilibrium analysis might lead to the calculation of deformations that are in contradiction with assumptions on which the soil loading is based. As an example the model cannot cope with the fact that active soil loading is assumed for all levels, on the side of the flexible retaining wall with the highest ground level. One of the premises is that the wall will move away from the retained soil mass. Due to the rotation of the wall, the wall might deform, and parts of the wall might rotate against the soil mass. For the zone above the anchor, the assumption of active soil loading would not be valid anymore then. To deal with this drawback in practice, additional relations for the soil loading in the active zone were adopted. According to the EAU (1996), a redistribution of the soil loading has to be taken into account as a function of the depth of the anchor in relation to the retained soil height.

When in the late seventies and early eighties computer facilities expanded, numerical schemes were considered to eliminate these problems. Among others in the 1970's the Dutch Public Works department developed the computer-code DAMWAND, a subsystem of the Genesys computer system. DAMWAND was based on Finite Element techniques. Verruijt (1983), developed an approach based on Winkler's theory (i.e. a subgrade reaction model). This development enabled the analysis of, multi-anchored structures and staged construction. The new approach calculates the soil loading depending on the loading path.

When 2D finite element analysis advanced sufficiently for Mohr-Coulomb

models of soil behaviour to be available, the possibility for further development of models for soil retaining structures, including 2D effects such as coupled soil behaviour, implicit evaluation of groundwater flow and consolidation was opened. The development of finite element techniques for the analysis of sheet pile retaining walls is the main topic of this chapter.

To start with some functional considerations on flexible retaining wall design is discussed, relating sheet pile design to a wider frame of reference. Recognising that functional analysis, and spatial design, always precedes structural analysis, some remarks on the functional value of the soil retaining walls are made.

Continuing the main line of methodology that is formulated in chapter 3 of this study, modes of failure are discussed. The knowledge of failure modes is thought to be fundamental for the development of concepts for the analysis of structures in the ultimate limit state.

The modelling of the structural behaviour is also discussed. To begin with, the empirical theory of Blum is described. Subsequently piecemeal developments, such as the addition of subgrade reactions and 2D finite element modelling are described. Within the framework of finite element analysis, the development of structural elements for the combination with 2D finite elements, for the computer code PLAXIS are discussed.

To give recognition to the fact that besides observation, logic is a powerful source for the development of models, verification is also discussed. Upper bound and lower bound solutions are derived and these are used to evaluate finite element results.

Finally within the framework of validation, the sheet pile test in Karlsruhe 1993 will be discussed. The class A prediction, see Lambe (1973), which was made will be described. Some of the main characteristics of the test itself, and a back-analysis of the test, are described. Based on this, some remarks on model uncertainty will be made, and finally some conclusions will be drawn.

6.2 FUNCTIONS OF FLEXIBLE RETAINING WALLS

A flexible retaining wall is a driven sheet, of wooden, steel or concrete piles or plates with flexibility to interact with the deformation of the soil, to bear the loading of the retained soil. Flexible retaining walls are mainly loaded perpendicular to the length axis and are used to retain soil and/or water, and to prevent erosion.

Flexible retaining walls are often used to stabilise the embankment of canals or rivers, or to form a deep excavation, or a quay wall. As a secondary function, the relatively low permeability of the wall as a screen is used. The latter function is not considered in further detail in this study.

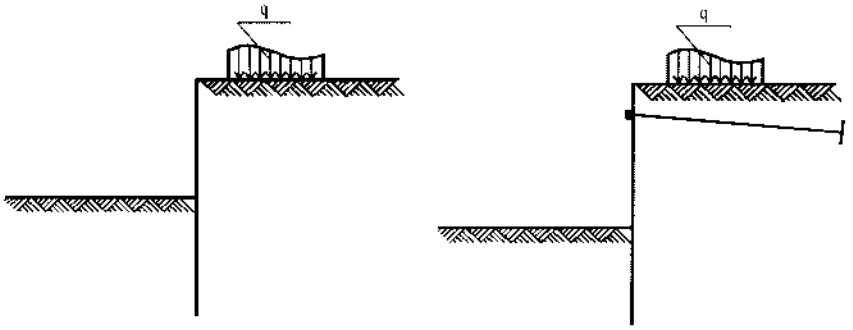

Figure 6.1 Flexible retaining walls. Left cantilever, right single anchored

From the point of view of structural analysis, two basic concepts may be recognised, see Fig. 6.1:

- *The free standing cantilever wall*
- *The anchored (or strutted) wall*
  - *free earth supported*
  - *with a fixed earth support*

Whereas the free earth supported anchored wall has a minimum of length, and therefore does not have an additional capacity to develop a cantilever bending moment at the toe of the wall, the fixed earth support has additional length and therefore additional capacity.

Here strutted walls will not be treated separately from anchored walls. In view of the mechanical performance, the behaviour is similar, and the slight differences that might occur will not be discussed.

For permanent structures, anchors are often used to limit the deformations, especially if the retaining height is large.

Although the free standing cantilever wall, and the free earth supported anchored wall, may be analysed as statically determined structures, if rigid plastic soil behaviour is assumed, if a more general view is taken, flexible retaining walls are multiple statically indeterminate. Therefore the mechanical model has to be simplified significantly, to reduce the calculation effort. These simplifications must be justified by the modes of failure, which are appropriate for the force distribution in the ultimate limit state. Before discussing failure modes in section 6.2.3, some of the main functions for a flexible retaining wall will be discussed in the next section.

6.2.1 *Functional aspects of flexible retaining walls*

For the development of the CUR Sheet-piling handbook (1993), functional analysis was put forward to derive a logical order in the content of the book. The extent of this functional analysis was only limited. Some elements of this functional analysis with be put forward in this section.

Table 6.1 Sheet piling configurations

Sheet pile structures	*- Cantilever*		
	- Anchored	*- Anchor rod(s)*	*- Single anchor*
			- Multiple anchor
		- Buttress type	
		- Stress relieve floor	
	- Celled wall type		
	- Other types	*- Double sheet pile type*	
		- Multiple strutted	

To begin with sheet pile functions were classified according to use and also in terms of the form of the structure. This classification considered:

- *The perspective of the user*
- *The perspective of the structural analyst*

The user perspective was concerned with the functions of a flexible retaining wall. The perspective of the structural analyst, which is summarised in Table 6.1, was more concerned with the mechanical aspects of the structure.
The perspective of the user leads to a more extensive set of functions as shown in Table 6.2

In this Table the structural types are listed on the vertical axis and the sheet pile functions to be considered are listed in the columns.
From the user perspective, the following functions have been recognised:

- *Soil retention*
- *Water retention*
- *Waterproofing*
- *Load bearing*
- *Erosion prevention*
- *Guidance*

The structural types are also classified with respect to time, i.e. temporary or permanent structures.
The necessary safety level is estimated from the functional characteristics and the estimated life span of the structure. These safety levels are given in Table 6.2, where one star (*) represents a low level and five star (*****) a high required level of safety.

This safety approach might be made more objective, balancing the marginal value of the functions with the marginal value of risk, as discussed in chapter 2. The more functions a structure has to perform, the more the marginal value of the risk shifts to higher safety levels. Assuming the economic 'law' of diminishing added value, a higher marginal value leads to a higher safety level. Further

Table 6.2 Sheet pile functions

	Retention		Bearing		Erosion	Water	Guidance	Temp./	Safety	Steel	Concrete	Wood	Plastics	Bentonite
	Soil	Water	Vert.	Hor.	protection	tightening		Perm.	High-M-Low					
Deep excavations														
Steel sheet piling	m	m	s	s	s			T	**	**				
Berlin wall	m		s	s	s			T	**	**	*	*		
Piled wall	m	s	s	s	s			T/P	***	*	**	*		
Deep wall	m	m	s	s	s	s		T/P	***		**			**
Combined wall	m	m	s	s	s	s		T/P	***	*				
Locks														
Chamber wall	m	m		s	s	s	s	P	***	**	**	*?		
Guide walls	m	s			s	s	s	P	***	**	*	**		
Seepage screen		m			m	s		P	***	**		**		**
Anchor walls				m				P	****	**	*			
Quay wall														
Guide walls	m	s	m	s	s	s	s	P	***	**	**	*?		
Combined wall	m	s	m	s	s	s	s	P	****	**	*			
Coffer dam	m	s	m	m	s?	s	s	P	****	**	*?	*		
Cell dam	m	s	m	s	s	s	s	P	****	**				
Bank protection														
Sheet pile wall	m	s		s	m		s	P	*	**	*	**	*?	
Toe protection	s			m	m		s	P	*		*	**		
Seepage screen		m			m		s	P	**	**			*?	
Environmental appl.														
Excavation	m	s	m?		s			T	**	**				
Isolation		s				m		P	*****	*	**		**	**
Noise retaining wall			s	m				P	*	**	**	**	*	*
Auxiliary														
Deepened roads	m	m			s	s		P	***	**	**		**	**
Dike reinforcement	m	m			m			P	****	**	**			
Pillar				s	s		s	P	****	**	**			
Stream guiding		m					m	P	*	**		**		
Skirts	m	m	m	m	m	s	s?	P	***	**				

m = main function
s = secondary function

discussion of this topic, however, is beyond the scope of this study.

In the next section, a discussion is given of the way in which functional value may be quantified.

6.2.2 *Functional value of soil and water retaining structures*

Soil Retention: The value of soil retention is related to the soil surface gained by avoiding a sloping interface between surfaces at a different level.

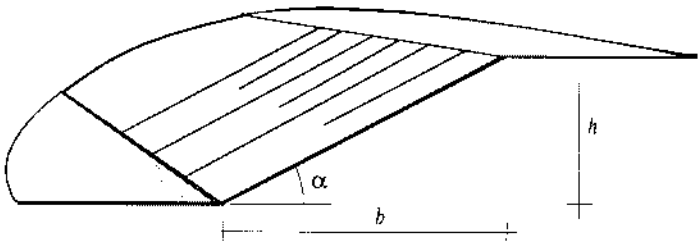

Figure 6.2 Sloping terrain

The functional value per length might be estimated as the area gained multiplied by the value of soil per unit area, C_a, to give:

$$Fw_{soilretain} = bC_a = \frac{h}{\tan\alpha} C_a \tag{6.1}$$

Where

b	=	*width*
C_a	=	*value per area*
h	=	*retained height*
α	=	*slope of the intermediate surface*

When the retaining wall is meant to fulfil an additional function, such as the transfer of cargo for a quay wall, the analysis is more complex. This will not be elaborated further.

Water Retention: The value of water retention might be estimated in analogy with the safety of a dike ring, for water defence purposes. For this situation an added value per unit metre area protected by the dike is estimated. This area can be identified by the length of the water-defence, multiplied by an influence length, λ_i.

The parameter λ_i might be estimated by considering the area enclosed of the water, divided by the length of the dike ring:

$$\lambda_i = \frac{A}{\oint_l dl} \tag{6.2}$$

Where A is the area enclosed of the water, and $\oint_l dl$ is the circumference.

For a rectangular excavation, $\lambda_i = \frac{b*l}{2*(b+l)}$, whereas for a circular polder, $\lambda_i = \frac{\pi r^2}{2\pi r} = \frac{r}{2}$. The added value must be related to the economic activity within the area.

If the area is an excavation for an underground car park in a city, the value will be different to that of an agricultural area such as a polder.

The functional value per length unit, with respect to water retention might therefore be:

$$F_{v\ water\_retainment} = \lambda_i C_b \tag{6.3}$$

where C_b = added value for activity

Erosion Prevention:_The value of erosion prevention is the market value of the rate of erosion depth, $D_{erosion}$, multiplied by the retained height, h, and the cost of repair C_r, giving:

$$F_{v\ erosion} = \sum_{i=1}^{n} \frac{1}{(1+r)^n} D_{erosion}\, hC_r \tag{6.4}$$

Load Bearing: The functional value of load bearing might be diverse and cannot be defined explicitly in advance. The value of bearing a crane on a flexible retaining wall placed for the retention of a deep excavation for 6 months, for example, is different from the situation that a flexible retaining wall is part of a quay wall in the Rotterdam harbour, where a container crane has to be supported for a life-span of, perhaps, 20 years.

6.2.3 *Failure modes: mechanisms for flexible retaining walls*

Introduction

In the preceding section external functions for the flexible retaining wall were regarded. External functions are related to the use, the purpose of the structure. In the next section the attention is shifted to mechanical aspects of the structure. One might regard these mechanical aspects with respect to the fulfilment of internal, (mechanical) functions.

To gain a better understanding of the mechanical functions, which are mainly related to soil retention and water loading, various failure modes may be identified as discussed below.

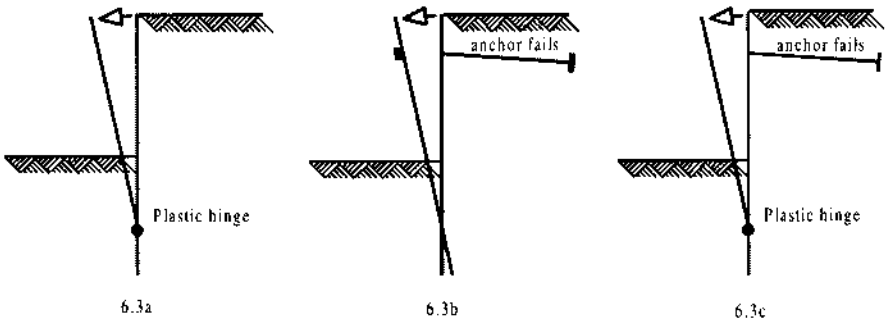

Figure 6.3 Structural failure mechanisms for walls with a fixed earth support: 6.3a, Cantilever plastic hinge, 6.3b, anchored, failure of anchor, 6.3c: anchored, combined.

Failure of flexible retaining walls can be classified in two ways.

- *structural failure*. Failure of the wall itself, i.e. the development of a plastic hinge in the wall, or failure of an anchor or a strut.
- *soil failure.*

Notice, that structural failure of a retained wall, implies that the soil fails too. The reverse is not always true.

Structural failure

For walls with a fixed earth support, the following mechanisms of structural failure are feasible.

1. For a cantilever wall, a plastic hinge develops near the base of the wall, see Fig. 6.3a. The soil mass will move forward above the position of the hinge.
2. Failure of the anchor, followed by failure of the soil mass, see Fig. 6.3b.
3. Failure of the anchor followed by large deformations in the soil mass and the

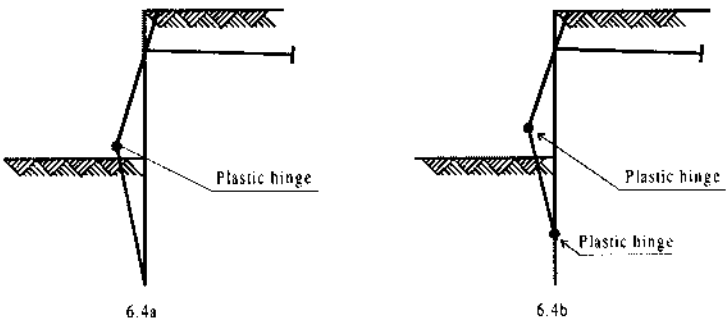

Figure 6.4 Structural failure in the flexible retaining wall. 6.4a. For a free earth supported wall, a plastic hinge in the 'field'. 6.4b. for a fixed earth supported wall, failure by two plastic hinges.

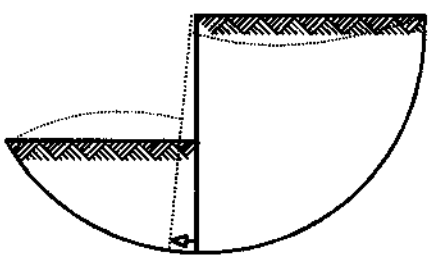

fig 6.5a

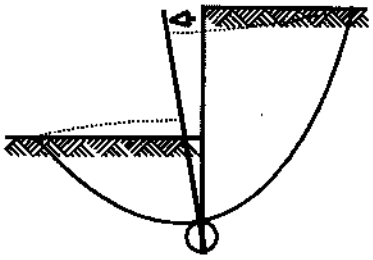

Fig 6.5b

Figure 6.5 Soil failure of a flexible retaining wall. 6.5a: Shear failure for wall that is too shallow. 6.5b. Shear failure where the top bends over formation of a plastic hinge near the base of the wall. See Fig. 6.3c

Two more structural failure mechanisms may be identified.

1. For an anchored wall with a shallow penetration, i.e. a free earth supported wall, a plastic hinge developing in the span of the wall. This leads to soil failure, and therefore failure of the whole wall. (see Fig. 6.4a).
2. For a fixed earth supported wall, two hinges need to develop for a mechanism to develop, see Fig. 6.4b.

These mechanisms are rarely observed because anchor failure usually precedes the development of plastic hinges in the wall. Apparently, in practice, anchors were often under-designed in the passed.

Soil failure

For the case where anchors are absent, and the wall is sufficiently strong, two more modes of failure may be identified.

- A traditional circular shearing failure in the soil, similar to the mechanism analysed for slope stability, (see Fig. 6.5a).
- A wedge shaped failure zone behind the wall, combined with a rotational soil failure in the sub soil, (see Fig. 6.5b).

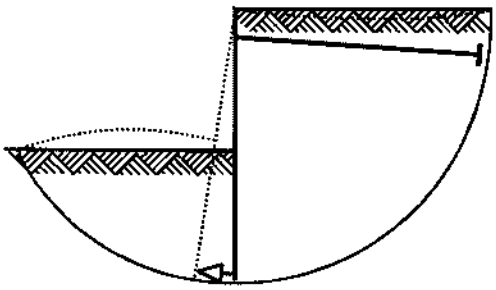

Figure 6.6 Shear failure of an anchored flexible retaining wall with a penetration which is too small.

Finally the case of a shearing failure for an anchored wall may be identified.

- This shearing failure, which is similar to case 6.4a, might occur for the case of a wall that is too shallow, where the passive zone in front of the wall is too small to provide sufficient resistance (see Fig. 6.6).

This overview is not exhausting, e.g. cases where plastic hinges occur at the anchor height were not discussed, because these are rarely observed in practice. It is thought, however, that basic insight into the failure modes that are described here contributes to a more objective approach for flexible retaining wall design.

6.3 STRUCTURAL ANALYSIS FOR FLEXIBLE RETAINING WALLS

6.3.1 *Soil loading*

In the previous section, failure modes for simple flexible retaining walls were described. One of the observations is that the primary direction of loading, and subsequently of deformation of the structure is horizontal. Only minor wall rotations occur. Based on this, a first assumption for the derivation of the soil loading on the wall is that:

> *' Interaction between soil and the structure has a negligible effect on the vertical stresses in the soil'*

A first estimate for the soil loading may therefore be derived using Rankine

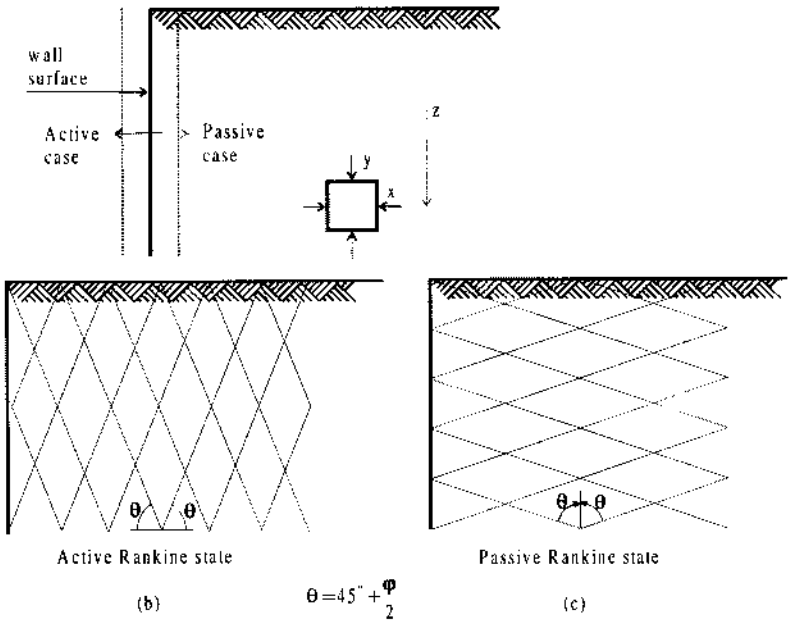

Figure 6.7 Active and passive failure for a smooth wall according to Rankine's theory, (see Craig (1978))

theory, see Craig (1978). This theory considers two main 'ultimate' loading conditions for the soil depending on whether the soil is compressed or extended. Active soil stresses are assumed for extension and passive stresses for compression, see Fig. 6.7.

As it is assumed that wall does not influences the vertical stresses in the soil, the horizontal stresses on the wall can be derived from the vertical soil stresses adjacent to the wall by only assuming equilibrium and the Mohr-Coulomb failure criterion. The effective vertical stresses are obtained by integrating the soil weight of the soil layers beginning at the soil surface and downward and then subtracting water pressures.

According to this theory, the effective horizontal stresses are;

$$\min(\sigma'_h) = \lambda_a \sigma'_v - 2c\sqrt{\lambda_a} \tag{6.5}$$

$$\max(\sigma'_h) = \lambda_p \sigma'_v + 2c\sqrt{\lambda_p} \tag{6.6}$$

Where c is the soil cohesion, λ_a is the coefficient of active soil pressure, λ_p is the coefficient of passive soil resistance and σ'_v is the vertical effective stress in the soil. Instead of λ_a and λ_p these parameters are sometimes indicated as K_a and K_p, which have the same meaning. Using these assumptions, the soil loading distribution for a wall without groundwater, such as shown in Fig. 6.8, can be derived.

The examples in this section are for the case without groundwater. If static groundwater is present, the influence can be included by assuming a hydrostatic pressure distribution and adding this to the effective horizontal stresses acting on the wall.

When deriving the effective horizontal soil stresses, the submerged weight of the soil must be used because active and passive soil coefficients are only relevant for effective stresses.

When there is seepage underneath the toe of the wall the approach described

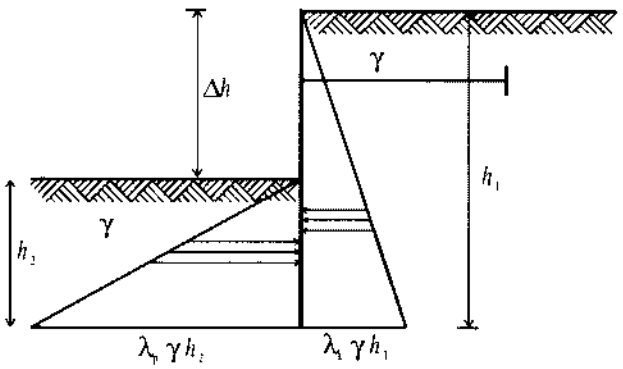

Figure 6.8 Effective soil pressures on a free earth supported sheet pile wall according to Rankine's theory

here is not valid. In that case groundwater flow models have to be used. Groundwater flow is discussed in chapter 5 and is not discussed further here.

Wall friction and the influence of curved shear surfaces

For a wall without adhesion, the coefficients for active and/or passive failure defined in equations 6.5 and 6.6 are given by

$$\lambda_a = \frac{1 - \sin(\varphi)}{1 + \sin(\varphi)} \tag{6.7}$$

$$\lambda_p = \frac{1 + \sin(\varphi)}{1 - \sin(\varphi)} \tag{6.8}$$

Were φ is the angle of internal friction of the soil. If there is friction at the wall/soil interface, the formulae have to be extended. According to Müller-Breslau (1947), (see also Gudehus (1980)), assuming straight shear surfaces, if both soil surfaces are horizontal and if the wall is vertical, the appropriate formulae are:

$$\lambda_a = \left(\frac{\cos(\varphi)}{1 + \sqrt{\frac{\sin(\varphi + \delta_a)\sin(\varphi)}{\cos(\delta_a)}}} \right)^2 \tag{6.9}$$

$$\lambda_P = \left(\frac{\cos(\varphi)}{1 - \sqrt{\frac{\sin(\varphi - \delta_p)\sin(\varphi)}{\cos(\delta_p)}}} \right)^2 \tag{6.10}$$

where δ is the angle of wall friction. Normally it is assumed that $\frac{1}{2}\varphi < \delta < \varphi$. It should be noted that for the more common cases, δ_a is positive and δ_p is negative. When δ is zero, the equations 6.9 and 6.10 reduce to 6.7 and 6.8.

From observations we have seen that for a high friction angle and/or a high wall friction the shear surfaces are not straight anymore, but curved. At the active, the soil retained side this will lead to a minor reduction in the soil loading. At the passive side however, curvature of the shear surface may lead to a major reduction in the capacity to give resistance. Therefore, for dense sand, which has a high friction angle φ, and consequently a high wall-friction angle δ equation 6.10 may overestimate the passive resistance. For a soil friction angle of 35° or higher a value for λ_p might be calculated with equation 6.10 of up to 10 or higher, which is unrealistic. In fact, for friction angles above 30° it is more likely that the soil behaviour will be determined by the curvature of the shear surface, which is

also influenced by the boundary conditions of the problem and cannot be generalised. In practice, any value of λ_p higher than 6 has to be treated with caution. In that case it is advisable to derive values for passive resistance based on non linear slip surface analysis, which tend to give a much lower value of λ_p.

Solutions for this problem have been published by Caquot & Kerisel (1948). These solutions seem to account for the wall friction in a more consistent way, as good agreement is obtained between empirical calculations based on Caquot and Kerisel, and finite element analysis, see section 6.4.2.

These assumptions about soil behaviour give a first estimate for soil loading on inflexible walls. The assumptions are based on the theory of plasticity. Deformations are assumed to be sufficiently large for plastic strains to develop. For a more refined model the development of stresses as a function of strains and 3D based material modelling is necessary. These advanced aspects are implicitly taken into account when the 2D finite element analysis is adopted. With the developments described in section 6.3.4, the material modelling such as introduced in section 4.6 become possible. First, however, the empirical model of Blum will be described.

6.3.2 *The method of Blum*

The first relatively powerful approach for the analysis of sheet pile walls was derived by Blum (1931). Blum took two equilibrium equations: $\sum H = 0$ (sum of horizontal forces), and $\sum T = 0$ (sum of moments), and combined this with the Rankine assumptions for soil loading. For a cantilever wall these equations can be solved analytically.

To extend this approach to anchored walls, Blum introduced the concept of a concentrated force at the toe of the wall. This assumes that the forces resisting rotation at this level are local and within the limits of engineering approximation can be modelled as a concentrated force. This concentrated force, denoted as C^p, is the resultant of the passive soil resistance. Since this resultant force needs

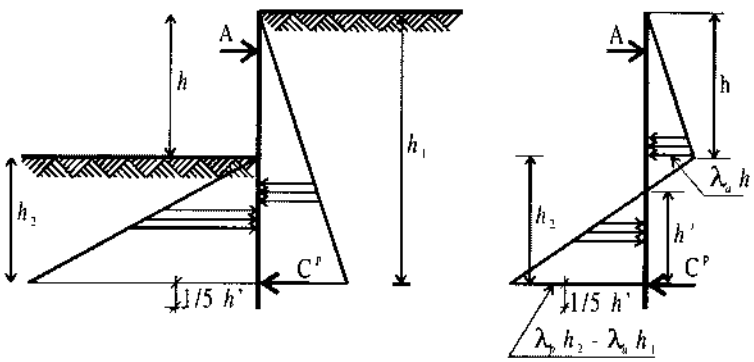

Figure 6.9 Anchored sheet pile wall. Resulting force , Scheme according to Blum (1931)

some spatial length to develop, Blum suggested extending the flexible retaining wall by 20 % of the height of the net passive zone. For the case shown in Fig. 6.9 this means 0.2 h', This supplementary length should, therefore, not be considered as extra in the sense of safety. It is simply needed to develop the force C^p.

The method of Blum is closely related to the graphical design method as shown in Fig. 6.10, which enables the integration of local soil loading recognising different soil layers, and the derivation of the bending moments diagram. As the introduction of an additional force to model the anchor introduces an over determination of the variables in the equations there is some freedom for the structural analyst to choose an equilibrium state. This is illustrated in Fig. 6.10 where the closing line in the graph may be chosen by the analyst. In my view, a calculation according to Blum means, that, the 'closing' line is drawn such that the cantilver moment at the toe is equal to the moment in the span. Subsequently, as discussed earlier, the penetration length is extended by 20 % of the height of the net passive zone.

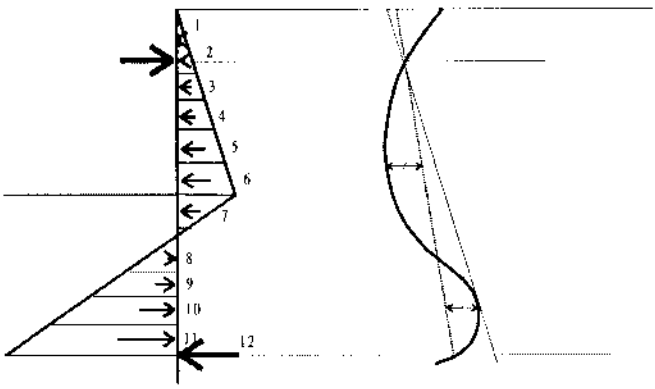

Figure 6.10 Graphical scheme proposed by Blum, (1931)

Safety considerations in combination with the application of Blum's scheme
After that the required pile length is determined the bending moments and anchor forces may be calculated. The shape of the sheet pile sections and the anchor 'thickness' can then be determined. For a wall in sandy soil it is usually practice to reduce the component of bending moment in the span corresponding to the effective soil stresses by a 1/3. For a wall in clay or peat, no such a reduction is allowed. For all cases, both for sand, clay or peat, the anchor or strut force used for design should be taken 15 % higher than values obtained from the analysis. (see EAU 1996: E 77).

These modifications to the values calculated using the Blum method are based on the observation, that prototype measurements indicate smaller bending moments and larger anchor forces than calculated.

6.3.3 *Subgrade reaction models*

According to Blum, active soil pressure is assumed for all of the retained side of the wall, even above the anchor. A more refined analysis taking into account deformations, however, might indicate compressive strains above the anchor, suggesting that a passive soil reaction is more likely. Similar behaviour might occur at the toe of the wall, although it is of minor importance because the concentrated force C^r implicitly takes this into account.

To include these effects, a more refined description of the structural deformation and soil behaviour is needed. The concept of a beam on elastic-plastic springs applying the subgrade reaction behaviour such as illustrated in Fig. 6.11 enables the modelling of these effects. The gradient of the inclined line between active and passive soil pressures is the subgrade reaction modulus. The difference in displacement between active and passive soil pressure, is denoted as the stretch. For sake of completeness, the neutral soil pressure for the situation of zero deformation has to be specified.

In literature several formulae can be found for the neutral soil pressure. A well known relation by Jaky (1944), for normal consolidation, is:

$$\lambda_n = 1 - \sin(\varphi) = K_0^{nc} \tag{6.11}$$

This parameter is often denoted as K_0 as well as λ_n

By Schmidt (1966), this relation is generalised, introducing the influence of the *Over Consolidation Ratio*, the OCR, which gives:

$$\lambda_n = K_0^{nc} \sqrt{OCR} \tag{6.12}$$

The next step in the development of this model, is the adoption of a numerical scheme. Several options are available including the use of finite elements. Where

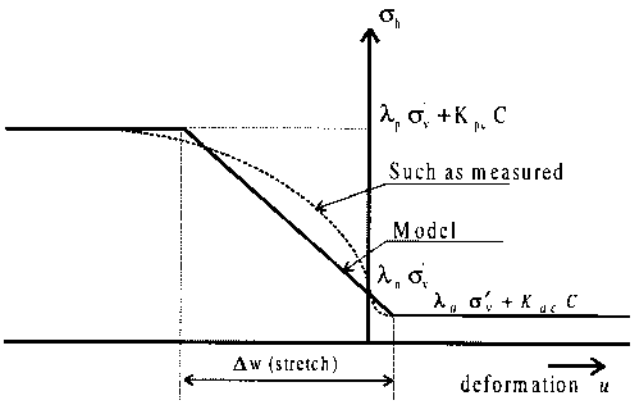

Figure 6.11 Spring characteristic for the calculation of flexible retaining walls using the beam on elastic-plastic springs concept.

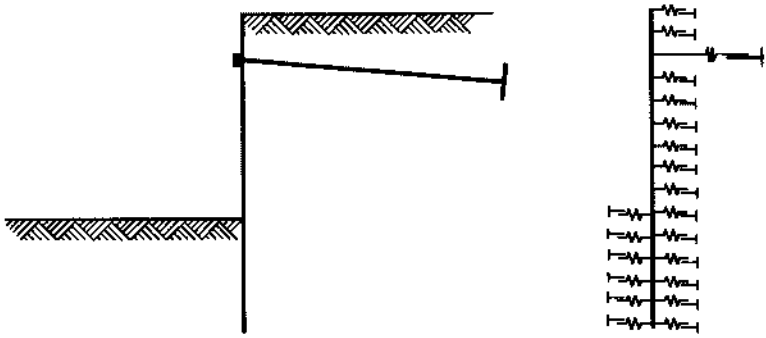

Figure 6.12 Flexible retaining wall modelled as a beam on elastic-plastic springs

the Public Works department developed a model based on Finite Element analysis, DAMWAND, Verruijt (1983) developed a mixed model (equations for forces and displacements) using finite differences. In both cases the wall is modelled as an assembly of small elements. The soil is discretized into a finite number of springs, as shown in Fig. 6.12.

Neutral soil stresses are assumed at the start of the procedure. If that does not result in an equilibrium state of stresses, then in subsequent steps the unbalance is removed taking into account the bending stiffness of the wall. Checking for all springs every iteration, this will lead to equilibrium.
Normally these programs have options to include more than one soil layer, and more than one construction stage.

The application of this type of model is not confined to situations where the analysis of deformations to verify the limit states of equilibrium is obliged. Often it is convenient to use this type of model for less complicated situations. If the model is used on a personal computer, the simplicity and speed of operation make the model easy to use for routine analysis.

6.3.4 *Finite element analysis for flexible retaining walls*

A next step in the development of models for the structural analysis of flexible retaining walls is the application of two-dimensional finite element analysis. Non linear finite element analysis is used in which an elastic-plastic constitutive model is used to describe the soil behaviour.

The basic equations for a finite element modelling have been discussed in chapter 4, and are not repeated here.

Structural elements for 2D plane strain analysis

In 1983 the computer code PLAXIS was mainly a finite element code for the analysis of problems in soil mechanics. Development of structural elements had not been carried out. The first development of structural elements, an inflexible

beam element is described below.

This development work began in 1983. The following two options were considered at the start of this development work:

- *an inflexible beam*
- *a flexible beam*

Both options were investigated thoroughly, and the inflexible beam option was implemented first. The inflexible beam option is appropriate for relatively stiff sheet piling. When approaching a soil failure, the soil stiffness decreases to zero as plastic failure develops. Hence the inflexible-beam option becomes more accurate as a soil failure is approached.

Inflexible beam elements

A short review of the theory of the computer modelling of inflexible beams is given below.

A rigid response of an element implies that nodes of that element if they are part of a straight line remain on a straight line during loading. Therefore a linear relationship between all the nodal displacements of the wall may be assumed. Formally this can be expressed as:

$$\mathbf{a} = \mathbf{T}\mathbf{a}^* \tag{6.13}$$

Where **a** is a vector of all nodal displacements **a*** is a vector of a reduced number of nodal displacements and **T** is a linear interpolation matrix. If there are n sheet piling nodes, giving $2n$ displacement components, then the difference between the number of unknowns in **u** and **u*** is $2n$-3. Note that three sheet pile nodes are retained for a full description of the sheet piling movement.

If this relation is adopted and implemented in the overall system matrix for a mesh, the following set of equations can be derived, (see also equation 4.76):

$$\mathbf{A}\ \mathbf{T}\Delta\mathbf{a}^* = \Delta\mathbf{q} + \Delta\mathbf{p} \tag{6.14}$$

Note that this new set of equations is not symmetrical. To obtain an efficient solution procedure however, symmetry is required. To re-establish the symmetry, both the left and the right hand side of equation 6.14 are multiplied by the transpose of the interpolation matrix **T** to obtain:

$$\mathbf{A}^*\Delta\mathbf{u}^* = \Delta\mathbf{q}^* + \Delta\mathbf{p}^* \tag{6.15}$$

Where

$$\mathbf{A}^* = \mathbf{T}^T\mathbf{A}\,\mathbf{T} \tag{6.16}$$

$$\Delta\mathbf{q}^* = \mathbf{T}\,\Delta\mathbf{q} \tag{6.17}$$

$$\Delta\mathbf{p}^* = \mathbf{T}\,\Delta\mathbf{p} \tag{6.18}$$

Thus, in the solution procedure a condensed stiffness matrix and load vectors can be applied. In practice the original dimensions of the matrix are maintained by introducing dummy variables and equations.

The procedure described here was implemented and verified. The performance of the model is described by Bakker (1987).

Hybrid beam elements

To improve the model, the computer code was extended with elements to model the flexibility of the structural elements. To avoid the use of rotational degrees of freedom, a hybrid formulation for a beam element was applied and implemented. The theory of this element, is described by Bakker (1990) and is only discussed here briefly.

In the derivation of the Euler type of beam element, the virtual work of material points is integrated by using a kinematics relationship between the strains and the curvature of the neutral axis of the beam. This is done by assuming that the relative displacement of a material point lying away from the neutral axis is determined by the change in rotation of the beam under the action of load according to:

$$u(x, y)=u(x)-y\theta(x) \tag{6.19}$$

Where $u(x,y)$ is the deformation at a point y from the neutral axis and $\theta(x)$ is the rotation of the neutral axis of the beam see Fig. 6.13. The longitudinal strain at a material point is the change in displacement with respect to the length axis of the beam giving:

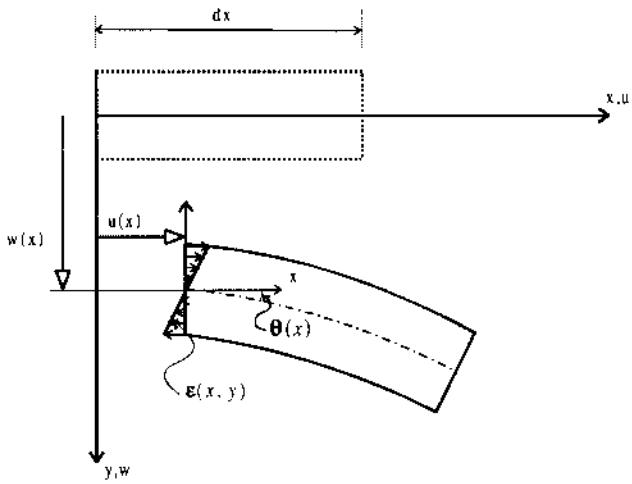

Figure 6.13 Kinematics relation between displacements and deformations in a beam element

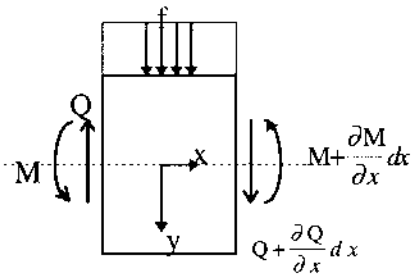

Figure 6.14 Equilibrium of a beam element in bending

$$\varepsilon_{xx}(x,y) = \frac{du(x,y)}{dx} = \frac{du(x)}{dx} - y\frac{d\theta(x)}{dx} = \varepsilon^n_{xx} - y\kappa \tag{6.20}$$

To satisfy compatibility between beam elements, for conventional 2D plane strain elements, compatibility between the global displacements u_x and u_y of common sides of adjacent elements is sufficient. However, as a beam element is a condensed element, it is not sufficient to impose compatibility for points only on the neutral axis. Compatibility of the rotation, θ of the neutral axis is obliged too. The introduction of compatibility of the rotation of the neutral axis, θ, is typical for structural elements, where displacements and strains are determined by a linear kinematics relationship such as given by equations 6.19 and 6.20.

For a rectangular beam element, the internal stresses can be integrated to derive condensed properties, such as normal force N, and bending moment M, as shown below:

$$N = \int_{-1/2h}^{1/2h}\int_{-1/2b}^{1/2b} \sigma_{xx}\,dy = \int_{-1/2h}^{1/2h} Eb\left(\varepsilon^n_{xx} - y\kappa\right)dy = \\ = Eb\left(\varepsilon^n_{xx} - \kappa\,\tfrac{1}{2}y^2\right)\Big|_{-1/2h}^{1/2h} = Ebh\varepsilon^n_{xx} = EA\varepsilon^n_{xx} \tag{6.21}$$

and,

$$M = \int_{-1/2h}^{1/2h}\int_{-1/2b}^{1/2b} \sigma_{xx}\,y\,dy = \int_{-1/2h}^{1/2h} Eb\left(\varepsilon^n_{xx}\,y - \kappa y^2\right)dy = \\ = Eb\left(\varepsilon^n_{xx}\,\tfrac{1}{2}y^2 - \kappa\,\tfrac{1}{3}y^3\right)\Big|_{-1/2h}^{1/2h} = -\frac{1}{12}Ebh^3\kappa = EA\kappa \tag{6.22}$$

Where $A = b\,h$ is the cross-sectional area, and I is the beam moment of area, $I = \frac{1}{12}bh^3$

More generally, for a symmetrical profile in uni-axial bending, the following constitutive relationship for a line element in bending and axial compression may

be identified:

$$N = EA\frac{du_x}{dx} \tag{6.23}$$

and:

$$M = -EI\frac{d^2w}{dx^2} = -EI\kappa \tag{6.24}$$

Where M is a bending moment, EI is the bending stiffness, κ is the curvature of the beam and w is the lateral displacement.

In addition to this, equilibrium requires that

$$\frac{dQ}{dx} + f = 0 \tag{6.25}$$

and

$$-\frac{dM}{dx} + Q = 0 \tag{6.26}$$

Where f is a distributed load, and Q is the shear force in the beam.

Combination of equation 6.25 and equation 6.26 gives the relation between bending moments and distributed load:

$$\frac{d^2M}{dx^2} + f = 0 \tag{6.27}$$

In the approach frequently used in structural mechanics, the equations 6.24 and 6.27 are combined to give the following differential equation relating distributed loads to displacements:

$$\frac{d^2(EI\frac{d^2w}{dx^2})}{dx^2} = f \tag{6.28}$$

As most finite element codes used in soil mechanics, are based on linear displacements only, (i.e. rotations at the nodes are not included), the combination of beam elements and continuum elements is not straightforward. Either rotations must be introduced as degrees of freedom, or an alternative scheme has to be adopted.

The implementation of rotational degrees of freedom would lead to modification of the existing code at that time (1985). An alternative scheme was therefore adopted. The choice was made for a scheme based on a mixed mode approach for the beam element, a hybrid element of the Reissner type. This scheme offered the opportunity to trade the compatibility of rotation for compatibility of bending moments. Structural elements to model sheet pile behaviour are

restricted to a small part of the mesh. This makes it feasible to adopt a condensation procedure to remove the degrees of freedom for the forces from the system matric.

The equations for bending 6.25 and 6.27 are used to derive the element equations. Here the interpolation of the geometry and of the displacements is based on the same functions, such as shown below:

$$x(\xi)=\sum_{i=1}^{n}\mathbf{N}_i\mathbf{x}_i\,, \qquad w(\xi)=\sum_{i=1}^{n}\mathbf{N}_i\mathbf{w}_i \qquad \text{and} \qquad M(\xi)=\sum_{i=1}^{n}\mathbf{N}_i\mathbf{m}_i\,,$$

where x_i, w_i, and m_i are nodal co-ordinates within the element local co-ordinate system, nodal displacements and nodal bending moments, respectively.

Applying Galerkin to discretise the equations 6.24 and 6.27 separately gives the following set of coupled equations: **D**

$$-\mathbf{F}\mathbf{m}+\mathbf{D}\mathbf{w}=\mathbf{0} \tag{6.29}$$

$$-\mathbf{D}^{\mathbf{T}}\mathbf{m}+\mathbf{O}\mathbf{w}=\mathbf{Q} \tag{6.30}$$

Where:

$$\mathbf{F}=\int_{-l}^{+l}\frac{\mathbf{N}^T\mathbf{N}}{E\,I}dx \tag{6.31}$$

$$\mathbf{D}=\int_{-l}^{+l}\mathbf{N}_{,x}^T\mathbf{N}_{,x}dx \tag{6.32}$$

and

$$\mathbf{Q}=\int_{-l}^{+l}\mathbf{N}_{,\mathbf{x}}^{\mathbf{T}}\mathbf{f}\,dx+\mathbf{N}_{,\mathbf{x}}^{\mathbf{T}}\mathbf{m}\Big|_{-l}^{+l} \tag{6.33}$$

To derive a suitable set of equations for implementation in PLAXIS, the equations 6.29 and 6.30 were combined to derive a system matrix. Equation 6.29 was rewritten therefore as:

$$\mathbf{m}=\mathbf{F}^{-1}\mathbf{D}\,\mathbf{w} \tag{6.34}$$

Equation 6.34 is now introduced into 6.30 to substitute the unknown bending moments **m** for unknown displacements **w**. This gives:

$$\mathbf{D}^{\mathbf{T}}\mathbf{F}^{-1}\mathbf{D}\,\mathbf{w}=\mathbf{Q} \tag{6.35}$$

A stiffness matrix suitable for implementation in the computer code can then be recognised as:

$$\mathbf{S}=\mathbf{D}^{\mathbf{T}}\mathbf{F}^{-1}\mathbf{D} \tag{6.36}$$

A disadvantage of this approach is that this condensation procedure cannot be

done for each individual element. As we have to impose continuity in the bending moments, before that the condensation can be performed, the matrices **F** and **D** have to be assembled for all of the adjacent beam elements. Fortunately, this usually involves only a limited number of elements in comparison with the number of soil elements. For the axial stiffness part, a conventional method based on virtual work may be adopted.

Note that equation 6.36 is derived in a local co-ordinate system. Before assembling the system matrix, a transformation to global co-ordinates is needed according to $\mathbf{A} = \mathbf{T}^T \mathbf{S}\, \mathbf{T}$. Here **T** is the transformation matrix relating the local to the global co-ordinate system, as given by:

$$\mathbf{T}\mathbf{w} = \mathbf{a} \tag{6.37}$$

Where **w** is the vector of local element displacements, and **a** are the global system displacements.

This procedure was implemented in the computer code PLAXIS in 1990. A 5-noded hybrid beam element, which is compatible with 15-noded continuum elements was used. A detailed formulation of this element is given by Bakker and Brinkgreve (1990).

Finite element modelling of flexible retaining walls in plane strain.
Since 1992 there is an increased interest in bored tunnelling in the Netherlands. The structural analysis of the tunnel lining for such a structure demands that curved beams are available. In order to meet this demand a further step in the development of structural element in the PLAXIS computer code was taken. A Mindlin type structural element was selected and implemented. The theory related to this is described in more detail in section 7.4.2

The advantages of this element are:

- the curvature of a beam can be taken into account;
- the influence of a rotation of the cross section, which is important for a beam which is short in comparison to its height, is implicitly taken into account, and
- Implementation of material non-linearity for the beam, (such as plasticity), becomes feasible.

Modelling soil structure interaction at the toe of a flexible retaining wall
The use of beam elements with a virtual thickness in a finite element mesh might lead to singularities in the deformation. Generally, if a stiff structure with edges or corners is combined with a soil continuum, singularities in the displacements might be introduced in the finite element mesh. This problem was examined by v. Langen (1991), for the problem of plate loading and for the modelling of pile penetration. The problem is not limited to those structures, also for a flexible retaining wall modelled with a beam element with virtual thickness this problem exists, as shown in Fig. 6.15. To avoid the problem of singular displacements at

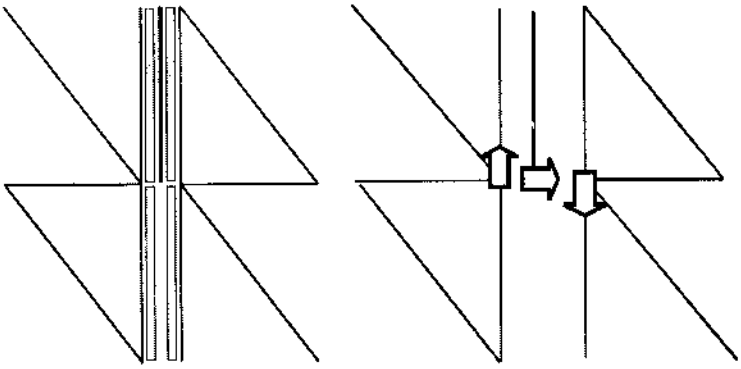

Figure 6.15 Interface elements at the toe of a flexible retaining wall. Singularities in the displacement field

the toe, interface elements between soil and wall are used. The interface elements should be extended at least one element beneath the toe to prevent this type of singularity.

For the mesh used in the calculations discussed in section 6.5.2, a double line of interface elements was used. Beam elements were placed between mesh blocks and are therefore sandwiched between the interfaces. The material behaviour of interfaces within the soil is based on the same parameters as used for the soil.

Theoretical studies have been carried out (see Bakker & Vermeer (1987)), to verify this model. Parts of this verification are described in the next section 6.4. Analysis of case studies have also been done including the back-analysis of the deep excavation for the Rotterdam Willems-spoortunnel, see Bakker & Brinkgreve, (1990). The Kalrsruhe sheet pile test is discussed in section 6.5

6.4 VERIFICATION OF THE FINITE ELEMENT IMPLEMENTATION

To check the accuracy of the inflexible beam elements described in section 6.3.4, analytical calculations have been compared with the results of finite element analysis. In this section two calculations are described. The first calculation is for a cantilever wall in a cohesive material, where the wall is loaded to failure by an external horizontal force applied at the top. The finite element results are compared with lower bound and upper bound solutions.

The second calculation concerns a cantilever wall in frictional soil, loaded to failure by a surface load. Here a non-associated flow rule is used, which means that the bounding theorems loose their significance. Moreover the collapse load is not necessarily unique. For this particular problem however, the range of non-uniqueness is small, as the kinematics boundary conditions are not very restrictive. This finite element computation appears to give a clearly identified collapse mechanism and similarly a clear collapse load. The latter is compared to the outcome of conventional engineering calculations.

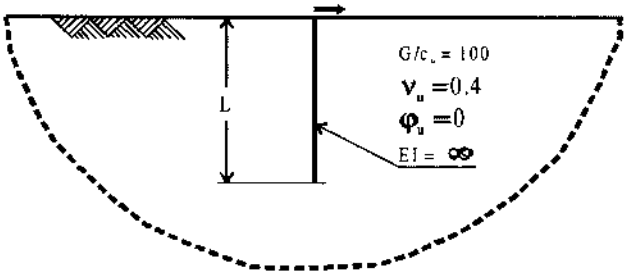

Figure 6.16 Anchor wall in cohesive soil

6.4.1 *Rough anchor wall in cohesive soil*

To verify the theory of section 6.3.4, for the inflexible wall implementation, a problem with an exact solution was sought. As the application pursued in the implementation was retaining walls, sheet pile problems in purely cohesive soil for undrained loading conditions were investigated. For this situation, $\varphi = \psi = 0$ and $c = c_u$ should be adopted. Ultimate limit states can than be bracketed by lower and upper bound solutions because the flow-rule is associated.

The first problem to be studied was a sheet pile wall in a half space with a constant undrained shear strength. The wall is loaded to failure by an external horizontal force at the top, as indicated in Fig. 6.16

This problem may be analysed analytically by deriving upper and lower bounds to the failure load. The statically admissible stress distribution, which is required to find a lower bound, was assumed as shown in Fig. 6.17.

Here stress discontinuities were used to separate regions of constant stress. Note that the soil weight might be taken into account adding a supplementary stress field according to:

$$\sigma_{yy} = \sigma_{xx} = \gamma \; y \tag{6.38}$$

Where the z-axis is taken perpendicular to the plane of analysis, x is horizontal,

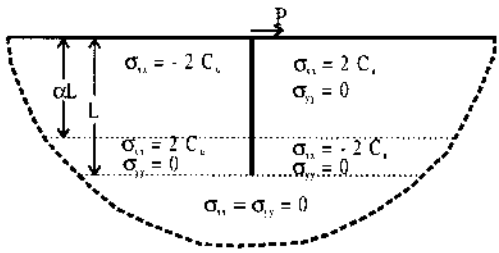

Figure 6.17 Statically admissible stress distribution around an anchor wall

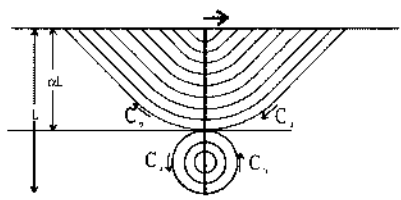

Figure 6.18 Assumed failure mechanism for upper bound analysis

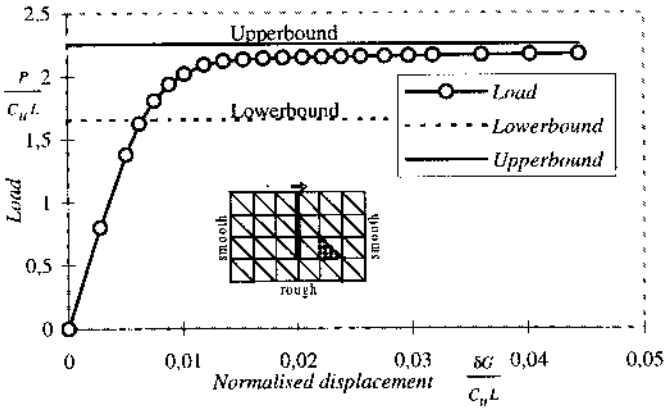

Figure 6.19 Computed load displacement curve for the anchor wall loaded at the top

and y is taken positive in the downward direction.

Both the position of the centre of rotation, and the lower bound P_{lower} can subsequently be solved from the equilibrium conditions for the wall using horizontal equilibrium and equilibrium of moments.

The result of this lower bound analysis is:

$$P_{lower} = 1.656\ c_u L \tag{6.39}$$

For an upper bound solution, a kinematically admissible velocity distribution is required. A suitable solution is proposed by Biarez (1958) and is illustrated in Fig. 6.18. Having formulated the displacement field, by an active and a passive wedge, and an earth roll at the bottom, it was possible to find the matching stresses, see Bakker & Vermeer (1987), which gave the following upper bound for the failure load:

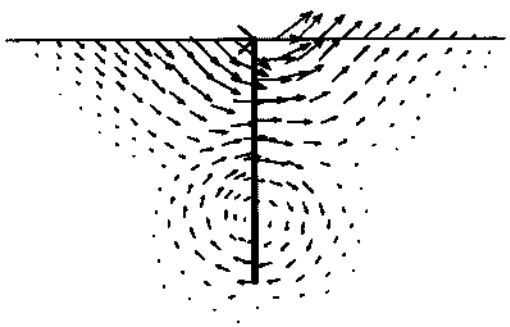

Figure 6.20 Finite element prediction of failure mechanism

$$P_{upper} = 2.256 c_u L \tag{6.40}$$

It should be noted that the assumed collapse mechanism involves deforming wedges rather than rigid ones.

Finite element analysis

The problem shown in Fig. 6.16, was analysed using the inflexible beam implementation in PLAXIS, with the mesh shown in Fig. 6.19. A mesh with 15-noded triangular elements was used, giving a cubic strain distribution and, as a result, a mesh with a large freedom with respect to deformations.

The load-displacement curve as indicated in Fig. 6.19, was obtained from 22 displacement increments using an average of 4 iterations per increment. The calculation showed a clear limit load of

$$P_{\max} = 2.174 \ c_u L \tag{6.41}$$

This result lies well in between the theoretical bounds as expected. Well before the end of the analysis a plastic failure mechanism developed as shown in Fig. 6.20. The mechanism obtained from the finite element analysis agrees well with the assumed mechanism in Fig. 6.18.

During the verification of the inflexible beam implementation a second plasticity analysis solution was used for a free cantilever wall in purely cohesive soil. The analytic solutions derived and used for the verification are given by Bakker & Vermeer (1987), and not repeated here. The finite element solution was found to be between the upper and lower bound solutions as expected.

6.4.2 *Cantilever wall in frictional soil*

The problem described in the previous section is of a theoretical nature. To check the accuracy of approximate engineering methods, a wall in frictional soil was studied. The dimensions and soil parameters were chosen quite arbitrary, as indicated in Fig. 6.21.

The problem concerns a cantilever-retaining wall in a frictional material with a height of 10 m. In practice, of course, for a wall of that size, normally an

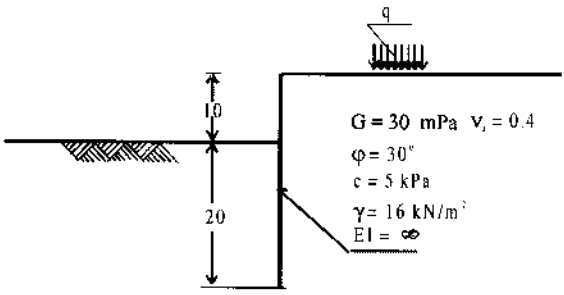

Figure 6.21 Cantilever wall in frictional material

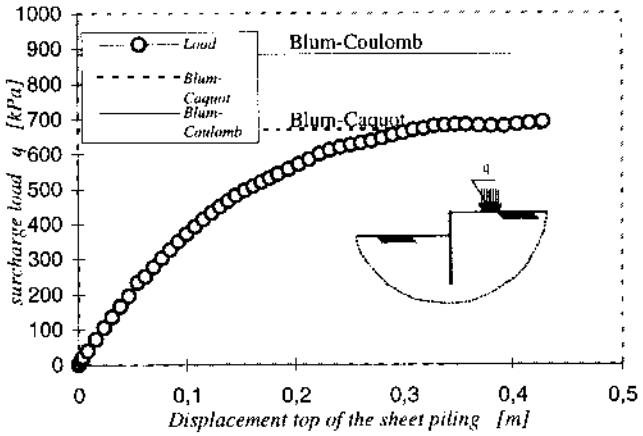

Figure 6.22 Computed surcharge-displacement curve for frictional soil

anchored wall would be used to limit the deformations. For analysis purposes however, the configuration is suitable

The soil parameters chosen were based on a sandy soil, i.e. a frictional model was assumed. For simplicity, because verification is the purpose and not validation, the soil parameters were assumed to be homogeneous for the entire soil mass.

In contrast to the problem described in section 6.4.1, if only soil-weight would be increased, a limit load would not be calculated. Indeed, for a frictional soil an increase of γ would simply give a proportional increase of the stresses causing an elastic response, because the stress paths would not intersect the conical Mohr-Coulomb yield surface in stress space.

For this reason, a uniform external surface load, as indicated in Fig. 6.21, was applied to the top of the soil. In the finite element analysis this load was increased incrementally up to the point that a limit load was calculated, see Fig. 6.22.

The finite element mesh, such as indicated in the in-set of Fig. 6.23, was adopted, as it was assumed that this would allow a Rankine-type failure of the soil without any interference from the mesh boundaries. A quadrilateral in this mesh is made up from two 15-noded triangles.

The analysis was performed in two stages. First the soil weight was incrementally increased to $\gamma = 16$ kN/m^2, using 12 load increments and an average of 5 iterations per increment. Next the external load was applied on the basis of an arc-length control procedure. The curve in Fig. 6.22 is made up of 50 load increments, each with approximately 7 equilibrium iterations per increment. The total number of iterations for the entire analysis sums to about 350. For the sheet pile wall in purely cohesive soil (see section 6.4.1), however only 60 iterations in total were needed.

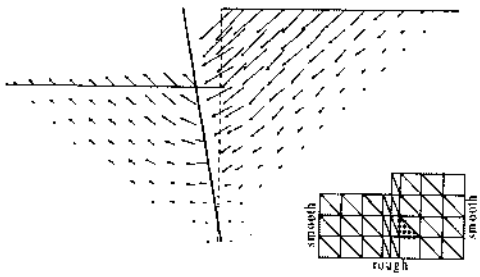

Figure 6.23 Predicted failure mechanism for retaining wall in frictional soil

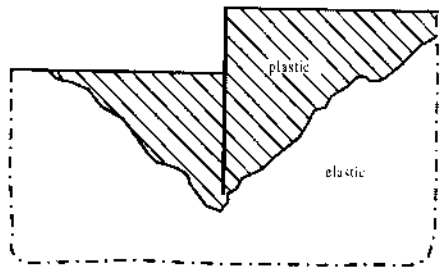

Figure 6.24 Computed plastic zones at failure

This indicates that an increase of the friction angle leads to a considerable increase of the computational effort. Similar behaviour is reported by De Borst and Vermeer (1984).

The predicted failure mechanism in Fig. 6.23 shows an active and a passive Rankine wedge. Notice that the slip lines are slightly curved due to the roughness of the wall. Underneath the Rankine wedges we observe a small roll, similar to the one in Fig. 6.20. The wall roughness is particularly important for the failure load. A smooth wall would give a failure load of about 270 kPa, whereas the finite element solution for a rough wall is:

$$q_{\max} = 680kPa \tag{6.42}$$

In Fig. 6.24, the plastic zones are shown. As can be observed the mechanism remains well inside the boundary of the mesh. Fig. 6.25 gives an indication of the inclination and magnitude of the principal stresses. Notice that the direction of the major principal stress is not perpendicular to the wall.

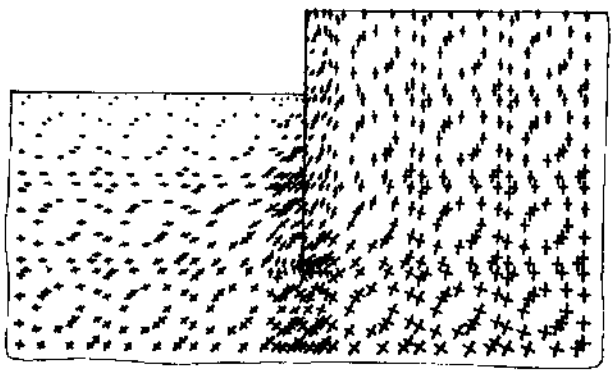

Figure 6.25 Computed principal stresses at failure

Engineering approaches

In Fig. 6.22 the results of analyses using Blum's method for this problem are also shown. For this purpose, two different approaches from practice have been followed for the calculation of the soil stresses, giving quite different values for the failure load.

The two methods used for the calculation of the soil stresses are; wall friction according to:

- *Coulomb/Muller-Breslau*
- *Caquot & Kerisel*

The failure load is calculated combining this with Blum's method (1931), by considering moment equilibrium about the toe of the sheet pile wall.

The same coefficient of active soil pressures is applied for both calculations. For the interface friction angle δ, $\tan \delta = \sin \varphi = 0.5$ is used, which means that $\delta = 26.57°$. This corresponds to the interface behaviour in the finite element analysis. The difference between the two engineering methods is more explicitly seen in relation to the passive earth pressure.

Using the coefficients of Caquot & Kerisel a failure load was obtained of

$$q_{Caquot} = 670 kPa \tag{6.43}$$

Application of the Coulomb/Muller-Breslau, (see Gudehus 1980), equation 6.10, gives:

$$q_{Coulomb} = 885 kPa \tag{6.44}$$

When comparing these values with the result of the finite element computation, Caquot's approach appears to give a much better result. This method is being incorporated in the British Code of Practice, see Potts and Burland (1983), and also in the German Code of Practice. The analysis presented here supports these decisions. Caquot & Kerisel's method has the advantage that it is based on a more refined analysis based on curved shear surfaces instead of straight shear surfaces, (see section 6.3.1).

6.4.3 *Conclusions*

The inflexible beam model seems to be reasonably successful for the analysis of sheet pile wall behaviour. Computed limit loads were found to lie in between theoretical upper and lower bound solutions. The computational effort remained modest for friction angles up to 30°. However, computer run times increased significantly with increase in the friction angle.

Practical engineering calculations give varying results due to different ways of dealing with the wall friction angle. The formulae of Caquot & Kerisel (1948) are thought to be the most appropriate, because it is based on curved shear surfaces. This approach gives better agreement with soil behaviour when compared with

field measurements and the results of numerical analysis.
Here the discussion of verification is limited to the inflexible beam implementation. The application of analytic solutions for verification purposes, such as described here is regarded as meaningful.

After implementing the hybrid beam elements in PLAXIS similar verifications as for the inflexible beam were performed. In addition, the hybrid beam element implementation was compared with subgrade reaction models and field measurements of the deep excavation for the Willems-spoortunnel in Rotterdam. A thorough validation using these field measurements was not possible, however, because adequate measurements of the displacements before excavation were not available. For further details see Bakker (1991).

In the next section validation is taken a step further with the sheet pile test in Karsruhe for which an excellent set of field data is available.

6.5 FIELD STUDY OF A SHEET PILE WALL

6.5.1 *Preface*

In 1993 at the test site Hochstetten near Karlsruhe, a sheet pile wall test was performed. The test was organised by the University of Karlsruhe in co-operation with the Dutch Centre for Civil Engineering, Codes and Specifications (CUR). The test, which was heavily instrumented, was carried out from the end of May and finishing in the second week of June 1993. The final loading was applied on the 8th of June 1993.

A prediction contest was held before the start of the test. The Civil Engineering Division of the 'Rijkswaterstaat' made two predictions. The prediction as

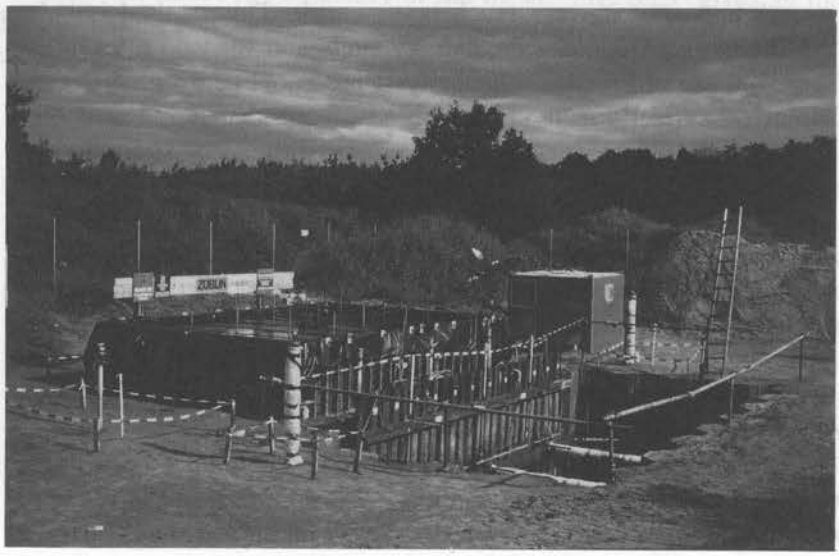

Figure 6.26 The construction excavation at the test site

published by Bakker & Beem (1994) is discussed below.

The test and the prediction results where published by Von Wolffersdorff (1996). In his report on the experiment, Von Wolffersdorff included a back-analysis based on a hypo-plastic model. The best fit for the parameters was found by trial and error. Details of the prediction results, as well as some details of the measurements to be used in the back-analysis, are described below.

Finally in this section, a back-analysis, based on Bayesian analysis (see Ledesma (1989)) is described. This back-analysis uses PLAXIS as mechanical model.

6.5.2 *The prediction of Rijkswaterstaat*

The experiment consisted of the staged construction of a small excavation as shown in Fig. 6.27. The trial wall, consisting of slender KD VI profiles was placed opposite a much heavier and stiffer Arbed PU 8 wall, for which the deformations, in comparison to the trial wall were negligible. The test wall was supported at a distance of 1.25 m below the soil surface by a strut supported by the opposite wall. To guarantee a 2D situation as far as possible at both sides of the 7 m. wide test, a 5 cm. thick bentonite slurry sheet was installed. This bentonite slurry sheet reduced the friction at the sides of the experiment down to

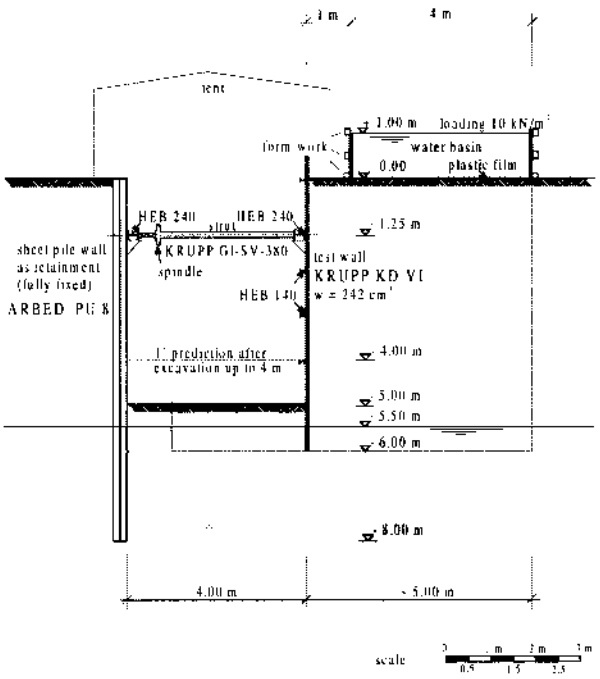

Figure 6.27 The construction excavation for the Sheet pile-wall test at Hochstetten (near Karlsruhe, Germany)

a negligible level. The excavation process is described in more detail in section 6.5.2 and Table 6.4

The Public Works department in Utrecht was one of the 39 organisations who made a prediction of the test results. This prediction was published, see Bakker & Beem 1993. The main items and results of this prediction are described below.
For an adequate prediction it was necessary to interpret the soil data provided by Karlsruhe University. Here the evaluation of the main parameters used for the prediction is discussed. An important aspect was the low groundwater level, and so an apparent cohesion due to suction had to be considered. A second aspect considered to be important was the staged execution. In the prediction this aspect was implicitly solved by calculation of a number of analysis steps: construction/loading/unloading.

The discussion here is concerned with the finite element prediction carried out using PLAXIS 4.5, and the subsequent back-analysis performed using PLAXIS version 7.0
Because correct modelling of soil structure interaction effects is important, special care was taken to model the singularity at the sheet pile toe. This procedure and the Mindlin type element used for the analysis are described in section 6.3.4.

The interpretation of the soil data, and the staged construction are described below.

Interpretation of Soil Data and determination of other parameters
Information of two kinds is needed for a finite element prediction. Firstly information about the geometry of the model, the forces acting upon it and the construction process is required. Secondly a material model and the parameters to be adopted is needed.

The first kind of information can be derived from the structure itself. The second type of information depends on the chosen material model. This section deals with the choice of the material model and the relevant material parameters. This was derived from the information for the sheet pile test, distributed by the University of Karlsruhe.

In 1993, the time that the prediction was made, the material models available ranged from relatively simple models such as the Elasto-plastic Mohr-Coulomb model, up to more complex models such as the Cam-Clay model. As a general rule the more complex the model, the more soil parameters are needed.

The purpose of the test was to study the collapse of the soil body. The material model should therefore be able to model soil plasticity as well as elasticity. As the test was carried out in sandy soil, the Mohr-Coulomb model was thought to be appropriate. At that time the difference between first loading and unloading/reloading was not recognised by most practitioners, and therefore not included in their analyses. For our prediction, the elasto-plastic version of the Mohr-Coulomb model with five parameters was used, see section 4.6

The material parameters needed for the material model had to be extracted from the geotechnical information which was included in de documentation which was assembled by the University of Karlsruhe. This documentation included results from a large number of geotechnical tests on the test site.

These included:

- *boring profiles*
- *dynamic probing*
- *grain size distributions*
- *oedometer tests*
- *shear box tests*
- *tri-axial tests*
- *plate loading tests*
- *capillary cohesion tests*
- *pressuremeter tests*
- *cone penetration tests*
- *Menard pressuremeter tests*

To obtain a stiffness modulus, the oedometer tests and the tri-axial tests might be used. In this case the tri-axial test results were preferred because the effect of shearing is taken into account more effectively. The strains measured in the tri-axial tests however where considered to be large (up to 10%), compared with the strains expected during the test. Furthermore the loading curves, see Fig. 6.28, did not show a peak. This effect was ascribed to the high density of the sand or the size of the sample. The German tri-axial tests where carried out on samples of size 10x10 cm, whereas Dutch samples normally measure 7x3.5 cm. A more slender sample might develop shear bands earlier, possibly leading to a peak in the load-displacement curve.

For the derivation of the shear modulus, the G_{50}, the secant shear modulus at 50% of the ultimate stress was used. This value was derived for three levels of cell pressure (see Table 6.3).

These data were used to develop a stress dependant relationship for the shear modulus in order to model the increase of G with depth. The relationship that was adopted is:

$$G = G_{50}^{ref} * \left(\frac{p}{p_{ref}} \right)^m \tag{6.45}$$

If a reference pressure was applied of $P_{ref} = 100$ kPa, this gave:

Table 6.3 Tri-axial test results for varying cell pressures

cell pressure MPa	Indication number	$sin\varphi$ at 4% strain	G50 MPa
100	S5KD13	0.63	13115
	S5KD15	0.60	11538
200	S5KD21	0.63	26231
	S5KD22	0.63	26321
300	S5KD31	0.61	30096
	S5KD32	0.61	30096

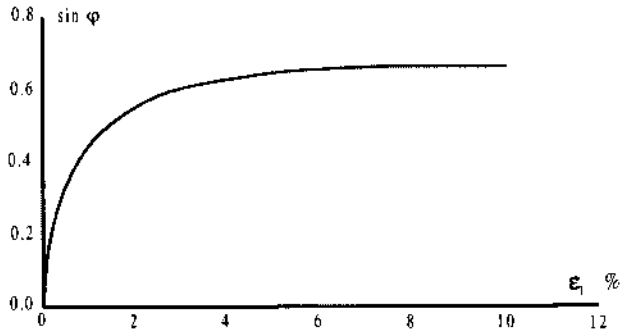

Figure 6.28 Tri-axial test result for lab.no. S5KD21

G_{50}^{ref} = 13314 kPa

m = 0.8 [-]

To derive the shear modulus from the Young's modulus, a Poisson's ratio of 0.3 for all the tri-axial tests was used.

The tri-axial tests results were also used to determine the friction angle of the sand. As this parameter is considered to be insensitive to the cell pressure, the value of this parameter should not vary too much between the different tests. For the derivation of the friction angle, characteristic for the analysis, the friction angle related to yielding of the sand at a strain of 4% (see Fig. 6.28) was used.

A comparison of the derived friction angle for the different stress levels enabled the consistency of the tests to be checked. The tests gave a mean value of the friction angle of 38°, which was thought to be relatively high for sand. It has to be considered, however, that the representative values normally adopted for design, implicitly include a safety margin because the laboratory will deliver characteristic values that are exceeded for 95% of the tests. Here however we had to predict the average soil behaviour.

For the angle of dilation, engineering judgement was adopted by assuming $\psi \approx \varphi - 30°$. For the prediction, this value was in fact reduced to 5°. For the wall friction, a friction angle of $\delta = 2/3\ \varphi$ was assumed. Furthermore, the advanced Mohr-Coulomb model (which included stress dependant elasticity in the elastic domain) was used. This model did not allow tension to occur.

The last parameter to determine was the cohesion. The in-situ tests showed that the top layer on the test site showed groundwater at less than atmospheric pressure. This was attributed to suction causing an apparent cohesion. Two series of 3 tests of excavated soil cubes were averaged to indicate an apparent cohesion between 2.7 and 4.0 kPa. Furthermore the plate loading tests were investigated using back-analysis. As the diameter of the plate was 30 cm, the shear plane goes mainly through the top metre of the soil. As the apparent cohesion is presumed to be dominant in the top metre of the soil, this test was considered to be suitable to estimate the apparent cohesion. Unfortunately, however, the results of the two

plate loading tests were quite different, and so it was not possible to estimate, with confidence, a value for the apparent cohesion. On basis of the tests on excavated soil cubes, and the plate loading tests, cohesion for all the soil layers of 3 kPa was assumed.

The initial stresses were calculated according to equation 6.11, see Jaky (1944).

Parameters of the wall

The wall tested was a profile by 'Krupp': Kanaldielen KD VI with the following properties

The bending stiffness was EI = 2033 kNm^2 and the axial stiffness was EA = 2200000 kN/m. The strut stiffness' (EA/L) was 20938 kN/m

Analysis of the construction sequence

The predictions for the test were performed with PLAXIS, version 4.5. The test itself was modelled in plane strain and so 3D effects were neglected. The mesh is illustrated in Fig. 6.29. The elements are fifteen noded triangles. The mesh displayed corresponds to a certain stage of construction; the initial mesh starts with a level soil surface. In Fig. 6.29, soil elements in the excavation have been removed. To obtain an accurate prediction for the sheet pile, the construction of the sheet pile is also modelled in the calculations.

The test was carried out in 8 stages of construction, see Table 6.4. At all the stages of the test the strains and stresses in the wall and the soil were monitored. Here for the numerical analysis eight stages of construction were recognised, whereas for the prediction contest only results for four stages of construction

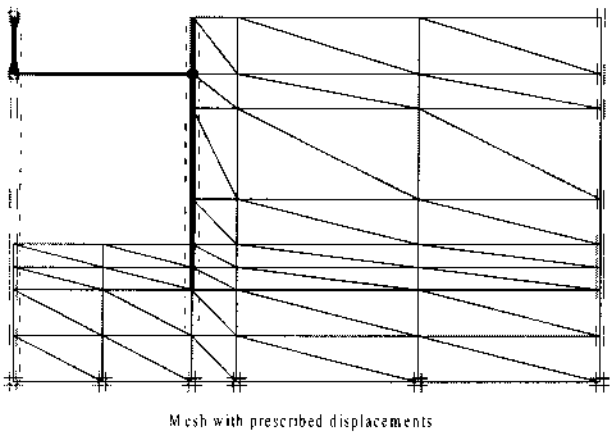

Figure 6.29 Element mesh with boundaries, sheet pile-wall, strut, soil elements and interface-elements. At the construction stage that the soil is excavated

Table 6.4 Stages of construction and stages for the predictions

Stage for numerical analysis	*Stage for prediction*	*Description*
0		Initial conditions
1		Excavation up to 1.00 m.
2		Excavation to -1.75 m.
3		Installation of the struts and pretension to 4.5 kN/m.
4		Excavation to -3.00 m
5	*I*	Excavation to -4.00 m.
6	*II*	Excavation to -5.00 m
7	*III*	Surface load (to reduce the effect of the apparent cohesion).
8	*IV*	Reduce the strut length up to 'failure'

were asked. In order to make clear which is which, the stages for numerical analysis are indicated with normal ciphers, whereas the stages for the prediction are indicated with Roman ciphers. One of the aims of the sheet pile test was to determine the behaviour of a yielding sheet pile in sandy soil. The yielding of the sheet pile was achieved by slowly shortening the struts, using the spindle in the struts, see Fig. 6.27.

To obtain an accurate prediction of the stresses and strains in the sheet pile wall, during the shortening of the struts, the initial earth pressure distribution has to be known. Modelling the construction process of the test site using the finite element procedure described below did this.

The prediction was performed as follows:

- *Activation of all the soil elements with all structural elements remaining inactive. This provides a set of equilibrium initial stresses.*
- *Activation of the beam elements to model the installation of the sheet pile. The interface elements are activated automatically when appropriate.*
- *De-activation of soil elements in the excavation to a level of -1.75 metres.*
- *Activation of the spring elements to model the struts. Initial pre-stress was 4.5 kN.*
- *De-activation of soil elements in the excavation up to -4.00 metres*
- *De-activation of soil elements in the excavation up to -5.00 metres*
- *Activation of the surface load (to reduce the effect of the apparent cohesion*
- *De-activation of the spring elements that model the strut. Failure is assumed when the strut force reduces to a limiting value.*

The prediction results of Rijkswaterstaat

In Fig. 6.30 the strut force as a function of the sheet pile wall deformation is shown. According to the numerical calculation it was expected that the strut

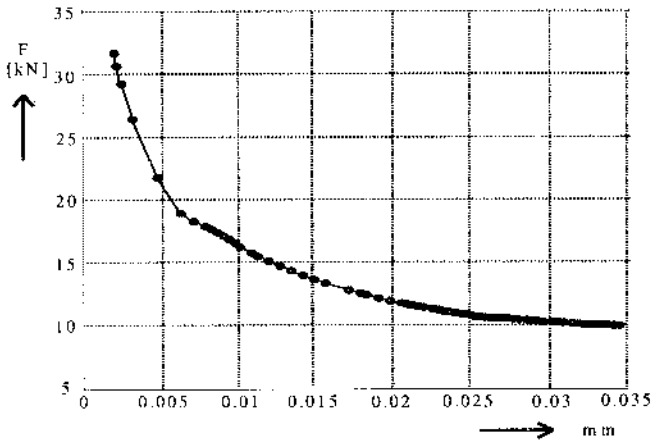

Figure 6.30 Strut force as a function of the sheet pile wall deformation measured at strut level

would have to be shortened several centimetres to have a significant decrease in the force level. After that, the strut force gradually reaches a limiting value. For the prediction, the ultimate limit state of the structure was taken from the calculations that correspond to the point that a displacement of the strut of 35 mm was calculated. The deformed mesh and the bending moments in the sheet pile wall related to that situation, are shown in Fig. 6.30 and Fig. 6.32. The tabulated summary of the prediction is given in Table 6.5 on page 132.

As can be observed from Fig. 6.30, the strut force significantly decreases when the strut is decreased in length. The bending moment in the span, however, increases only slightly, from M = 8.14 kNm/m after the excavation to 13.2 kNm/m at failure

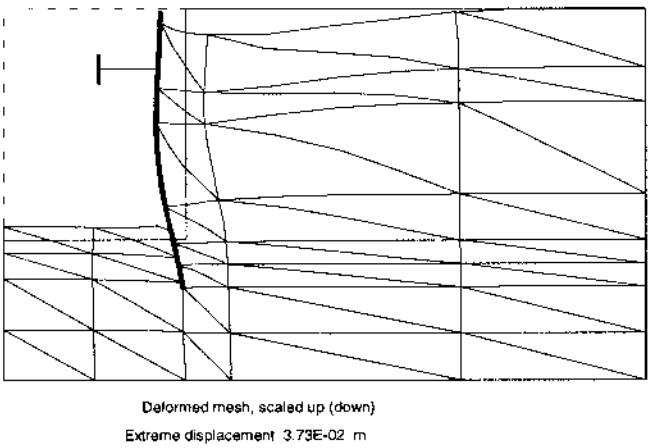

Figure 6.31 Deformed mesh at failure

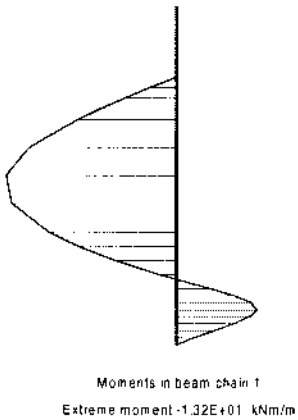

Figure 6.32 Distribution of bending moments at minimum strut force

Fig. 6.32 shows the distribution of the predicted bending moment in the sheet pile wall. The lack of any significant bending moment above the strut was thought to be caused by the apparent cohesion in the upper layers due to suction. The deformed mesh at wall failure is shown in Fig. 6.31.

Prediction contest

The prediction described in this section was not the most accurate, although the results were comparable to all the other finite element predictions. It should be

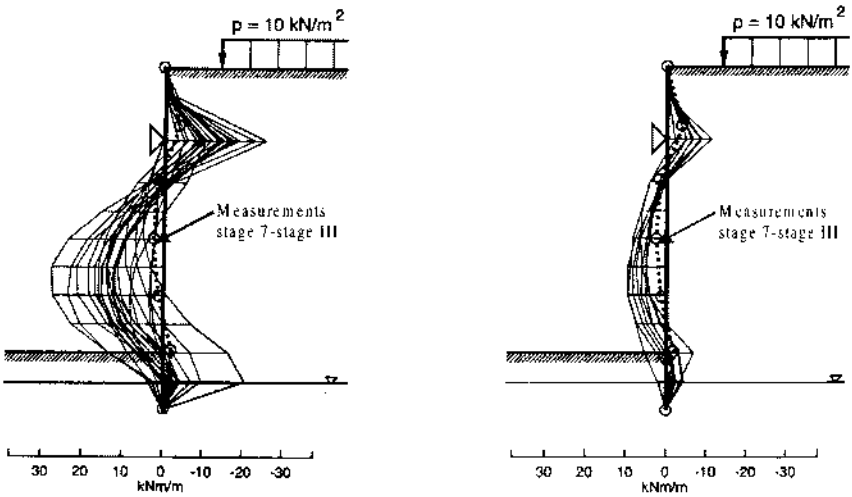

Figure 6.33 Prediction results for the bending moments at stage7/stage III, after excavation and surface load:
left: a), Subgrade reaction models.
right: b) PLAXIS predictions using Mohr-Coulomb model

noted that the measurements of the bending moments and the deformations were out of the range for all these predictions. In that sense the Rijkswaterstaat prediction was not better or worse than any other. A numerical comparison of prediction and measurement together with the results of back analysis calculations are summarised in Table 6.7, see page 139.

The test results and the predictions were presented by Von Wolffersdorff (1994), at a Workshop at Delft University, on October 6 and 7, 1994.

In his presentation v. Wolffersdorff made an arranging of the prediction results in such a way that the characteristic results for different classes of models, i.e. subgrade reaction models, finite element models, and for all the models, could be compared. Here in Fig. 6.33a, the bending moments respectively for the predictions with subgrade reaction models, and in Fig. 6.33b for the predictions with PLAXIS, both for stage III of the test are shown.

It is tempting to estimate the standard deviation of the results of the various models, to derive an estimate for the standard deviation of models by this. It should be noted however that all the predictions where based on the same set of parameters. A part of the standard deviation thus established is related to the interpretation of the geotechnical survey data. It would therefore be wrong to interpret the derived standard deviation as characteristic for the model; the derived value is both related to the model and the interpretation of the soil data.

6.5.3 *Test execution and measurements*

The test, was performed, in sandy soil, and was heavily instrumented. The test was started late in May 1993. The final loading was carried out on the 8th of June.

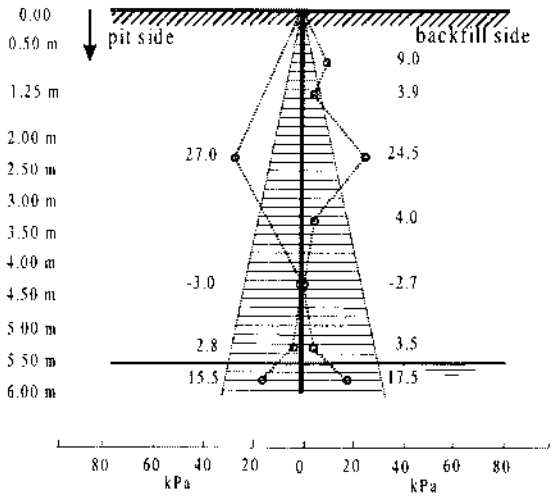

Figure 6.34 Measured earth pressures, after installation of the test wall, (at stage T_0)

Table 6.5 The main prediction results and Measurements

				Prediction	*Measure-ment*
Head moment stage	*7 (III)*	*[kNm/m]*	M7(1.25)	-6.78	-5.06
Moment in the span, stage	*7 (III)*	*[kNm/m]*	M7(3.00)	6.72	2.76
Strut force stage	*7 (III)*	*[mm]*	F7	30.07	33.72
Top displacement Stage	*7 (III)*	*[mm]*	U7(0.00)	-0.586	5.15
Displacement in the span, Stage	*7 (III)*	*[mm]*	U7(3.00)	7.19	3.4
Ultimate bending moment	*8 (IV)*	*[kNm/m]*	M8(2.00)	5.99	4.67
Ultimate bending moment	*8 (IV)*	*[kNm/m]*	M8(3.00)	12.2	3.41
Ultimate strut force	*8 (IV)*	*[kN/m]*	F8	10.0	4.22

The groundwater level was 5.5 m below soil surface. As a result the sand showed some apparent cohesion. The test was performed by executing the stages of construction summarised in Table 6.4.

After installation of the instrumented sheet piles but before excavation, horizontal soil stresses where measured, see Fig. 6.34. According to Von Wolffersdorff (1994): *'the initial horizontal stresses as observed are quite in disagreement with 'as expected' distributions, but nevertheless have to be considered accurate as the measurement was repeated four times independently, and showing a coherent picture'*. The measured initial stresses did not agree with the common theory according to Jaky, especially near the soil surface. This effect is taken into consideration in the back-analysis calculations. A tabulated summary of the main test results is given in Table 6.5

One of the critical things to predict was the deformation of the structure at soil failure. At soil failure, the structure is close to a mechanism. Therefore one might

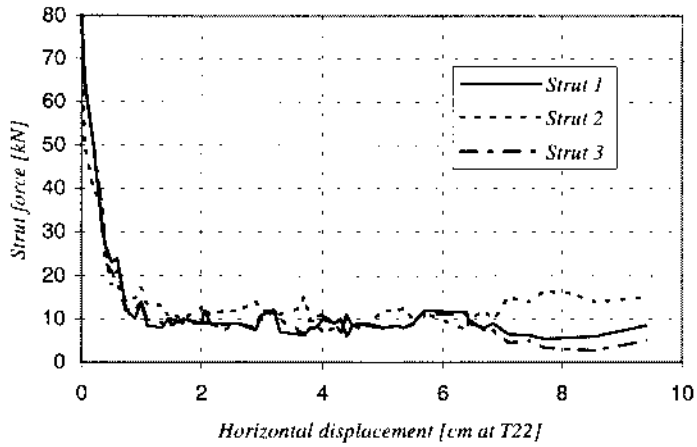

Figure 6.35 Strut force as a function of deformations.

argue that the deformations at soil failure are not well defined. To overcome the problem whether the deformations at soil failure are well posed, here in Fig. 6.35, the strut force as a function of the deformation is given. As one can observe, only small deformations of the wall lead to significant reductions in strut force (and presumably to the soil loading on the wall).

A quick comparison between the predictions and the measurements showed that the measured deformations were less, at least a factor two than expected from the predictions. Initially in the prediction, a critical value to predict was the ultimate level of the strut force. When measured data became available, however, attention became focussed on understanding the small deformation behaviour of the wall.

From the measuring data it was observed that the pre-stress of the anchor was 4.29 kN/m, rather than 4.5 kN/m which was assumed in advance.
More detailed information about the measurements will be discussed in section 6.5.4 where the measurements are evaluated taking into account both the prediction and the back-analysis results.

6.5.4 *Back-analysis*

Theory

To perform a back-analysis for the Karlsruhe sheet piling test, inverse analysis Ledesma (1989), Nova (1995), was applied.

To apply this theory, an explicit model relating parameters $\mathbf{x}$, and analysis results $\mathbf{f}^c$
(Where the superscript ^{c}, stands for 'calculation'), has to be available, i.e.:

$$\mathbf{f}^c = \mathbf{M}(\mathbf{x}) \tag{6.46}$$

The results of the model may then be compared with the measurements, $\mathbf{f}^t$ (where the superscript ^{t}, stands for test). Both $\mathbf{f}^c$ and $\mathbf{f}^t$ are assumed to be vectors, with a length n; the number of relevant measurements. Here only a limited number of measurements will be used to fit the parameters. For this case, these parameters include a maximum bending moment, a strut force and/or strut deformation, for a number of successive steps in the excavation. The parameters evaluated might be judged as a set of engineering parameters common for the evaluation against structural criteria.

The measurements being taken in consideration and the corresponding calculation results are ordered in vectors according to:

$$f_i^t = (f_1^t, f_2^t, \ldots\ldots, f_n^t)^T \tag{6.47}$$

and

$$f_i^c = (f_1^c, f_2^c, \ldots\ldots, f_n^c)^T \tag{6.48}$$

After Ledesma, (1989), it is assumed that the probability density of the prior

information of the parameters and the measurements are multivariate Gaussian:

$$P(\mathbf{x})=\left|\mathbf{C}_{\mathbf{x}}^{\mathbf{0}}\right|^{-1/2}(2\pi)^{-m/2}\exp\left[-\frac{1}{2}\left(\mathbf{x}-\langle x\rangle\right)^{\mathrm{T}}\left(\mathbf{C}_{\mathbf{x}}^{\mathbf{0}}\right)^{-1}\left(\mathbf{x}-\langle x\rangle\right)\right] \tag{6.49}$$

and

$$P(\mathbf{f}^{\mathbf{c}})=\left|\mathbf{C}_{\mathbf{f}}\right|^{-1/2}(2\pi)^{-n/2}\exp\left[-\frac{1}{2}\left(\mathbf{f}^{t}-\mathbf{f}^{\mathbf{c}}\right)^{\mathrm{T}}\left(\mathbf{C}_{\mathbf{f}}\right)^{-1}\left(\mathbf{f}^{t}-\mathbf{f}^{\mathbf{c}}\right)\right] \tag{6.50}$$

Where:

$\mathbf{C}_{\mathbf{x}}^{\mathbf{0}}$ *is the covariance matrix, based on the available 'a priori' information.*

$\mathbf{C}_{\mathbf{f}}$ *measurements covariance matrix*

$\langle x\rangle$ *' a priori' estimated values of parameters, e.g. the mean values*

$\mathbf{f}^{t}$ *the measured variable values*

m *is the number of parameters evaluated*

n *is the number of measurements*

$(\ )^{T}$ *is used to indicate a transpose*

If the measurements and the a priori estimates for the parameters are independent, the likelihood of a combination of a priori parameters and measurements is assumed to be:

$$L(\mathbf{x})=k\,P(\mathbf{x})P\left(\mathbf{f}^{\mathbf{c}}\right) \tag{6.51}$$

Where k is an arbitrary constant.

The most likely combination of parameters to fit the measurements can be found solving the minimum of the natural logarithm, which gives the same optimum, if the function to be analysed is monotonic. Therefore an additional function S is postulated to be minimised;

$$S=-\ln L(\mathbf{x}) \tag{6.52}$$

Which may be expressed in the form:

$$\begin{aligned}S=&\left(\mathbf{f}^{t}-M(\mathbf{x})\right)^{T}\mathbf{C}_{\mathbf{f}}^{-1}\left(\mathbf{f}^{t}-M(\mathbf{x})\right)+\left(\mathbf{x}-\langle x\rangle\right)^{\mathrm{T}}\left(\mathbf{C}_{\mathbf{x}}^{\mathbf{0}}\right)^{-1}\left(\mathbf{x}-\langle x\rangle\right)+\\&+\tfrac{1}{2}\ln\left|\mathbf{C}_{\mathbf{f}}\right|+\tfrac{1}{2}\ln\left|\mathbf{C}_{\mathbf{x}}^{\mathbf{0}}\right|+\tfrac{n}{2}\ln(2\pi)+\tfrac{m}{2}\ln(2\pi)-\ln k\end{aligned} \tag{6.53}$$

If the error structure of the measurements and parameters is fixed, only the first two terms of the equation have to be considered in the minimisation process, the other terms being constants. This leads to the following modified function:

$$S^{*}=\left(\mathbf{f}^{t}-M(\mathbf{x})\right)^{T}\mathbf{C}_{\mathbf{f}}^{-1}\left(\mathbf{f}^{t}-M(\mathbf{x})\right)+\left(\mathbf{x}-\langle x\rangle\right)^{\mathrm{T}}\left(\mathbf{C}_{\mathbf{x}}^{\mathbf{0}}\right)^{-1}\left(\mathbf{x}-\langle x\rangle\right) \tag{6.54}$$

It is assumed that the results of the numerical analysis, f^{c}, may be expanded using a linear Taylor's expansion according to;

$$\mathbf{f}^{\mathbf{c}} = \mathbf{f}_{\mathbf{0}}^{\mathbf{c}} + \frac{d\mathbf{f}^{\mathbf{c}}}{d\mathbf{x}}\Delta\mathbf{x} = \mathbf{f}_{\mathbf{0}}^{\mathbf{c}} + \mathbf{A}\Delta\mathbf{x} \tag{6.55}$$

Where A stands for the influence matrix. Combining equations 6.54 and 6.55 gives:

$$S^* = \left(\mathbf{f}^{\mathbf{t}} - \mathbf{f}_{\mathbf{0}}^{\mathbf{c}} - \mathbf{A}\Delta\mathbf{x}\right)^T \mathbf{C}_{\mathbf{f}}^{-1}\left(\mathbf{f}^{\mathbf{t}} - \mathbf{f}_{\mathbf{0}}^{\mathbf{c}} - \mathbf{A}\Delta\mathbf{x}\right) + \left(\mathbf{x} - \langle x\rangle\right)^{\mathbf{T}}\left(\mathbf{C}_{\mathbf{x}}^{\mathbf{0}}\right)^{-1}\left(\mathbf{x} - \langle x\rangle\right) \tag{6.56}$$

It is intended to improve the solution by adjusting trial values of the parameters $\boldsymbol{x}$, i.e. $\boldsymbol{x}^{tr}$. ($\boldsymbol{x}^{tr}$ are the parameters related to the trial values of $\mathbf{f}^{\mathbf{c}}$). The procedure is started with starting values x_0^{tr} and accordingly $\mathbf{f}_{\mathbf{0}}^{\mathbf{c}}$. If we use the notation $\Delta\mathbf{f} = \mathbf{f}^{\mathbf{t}} - \mathbf{f}_{\mathbf{0}}^{\mathbf{c}}$, equation 6.56 gives:

$$S^* = \left(\Delta\mathbf{f} - \mathbf{A}\left(x - x^{tr}\right)\right)^T \mathbf{C}_{\mathbf{f}}^{-1}\left(\Delta\mathbf{f} - \mathbf{A}\left(x - x^{tr}\right)\right) + \left(\mathbf{x} - \langle x\rangle\right)^{\mathbf{T}}\left(\mathbf{C}_{\mathbf{x}}^{\mathbf{0}}\right)^{-1}\left(\mathbf{x} - \langle x\rangle\right) \tag{6.57}$$

Equation 6.57 can be minimised by differentiating with respect to $\boldsymbol{x}$:

$$\frac{\partial S^*}{\partial x} = -\mathbf{A}^{\mathbf{T}}\mathbf{C}_{\mathbf{f}}^{-1}\Delta\mathbf{f} - \mathbf{A}^{\mathbf{T}}\mathbf{C}_{\mathbf{f}}^{-1}\mathbf{A}\,\mathbf{x}^{\mathbf{tr}} + \mathbf{A}^{\mathbf{T}}\mathbf{C}_{\mathbf{f}}^{-1}\mathbf{A}\,\mathbf{x} + \mathbf{C}_{\mathbf{x}}^{-1}\mathbf{x} - \mathbf{C}_{\mathbf{x}}^{-1}\langle x\rangle = 0 \tag{6.58}$$

Rearranging the equation with the unknown parameters, $\mathbf{x}$, on the left side, and the a priori information, trial values and a priori values of the unknowns on the right hand, gives:

$$\left(\mathbf{A}^{\mathbf{T}}\mathbf{C}_{\mathbf{f}}^{-1}\mathbf{A} + \mathbf{C}_{\mathbf{x}}^{-1}\right)\mathbf{x} = \mathbf{A}^{\mathbf{T}}\mathbf{C}_{\mathbf{f}}^{-1}\left(\Delta\mathbf{f} + \mathbf{A}\,\mathbf{x}^{\mathbf{tr}}\right) + \mathbf{C}_{\mathbf{x}}^{-1}\langle x\rangle \tag{6.59}$$

Equation 6.59 is the general form of the maximum likelihood formulation for back-analysis. If the a priori information is not taken in consideration, the equation simplifies to:

$$\left(\mathbf{A}^{\mathbf{T}}\mathbf{C}_{\mathbf{f}}^{-1}\mathbf{A}\right)\mathbf{x} = \mathbf{A}^{\mathbf{T}}\mathbf{C}_{\mathbf{f}}^{-1}\left(\Delta\mathbf{f} + \mathbf{A}\,\mathbf{x}^{\mathbf{tr}}\right) \tag{6.60}$$

Finally, if the error structure matrix is the identity the more common form of the least squares formulation is obtained:

$$\left(\mathbf{A}^{\mathbf{T}}\mathbf{A}\right)\mathbf{x} = \mathbf{A}^{\mathbf{T}}\left(\Delta\mathbf{f} + \mathbf{A}\,\mathbf{x}^{\mathbf{tr}}\right) \tag{6.61}$$

The equations 6.59 to 6.61 are in essence highly non-linear; i.e. the matrix A is non linear. Therefore to derive a solution of these equations is not straightforward. To begin with, here in this study the derivation of a solution is tried out with a linearised approach. Matrix A is derived from a variation of a trial solution with the finite element method. Further a solution of the above presented equations is sought maintaining the thus derived matrix A, and subsequently making a number of finite element calculations, updating the solution with the outcome of the former iteration.

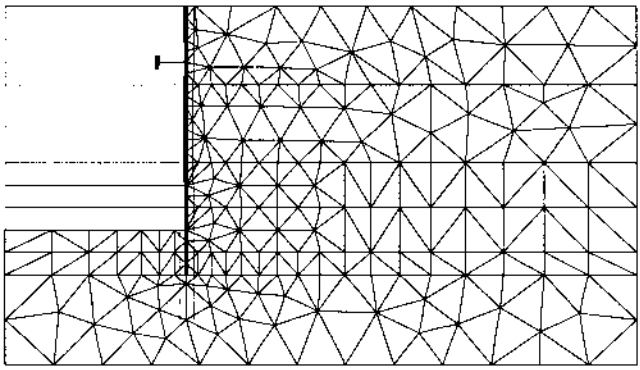

Figure 6.36 Finite Element model for back-analysis

Finite Element Modelling

The finite element analyses both for the prediction and for the back-analysis were performed with PLAXIS. The prediction with version 4.5, and the back-analysis with version 7. The test was modelled in plane strain. The mesh for the back-analysis is given in Fig. 6.36. The mesh displayed corresponds to the construction stage when excavation is complete. In the initial situation a level soil surface is modelled. To improve the analysis, with respect to the stress path of the soil, all stages of construction are modelled and calculated. Here in contrast with the prediction, 6-noded elements were used. Experience shows that for plane strain, these elements provide sufficient accuracy.

The shortening of the struts in the final stage of the analysis was performed by removing the strut in a staged construction analysis, until the point in the analysis where the soil fails.

Evaluation of the Input for the Back-analysis

For the material model the PLAXIS Hard-soil model was chosen, (see Vermeer & Brinkgreve (1995)). The hard soil model has a stress dependent stiffness, and a hyperbolic relation between deviatoric strain and deviatoric stress in the elastic range, proposed by Duncan & Chang (1970). This soil model uses an initial Young's modulus, E_i and an unloading-reloading Young's modulus E_{ur}. For shear a failure criterion according to the Mohr-Coulomb theory is used. In later years the Hard-soil model has been slightly extended with a cap to model compressible soil. The extended model is named Hardening soil model now.

After the test, the measurements were evaluated and compared with the predictions in order to derive an appropriate set of a-priori data for the back-analysis calculations. In this evaluation the focus was put on:

1) *The soil stiffness, i.e. for small strains,*
2) *Apparent cohesion due to suction,*
3) *Initial stresses due to the installation procedure.*

Here the following considerations where made;

Friction angle: The evaluation of the monitoring data suggested that the soil is 'stronger' than initially anticipated. As a result the bending moments and strut forces were largely overestimated in the predictions. Therefore, in the back-analysis to begin with a friction angle at failure (φ_m at 4% strain), will be assumed, i.e. $\varphi = 42^{\circ}$.

Apparent cohesion: In the back-analysis by Von Wolffersdorff (1996), it is mentioned that for the top layer of approximately 1.5 m a capillary suction of about 13 kPa exists, leading to an apparent cohesion of $c_{suct} = 13 \tan(42) = 11.7$ kPa.

Elasticity of the soil: In the prediction by Bakker & Beem (1994), the advanced Mohr-Coulomb model with a G_{50} was used. With this approach, the stiffer behaviour of the soil in unloading was neglected. In the back-analysis, the PLAXIS 'hard-soil' model was used.

The modulus from the Tri-axial-test results is $E_{50} \approx 2(1+\nu)G_{50}^{ref} \approx 35000$ was used. This value was initially adopted for the analysis. Subsequently the cone-penetration results were considered in conjunction with the empirical relation that $E \approx (3 \text{ to } 5)q_c$. Based on this, 5 layers with different stiffness were identified and applied in the analysis (see Fig. 6.37 and Table 6.6).

The stiffness ratio, for unloading-reloading was assumed to be 1.6, based on the plate loading tests. The initial stiffness, E_i, assuming a hyperbolic shape of the hardening curve, is twice the value of E_{50}. The Young's modulus for unloading-reloading, E_{ur}, was therefore assumed to be 1.6*2 = 3.2 times E_{50}. The Young's moduli used are listed in Table 6.6.

Initial stresses:The earth pressure measurements before excavation, (see Fig. 6.34) indicate that in the top 2.0 m of soil an increased horizontal stress is active. Below a depth of 3.5 m however, the horizontal stresses seemed to be inconsistent with plasticity theory, as for active failure:

$$K_0 \approx \frac{1-\sin\varphi}{1+\sin\varphi} - \frac{c}{\sigma_v}\cos\varphi$$

this would mean that for a depth of 3.5 m with an approximate vertical soil stress of $\sigma_v \approx 3.5*16.5 \approx 58$ kPa, a soil friction of approximately $\varphi \approx 42^{\circ}$ and a cohesion of $c \approx 5$ kPa the minimum value of K_0 would need to be larger than 0.14; i.e. $K_0 \geq 0.14$

The observed K_0 value however is approximately zero (0.0) which suggests that there is a cohesion of more than 15 kPa which is considered to be unrealistic. In the back-analysis, a K_0 value of 0.2 is used for the zone below 3.5 m. For the upper layers an a priori value for K_0 of 0.3 $\approx$ (1-sin φ) was used. During the

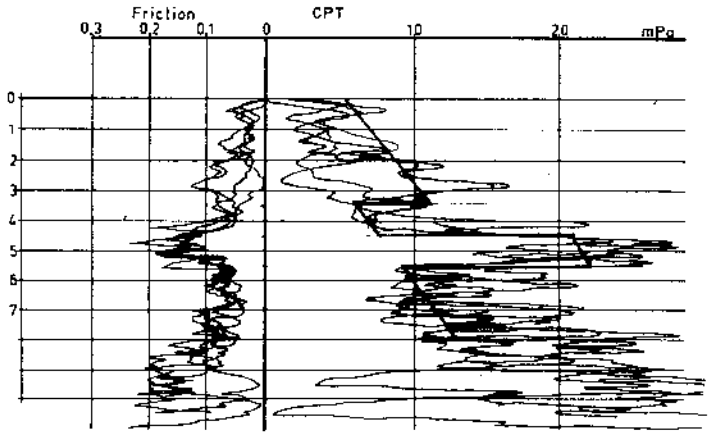

Figure 6.37 Cone penetration test result, and layer identification

analysis this value was updated based on the likelihood calculations.

Parameters to evaluate

The measurements adopted for the back-analysis, is a subset of the total amount of measured data. This subset of characteristic measurements, such as anchor force, bending moment, and maximum deformation is evaluated for several stages of construction.

The measurements are: M2(2.0), which represents the bending moment in the second stage of excavation, see Table 6.3, at the point 2.0 m. below the top. In a similar way the bending moment in the sixth stage of construction at a point 1.0 m and a point 3.0 m. below the top were considered, i.e. M6(1.0) and M6(3.0). The strut-force in the sixth stage was considered; F6. And the deformations at the top and at a point 3.1 m below the top in the seventh stage of construction were considered, U7(0.0) and U7(3.10). Finally the bending moment at 2.0m. and at 3.0 m. below the top and the strut-force, at soil failure (stage 8), were considered, i.e. M8(2.0), M8(3.0) and F8.

Table 6.6 Soil data used as input values for the back-analysis

Layer top	γ_d	γ_n	φ	ψ	c	c_{depth}	*Ref* c_{depth}	E_{50}^{ref}	E_{ur}	υ
+. MSL	kN/ m^3	kN. m^3	[°]	[°]	kPa	kPa	m	kPa	kPa	[-]
+0.00	16.9	-	42.0	12.0	11.7	-	-	65000	208000	0.3
- 1.25	16.5	-	42.0	12.0	11.7	-2.52	-1.25	65000	208000	0.3
- 3.50	16.5	-	42.0	12.0	11.7	-2.52	-1.25	35000	112000	0.3
- 4.50	16.5	-	42.0	12.0	1	-	-	70000	224000	0.3
- 5.50	16.5	19.0	42.0	12.0	1	-	-	35000	112000	0.3

The solution of the equations 6.59 and 6.60 demands that a covariance matrix for the measurements is established. This would not be necessary for the conventional least squares analysis given by equation 6.61, which implicitly assumes a standard deviation for the measurements of 1.0.

In order to assess the importance of the measurements, and to do this in a way that is not too subjective, it was assumed that measurements are independent. Which means that the covariance matrix becomes a diagonal matrix. For the diagonal terms, a variance of $\sigma_i/\mu_i = 0.1$ is adopted. In addition to that errors (Δf_i) with respect to bending moments and strut forces are weighted heavier in comparison than deformations, by a factor of 5.

Back analysis, calculations and results

The back-analysis was started with the weighed least square approach given by equation 6.60.

The method itself was applied by extracting the gradients assembled in matrix **A**, from the finite element model only once. Subsequently the solution improved iteratively, updating the trial value of the parameters based on the result of the least square solution. The assumption made implicitly was that the derivatives of the model assembled in matrix **A** are not too sensitive to the final solution. This was necessary because the finite element model was not linked in with the least square analysis so that the derivatives for matrix **A** could not be computed automatically.

This procedure appeared to be reasonably stable, giving convergence in approximately 15 steps. Within this process, the equations were solved using Mathcad © (1995), which was suitable for this application because there is only a small system of equations to be solved.

Table 6.7 Comparison Measurements and back-analysis

			Prediction	*Measure-ment*	*Back analysis Weighed Least Squares*	*Back analysis Maximum Likelihood*
Bending moment stage 2	*[kNm/m]*	M2(2.00)	p.m.	2.26	1.93	1.99
Bending moment stage 6	*[kNm/m]*	M6(1.00)	-5.8	-4.41	-5.159	-4.96
Moment in the span, stage 6	*[kNm/m]*	M6(3.00)	5.38	2.2	1.778	1.65
Strut force stage 6	*[kN/m]*	F6	23.36	28.64	29.68	28.38
Displacement in the span, stage 6	*[mm]*	U6(3.00)	3.51	2.99	2.637	2.49
Head moment stage 7	*[kNm/m]*	M7(1.25)	-6.78	-5.06	-6.234	-6.03
Moment in the span, stage 7	*[kNm/m]*	M7(3.00)	6.72	2.76	2.138	1.99
Strut force stage 7	*[mm]*	F7	30.07	33.72	34.86	33.91
Top displacement Stage 7	*[mm]*	U7(0.00)	-0.586	5.15	2.86	2.90
Displacement in the span, Stage 7	*[mm]*	U7(3.00)	7.19	3.4	3.27	3.14
Ultimate bending moment	*[kNm/m]*	M8(2.00)	5.99	4.67	3.919	3.87
Ultimate bending moment	*[kNm/m]*	M8(3.00)	12.2	3.41	9.41	9.44
Ultimate strut force	*[kN/m]*	F8	10.0	4.22	3.035	3.38
Objective function S^*	*[-]*				72.5	61.17

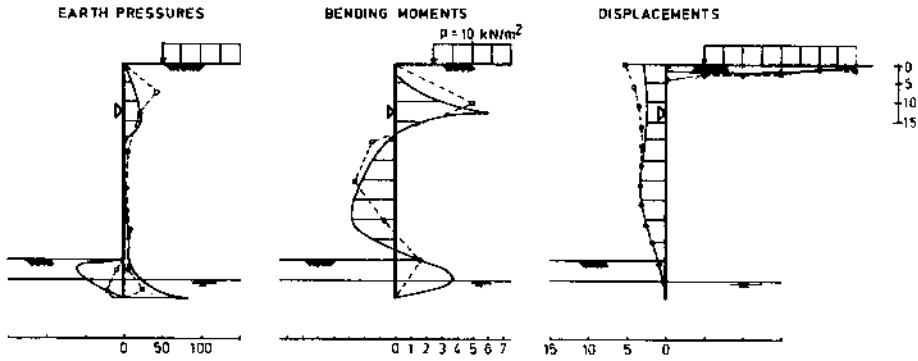

Figure 6.38 Comparison of back-analysis results and measurements

A comparison of back-analysis results and measurements is given in Table 6.7. The terminology is that M indicates bending moment, U indicates displacements, and F indicates the strut force. The parameters derived in the subsequent analyses are listed in Table 6.8

One of the results of this analysis was that the ratio for the Young's modulus came out nearly four times as high as the value extracted from the tri-axial test results, presented in Table 6.5. After that the weighted least squares result according to equation 6.60 was derived the analysis was continued with the maximum likelihood formulation. Therefore equation 6.59 was used in a trial to improve the result. It soon became clear that the procedure without updating matrix **A** did not converge well. The improved solution is also given in Table 6.7, although it has to be mentioned that only 2 or 3 convergent iterations could be

Table 6.8 Back-analysis results

	k0(1)	*K0(2)*	*φ*	*ψ*	*R(δ)*	*C(1)*	*C(2)*	*R(E)*
Prediction	0.38	0.38	38	5	0.66	5	5	1.0
Weighted Least squares (eq. 6.60)	2.85	0.6	42.7	4.7	1	6.35	5.5	4.25
Maximum Likelihood (eq. 6.59)	2.92	0.59	42.5	6.0	1	7.2	5.85	4.1

where

$K_0(1)$ = the K_0 in the upper soil layer (less than 1.25 m deep)
$K_0(2)$ = the K_0 in the soil layer between 1.25 m. and 3.5 m. deep
$C(i)$ = the cohesion in soil layer (i) (numbering starts at surface level, and continues downward)
$R()$ = ratio; multiplier to establish what the effective value of a parameter is.

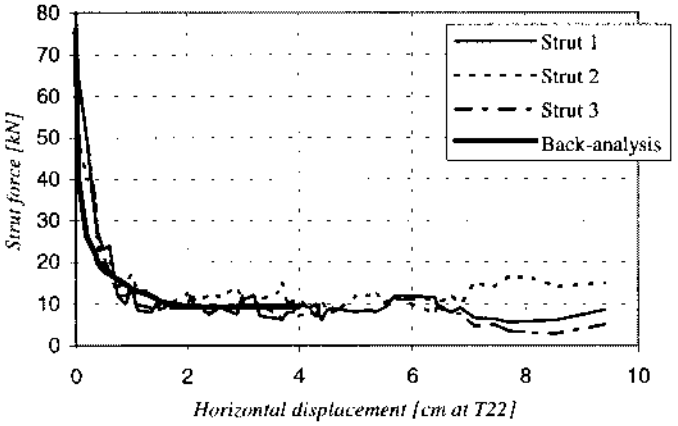

Figure 6.39 Strut force as a function of deformations; comparison with back-analysis.

done, depending on the relaxation factor applied. Taking smaller steps only resulted in a slower convergence. Even then, after some iterations, the process diverges. The influence of the a priori information seems to be that the calculations lead to higher values of the cohesion.

This concept is used for 1) δ, wall friction and 2) E, Young's modulus, (for all soil layers). $R(\delta) = 1.0$, (which implicitly is related to the wall friction according to $\tan\delta = \sin\varphi$), φ and ψ are varied for all soil layers.

In Fig. 6.38, the earth pressure, bending moments and displacements are displayed for stage 7. Finally in Fig. 6.39 the displacement strut force plot is given. As one can observe, for the values of stresses and bending moments, a reasonable agreement is obtained. However, the distribution of the bending moment indicates that the effective soil loading is located on a higher level than in the model. This suggests that the stiffness of layer 3 is different from that assumed in the analysis. In theory the distribution of stiffness could also have been subjected to an optimisation process but this analysis was not done.

If the displacements from the measurements and the back-analysis are compared, one can observe that the largest differences occur above the level where the strut is active. The conclusion drawn was that the displacements at the level of the strut, before strut installation, seem to have been larger than in the analysis. The relative rotation, which is implicated by this, intensifies the difference for the upper layer.

Concluding remarks on the back-analysis

A reasonable fit of the parameters has been obtained. Apart from the importance of initial stresses, and the underestimated influence of soil suction, it appeared

that the stiffness based on tri-axial cell tests underestimated the observed behaviour in-situ.

It might be argued, however, that the factor of four for the Young's modulus, between the tri-axial results and the back-analysis is too high. Such a factor leading to values for the Young's modulus of sand of over 800 mPa, contradicts literature, which indicates that maximum Young's modulus for sand, for small strains of 400 mPa is more realistic, see Tatsuoka et al. (1997). The latter paper indicates that the influence of de-structuring on the Young's modulus of sand is in the order of 2. Re-evaluating Fig. 6.38 the difference between the stiffness of the construction as back-analysed and observed indicates that a factor of 2, to account for de-structuring is not unrealistic.

The friction angle at the wall/soil interface was found to be greater than the common assumption that it is 2/3 of the angle of soil friction.

It is thought that the hard soil model provides an improved description of small strain behaviour. For convergence of the maximum likelihood analysis, an update of the gradient matrix **A** seems to be necessary to ensure convergence.

6.6 CONCLUSIONS

In this chapter the hierarchy in models for the analysis of flexible retaining wall is discussed. Within this context it is shown that a subsequent addition of more refined models leads to an increasing expansion of the modelling space.

The verification of the inflexible beam implementation shows that for the calculation of ultimate limit states, the flexibility of the sheet pile wall is of minor importance. A comparison of numerical analysis and analytical solutions for ultimate limit states supports this conclusion.

Validation of the flexible beam implementation is less decisive. When the model is compared with the results of test measurements it became clear that an adequate determination of parameters is at least as important as a good formulation of the model. On the one hand the prediction contest in Karlsruhe supports the conclusion that finite element calculations lead to a smaller bandwidth of the results in comparison to other models. On the other hand as the models become more and more capable of describing different effects, it becomes increasingly difficult, in back-analysis, to determine whether a difference between measurement and analysis is caused by one or the other input parameter.

With the expansion of parameters being used in the model, the solution space expands too, which requires that the parameters are adequately determined. To improve the determination of model parameters, the application of maximum likelihood type of analysis may be appropriate. To enhance the performance of such an analysis, the direct coupling between the finite element code and the optimisation procedure is thought to be necessary.

CHAPTER 7

Bored tunnels in soft soil

7.1 INTRODUCTION

In the Netherlands up to 1994 little attention was given to the development of a design philosophy for bored tunnels. When in 1994 the design of the Second Heinenoord tunnel had to be undertaken, models and a design philosophy for the tunnel structure were adopted from abroad. With this a risk was taken in the application of these models for the soft soil conditions in the Netherlands, because these, mainly empirical models, where validated, for stiffer soil conditions. Examples of the adopted models were; the relations of Peck (1969a) for surface settlements, the model of Horn (1961), for tunnel face stability or adapted by Janscec & Steiner (1994), and the subgrade reaction model of Duddeck (1980) for tunnel lining design.

In this chapter the main topic is the development of models for the structural design of the lining of a bored tunnel, for soft soil conditions. The view is taken that a tunnel after construction is essentially a soil retaining structure. Therefore a similar approach is taken as for the other types of soil retaining structure in this study. Following the line of development such as formulated in chapter 3 and 4, the application of the finite element method is leading. The finite element method is regarded as a step forward in comparison to the empirical models, because with this, potentially the empirical models described above might be replaced by a single model.

This chapter is concerned with the design model for the tunnel lining. The model of Duddeck is taken as a starting point.

In section 7.2 the main problems related to bored tunnelling in soft soil will be discussed. After a general introduction, followed by a short description of the geology in the western part of the Netherlands, various tunnel boring issues, relevant to Dutch soft soil conditions, will be discussed.

In section 7.3, in line with the main methodology of this study, the limit states will be discussed.

In section 7.4, in line with the thought that an hierarchy between models can be distinguished, a number of models, to begin with the analytical model and the model by Duddeck (1980), is discussed. Subsequently finite element models are discussed. As the finite element models discussed in chapter 6, are insufficient for the modelling of a curved tunnel lining, a new Mindlin beam type of element is introduced.

Though the effect of jack pressures is an important issue for the design of the reinforcement of a tunnel lining segment, in this chapter the attention is focused on the soil loading, because this is a long term load, increasing due to creep and consolidation, whereas the jack pressure is only applied during tunnel construction.

In addition to ring action, the beam action of a tunnel tube is evaluated. Though recognising that the ultimate limit states for a tunnel lining are mainly based on two-dimensional ring action, for the serviceability limit state, the longitudinal stresses are also important.

The monitoring of the Second Heinenoord tunnel has produced a large database of information. In section 7.5, an overview of the monitoring of the Second Heinenoord tunnel will be given. Subsequently, attention is focused on the structural observations. Both the ring action and the longitudinal action will be evaluated. Both the analytical models as well as the models based on the finite element method are evaluated.

Parts of this chapter have been published earlier in Bakker et al. (1997), Bakker (1999[a]), Bakker et al. (1999[b]) and Bakker et al. (1999[c]).

7.2 BORED TUNNELS IN THE NETHERLANDS

The use of subsurface infrastructure is not new for the Netherlands. In a typical delta country, such as the Netherlands, dominated by natural and artificial waterways, tunnels are traditionally used instead of bridges to cross the waterways, to facilitate the water traffic. Up to 1995 some 55 km of motorway and rail tunnels were constructed in the Netherlands. Most of these tunnels were constructed as immersed tubes. Before 1995, the shield tunneling method had not been applied in the Netherlands for tunnel diameters larger than 4 m. But this has now changed; as a result of a national debate on more underground infrastructure, the Dutch Government decided in 1993 to finance two experimental TBM tunneling projects:

- *a second tunnel under the Oude Maas near Heinenoord (Rotterdam).*
- *a new railway tunnel also under the Oude Maas near Botlek (Rotterdam).*

Since then, a number of other projects with bored tunneling have been taken under design. Of which the following have been taken under construction (2000).

- *the motorway crossing of the Western-Scheldt inlet.*
- *the Sofia tunnel in the 'Betuwe' route, for cargo rail*

In the near future, a number of other major TBM-tunneling projects will be undertaken:

- *the north-south metro line under the city of Amsterdam*
- *the tunnel for the high speed rail line in the line between Amsterdam and Rotterdam*
- *the tunnel under the Pannerdensch canal in the 'Betuwe' route, for cargo rail*

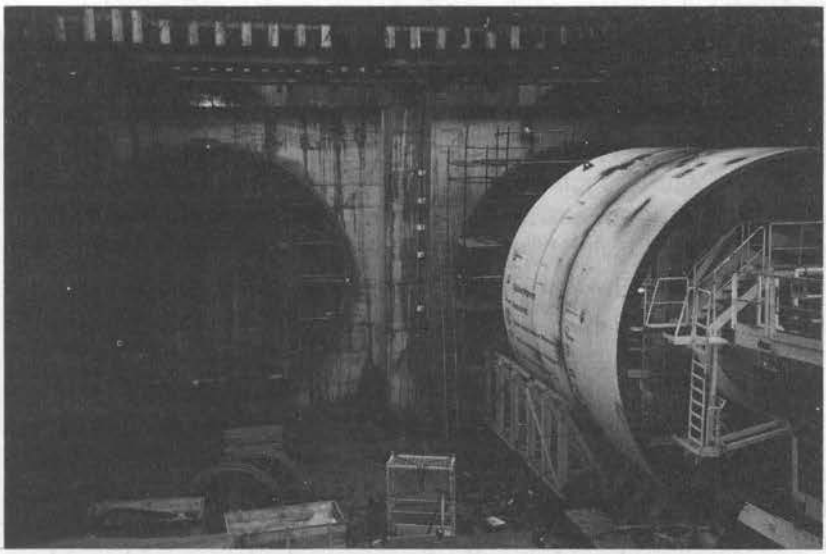

Figure 7.1 Tunnel boring machine installed for the start of the second Heinenoord tunnel

One of the topics given much attention in the preparations for the monitoring of these tunnels, is the structural design of the tunnel lining.

To begin with some typical aspects of the soil condition in the Western part of the Netherlands will be discussed.

7.2.1 *Geology of the Netherlands*

The top-section of the stratification of the western part of the Netherlands consists of peat and soft to very soft clay (formed during the Holocene (alluvial) period) laying on top of a thick layer of sand, coarse sand and gravel (formed during the Pleistocene (dilluvial) period). The groundwater level is often almost at the soil surface. The Pleistocene sand layers were mainly formed during the glacial periods, when the water level of the North Sea was relatively low. During the interglacial times of high sea level, the west coast was below sea level and marine clays were deposited. The sedimentation of coarse sand and gravel was related to meandering river systems.

Windblown sands where deposited during interglacial periods. At the beginning of the Holocene period, the last sea level rise, tidal zones reached the south west of the Netherlands again. Peat formation started nearby in the flood plains. These peat layers were sometimes overlain by marine clay and sometimes eroded by the sea.

About 5000 years ago a coastal barrier system formed as dune formation began. In the areas behind the coastal barrier, out of reach of the aggressive sea, thick peat layers were formed. Locally, these layers were eroded by the sea again

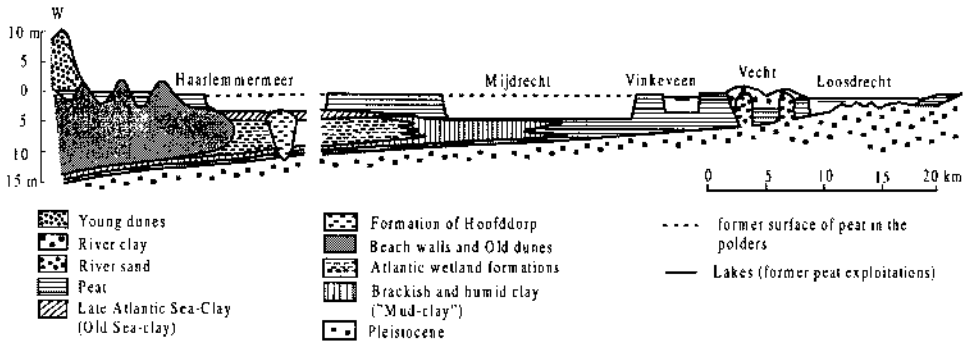

Figure 7.2 Geological cross-section of West-Netherlands, over Mijdrecht and near Delft, after Buisman (1978)

and were partly replaced by marine clay sediments.

Because of the low stiffness and strength of the upper Holocene layers, the construction of bored tunnels was for long regarded as difficult.

In the next section the main issues relating to tunneling are described. Subsequently, the difficulties which might occur when tunneling in soft soil will be discussed.

7.2.2 *Typical problems of bored tunnelling in soft soil*

According to Peck (1969[a]), the main problems related to bored tunneling are;

1. *Keeping a stable tunnel face,*
2. *Limiting the impact on the surrounding soil and foundations and*
3. *Keeping the tunnel safe and operational during use.*

Typical aspects which might lead to problems in relation to the construction of bored tunnels in the Dutch situation might be;

- *The geology. Very soft soil on top of Pleistocene sand*
- *Piled foundations in the Dutch cities,*
- *Groundwater level close to the soil surface*

Some of these difficulties are described in more detail below.

Feasibility of boring:

The feasibility of boring is discussed by various authors, for example by Peck (1969[a]).

Relevant aspects are:

- *Face stability.*
- *Excavation efficiency with respect to the soil encountered*
- *Maintenance and unexpected wear of cutter bits*
- *Unexpected objects*

Face stability: For a slurry shield, the working pressure for the slurry support is on the underside bounded by active failure of the soil and on the upper side by passive failure or blow out. Active failure might occur if the support pressure is too low to maintain equilibrium in the soil mass. Passive failure or blow out might occur if the support pressure is too high for the equilibrium of soil stresses. A blow out might lead to uncontrolled loss of support fluid.

Fig. 7.3 shows how the boundaries for the support pressure P_a are affected by the strength of the soil. It is indicated how the boundaries for the support pressure will be affected if the soil gets weaker; narrowing the bandwidth which is available for the support pressure.

In Fig. 7.4 the effect of the uncertainty in the upper and lower bound support pressure by means of the probability density of instability is indicated. For soft soils a problem arises if the safe range between lower and upper limit leaves a too small range for operating the working pressure of the face support.

A complicating factor might be if the vertical soil stresses are partially determined by water loading under the influence of tidal movements. The machine driver might have to compensate his slurry support pressure as a function of these tidal movements.

Maintenance and wear of cutter bits: It is not likely that this is an important issue in soft soil. The handling of very soft clay, however might give more problems.

Excavation efficiency. If there is a large diversity in soil layers; e.g. in the upper Holocene layers, the excavation efficiency might be affected. It will be difficult, then, to optimise the type of TBM on a single type of soil. Even during a

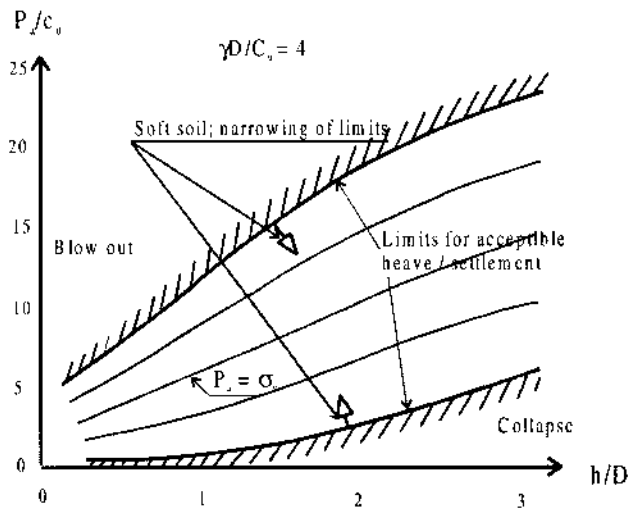

Figure 7.3 Face support pressure required for stability, for undrained conditions, (according to Mair (1987)), here C_u = undrained shear strength.

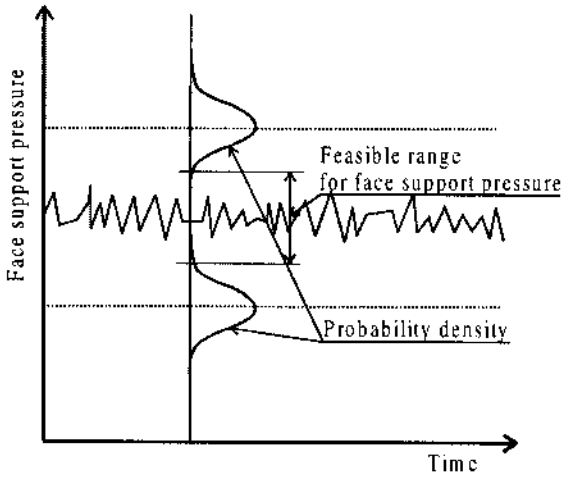

Figure 7.4 Stability range for face support pressure at a certain ratio for *h/D*

tunnel drive of only hundreds of metres, several types of soil might be encountered, often only in thin layers. The tunnel face might not be homogenous, and may exist of several soil layers of materials with a different permeability. This, coupled with the probability of water bearing layers, might give rise to local instabilities. For situations with a large variation in soil layers it is advisable to reduce the speed of excavation to ensure that the 'cake' formation on the front is not too much affected.

Unexpected objects: In the Netherlands, subsoil fossil wood might be encountered. During exploration for the sand closures during the Delta project, when large amounts of sand where needed, special consideration was given to this aspect. Seismological surveys in the Eastern Scheldt estuary indicated the existence of fossil wood in the subsoil. In practice however no problems where observed. The encountering of tree trunks however cannot be excluded.

In the Northern parts of the Netherlands, in the zone that was covered with ice in the last glacial period, boulders where carried by the ice from the Scandinavia to the Netherlands. The megalithic chambered tombs which can be found in the province 'Drente' are artefacts of that. Boulders might be encountered north of the 'Haarlem-Nijmegen' line in the Netherlands, and on the 'Utrecht chain of hills'

Limiting the impact on the surrounding soil and foundations

The impact on the surrounding soil and foundation, can be classified as follows

1. *Settlement trough, developing during tunnel excavation*
2. *Settlement in the surroundings of the tunnel due to drainage of the underground*
3. *Influence of tunnelling on settlements of foundations and/or reduction of pile bearing capacity*

Settlement trough. Numerical and analytical models indicate that the settlement trough is a function of the volume loss. The volume loss develops both at the tunnel face, and at the tail of the tunnel boring machine. The question is whether the volume is strongly related to the stiffness and or the strength of the soil. To begin with it is assumed that the main mechanism is kinematical.

Drainage: The effect of leaking tunnels on the global hydrology of an area must not be under estimated. Though the leakage water in tunnels can be pumped away; the pumping systems must be shown to be capable of solving such a problem. The effect on the surrounding area and settlements related to that can be larger than the initial settlements due to construction itself.

A case history was reported by O'Reilly et al. (1992), where the development of settlements above a tunnel were measured over a period of eleven years. The tunnel itself was located in very soft clay soil. Back-analysis revealed that the relative permeability of the lining in such a situation is high. Such is surely the case if the permeability of the surrounding soil is low.

Influence of tunnelling on piled foundations: In the western part of the Netherlands, most buildings are founded on piles. The length of these piles is often between 15 and 20 metres. It is to be expected that tunnel boring processes if undertaken in the Dutch cities will take place at or around that level of depth.

Normally during tunnelling, the volume of soil that is removed, is larger than the volume of the tunnel itself. Using the present techniques, this volume loss may be in the order of 1% of the tunnel volume. This volume loss influences the state of stress in the surrounding soil, which may cause additional settlement of nearby piles and a reduction in the bearing capacity of foundations.

The interaction between loaded foundation piles and a tunnel under

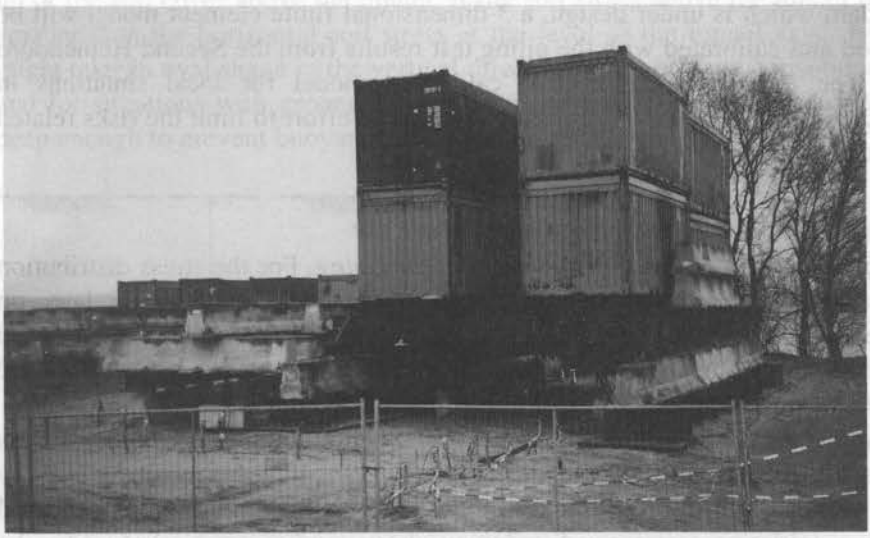

Figure 7.5 Test site for interaction Piled-foundation and tunnel boring at the site of the second Heinenoord tunnel

construction is complex. The problem is typically 3-dimensional and the stress distribution in the soil around a driven pile is still a point of discussion. Although numerical models for 3D analysis are available, the results need validation either by full scale measurements or by model tests in the centrifuge.

In 1994, this problem was modelled by centrifuge testing, (Bezuijen and van der Schrier, 1994). The tunnelling process was simulated using a model tunnel which consisted of a cylinder with a diameter which could be varied in a controlled way. Six piles at different distances from the tunnel, loaded to 75% of the ultimate bearing capacity, were used to investigate the pile-tunnel-interaction. During the test, in which the diameter of the tunnel was reduced, the settlement of the piles was monitored. Three different tests were performed; one preliminary test with limited instrumentation for a tunnel in homogeneous saturated sand, and two subsequent tests with a layered soil model analogous to the typical Dutch conditions, i.e. a (Holocene) clay layer on top of a (Pleistocene) sand layer. Based on these test, it was concluded that additional pile settlement due to tunnelling might become significant if the volume loss is above 1% and the distance between the pile and the tunnel is less than about one tunnel diameter. The settlement observed during the test concerned cases where the tunnel was located in the foundation (sand) layer. Extrapolation of the test results indicate that if the tunnel is located in the overlaying clay layer, the influence of the tunnelling process is less significant.

During construction of the Second Heinenoord tunnel, full scale tests were carried out using concrete and wooden piles, see Fig. 7.5. The results indicate that the pile bearing capacity is hardly influenced if the pile is further away than 1.0 tunnel diameter from the tunnel. Settlements follow more or less the settlement trough found at the soil surface. For the North-South metro line in Amsterdam which is under design, a 3 dimensional finite element model will be developed and calibrated with the piling test results from the Second Heinenoord tunnel. The application of such a calibrated model for local situations in Amsterdam, is thought to be a powerful tool in the effort to limit the risks related to the construction of this metro line.

Keeping the tunnel safe and operational during use

Soil stiffness effects on bending moments in the lining. For the stress distribution in the tunnel rings, the model developed by Duddeck (1980) and later on evaluated with respect to the influence of the stiffness of the bedding can be used to illustrate the influence of soft soil. This will be discussed in section 7.4.2 where the models for the analysis of tunnel lining behavior will be discussed.

Buoyancy. As the weight of the tunnel lining and the tunnel installation is less then the soil (including the groundwater) that is removed, the structure is initially not in vertical equilibrium. In order to gain equilibrium a slight upward movement, initiating a stress redistribution above, and a stress relief under the tunnel will occur until vertical equilibrium is reached. The effects of this are

related to the beam action of a tunnel, see section 7.4.2.

Axial equilibrium; At the stage of entering the receiving shaft after completion of a tunnel track, the axial stresses at the front, will diminish because the face pressure will be released when entering the free air. If no adequate measures have been undertaken, the axial stresses in the tube may reduce significantly. The axial stresses in the tube however contribute to the capacity of the tube to sustain shear forces, and therefore a procedure has to be developed to secure a sufficient shear force capacity between the rings.

7.3 MODES OF FAILURE FOR A TUNNEL LINING

In general a tunnel without artificial support, might fail either due to an inability to sustain the stresses in the roof of the tunnel, see Fig. 7.6a, or by overloading of the soil at the sides of the tunnel, see Fig. 7.6b.

Failure of the roof might be classified as a shearing failure, whereas, overloading of the sides is essentially a compressive failure. Both modes of failure might in practice be observed as a combined failure, such as illustrated in Fig. 7.6c. In order to avoid these types of failure, for situations where the soil is insufficiently strong to maintain an underground opening, a lining is added to the tunnel surface. If the lining is designed adequately, soil failure can be avoided.

If the tunnel lining is below the groundwater level, than a sufficient soil cover has to be available to prevent the tunnel to float and move upwards, see Fig. 7.7. This problem is solved in practice by ensuring a soil cover of approximately one diameter above the crown of the tunnel. Theoretically, for a very shallow tunnel which is above the groundwater table, another failure mechanism exists; breaking up of the soil cover above the tunnel. If the soil stress above the tunnel becomes smaller than the horizontal soil stress at the level of the tunnel axis, the tunnel might take an oval shape in the vertical direction. For normally consolidated soil, and for situations with groundwater, it is thought that if the tunnel is designed deep enough to prevent buoyancy, then breaking up is also prevented.

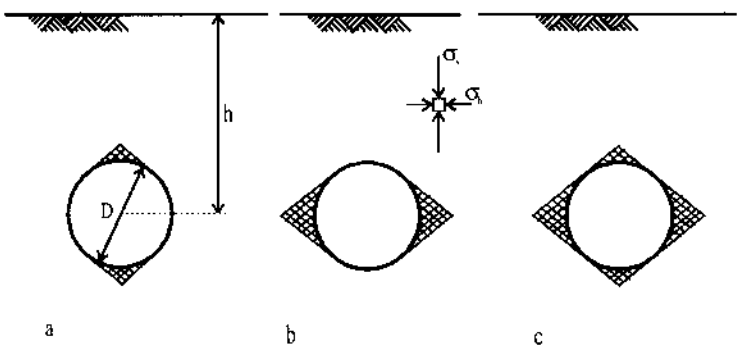

Figure 7.6 Failure modes for a (deep) tunnel (without a lining) in homogeneous soil

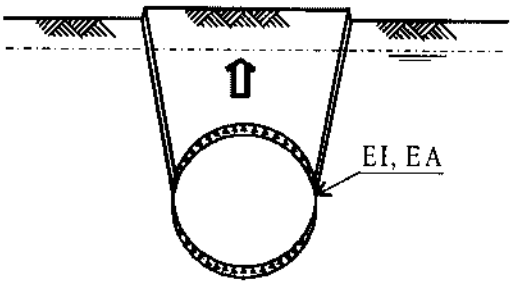

Figure 7.7 Buoyancy of a shallow tunnel with high groundwater level

Finally, for a lined tunnel, which is safe with respect to buoyancy and breaking up (i.e. if the tunnel is sufficiently deep) the normal deformation mode to be expected is horizontal ovalisation. This is associated with a minor stress relief above the tunnel, and a greater one below. Due to compression of the soil at the sides of the tunnel, a lateral stress increase will be observed, which tends to diminish the difference between the vertical stresses and horizontal stresses. For a flexible tunnel in stiff soil, the tunnel lining will be deformed by the soil stresses in such a way that the lining stresses are mainly due to hoop compression. This process is illustrated in Fig. 7.8, where the plastic zones around the tunnel are indicated. Due to this process, bending moments in the tunnel lining would ultimately vanish, and the only mode of failure left would be compressive failure of the lining.

Before we decide to design on the compressive strength of the tunnel lining only, we have to consider that additional bending moments might be introduced in the tunnel lining due to large deformation effects. We have to consider that the increase of these second order bending moments due to geometric effects might

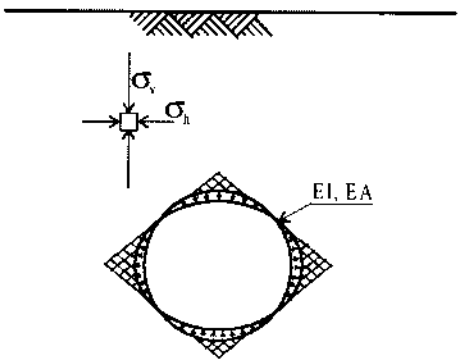

Figure 7.8 Compressive failure of a tunnel lining, in combination with soil failure around the tunnel. The plastic zones are indicated

exceed the decrease due to diminishing stress differences in the surrounding soil.

In order to evaluate this, an analysis of this mechanism has been done (see Appendix B). For this purpose a simple ultimate limit state model has been developed, where the relationship between the plastic bending moment and the deformations is derived. (This model assumes rigid plastic behaviour of the tunnel lining). The analysis gives:

$$M_{pl} = \frac{(1-K_0)}{4}\sigma'_v r^2 + \frac{(\sigma_v + \sigma_h)}{2} ru - \frac{E_g u r}{4} \tag{7.1}$$

Where the first part of equation 7.1 is related to bending moments caused by the initial stresses in the soil; (i.e. the distortional part). The second part is related to the compressive part of the soil loading; (i.e. only contributing if the tunnels deforms as a result of distortional loading). This part can be recognised as the influence of second order deformation contributions. The third part is related to the soil-structure response. Due to the compression of the soil at both sides of the tunnel, the difference between the magnitude of the soil stresses above and at the sides of the tunnel reduces.

To develop some insight into this relation, the relationship between bending moment and displacement has been worked out for a tunnel with a radius of $r = 4$ m, with a depth ratio $h/r = 4$, a $K_0 = 0.5$, a wet soil weight of $\gamma_w = 20$ kN/m^3 and for a groundwater table near the soil surface (see Fig. 7.9). This figure is drawn for the parameters which are representative for the situation at the Second Heinenoord tunnel. As one can observe the bending moment strongly reduces for a minor deformation of the tunnel lining. Based on this analysis, it must be doubted whether the choice for a high partial safety factor on the capacity for bending moments is a good investment. Maybe it would be more beneficial to

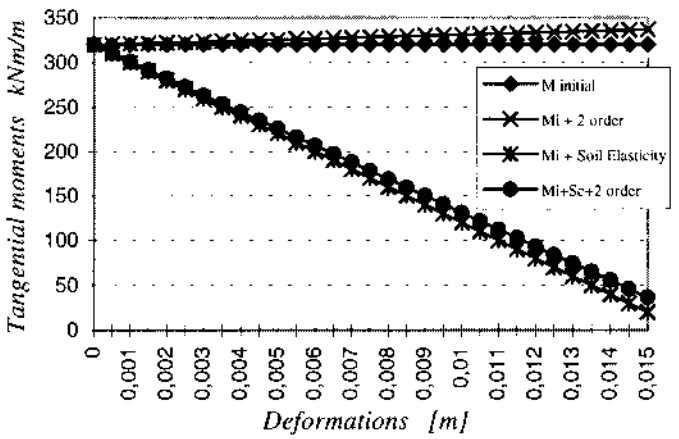

Figure 7.9 Bending moments as a function of deformations for a tunnel with a diameter of 8 *m.*, with a depth ratio of $h/r = 4$, for a soil stiffness of $E = 20000$ *kPa*, for a $K_0 = 0.5$

assure that the tunnel lining has a high flexibility, i.e. only a minor deformation of the lining will assure equilibrium of stresses due to the soil reaction.

Finally, special effects such as local failure in the tunnel lining, when the lining is composed of segments have to be accounted for. The shear force distribution calculated using equations A-3 and A-32 of Appendix A which gives:

$$Q = -\frac{(\sigma_v - \sigma_h)}{2} r \sin(2\theta)$$

whereas the distribution of the normal forces is according to

$$N = -(\frac{\sigma_v + \sigma_h}{2})r + (\frac{\sigma_v - \sigma_h}{2})r\cos(2\theta)$$

If there is an axial joint at a location where the ratio between normal and shear force is high, local shearing and subsequent failure of the tunnel might occur. If there is a friction modulus f, at the joint this would mean that

$$Q \leq N \ f \tag{7.2}$$

Working out a yield criterion for the analytic solution assuming K_0 for the initial soil stresses and disregarding the stress reduction due to soil structure interaction gives:

$$\left(\frac{1+K_0}{2}\sigma'_v + u\right) f \geq \frac{1-K_0}{2}\sigma'_v \tag{7.3}$$

where u is the groundwater pressure.

If u is zero, (i.e. for the situation without groundwater), the criterion becomes:

$$f \geq \frac{1-K_0}{1+K_0} \tag{7.4}$$

For a specific design, when there is soil-structure interaction and when the soil is layered and heterogeneous, the more general criterion given by equation 7.2 has to be evaluated.

Besides shearing at the axial joints as indicated above, shearing at the ring joints has to be considered because this may damage the waterproof sealing between the tunnel segments. If the capacity of the rubber sealing is exceeded, the sealing might fail and cause leakage, see also Fig. 7.33

In the next section the attention will be shifted to models for the analysis of the stress and strain distribution in a tunnel lining. The influence of the soil stiffness on the stress distribution in a tunnel ring is also described. This discussion starts by considering the design methodology.

7.4 STRUCTURAL ANALYSIS OF THE TUNNEL LINING

7.4.1 *Design methodology*

Soil loading is not the only loading to be evaluated for the dimensioning of a tunnel lining. This section, however, is limited to the evaluation of soil loading, because failure to support the soil leads to an ultimate limit state with major consequences.

According to NEN 6740 soil retaining structure should be evaluated for three states;

1. *Ultimate Limit State 1a*
2. *Ultimate Limit State 1b*
3. *Serviceability Limit State 2*

For the ultimate limit state 1a; ULS 1a, only the stability of the structure as a whole is regarded. We have to realise however that before the ULS 1a state is reached, in an earlier stage of loading the deformations might have a negative effect on the stability of other nearby structures. For that situation the ULS 1b criteria are formulated.

The criteria for the serviceability limit state are also related to deformations, but for the serviceability conditions of the structure itself.. The criteria for the SLS 2 state are related to the functioning of the structure. The partial safety coefficients for the different states, according to NEN 6740 are given in Table 7.1:

With respect to external loading, the partial safety factors for state 1a and 1b may be taken as 1.4 during construction, rather than 1.7. The consideration is that loads during construction, when considered and evaluated have a smaller variation, than has to be accounted for the loads during operation.

Essentially the factors given in table 7.1 should be used for all geotechnical structures, not being piled or raft foundations. Objectively however, determination of partial safety factors depends on the structural behaviour, and an

Table 7.1 Partial safety factors as given by NEN 6740

Limit State	*Ultimate*		*Serviceability*
Loading	*construction*	*unfavourable deformations*	
	1a	*1b*	*2*
Soil weight; $\gamma_{m,g}$	1.1	1.1	1.1
Groundwater pressures; $\gamma_{m,u}$	1.3	1.3	1.0
External load; $\gamma_{m,b}$	1.7/1.4	1.7/1.4	1.0
Soil friction; $\gamma_{m,\varphi'}$	1.2	1.2	1.0
Cohesion; $\gamma_{m,c}$	1.5	1.5	1.0
Material strength; $\gamma_{m,str}$	1.0	1.0	1.0

economic evaluation, see also chapter 2. In practice however, the derivation of partial safety factors is not restricted to such an evaluation.

As a tunnel is a flexible structure where soil structure interaction plays an important role in the development of the equilibrium stresses that determine the loading of the structure, there is a similarity between the lining on a bored tunnel, and a sheet pile wall such as discussed in chapter 6. For sheet pile structures based on probability theory and a balance between economic benefit and investment, a dedicated set of partial safety factors was derived, see the CUR 166 Sheet piling handbook, (1993).

For underground construction a similar approach has been undertaken by COB L510 (1996) which gives a more detailed set of partial safety factors for tunnel lining, depending on the loading combination.

In her studies for ITM, Mendez Lorenzo (1998), after Ruitenberg (1998) and van Kinderen (1995), investigated the reliability index of a tunnel lining. The purpose of this study was the derivation of partial safety factors for the ultimate limit state 1a, using the Approximate Full Distribution Approach (AFDA), applying Duddeck's model (1980). As Mendez Lorenzo wanted to optimise the design, she back calculated the Reliability index β, for a steel fibre reinforce concrete wall for several levels of steel fibre content α_{SFRC}. Having started with a lining thickness of 0.4 m, (d/D = 0.0444), she found an increase in the reliability index β, for a decreasing lining thickness, see Fig. 7.10.

Mendez Lorenzo extended her initial linear model to incorporate both geometrical and material non-linear behaviour. With respect to geometrical non-linear behaviour, for the lining thickness of 0.4 m, she found an amplification factor of 1.07 (M_{II}/M_I). Whereas this value increases for smaller lining thickness, finally leading to buckling for a lining thickness between, 0.17 and 0.22 m., depending on whether short or long term loads where considered. Mendez

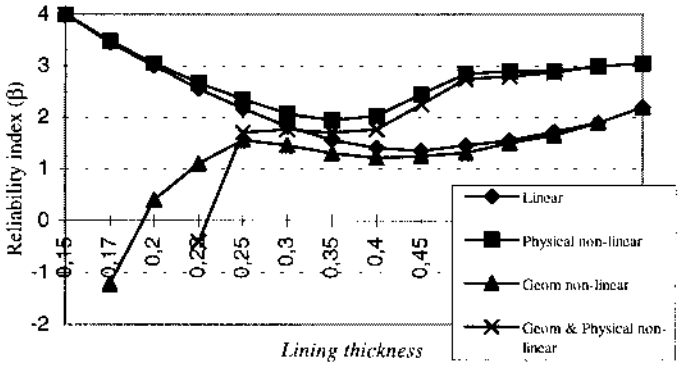

Figure 7.10 Reliability index as a function of lining thickness, according. to Mendez Lorenzo (1998) for α_{SFRC} =0.05 ;B45 and R = 4.7 m

Lorenzo concluded that for a lining thickness of 0.3 m (d/D = 0.033), see also Fig. 7.10, geometrical non-linear effects become important. For a lining thickness, of more than 0.3 m, she claims that the material non-linear behaviour of the concrete lining, is of more importance than the geometrical non-linear behaviour.

As she introduced partial factors of safety both for the model and for the parameters, a comparison of her results with Table 7.1 is not straight forward and is not attempted here.

The main recommendations from the work of Mendez Lorenzo on partial safety factors are

1. *the use of a partial safety factor on the elastic properties of the soil; E_s and ν_s, between 1.2 and 1.3*
2. *A partial safety factor of 1.1 with respect to the groundwater level*
3. *All other partial safety factors being kept 1.0*

It must be noted here, that the assumption of a variation coefficient of 0.1 and the rigorous adoption of $K_0 = 1 - \sin\varphi$, according to Jaky (1944), are doubtful. For the over-consolidated Pleistocene sand layers, K_0 values of more than 1.0 might be expected, which deviate significantly from the values given by the Jaky relation.

In contrast to flexible retaining walls, the tunnel lining in soft soil is not a flexible structure. In that sense there is more resemblance with a concrete panel wall. For such a situation the soil loading is more depending on the stiffness ratio between structure and soil than on the plastic parameters of the soil. The adoption of partial safety factors on the friction angle or the cohesion would indeed be peculiar than. In that light one of the outcomes of the study of Mendez Lorenzo, i.e. that the uncertainty with respect to stiffness becomes dominant, and therefore it can be understood that it is advised to adopt partial safety factor on the elastic properties of the soil.

Before a more definite set of partial safety factors for the design of tunnel lining can be established, two more steps have to be taken:

1. *General agreement on the definition of the ultimate limit states*
2. *Agreement on a sufficiently efficient model*

If these requirements are met, the establishment of a set of (partial) safety factors is relatively straight forward.

The discussion related to the adoption of an efficient model for the description of stress and strain in the tunnel lining is given in the next section.

7.4.2 *Models for the analysis of stresses in the tunnel lining*

Ring action; analytic solutions

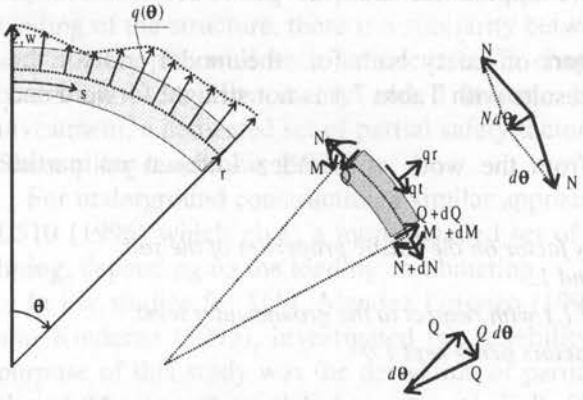

Figure 7.11 Equilibrium of a curved beam

According to Hetenyi (1946) and Bouma (1993), see Fig. 7.11, the stresses in the curved wall of a lining with a linear soil reaction, are governed by;

Radial equilibrium:

$$\frac{d^2M}{ds^2} - k_r w_r + \frac{N}{r} - q_r = 0 \tag{7.5}$$

Tangential equilibrium:

$$\frac{dN}{ds} - k_t w_s - \frac{Q}{r} + q_t = 0 \tag{7.6}$$

and a Kinematics equation:

$$EI\left(\frac{d^2 w_r}{ds^2} + \frac{w_r}{r^2}\right) + M = 0 \tag{7.7}$$

where k_r is the radial subgrade reaction modulus of the soil and k_t is the tangential subgrade reaction modulus. The variables u_r and u_s are the radial and the tangential displacements.

These expressions lead to the following differential equation:

$$\frac{d^5 w_r}{ds^5} + \frac{2}{r^2}\frac{d^3 w_r}{ds^3} + \left(\frac{k_r}{EI} + \frac{1}{r^4}\right)\frac{d w_r}{ds} - q + \frac{K_r}{r} w_s = 0 \tag{7.8}$$

For the more simple situation of a loaded curved beam without bedding, (i.e. $k_r = 0$, $k_t = 0$ and $q \neq 0$), Bouma derived a characteristic solution which can be

compared to a stiff tunnel in very soft soil, for a rough wall (including the tangent loading). A description of this derivation, is given in Appendix A.

The main results of the analysis are:

Normal force:

$$N = -\frac{(\sigma_v + \sigma_h)}{2} r + \frac{(\sigma_v - \sigma_h)}{2} r\cos(2\theta) \tag{7.9}$$

Shear force:

$$Q = \frac{\sigma_v - \sigma_h}{2} r\sin(2\theta) \tag{7.10}$$

Bending moment:

$$M = -\frac{(\sigma_v - \sigma_h)}{4} r^2\cos(2\theta) \tag{7.11}$$

Where σ_v = vertical soil stress, σ_h = horizontal soil stress and r = the radius of the tunnel.

Finally the deformation of the tunnel lining with respect to its centre can be calculated according to:

$$w = -\left(\frac{\sigma_v + \sigma_h}{2}\right)\frac{r^2}{EA} - \left(\frac{\sigma_v - \sigma_h}{12}\right)\frac{r^4}{EI}\cos(\theta) \tag{7.12}$$

This solution disregards the influence of stress redistribution due to differences in stiffness between soil and structure. To overcome this shortcoming, subgrade reaction models have to be used.

Subgrade reaction models

When the tunnel tube liner and the soil interact; a subgrade reaction, (such as included in equations 7.5, 7.6 and 7.7), has to be accounted for. In that case an analytic solution is difficult to derive. Numerical solutions such as those derived Duddeck (1980, 1984 & 1991) are more appropriate then. These solutions can be shown with graphs such as given in Fig. 7.12

In the following description, an evaluation will be given of the influence of the soil stiffness on the circumferential stresses in the tunnel lining, in order to clarify the behaviour of the concept developed by Duddeck.

For the situation that $\sigma_h = K_o\sigma_v$ and for the condition that $K_o < 1$, for a tunnel which is situated not too shallow, the tunnel will take an oval shape in the horizontal direction, giving an increase in horizontal soil stresses and a reduction in the stress difference. In the limiting case of a very weak soil reaction the subgrade reaction model implicitly describes the results of the analytical model as discussed in section 7.4.2 Which means that for bending moments and normal

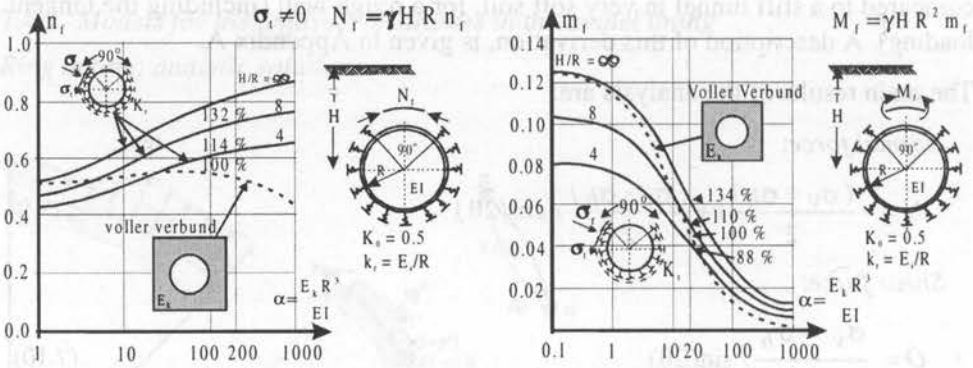

Figure 7.12 Results of the Duddeck model for tunnel analysis as a function of the subgrade reaction ratio

forces in a tunnel lining, the effect of the relative stiffness can be 'visualised' as a reduction factor on the rigid solution (see Fig. 7.12). The reduction is a function of two elasticity parameters:

$$\alpha = \frac{E_g r^3}{E_b I_d} = \frac{E_g D^3}{8 E_b I_d} \qquad (7.13) \qquad \text{and} \qquad \beta = \frac{E_g r}{EA} = \frac{E_g D}{2Ed} \qquad (7.14)$$

where

E_g = The Young's modulus of the soil
D = The diameter of a tunnel; $D = 2r$
E_b = The Young's modulus of the concrete wall
I_b = The moment of inertia of the cross-section of the tunnel wall; $I_b = 1/12\, d^3$
d = The thickness of the concrete liner

The evaluation is made for horizontal stresses given by $\sigma_h = K_0\, \sigma_v$ and using an adapted notation, where a new parameter m is introduced, according to $m = \frac{(1 - K_0)}{4}$, which is equivalent to reading the relationship between circumferential bending moment and soil loading according to $M_{max} = m\sigma_v r^2$ (which can be compared with equation 7.11).
For the relations derived by Duddeck, which are illustrated in Fig. 7.12, approximate empirical relations are found in literature, see Vrijling (1998). For the circumferential normal force, according to:

$$N = -C_0^N \frac{(\sigma_v + \sigma_h)}{2} r + C_2^N \frac{(\sigma_v - \sigma_h)}{2} r \cos(2\theta) \qquad (7.15)$$

and for the circumferential bending moment that operates in the tangential cross-sections according to:

$$M = -C^M \frac{(\sigma_v - \sigma_h)}{4} r^2 \cos(2\theta) \tag{7.16}$$

where:

$$C_0^N = \frac{2}{2+1.54\beta} \text{ (7.17)}, \quad C_2^N = \frac{2(1+0.064\alpha)}{2+0.171\alpha} \text{ (7.18)}, \quad C^M = \frac{4}{4+0.342\alpha} \tag{7.19}$$

Fig. 7.12 is drawn for $K_0 = 0.5$, and for a homogeneous soil. Duddeck indicated a region of application between $5 < \alpha < 200$ which would mean a reduction in the bending moment with respect to the initial situation (no stress redistribution) of between 20 and 80 %.

Two-ring subgrade reaction models

In practice the liner of a bored tunnel is often constructed by mounting rings of curved segments at the end of the liner build in the previous construction phase. Therefore the tunnel ring is not continuous but segmental, (see also Fig. 7.18). The liner will have 'ring' joints between adjacent rings, and axial joints, between the segments in a ring.

An evaluation will be made of the approximate behaviour of the model, for values of the parameters which are representative for the Dutch soft soil situation.

Before the evaluation is possible some assumptions and simplifications are made. To begin with the elasticity of the segmental liner for bending for a unit width is assumed as: $I_d = \frac{1}{12} d^3$.

A direct relationship between the liner thickness and the tunnel diameter is assumed according to: $d = \frac{D}{20}$. Furthermore the evaluation is made for a feasible range of the ratio between elasticity of the liner and elasticity of the soil of: $\frac{E_b}{E_g} \approx (1 \text{ to } 10) * 10^3$.

For soft soil conditions, this leads to a feasible range for the flexibility parameter α, according to:

$$\alpha \approx \frac{12 * 10^3 E_g}{Eb} = \frac{12 * 10^3}{(1 \text{ to } 10) * 10^3} \approx (1 \text{ to } 12) \tag{7.20}$$

This means that for soft soil conditions we are nearly out of the range of application $10<\alpha<200$ as indicated by Duddeck. The reduction of circumferential stresses in the liner (bending moments) will therefore be much less than indicated for the range of application, only 10 to 30 %, instead of 20 to 80%. In practice the bending moment is not only determined by the flexibility parameter α, but also by the grouting process and the stress relieve in the surrounding soil associated with this. The latter effect is not included in the model derived by Duddeck.

If the liner is composed of segments there will be joints between the segments.

These joints may limit the capacity to sustain bending moments. If the joint is loaded with an eccentric normal force, (i.e. if the eccentricity is larger than the centre 'core' of the beam), tensile stresses would develop at one side of the beam. Tensile stresses cannot develop in the joint however, and this will lead to an increase in local compressive stresses, and/or a redistribution of stresses to adjacent segments. This behaviour might significantly reduce the bending stiffness. A first assumption might be to neglect the bending stiffness and strength of an axial joint. However, a single ring with such joints but without soil support is not in stable equilibrium. Since the variation in the soil parameters is such that it is not recommended to rely on the stiffness of the soil to achieve equilibrium, the problem is normally solved by accounting for the interaction between adjacent rings to deliver the necessary stability.

Finite element analysis

Mindlin beam elements

In section 5.3.5 the theory for straight structural elements was described. With the increased interest in bored tunnelling the demand for a curved beam elements to model circular tunnels increased. Therefore in 1992 curved beam elements were developed for use in the computer code PLAXIS. The development and implementation of curved beam elements can be viewed upon as an upgrade in

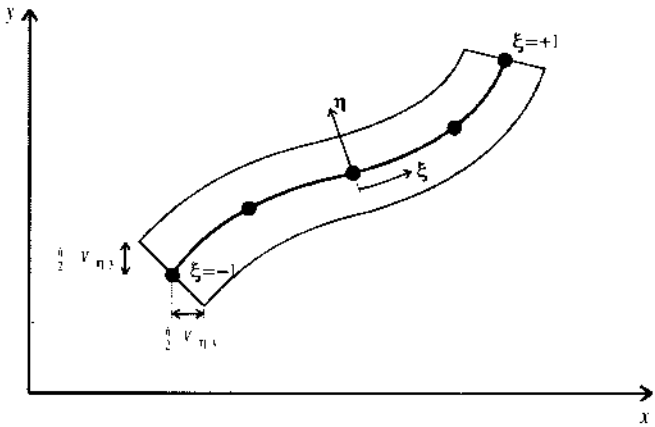

Figure 7.13 Five noded Mindlin beam element

comparison with the hybrid beam element which is discussed in section 6.3.4 which before 1992 had been the standard for PLAXIS. After a short review of the literature with respect to structural elements, the Mindlin type beam element, as described by (Bathe 1982) was adopted.

According to Mindlin beam theory, the beam is modelled as a two-dimensional plane-strain element, where the degrees of freedom are all located in the neutral axis of the element. This enables the use of the element as a thin element, similar

to the Euler beam theory, or the Reisner type of structural element such as discussed in section 6.3.4

The displacements within a Mindlin Beam element are interpolated according to:

$$\begin{Bmatrix} x(\xi,\eta) \\ y(\xi,\eta) \end{Bmatrix} = \sum_{i=1}^{5} N_i(\xi) \left[\begin{Bmatrix} X \\ Y \end{Bmatrix}^i + \frac{h}{2}\eta \begin{Bmatrix} V\eta x \\ V\eta y \end{Bmatrix}^i \right] \tag{7.21}$$

where $\boldsymbol{V}$ contains the vector elements of the normal to the axis of the beam, X_i and Y_i are global nodal co-ordinates and h, (see Fig. 7.13), is the height of the beam element. N_i contains the vector of interpolations.

The deformations within the element are given by:

$$\begin{Bmatrix} u(\xi,\eta) \\ v(\xi,\eta) \end{Bmatrix} = \sum_{i=1}^{5} N_i(\xi) \left[\begin{Bmatrix} u \\ v \end{Bmatrix}^i + \frac{h}{2}\eta \begin{Bmatrix} -V\eta y \\ V\eta x \end{Bmatrix}^i \theta^i \right] \tag{7.22}$$

where Θ_i is the rotation at node *i*

The advantages of this element are:

1. *the curvature of a beam can be taken into account*
2. *the influence of a deflection of the cross-section, which is important for a relatively deep beam, is implicitly taken into account, and*
3. *a more straight forward extension of material non-linearity, such as plasticity, becomes feasible.*

The Mindlin beam element was successfully implemented and verified in the computer code PLAXIS, see Song (1993)

Phased analysis scheme

One of the features enabled by finite element analysis is the ability to model the

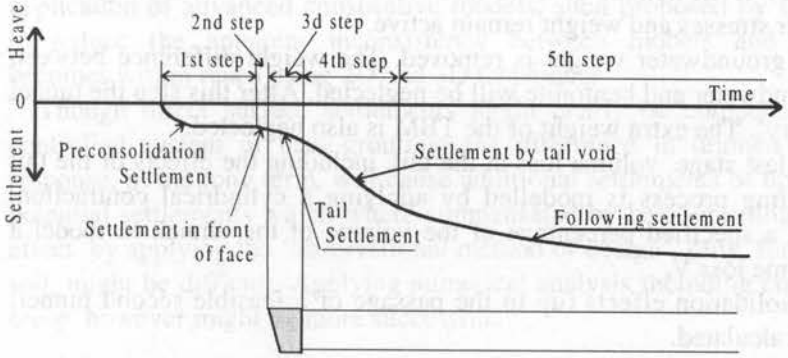

Figure 7.14 Five steps in ground displacements (Fujita 1993)

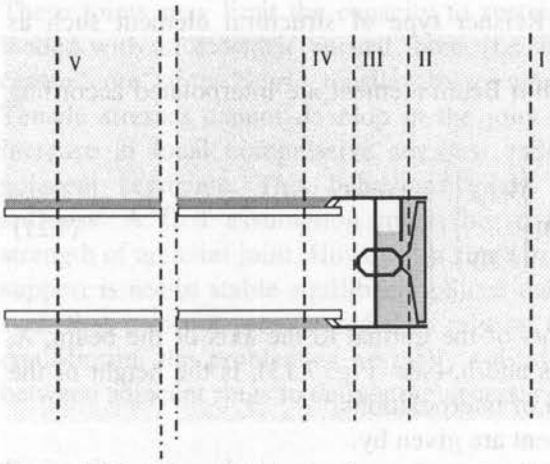

Figure 7.15 Phased analysis of tunnel construction

staged excavation of the tunnel structure. According to Fujita (1993), see Fig. 7.14, a number of steps are recognized in the staged construction of a bored tunnel. An important step is the volume loss V_s of the soil at the tail of the boring machine. This volume loss is of the order of 1 to 2 % of the tunnel area. Though this volume loss might be more or less compensated by grouting of the tail void, consolidation and creep effects lead to the situation that a partial volume loss of 0.5 to 1.0 % cannot easily be avoided. Volume loss causes surface settlements, and stress relief. The latter is important for the analysis of stresses in the tunnel lining. This volume loss cannot easily be modeled with a subgrade reaction model.

The development of the structure, such as illustrated in Fig. 7.15, can be modelled by applying staged construction features, (i.e. contraction and de-watering), and ensuring equilibrium of the structure.

The following stages of analysis are proposed, Bakker (1996):

stage I: initial stresses are calculated using the K_0 procedure.

stage II: The tunnel lining is activated while simultaneously the soil inside the tunnel is de-activated. This also de-activates the soil weight. The water stresses and weight remain active.

stage III: The groundwater weight is removed. The weight difference between groundwater and bentonite will be neglected. After this step the tunnel is 'dry'. The extra weight of the TBM is also neglected.

stage IV: The last stage, volume loss at the tail, including the effects of the tail grouting process is modelled by applying a cylindrical contraction, with a specified percentage of the volume of the tunnel, to model a volume loss V_s .

stage V: Consolidation effects (up to the passage of a feasible second tunnel) are calculated.

stage VI: For a second tunnel, the stage II, III, IV and V are repeated.

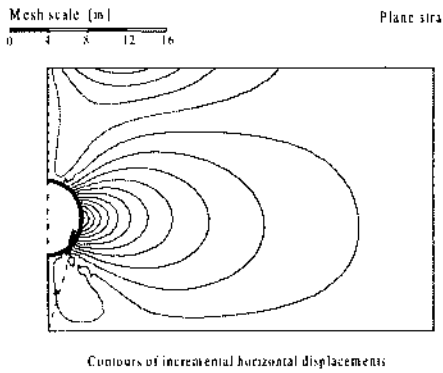

Figure 7.16 Contours of horizontal displacements due to tunnelling

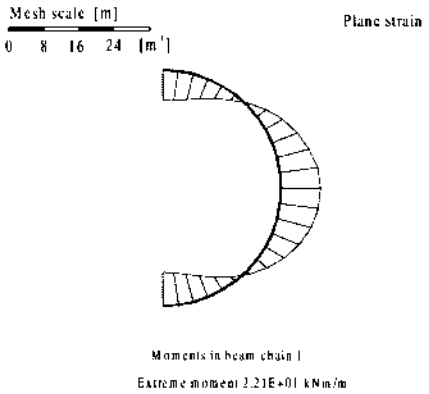

Figure 7.17 Bending moments in lining

Since 1996, as a result of the monitoring of the Second Heinenoord tunnel it came clear that this scheme is unable to give a good description for the surface settlements. For that a more refined approach taking into account the pressure distribution in the annulus grouted behind the tail of the tunnel boring machine is needed. As surface settlements are not the main focus in this study, the analyses performed here are mainly based on the staged construction scheme given above, using the contraction model.

In order to illustrate the relationship between finite element analysis and empirical models the results of a typical finite element analysis is illustrated in Fig's 7.16 and 7.17. In Fig. 7.16 the horizontal displacement contours are given to illustrate the similarity with the results of a more simple subgrade reaction model. For a tunnel in homogeneous soil even the symmetry in the distribution of bending moments are reproduced, as shown in Fig. 7.17.

The use of finite element analysis for tunnel analysis allows time-dependent phenomena such as consolidation and creep to be modelled. In addition, the application of advanced constitutive models, such proposed by Duddeck (1991) to reduce the apparent inconsistency between models and measurements, becomes within reach using 2D and 3D techniques.

Though direct surface settlements might nearly be compensated by a well controlled system of back-grouting, the difference in drained and undrained response, in the long term, will cause additional settlements of up to 60 % of the potential settlements which where compensated by back-grouting. Avoiding this effect by applying the 'observational method of design' only, for low permeable soil, might be difficult. Applying numerical analysis including consolidation and creep, however might be more successful.

Segmental lining and 3D finite element modelling

Up to this point, in this chapter, soil-structure interaction, and the effect of the stiffness ratios between soil and structure have been discussed with only minimal attention to the fact that the lining is composed of segments. Segmental linings however can be viewed as an assembly of blocks, connected by joints. This construction is similar to that of stacked structures such as masonry, brickwork and pre-cast concrete assemblies. In essence this aspect is truly three-dimensional. To gain insight into the staged development of stresses in a tunnel-ring during construction, three-dimensional models are needed.

A non-linear finite element strategy whereby the segments are modelled by continuum elements and the joints by interface elements might be feasible. The non-linear behaviour will mainly be concentrated in the relatively weak and flexible joints while the relatively strong concrete segments can be modelled as linear elastic. With this approach the total strength and stiffness, (flexibility), of the assembly might be analysed.

Due to the reduced stiffness at the axial joints a transfer of bending moments to adjacent segment rings might occur, leading to an increase in the magnitude of the bending moment by up to a factor of two. The flexibility of axial joints also act to reduce the bending moments, due to soil structure interaction. In this case, numerical analysis indicates that the bending moments for this type of configuration are about 1.6 times greater than values calculated for the solid ring configuration, see Visschedijk (1996).

To illustrate this behaviour, one of the predictions for the instrumented rings used to monitor the Second Heinenoord tunnel is shown in Fig. 7.18. This monitoring project showed that to understand the deformation behaviour of a segment it is not sufficient to monitor stresses and strains only. The differential displacements between segments must also be monitored. At the Heinenoord tunnel, special instrumentation was installed for this purpose.

Finally, the analysis of segmental behaviour is important, especially in the case of soft soil and a high groundwater table. A lining composed of separate stressed

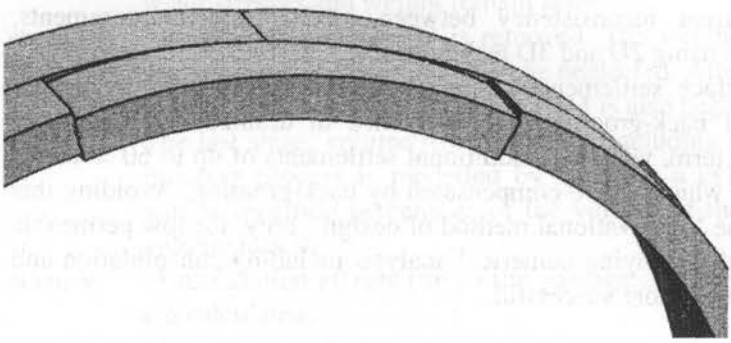

Figure 7.18 Deformation of a segmental lining

segments, with hinged joints, that is compressed by the surrounding soil is an unstable structure. Large differential movements between segments might influence the water tightness of the lining, and therefore affect the serviceability of the structure.

Special aspects; second order bending moments

In cross-sectional equilibrium, the circular lining of a tunnel will react to the external soil loading both by circumferential hoop forces, as well as bending moments. In the sense that a lining attracts both normal forces as well as bending moments, it is comparable to an eccentrically loaded column. The latter is, for the ultimate limit state, evaluated including second order large deformations According to Timoshenko (1936), in the ultimate limit state, the critical circumferential load (or hoop-force), for the lining is

$$N_{cr}=\frac{3EI}{r^3} \tag{7.23}$$

Where r is the tunnel radius. According to, among others, Besseling (1975), the bending moments including second order effects, can be approximated by:

$$M^2=M^1+\frac{n}{n-1}N^1\delta^1 \tag{7.24}$$

where

$$n = \frac{N_{cr}}{N^1}$$

M^1 = *the first order, (small deformation) bending moment*
N^1 = *the acting normal force*
δ^1 = *the first order amplitude in deformation*

Based on this assumption, Mendez Lorenzo (1998) related the reliability index to the lining thickness, for an homogenous tunnel ring theory, using probability theory. She made her analysis for a standard tunnel with a radius of r = 4.7 m, a wall thickness of 0.4 m, concrete with a compressive strength of 45 mPa, (B45 according to the Dutch code of practice), and a ratio of steel fibre content of $\alpha_{sfrc}=0.05$, see also section 7.4.1.

Mendez Lorenzo reached the unexpected conclusion that the reliability index β increased for a decreasing lining thickness, see Fig. 7.10. This unexpected behaviour can be explained by the fact that an increasing flexibility of the lining leads to an increased capacity to adjust to the differential loading and subsequently to a decrease in bending moments in the lining. We have to consider however, that if the lining thickness is decreased beyond a critical value, this behaviour is overtaken by second order effects, and bending moments will increase again. Mendez Lorenzo established a critical lining thickness of 0.3 m. see Fig. 7.10, for a tunnel with a diameter of 9.4 m. Beyond this, second order

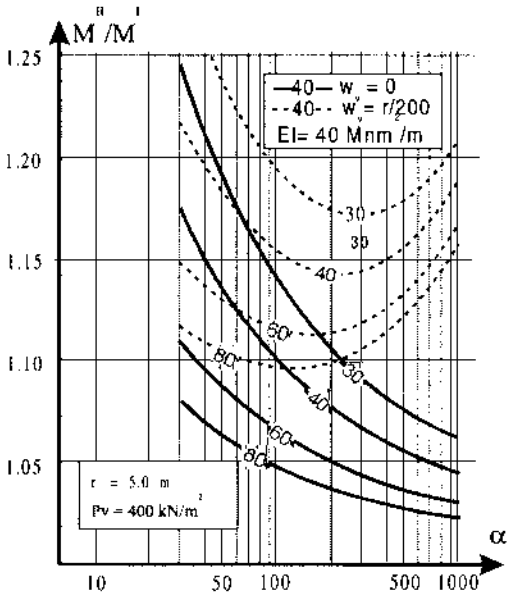

Figure 7.19 Second Order Bending moments, Ahrens (1982)

effects dominate the behaviour.

Ahrens (1982) carried out an extensive study of second order effects for tunnels too. The results, see Fig. 7.19, confirm that second order geometric non-linearities will be more important for lower values of the α factor. In the example of Mendez Lorenzo a multiplier of 1.17 was found comparing to first order analysis. This value fits in well, for example in the graphs given by Ahrens, who gives a value of this multiplier as a function of α, see Fig. 7.19, where α is the flexibility index as introduced by Duddeck.

In a study of TNO, Steenhuis (1995) indicates that for soft soil conditions, if the influence of imperfection in the configuration is included, the bending moment might even be as high as 1.42 times the first order bending moment, especially for the low α values. In his study Steenhuis takes into consideration that the assembly of the segments might introduce imperfections with respect to the ideal ring which explains the difference between his work and that of Ahrens.

Just after that the segments are placed and still within the tail of the TBM machine and not yet subjected to the prestressing support of the soil, they have to support heavy loading by the jacks pushing the TBM forward. This may cause irreversible deformations in the joints. Well considered placing of coupling bolts might mitigate this effect. Analysis of the phenomena might be carried out using 3D finite element techniques as illustrated in Fig. 7.18

Longitudinal action and beam action

Due to the staged construction of a tunnel lining, the tube is loaded in longitudinal direction as well as in the circumferential direction. Due to this process, bending moments and shear forces develop along the tunnel length. The development of these distributions of force and bending moment is influenced by the construction method. The construction may be characterised as adding tunnel rings onto the tube which are subsequently loaded by the groundwater due to the buoyancy forces, but also due to actions from the tunnel boring machine. These actions are, an (eccentric), axial load, and a vertical (shear) force, see Fig. 7.20. The axial loading by the tunnel boring machine is not considered further, because

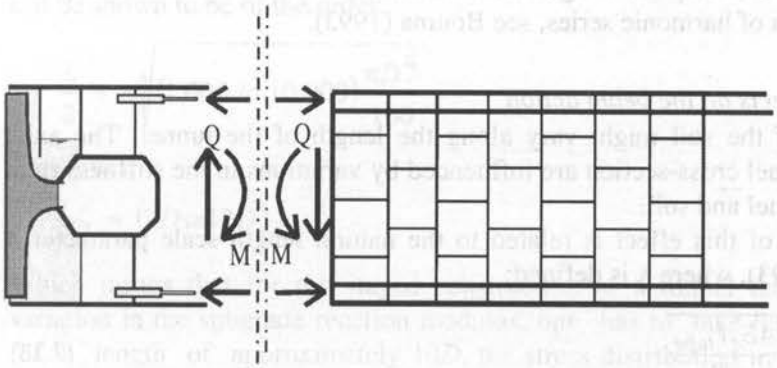

Figure 7.20 Loading. of the tunnel beam by the tunnel boring machine

in the model developed here, the axial force itself has no direct influence on the longitudinal bending moment. The eccentricity is, however, important and is modelled here as an external bending moment.

Subgrade Reaction Model for the Longitudinal Stresses

The differential equation which describes the beam action of a bored tunnel is derived from the well known concept of a beam on elastic foundation. According to Hetenyi (1946), this equation was first developed by Winkler in 1867. Assuming a subgrade reaction which is proportional to the deflection of the beam an extended equation for the lateral equilibrium of a slender beam in bending may be written as:

$$EI\frac{d^4w}{dx^4}+kw=q \tag{7.25}$$

where:

w = *the deflection of the beam*
k = *the subgrade reaction modulus of the soil*
q = *the distributed load on the beam (per Unit of width)*
EI = *the bending stiffness (per unit of width)*

The solution of this equation is simplified by the introduction of the additional parameter β_s, according to:

$$4\beta_s = \frac{k}{EI} \quad or \quad \beta_s = \sqrt[4]{\frac{k}{4EI}} \tag{7.26}$$

The differential equation then simplifies to

$$\frac{d^4 w}{dx^4} + 4\beta_s^4 w = q \tag{7.27}$$

For the homogeneous equation a general solution is available which is composed of a combination of harmonic series, see Bouma (1993).

Soil stiffness effects on the beam action

The stiffness of the soil might vary along the length of the tunnel. The axial stresses in a tunnel cross-section are influenced by variations in the stiffness ratio between the tunnel and soil.

The measure of this effect is related to the natural length scale parameter λ (see Bouma, 1993), where λ is defined:

$$\lambda = \frac{2\pi}{\beta_s} = 2\pi \sqrt[4]{\frac{4E_t I_{tube}}{K}} \tag{7.28}$$

The value of λ (in fact half this value), might be interpreted as a measure of the distance on which a local force makes balance with the subgrade reactions. Furthermore, the maximum of the induced bending moments is proportional to λ^2.

The parameters which are determinate for λ are:

E_t	=	*the Young's modulus for the material of the tube*
I_{tube}	=	*Moment of inertia for bending of the tube*
K	=	*subgrade reaction modulus for the soil (note that here the notation K is taken instead of k, because now the width of the beam is included in the equation; i.e. k is multiplied with the beam's width to derive K*

We can estimate the value of the length λ, using the following assumptions and simplifications:

1) The moment of Inertia for a thin lined tube is estimated as: $I_{tube} \approx \frac{\pi}{8} dD^3$,

   where

   D = *Diameter of the tube,*
   d = *Thickness of the liner.*

2) A continuous bedding is assumed both under and above the tunnel, and therefore the subgrade reaction for the tube is approximated, as: $k \approx 2\,D\,k$,

3) The subgrade reaction modulus for the soil is approximated as; $k \approx 2E_s/D$, where

   E_s = *the Young's modulus for the soil.*

Subsequently if we apply these assumptions, in combination with equation 7.28, an estimate can be made of this influence length according to:

$$\frac{\lambda}{2}=\pi\sqrt[4]{\frac{\pi E_t dD^3}{8E_S}} \tag{7.29}$$

If it is assumed that $E/E_s \approx$ (1.000 to 10.000), and $d \approx D/20$, then the length scale can be shown to be of the order:

$$\frac{\lambda}{2} \approx \pi\sqrt[4]{(1.000 \text{ to } 10.000)\frac{\pi D^4}{160}}$$

This gives:

$$\lambda/2 \approx (7D \text{ to } 12D) \tag{7.30}$$

Which means that for the staged construction of a tunnel tube, if there is a variation in the subgrade reaction modulus, one has to take into account that for a length of approximately $10D$, the stress distribution in the tube will be influenced.

The lower the stiffness of the soil, and/or the higher the stiffness of the tube (larger diameter), the more inaccurate becomes the assumption that every ring in the tube is in distinct equilibrium with the supporting soil. Generally, a low stiffness of the soil will cause larger deformations before equilibrium is achieved.

Quantitative analysis of the beam action

Bogaards (1999) has developed a method for the analysis of the stresses in a tunnel lining behind a tunnel boring machine. In order to illustrate the scheme he developed, in Fig. 7.21, the addition of subsequent segments (tunnel-rings), is sketched. The assumption is made that at each successive stage there is a stable equilibrium of forces and stresses. In each successive step a new tunnel ring is added, thus extending the length of the tunnel. We can recognise in Fig. 7.22, where 7.22a is the old stage of construction, and 7.22c is the new stage of construction, that 7.22b has to be added to the system to derive the desired equilibrium state. That is; putting the external forces on the one side of the new segment, and releasing the forces on the other side of the segment. This scheme indicates, that to derive the stress state at a certain stage of construction, the former stages of construction have to be summed up, as illustrated in Fig. 7.21.

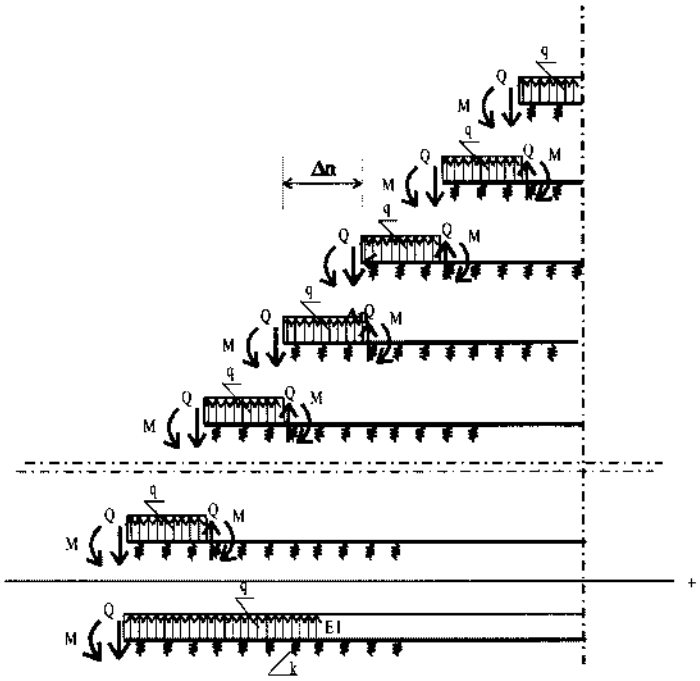

Figure 7.21 Conceptual model for the analysis of longitudinal stresses in a tunnel lining

In more detail, Fig. 7.22 shows that three partial contributions have to be considered. These are:

1. *The distributed load q due to buoyancy*
2. *The shear force Q produced by the tunnel boring machine*
3. *The eccentric axial force introduced by the tunnel boring machine, modelled as an external bending moment M.*

Distributed load: For the distributed load due to buoyancy an analytical solution, by Boogaard (1998) is available. This solution gives:

$$M_q(m) = -EI\beta^2 \sum_{n=1}^{m} e^{-\beta n \Delta_n} \left(-2C_1 \cos(\beta n \Delta_n) + 2C_2 \sin(\beta n \Delta_n)\right) \tag{7.31}$$

where

$$C_1 = -\frac{q}{k} e^{-2\beta\Delta_n} \sin^2(\beta\Delta_n) \tag{7.32}$$

and

$$C_2 = \frac{q}{k}\left[\left(\sin^2(\beta\Delta_n) - \frac{1}{2}\right)e^{-2\beta\Delta_n} + \frac{1}{2}\right] \tag{7.33}$$

where Δn is the element length, (i.e. the width of a tunnel ring which is being constructed).

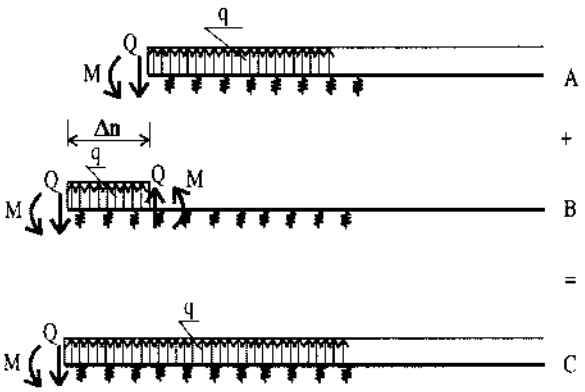

Figure 7.22 Staged construction of a tunnel tube, adding segments

To obtain more insight into this concept, additionally an approximate derivation will be given. For this approximate concept, a new element with a distributed load is modelled in a different way, as shown in Fig. 7.23. Here, the interaction at the tunnel ring is neglected. The load of the new segment is modelled with a force and an external moment at the point of connection only.

The force is derived from the general solution for a point load on the end of an half infinite beam, see Bouma (1993), which gives:

$$M_q^1(m)=\sqrt{2}\sum_{n=1}^{m}\frac{1}{2}q\Delta_n^2 e^{-\beta(n-1)\Delta_n}\sin(\beta(n-1)\Delta_n+\frac{\pi}{4}) \tag{7.34}$$

The second part, is derived from the solution for a bending moment, which is:

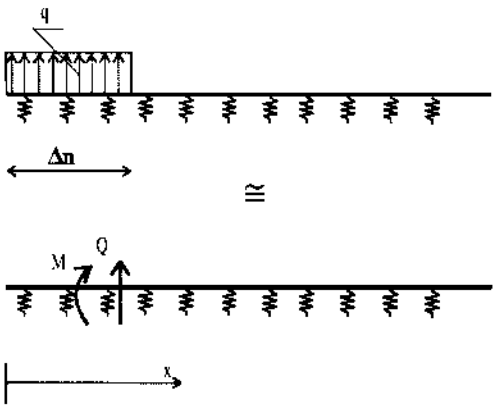

Figure 7.23 Modelling the distributed load, as the sum of an external moment and a shear force

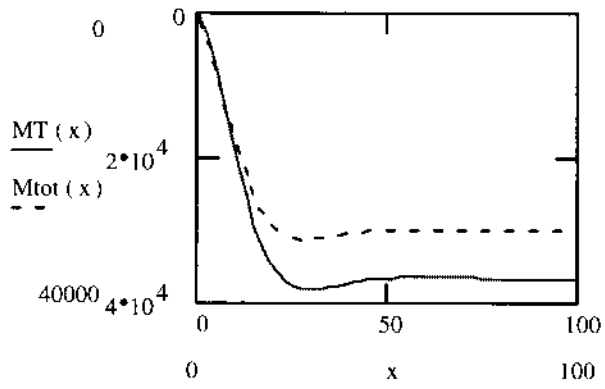

Figure 7.24 Comparison between analytical solution, eq. 7.26, (here indicated as Mtot), and the approximate solution, (here indicated as MT). Here in this graph, x denotes the number of rings of 1.5 m

$$M_q^2(m) = \frac{1}{\beta}\sum_{n=1}^{m} q\Delta_n e^{-\beta(n-1)\Delta_n}\sin(\beta(n-1)\Delta_n) \tag{7.35}$$

The effect of the buoyancy is than calculated by summing $M_q = M_q^1 + M_q^2$

The difference between the approximate solution of 7.34 and 7.35, and the solution of 7.31, is illustrated in Fig. 7.24

For small values of Δn, the solutions are identical. For larger, more realistic, values of Δn the approximate solution overestimates the bending moment, because the stress reduction of the interaction at the segment due to the bedding in the interval Δn is neglected.

Eccentric load: For the eccentric axial loading, in this simplified model, a constant eigen moment is introduced in the tube by the tunnel boring machine

$$M_{exc} = M_{TBM} \tag{7.36}$$

Shear force: For the shear force introduced by the TBM, the following relation is derived:

$$M_Q(n) = -\sqrt{2}\sum_{m=1}^{n} Q\Delta_n e^{-\beta m\Delta_n}\left[\sin\left(\beta m\Delta_n + \frac{\pi}{4}\right)\right] \tag{7.37}$$

The bending moment at segment n, can than be calculated by summing up the three partial contributions:

$$M(n) = M_{distr} + M_{exc} + M_Q \tag{7.38}$$

In section 7.5.5, this theory is compared with measurements of the 2nd Heinenoord tunnel.

7.5 FIELD STUDY SECOND HEINENOORD TUNNEL

7.5.1 *Introduction*

In 1993, two pilot projects for bored tunnelling were started, as described in section 7.2. Both projects were accompanied by an extensive monitoring programme. At the time of writing of this section, 2000, the construction of the Second Heinenoord tunnel, see Fig. 7.25, has been completed. The tunnel was opened for the public on 16 September 1999. In this section, a brief overview of the monitoring project with respect to the research related to the tunnel lining is given.

To begin with some general information about the project will be given. Then the the instrumentation of the measuring rings will be described.

In between, a simple model will be described which relates the uncertainties with respect to the positioning of tunnel segments with additional stresses in the lining.

A back-analysis of the stresses in the tunnel lining will be described, where it will be shown that a distinction between stresses due to installation and due to soil loading has to be made. Finally the measurements of the longitudinal stresses will be compared in a back-analysis using the Bogaards model described in section 7.4.2

7.5.2 *The second Heinenoord tunnel*

The existing Heinenoord tunnel in motorway A 29 used to be a source of daily congestion for the traffic to and from the Rotterdam Europoort area. To extend the motorway capacity from 2 x 2 lane to 2 x 3 lanes a new water crossing had to

Figure 7.25 Artistic aerial view of the Heinenoord tunnels

be constructed for local traffic. This new crossing was originally designed in 1990 as an immersed tunnel. Due to budget problems, however, the project was postponed until 1993. The opportunity to use this tunnel as a pilot project for bored tunnelling has stimulated the construction of the tunnel.

In 1996 the construction of the project was started with the simultaneous construction of shafts and ramps. TBM tunnelling was began in February 1997 from the North Bank and the machine was turned on the South Bank to start the construction of the second tube in the reverse direction. Finally the tunnel drive was completed in June 1998, on the North Bank. The total length of the tunnel is 1350 m. (one way), with a TBM part of 950 m. The cross-section consists of two tubes with an external diameter of 8.30 m. There are no cross passages. A detailed study of the suitability of machine types for the soil in-situ, showed a slight preference for a slurry type machine above an earth pressure balance (EPB) shield. The former was therefore chosen.

Geological profile and soil properties at Heinenoord

To investigate the geological situation at the site, an extensive site investigation program was carried out. This included, bore-holes, vane-tests, CPTs, dilatometer- and pressuremeter tests. Parameters such as strength and weight where derived from laboratory tests.

On the North Bank and the South Bank of the river Oude Maas, measuring sites with a size of approximately 50 x 75 square metres each were installed for geotechnical monitoring, see Fig. 7.26 and K100-01 (1995). The approximate location is indicated by the marks A and B in Fig. 7.25. The side of the field nearest to the start shaft is at a distance of 75 metres, where there is a soil cover of 12 metre on top of the roof of the tunnel, increasing up to 13 metre at the other side of the measuring field. To measure the influence of the tunnelling process on ground parameters, a measuring system was installed, including surface level points, inclinometers, extensometers, soil pressure cells, and water-pressure gauges.

The tunnel cuts through cohesive Holocene layers and sandy Pleistocene layers. At the test site on the North Bank, the tunnel goes mainly through Holocene deposits and sand layers. At the test site on the South Bank, however, peat and clay layers are also present. On both test sites, only the invert is bedded into the Pleistocene sand. The tunnel is driven entirely below the ground water table, which lies at +0.60 N.A.P. (N.A.P. is the Dutch reference level).

7.5.3 *The monitoring scheme*

During the preparations for a monitoring scheme it was realised that a fruitful project would need a frame of reference to work within. If monitoring is developed from the objective of the Observational method, see Peck (1969[b]), the objective of monitoring is clear; i.e. limiting the risks, and preventing unnecessary investments. Here monitoring was developed from a much broader

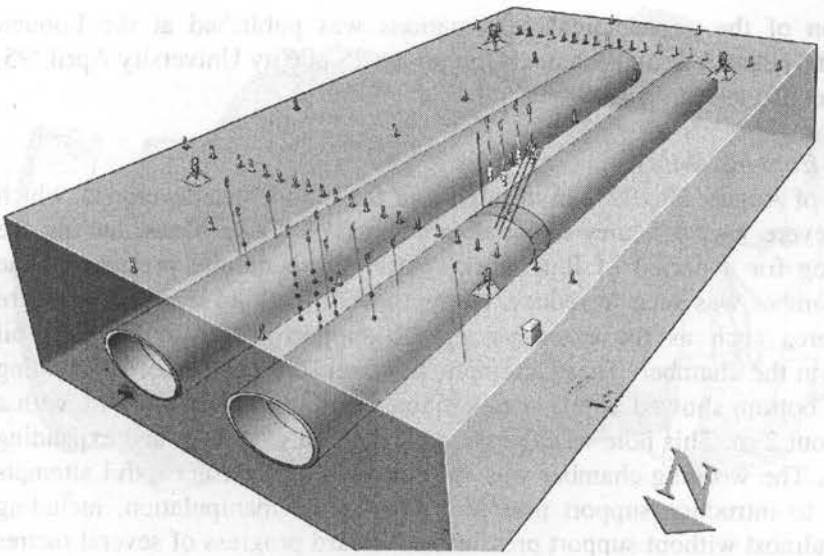

Figure 7.26 Measuring field at North Bank of river 'Oude Maas'

feeling that the Dutch engineering industry would benefit from the monitoring of the first large diameter bored tunnel in the Dutch soft soil. Such a scope does not offer clear limits what to monitor, and therefore the methodology of model development was adopted.

Without such a frame of reference, if was felt that the objective for the monitoring would not be clear enough. The risk might be there, that one collects data which later proves to be unnecessary. Alternatively, essential data might be missing. In order to provide a suitable frame of reference, two statements have been proposed:

'Measuring is knowing'
'A measurement which has been preceded by a prediction has added value'.

Therefore, it was decided to make predictions related to the measurements, and to evaluate the measured data in the light of these predictions. The predictions, based on empirism, numerical analysis and the use of physical models were executed and reported before the construction phase of the tunnel, see K100-04 (1997).

A statement of the areas where further geotechnical knowledge relating to boring of tunnels in soft soil is needed was reported by Bakker et al. (1997).
The monitoring scheme consisted, of three separate parts.

1) *Monitoring the processes related to the tunnel boring machine*
2) *Monitoring of the geotechnical deformations*
3) *Monitoring of the structural behaviour of the tunnel lining.*

A prediction of the geotechnical deformations was published at the London meeting and Symposium of Technical Committee 28 at City University April '95, see Bakker et al. (1996)

7.5.4 *Bore front instability*

In the night of August 28 1997, an instability of the tunnel face developed, which lead to a severe loss of slurry material into the river Oude Maas, halting the tunnel boring for a period of four weeks. After the bentonite pressure in the working chamber was seen to reduce, attempts were made to maintain pressure with measures such as the extension of the support plates to prevent soil penetration in the chamber. These attempts, however, did not succeed. Sounding of the river bottom showed a hole with a diameter of approximately 6 m. with a depth of about 2 m. This hole was excavated and filled with sand and expanding clay pellets. The working chamber was then cleaned, and unsuccessful attempts were made to introduce support pressure. After some manipulation, including excavation almost without support pressure, a forward progress of several metres without excessive displacements was achieved. After this the support pressure could be increased. Thus moving the construction on from the location of the incident.

Although the machine, at the time of the instability, had been operated with a support pressure much higher than the vertical soil pressure, the main cause of the incident was blamed on heterogeneity in the subsoil, possibly due to the fact that somewhere in the vicinity of the incident, during the construction of the first immersed Heinenoord tunnel, a mooring pole had been present.

7.5.5 *Structural behaviour of the tunnel lining*

In two locations under the measuring fields, one under the North Bank, and one under the measuring field on the South Bank, a tunnel lining ring was equipped with strain gauges placed in various different directions (ten strain gauges per segment).

All seven segments in a ring were instrumented to measure the entire stress distribution in the ring (see Fig. 7.27), as a function of time and distance behind the TBM. Pressure cells were put on the outer surface of the segments, (two pressure cells per segment on 7 segments), to compliment the strain gauges.
To measure differential deformations between segments, special devices where placed, bridging the joints between segments. Details of these instruments are given by Leendertse (1997[a]).

To measure the deformations of the tunnel lining at the time that the tunnel rings are loaded by the soil, (and the tail grouting), if the tunnel boring machine moves forward during excavation, a special laser equipped theodolyte system, which automatically measures inclination and distance of a number of pre positioned points on the lining was developed. This to overcome the problems related to insufficient space for ordinary position measurements in the cramped

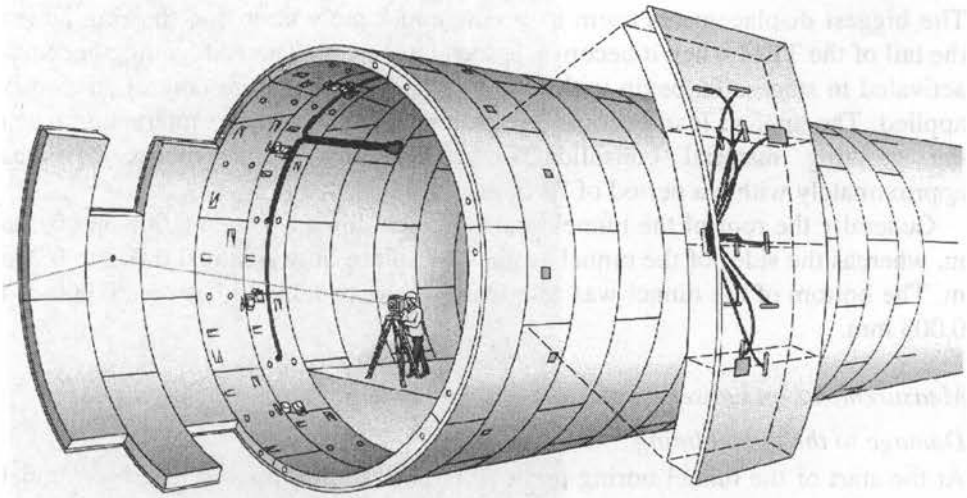

Figure 7.27 Measuring ring and instrumentation

workspace just behind the tunnel boring machine in front of and besides the train with support equipment of the TBM.

This system measured the deformations of the lining during the period that the unloaded ring leaves the tail of the TBM and becomes loaded by the soil. This is the position where the largest gradient in deformation with respect to time was expected. An indication of the measured radial displacements is given in Fig. 7.28

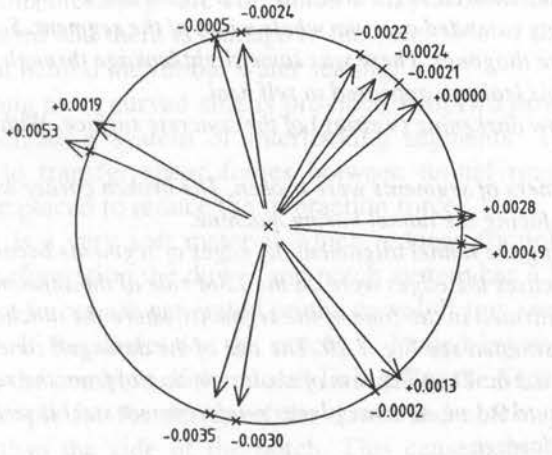

Figure 7.28 Deformations of the lining, Ring 568, measurement series 200, cycle, 148 and 149 just after installation and soil loading. Deformation with respect to the tunnel centre.

The biggest displacements seem to occur immediately after that the ring leaves the tail of the TBM when it becomes loaded by the soil. The soil loading becomes activated in stages. To begin with, due to grouting, a pressure controlled load is applied. The applied load becomes dominated by soil structure interaction when the grouting material consolidates and hardens. This process develops approximately within a period of 24 hours.

Generally the roof of the tunnel tends to come down between 0.002 and 0.006 m, whereas the sides of the tunnel seems to displace outwards just 0.002 to 0.005 m. The bottom of the tunnel was relatively stable, coming up between 0.000 and 0.003 mm.

Measurements and observations at the tunnel lining

Damage to the tunnel lining

At the start of the tunnel boring process, (when the constructed length of tunnel was less than 100 m.), damage to the lining was higher than expected. To obtain a better understanding of this damage, a project was issued and carried out by Leendertse (1997[b]). Some characteristic conclusions of his report are reported here. A simple kinematics model will also be described relating inaccuracies in assembly of the tunnel ring to the observed damage.

A description of the damage pattern is given below:

1. *Nearly all the joints were subjected to differential deformations which might be as much as 30 mm. The differential deformations on the longitudinal joints within one ring, however, are significantly smaller.*
2. *In many places there was leakage between adjacent segments. There is not a clear relationship between the observed differential deformations and the amount of leakage water.*
3. *Some of the segments showed slight cracking, over about half of their length. This cracking extended over the whole width of the segment. Some of these cracks were diagonal. There was some slight leakage through these cracks, but this leakage appeared to self heal.*
4. *Some segments show darkening (wetting) of the concrete surface. Without any visible cracks.*
5. *At some places corners of segments were broken. The broken corner was always on the side facing the tunnel boring machine.*
6. *In many places along the tunnel alignment the edges of segments became snapped off. In all cases the edges were on the TBM side of the segment. The damage concentrated in the zone of the segments where the notches for the dowels are situated see Fig. 7.29. The size of the damaged zones were up to 0.4 m x 0.5 m. The thickness of shales coming of from the ring surface might be up to 0.1 m. At some places reinforcement steel is visible due to this type of damage*
7. *On more than one occasion, the edges of segments adjacent to the key segment (the closing segment of the tunnel ring), became damaged. Often the damage to edges of the key segment has extended to the entire segment width.*

Figure 7.29 Damage to the tunnel lining; i.e. damage near the dowel and notch system

As described above, the damage was not exclusively concentrated near the key segment but appeared, to a lesser degree at the flanks of the tunnel too. Apart from cases where edges snapped of, most of the damage is concentrated on the dowel and notch locations. Although there is not a one-to-one correlation between places with leakage and places of damage, there is a strong feeling that the locations of leakage are correlated with places where the back wall of a notch is overloaded and there is damage to the outer side of the tunnel segment forming a short cut behind the rubber water sealing.

Each ring at its curved side is provided with two dowels (or notches), see Fig. 7.30, to create a system of interlocking segments. This ensures that there is capacity to transfer shear forces between tunnel rings. On the dowel, kaubit stripes are placed to reduce the interaction forces.

Kaubit is a very soft material which reduces friction (if there is any). In the design configuration the dowel and notch system has a free deformation of 6 to 7 mm before forces are generated on the dowel. If this space is exceeded, the dowel is loaded. If the dowel (or the notch) is loaded beyond its capacity, damage is caused to the concrete of the tunnel lining. For the Second Heinenoord tunnel the main principle for the design of the dowel and notch system is that the dowel is stronger than the side of the notch. This caused the breaking of fragments on either sides of the wall, depending on the direction the dowel is loading the side of the notch.

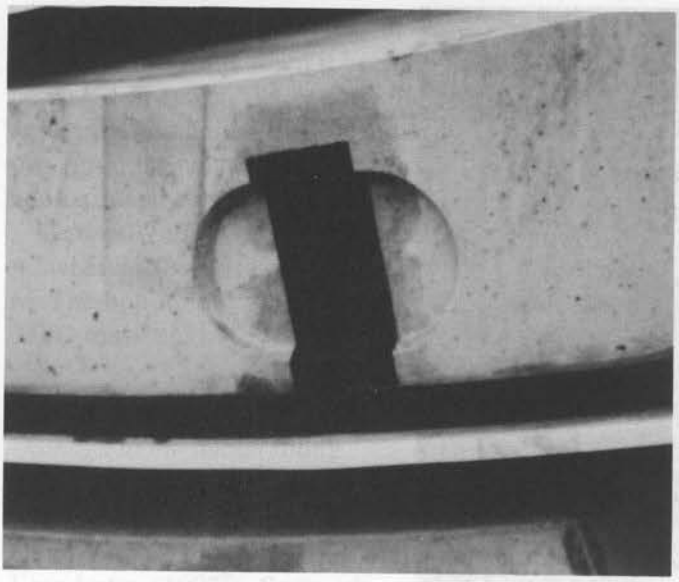

Figure 7.30 Dowel and notch connection in the ring joint. Here the notch with Kaubit strip is shown.

At the ring joint triplex wood plates were used instead of Kaubit to avoid damage due to assembly stresses. It is a topic of further research at this moment whether these wood plates were effective.

Evaluation of the structural observations

To understand the possible causes of the damage, three mechanisms are recognised and analysed:

- *Compression of the ring due to loading, when a tunnel ring leaves the tail of the TBM machine.*
- *Oval distortion of the ring due to the distortion part of the loading on the ring.*
- *Inaccurate installation of the segments of a tunnel ring*

Quantitative estimates are described below of the extent to which these mechanisms contribute to the to differential deformations.

Compression of the ring: The distribution of the compression of the ring can according to den Hartog (1952) be modelled with the theory of a beam on elastic foundation, with a bedding modulus of $k = Ed/r^2$

where

E = *the Young's modulus of the lining material*
d = *the lining thickness*
r = *the tunnel diameter.*

Table 7.2 parameters for the Second Heinenoord tunnel

r	= 3.975 m, (tunnel radius)
d	= 0.35 m (lining thickness)
h/r	= 3
K_0	= 0.5
γ_n	= 18 kN/m^3
E	= 30.000.000 kPa

For a first estimate however it is not necessary to calculate the distribution of the compression of a tunnel ring. An estimate of the decrease of radius for the second Heinenoord tunnel will be made. This estimate can be derived with the first term of equation 7.12.

The mean loading on the tunnel wall is estimated to be of the order $q_1 = \bar{\sigma} = \frac{3r((1+K_0)(\gamma_n - 10)+10)}{2}$. This is equivalent to the mean stress level at the depth of the centre of the tunnel, here for an estimated depth of the roof of the tunnel of one diameter.

The radial displacement of the tunnel is given by:

$$\frac{\delta w_1}{r} = -3\left(\frac{((1+K_0)(\gamma_n - 10)+10)}{2}\right)\frac{r^2}{Ed} \tag{7.39}$$

Based on the parameters of Table 7.2 the change in diameter is estimated to be $\delta w_1 = 0.00025m$.

Ovalisation of the ring: assuming a first order approximation in a similar way, the distortion deformation of the ring due to a Fourier loading can be calculated from the analytic solution of section 7.4.2

$$\frac{\delta w_2}{r} = \frac{1}{6}\frac{q_2 r^3}{EI}\cos(2\theta) \tag{7.40}$$

The parameter q_2 can be estimated in a similar way to q_1 as $q_2 = 3r\frac{(1-K_0)}{2}(\gamma_n - 10)$.

The second moment of area is given by $I = \frac{1}{12}1(d)^3 = \frac{d^3}{12}$

Combining these components gives the lateral deflection:

$$\max\left(\frac{\delta w_2}{r}\right) = 3(1-K_0)(\gamma_n - 10)\frac{r^4}{Ed^3} \tag{7.41}$$

For the parameters of Heinenoord tunnel as presented in Table 7.2 and taking in consideration that the flexibility of the lining is less than for a homogeneous one by dividing the stiffness by 2, gives $\max(\delta w_2) \approx 0.005\ m$. This is not a negligible

deformation. Apparently the free space in the dowel is just enough for a segment ring to adjust to the soil loading without loading the dowels. Inadequate positioning of the notch and dowel system however will exceed the tolerance though.

Inaccurate installation: The third mechanism to evaluate is the influence of irregular installation of lining segments, and the subsequent influence on the installation space for the key block.

The geometry model being used assumes an objective frame of reference for the centre of the tunnel to be constructed. Installation of adjacent segments is assumed to be such that:

- *segments are not rotated with respect to their ideal inclination in space.*
- *segments have an arc length S with a mean value of* $\mu_s = 2\pi r/n$, *and a standard deviation of* σ_{s_0}
- *segments are placed adjacent to the previously placed segments with its connection side on the line from the centre of the frame of reference going through the end of the previously placed segment.*

Observed from the centre of the tunnel, the projection of the segment on the ideal ring gives a wedge with an arc which depends on the radius of the segment to the objective centre and its structure size. The assumption underlying this concept is that the arc length (on the ideal circumference) is influenced by the accuracy with which the segments are placed in the radial direction, see Fig. 7.31

An inaccuracy of δr in the radius of a tunnel will add up to an in the total circumference of the tunnel ring of $2\pi\delta r$. If we transform this relationship for

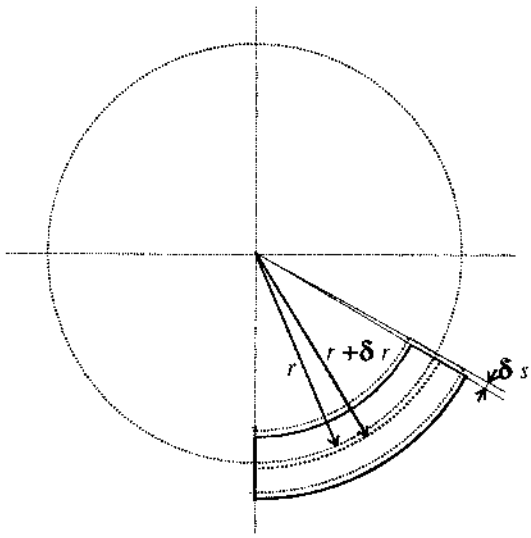

Figure 7.31 Geometry model for the installation of lining segments

an tunnel segment, we have to divide this by the number of segments. Thus the contribution to the projection on the ideal tunnel ring circumference, based on error in the radius is for a single element calculated as $\delta l = \frac{2\pi}{n}\delta r$

For sake of simplicity of the model, a rotation of the segment is not considered, as the contribution of a rotation is only of a second order.

If we combine this with the inaccuracy of the arc length of the segment itself, caused by the fabrication inaccuracy, we can calculate a standard deviation for the arc length of the projection of the segment on the ideal tunnel radius. This standard deviation is a weighted sum of the standard deviation of installation inaccuracy and fabrication inaccuracy according to:

$$\sigma_s = \sqrt{\sigma_{s_0}^2 + \left(\frac{2\pi}{n}\sigma_r\right)^2} \tag{7.42}$$

If we sum this up for n segments to make the circle, the standard deviation of the closing gap can be found. Given that the mean value of the gap will be $n\frac{(2\pi r)}{n} - 2\pi r = 0$, we only have to consider the standard deviation for which we have:

$$\sigma_o = \sqrt{n}\sqrt{\sigma_{s_0}^2 + \left(\frac{2\pi\sigma_r}{n}\right)^2} = \sqrt{n\sigma_{s_0}^2 + \frac{(2\pi\sigma_r)^2}{n}} \tag{7.43}$$

Furthermore we will look into the size of the gap for a reliability index of β, which means that

$$\Delta O = \beta\sigma_o = \beta\sqrt{n\sigma_{s_0}^2 + \frac{(2\pi\sigma_r)^2}{n}} \tag{7.44}$$

Subsequently it is assumed that for a negative gap, the only degree of freedom to fulfill a successful installation of the key block, (here sketched with zero dimension), is that the adjacent segments rotate with respect to the point with which these are connected to the other segments, such as indicated in Fig. 7.32. For simplicity, it is assumed here that the lining segments are rigid.

The space created by the rotational deformation, see Fig. 7.32, assuming symmetry is

$$\Delta w = \frac{\frac{1}{2}\Delta O}{\sin(\zeta/2)} \tag{7.45}$$

where ζ is the arc enclosed by a segment, that is: $\zeta = 2\pi/n$.

This finally gives a radial displacement according to:

$$\Delta w = \frac{\Delta O}{2\sin\varsigma/2} = \frac{\beta\sqrt{n\sigma_{s_0}^2 + \dfrac{(2\pi\sigma_r)^2}{n}}}{2\sin\varsigma/2} \tag{7.46}$$

Substituting $\varsigma = 2\pi/n$ into this equation gives:

$$\Delta w = \frac{\Delta O}{2\sin\varsigma/2} = \frac{\beta\sqrt{n\sigma_{s_0}^2 + \dfrac{(2\pi\sigma_r)^2}{n}}}{2\sin\pi/n} \tag{7.47}$$

We will evaluate this relationship for the following data related to the Second Heinenoord tunnel:

$$\sigma_s \approx 0.00025m = 0.25mm$$
$$\sigma_r \approx 0.002m = 2\ mm$$
$$n = 7$$

Equation 7.47 is linear in the reliability index. Therefore, if we evaluate equation 7.47 for the parameters given, assuming $\beta = 1.96$, we find that the gap is in excess of 0.011 m for 2.5 % of the rings. Here for the reliability index the relationship for a normal distribution is assumed. In combination with a reliability index of $\beta = 1.64$, that is, for 5 % of the rings, the displacement will be in excess of 0.009 m.

Depending on the distribution of the strength of the fixation with which the ring is fastened to the tube, this rotational deformation might develop with other couples of segments in the ring. Fig. 7.33 shows that this mechanism of displacement was in fact observed in the tunnel lining.

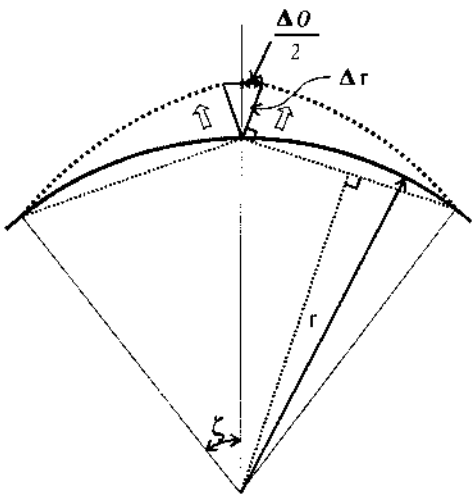

Figure 7.32 Rotational deformations of lining segments due to a lack of space near the key block.

Figure 7.33 Differential displacement as observed at the Second Heinenoord tunnel

These observations led to a more detailed numerical analysis of the construction stage of the tunnel lining. The results of this analysis support the conclusion that a proper control of the installation phase is crucial for an adequate control of the integrity of the lining segments. A detailed description of this analysis is given by Blom et al. (1998).

These analyses showed that the largest displacements are triggered by inaccurate installation, and to a lesser degree by ovalisation. In the tunnel itself, tilting of segments with respect to the axis perpendicular to the tunnel axis, in the horizontal plane, is also observed. This mechanism also contributes to the displacement as calculated here. Tilting might be triggered by the step-wise development of the grouting pressure on to a segment as the tail of the TBM moves forward. A quantitative evaluation of this effect is not attempted here however.

Measurements of stress and strain in the Lining

During the tunnel boring, as described in section 7.5.3, measurements of circumferential normal forces and bending moments in the tunnel lining were made. In this section these measurements are evaluated. In the preparation phase of the monitoring, predictions have been made with different models. The number of models used makes it difficult to discuss the advantages and disadvantages of the different models in a comprehensive way. In this section therefore a back-analysis with the analytical models such as described in section 7.4.2 is outlined. The result of this analysis will be compared with the measured

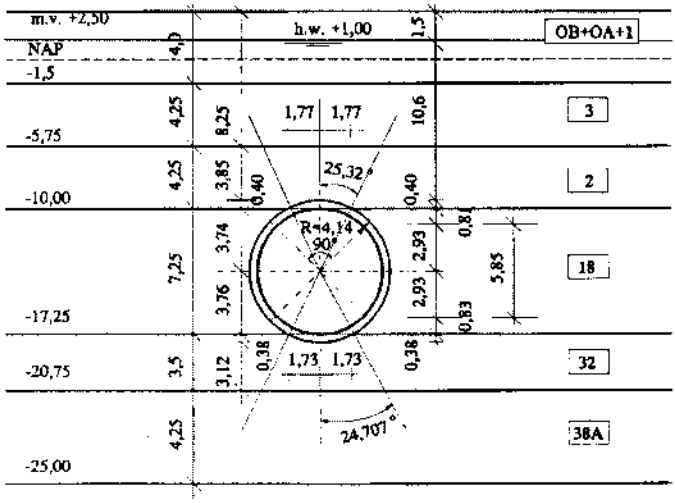

Figure 7.34 Cross-section measuring field North

data. Finally the differences are evaluated using a PLAXIS back-analysis.

Back analysis for measuring ring 'North Bank'

A summary of the main soil data from the 'K100 data set for predictions', is given in Table 7.3.

For the analytical model, the stresses, σ_v, and σ_h, in the soil at the level of the tunnel centre are calculated which are determinate for the bending moments in the tunnel lining. These stresses are calculated, summing up the soil weight, and accounting for the water pressure, using the data given in Table 7.3. The cross-section given in Fig. 7.34 was taken as a starting point.

Back analysis with the analytical model

The effective horizontal soil stresses, are calculated using the K_0 relationship. Based on the geology as indicated in Table 7.3 and Fig. 7.34, the horizontal and vertical soil stresses at the tunnel axis are calculated as: $\sigma_v = 300\ kPa$ and $\sigma_h = 218$ kPa. Subsequently with equation 7.11 and 7.9 the stresses in the tunnel lining are calculated for the situation that the wall of the tunnel would be inflexible:

$$M(\theta)=324\cos(2\theta)\quad [kNm/m] \quad \text{and} \quad N(\theta)=-1022+163\cos(2\theta)\quad [kN/m]$$

In a second step, the flexibility of the lining is considered. Flexibility leads to an increase in the horizontal soil stress. The effect of this is analysed according to the empirical relations of Duddeck. The coefficients α, and β, are approximated, using the data of Table 7.3, which gives:

Table 7.3 Description of layers and soil parameters for the North Bank

symbol	*soil type*	*top of layer[m] N.A.P.*	γ_{sat} (γ_{dry}) [kN/m^3]	c_u [kPa]	c' [kPa]	φ' [-]	ν [-]	E_{oed} [mPa]	K_0 [-]
OA/1/OOB	*mixture of sand and clay*	+ 2.50	17.2 (16.5)	-	3	27	0.34	5.2	0.58
3	*sand, local parts of clay*	- 1.50	19.5	-	0	35	0.30	26	0.47
2	*sand with clay*	- 5.75	19.0	-	0	33	0.31	25	0.47
18	*sand, local parts of clay*	- 10.00	20.5	-	0	36.5	0.30	40	0.45
32	*sand, gravel*	- 17.25	20.5	-	0	36.5	0.30	60	0.50
38A	*clay, local parts of sand*	- 20.75	20.0	140	7	31	0.32	16	0.55
38F	*sand*	- 25.00	21.0		0	37.5	0.30	80	0.55
38A	*clay, local parts of sand*	- 26.50	20.0	140	7	31	0.32	16	0.55

$$\alpha = \frac{E_g D^3}{8 E_b I_d} = \frac{30*10^6 \cdot 7.95^3}{8 \cdot 15*10^9 \cdot 1/12 \, 0.35^3} \cong 35, \text{ and } \beta = \frac{E_g D}{2Ed} = \frac{30*10^6 \cdot 7.95}{2 \cdot 15*10^9 \cdot 0.35} = 0.0227$$

For which the coefficients $C_0^N, C_2^N, and\, C^M$, see the equations 7.17 - 7.19, are calculated as;

$$C_0^N = 0.982 \qquad C_2^N = 0.81 \qquad C^M = 0.25$$

If we combine this with the equations 7.15 and 7.16 this gives:

$$M(\theta) = 81 \cos(2\theta) \quad [kNm/m] \quad \text{and} \quad N(\theta) = -1004 + 132\cos(2\theta) \quad [kN/m]$$

Due to the soil structure interaction, a large reduction in the amplitude of the bending moment is found.

The next step is a comparison of these results with the measurements. The first question to consider is: 'after what time does the stress distribution correspond to the final soil bearing condition ?' In Fig. 7.35 the bending moments in the lining, measured as a function of time, are plotted, for the first week after construction. We can observe that the largest changes in the lining stresses develop within a period of about five days. For comparison with the numerical calculations, the measurements after 9 days have been used.

If we compare the back-analysis results for the circumferential moments and hoop compression forces with the measurements at the North Bank of the 'Oude Maas', see the dotted line with the squared symbols in Fig. 7.36 and Fig. 7.37, it is clear that the differences are small for the bending moments. The measured bending moment does, however show some peaks which are difficult to explain based on soil loading only. A larger difference is observed for the normal forces.

The difference in normal forces will be discussed in more detail after the 2D finite element back-analysis is described.

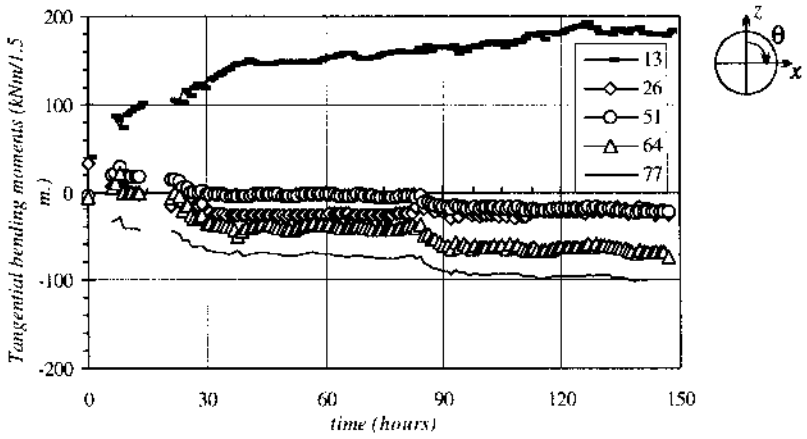

Figure 7.35 Bending moment in the tunnel ring 1; 3/4/97 up to 9/4/97, the numbering indicates the orientation in degrees with respect to the vertical axis

In order to make a comparison of the measured soil stresses with the model, an assumption has to be made to relate the analytical model with stresses. The following assumptions were used:

$$\frac{\sigma_v + \sigma_h}{2} = \frac{1004}{3.975} \qquad \text{and} \qquad \frac{\sigma_v - \sigma_h}{2} = \frac{2*81}{(3.975)^2}$$

This gives: σ_v = 262.8 *kPa* and, σ_h = 243.3 *kPa*, assuming that the calculated vertical soil stress is the intermediate principal stress.

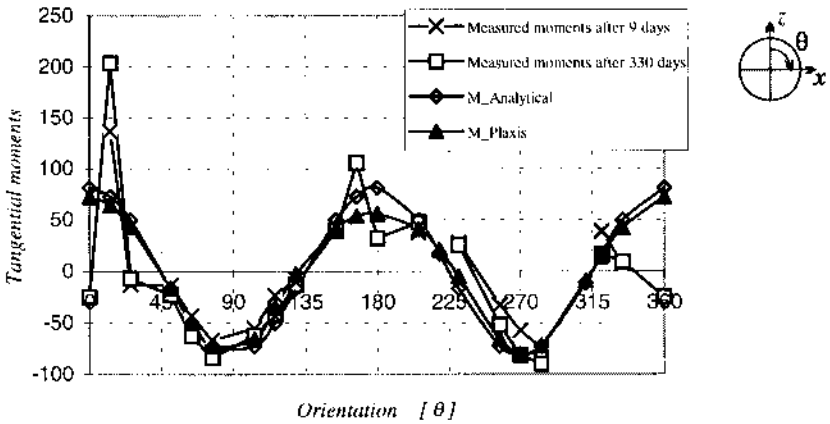

Figure 7.36 Bending moments as measured and back-calculated for the measuring ring on the test site at the North Bank.

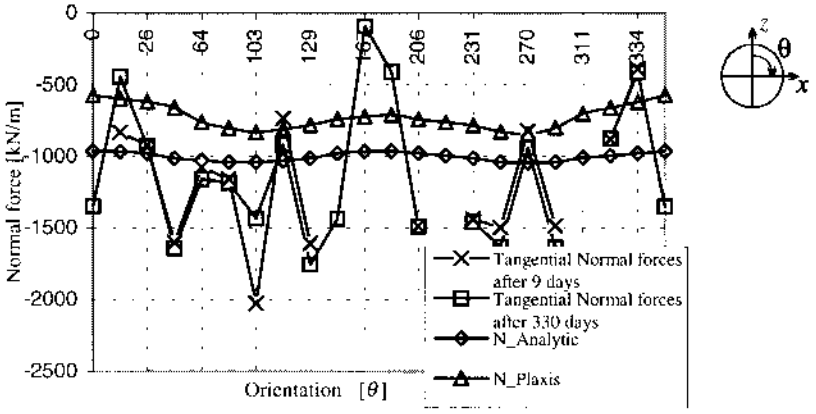

Figure 7.37 Comparison of Back-analysis for the Normal forces with Measurements at the North Bank

To compare this with measured soil stresses as a function of the orientation, the weight of the lining has to be accounted for. The result is given in Fig. 7.38.

If we compare the calculated soil stresses with the measured soil stresses on the tunnel lining the agreement is less good as in the comparison of the bending moments. This difference is thought to be associated with the volume loss that develops after that the TBM moves forward, and the tunnel ring comes free from the tail of the TBM. This volume loss is ignored in the analytical model. The effect of the volume loss is observed as a settlement trough at the soil surface.

This volume loss causes stress relief near the tail of the TBM. The stress relief is reduced by the back grouting process, but it cannot be ignored. Whether the stress relief might be undone by soil creep is uncertain.

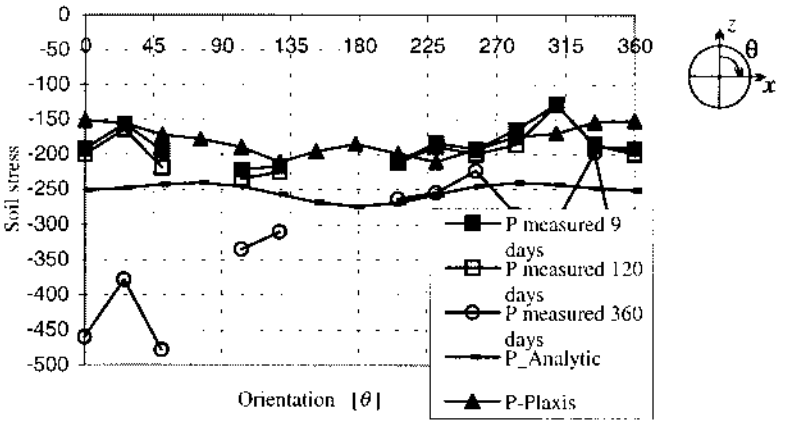

Figure 7.38 Radial soil stresses on the tunnel lining

Back analysis with 2D Finite Elements

To analyse the effects of the volume loss, a number of 2D finite elements calculations were performed using PLAXIS. The results are shown in Figures 7.36, 7.37 and 7.38 too. The soil data given in Table 7.3 and structural data, given in Table 7.2 was used. The radius of the tunnel was taken as the distance between the tunnel centre and the midst of the tunnel lining,
i.e. r = 3.975 m. Furthermore the axial stiffness of the wall was assumed to be equal to that of an homogeneous wall, whereas the bending stiffness of the wall was reduced by 50 %.

Fitting the finite element analysis to the data, led to the following conclusions:

1. *The best agreement was found for an assumed contraction of approximately 0.5 %. At this level of contraction good agreement was obtained for the low measured soil stresses, see Fig. 7.38.*
2. *In comparison to the analytical model, where a smooth wall always leads to higher bending moments, the results from a finite element analysis are less clear cut. With finite elements the highest bending moments are found for a smooth wall. Though this result was recognised by Erdmann & Duddeck, it is not included in the analytic solution as given by the equations 7.15 to 7.19.*
1. *If the finite element calculation is made for the situation without volume loss the agreement is much less. For that situation a smaller amplitude in the bending moment is calculated, i.e. M = 65 kNm/m, instead of 81 kNm/m. This effect will be discussed in more detail further on in this section*
2. *If we look at the soil stress level from the finite element analysis, and compare this with the measured soil stresses shortly after installation, better agreement is found than when applying the analytical model see Fig. 7.38.*

Looking at the normal forces the finite element calculation did not lead to much improvement, (see Fig. 7.37). It is as if the low soil stresses are not compatible with the normal forces being measured. A possible explanation would be that the measured soil stresses are related to an earlier time step of stress development than the normal forces. It is as if the stress level directly after grouting is 'frozen in' by the hardening process of the cement in the grout, and that after the grout has cemented, the effective soil stresses begin to increase. This stress increase would not be measured if the grouting material 'over-bridged' the pressure gauges. Therefore the accuracy of the soilpressure gauges is unclear, especially with respect to their capability to monitor the stress development. The strain gauges, on the other hand, are thought to have a high degree of reliability. Further on in this section the measurements over a much longer period, i.e. one and a half year are evaluated which give some weight to this assumption.

Before evaluating these longer term measurements, the vertical equilibrium and the effect of circumferential shear stresses is discussed. Looking at the stress distribution calculated with PLAXIS it is observed that the integrated normal

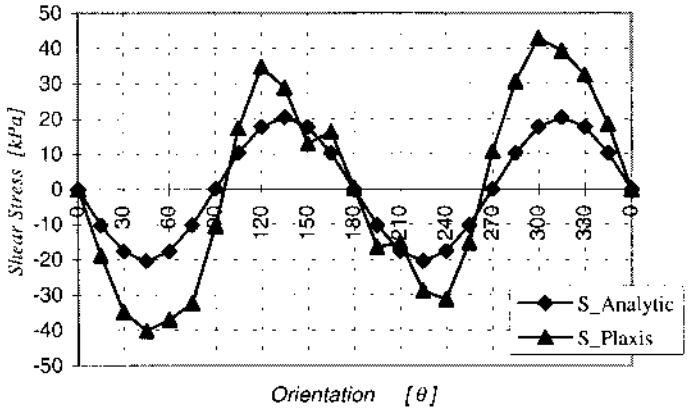

Figure 7.39 Comparison of Shear stresses around the tunnel, for the analytical model and according to PLAXIS.

stresses are not in vertical equilibrium. The stress level at the invert of the tunnel is much higher than at the crown. This can be explained, however, if we evaluate the shear stress distribution. For the analytical model and for the finite element model, see Fig. 7.39. It is observed that the shear stresses calculated with PLAXIS, at the crown of the tunnel, are higher and therefore contribute to the vertical equilibrium of the tunnel.

The bending moments, agree well with the back-analysis, although distinct differences are observed. These differences are attributed to the variations in the normal force, and interaction between adjacent tunnel rings. According to Visschedijk (1996), interaction at the joints in a ring might increase the bending moments by a factor up to 1.6. Variations in the normal force combined with variations of the midst of the segments, is calculated to cause an additional moment of approximately;

$$M_{ad} = N\delta \approx 1500 * 0.02 \approx 30 kNm/m$$

This suggests that the differences between the back-analysis and measurements can reasonably be explained by interaction between segments and the effects of installation.

Long term measurements of the soil stresses

After a period of one and a half years it was decided to evaluate the long term measurements, to gain insight into the time dependent effects. Initially measurements at one month intervals where extracted from the measurement database. These measurements proved to be difficult to interpret, however. After that, v. Oosterhout (1999[b]) extracted data at intervals of one day for a period of nearly 15 months. These data indicated that after about 240 days, a significant change in the radial soil stresses developed, see Fig. 7.40. The main changes

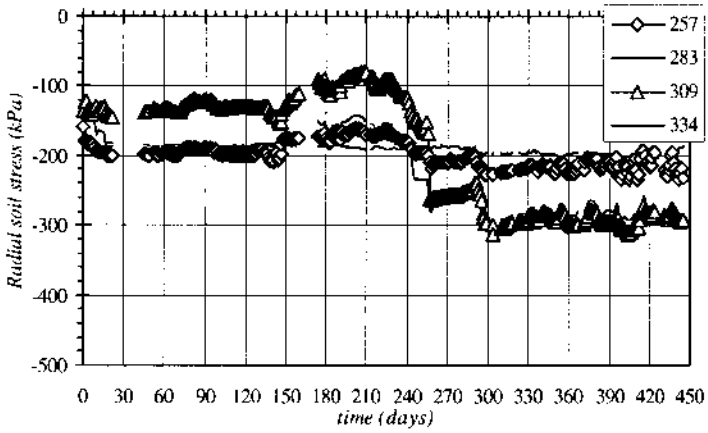

Figure 7.40 Radial soil stresses on tunnel ring 1 (North) from 3/4/97 up to 23/6/98, the number indicating the measurement indicate the orientation angle of the measuring device.

occurred around the date of 15 December 1997 when the support structure in the North starting shaft was removed.

A noticeable change also occurred a month later when the support on the South bank was taken away. Subsequently the question arose whether the soil stresses actually had changed, had risen, or that something had happened to the pressure gauges. A feasible explanation which was proposed was that the grouting material had cracked, causing a reduction in over-bridging effects. In order to evaluate this assumption the strain gauge measurements were looked upon.

From Fig. 7.41 it can be seen that although minor developments occur with

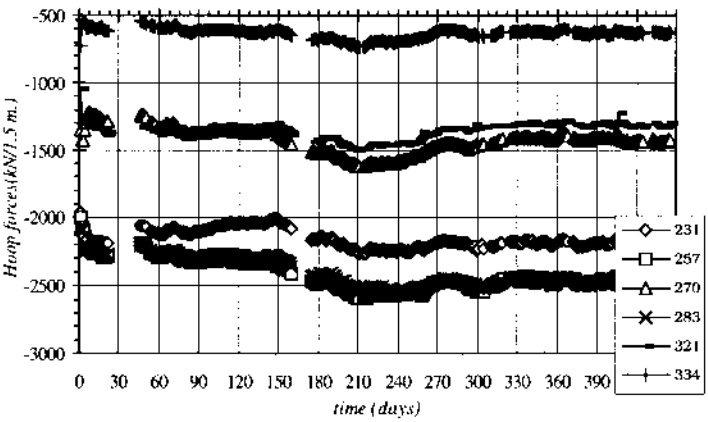

Figure 7.41 Circumferential hoop forces ring 1 (North) from 3/4/97 up to 23/6/98

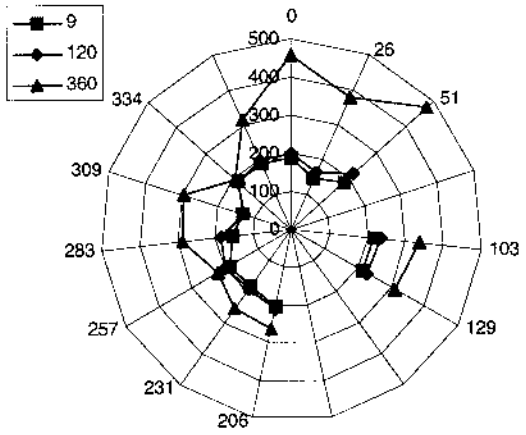

Figure 7.42 Radial soil stresses on the tunnel lining, 9, 120 and 360 days after construction

time, around the 240th day after installation there is not a sudden change in the normal forces. From this it was concluded that the change in measured soil stresses is related to the measuring device and not to a change in soil stress, which supports the argument that over-bridging of the pressure gauges by the grouting layer influences the measurements.

A second aspect to consider is that v. Oosterhout (1999[a]) did identify difficulties with respect to the interpretation of temperature effects on the pressure measurements. The measuring data as presented in the Figures 7.40 and 7.42 have been corrected for this effect. For the North measuring ring, in Fig. 7.42, the development of the soil stresses on the tunnel lining is displayed at three distinct times after construction. From this figure the increase in soil stresses, discussed above is distinctly visible. It must be mentioned here, however, that the temperature correction is not beyond discussion. The fact that the soil stresses, in the first quadrant increase to values distinctly higher than the overburden stress, (about 300 kPa) contributes to the doubts that still exist on the accuracy of the pressure measurements.

Measuring ring 'South Bank'

With the knowledge gained with the first measuring ring, and noting that installation stresses are significant, extra care was given to the measuring of stresses as early after installation as possible for the second measuring ring. Due to this care, it was possible to establish the additional stresses which developed due to the soil loading, by extracting the stresses which had developed before the ring had left the tail of the tunnel boring machine. In Fig. 7.43 both bending

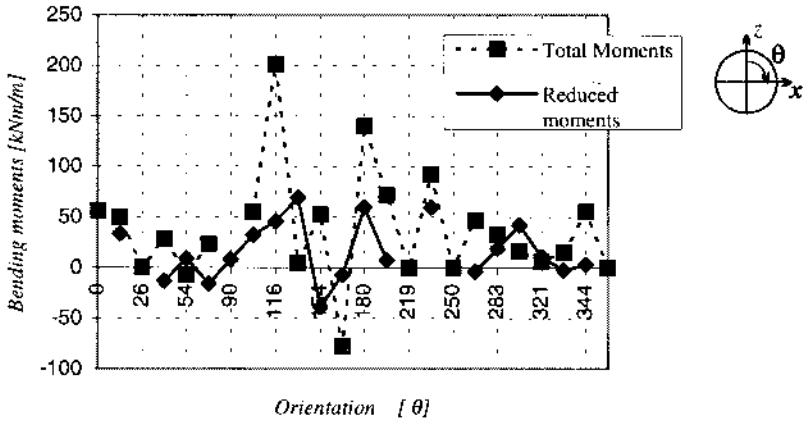

Figure 7.43 Comparison between back-analysis with PLAXIS and bending moments due to soil loading, for the measuring ring South

moment distributions are given; the total bending moment, as a function of orientation, and the bending moments after subtraction of the initial stresses.

Assuming the same procedures as for the North ring, PLAXIS was used to back-analyse the bending moments. In Fig. 7.44, the reduced bending moments are compared with the PLAXIS results.

A comparison between the back-analysis and the measurements shows that the amplitude of the maximum moment is adequately predicted by the model. A comparison of the distribution, however, shows that the fit is less successful. On the one hand it seems as if there is a shift in the orientation for certain parts of the

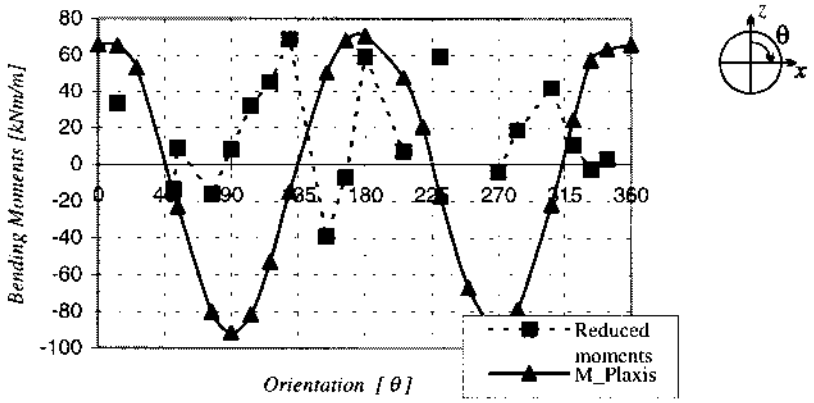

Figure 7.44 Measuring ring South, Total bending moments, and Bending moments after reduction with installation stresses.

distribution. On the other hand the measured distribution shows peaks which cannot be explained by the soil loading.

It is thought, see section 7.5.5, and Blom et al. (1998), that these peak stresses are caused by an inaccurate installation of segments when assembling a ring in the tail of the TBM. If the joints cannot adjust to the actual soil loading in an adequate way, such as when a smooth material such as Kaubit is put into the ring joint, peak stresses like this might develop.

Bending moments as a function of the volume loss

In the back-analysis, for both measuring rings, it was assumed that the volume loss was 0.5 %. The value of 0.5 % was estimated from the volume loss as observed at the soil surface, where a volume loss of approximately 0.8 % was measured. For small volume losses, assuming the analytical solutions, such as those of Sagaseta, the volume loss at the tunnel is back-analysed to be less by a factor of 1.6

Looking at the development of the stress in the lining, the force volume-loss relationship, it is observed that the (maximum) bending moment increases with the volume loss. For the given stiffness ratio between structure and soil, for the South measuring field, the relationship is given in Fig. 7.45, which indicates that the bending moment displays a maximum somewhere in the range between 0.5 and 1.0 % volume loss. For volume losses larger than this the bending moment appears to reduce.

For a typical tunnelling situation the volume loss is usually greater than 0.5 %. If the tunnel boring machine is well driven it should be possible to limit the volume loss to 1.0 %. For the design of the tunnel ring, an assumed volume loss between 0.5 - 1.0 %, is thought to be reasonable.

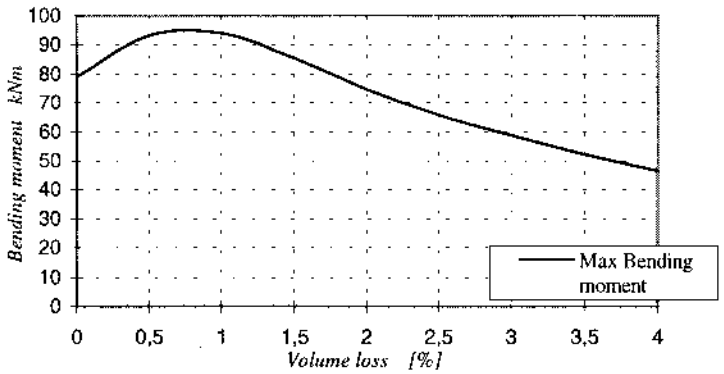

Figure 7.45 Bending moment as a function of the volume loss in %, for measuring field South (PLAXIS-analysis)

Consideration

The designer of a tunnel must consider that installation stresses are unfavourable, because they might cause damage to tunnel lining segments during construction. On the other hand, installation stresses may be classified as eigen stresses. A characteristic of eigen stresses is that for a redundant structure, they do not contribute to failure in the ultimate limit state. For failure calculations, therefore, it is only necessary to consider the stresses due to soil loading. A comparison of the back-analysis results with the measurements leads to the conclusion that the relationship between soil loading and bending moments is adequately modelled with 2D finite element analysis. With respect to the hoop forces there is a larger difference. For the ultimate limit state the hoop forces are related to the weight of the overlaying soil, which is usually straightforward to calculate.

Measurements of longitudinal bending moments

The theory described in section 7.4.2 has been used by Bogaards for the analysis of the measurements from the Second Heinenoord tunnel. The result of this study is illustrated in Fig. 7.46. As can be observed from this figure, the magnitude of the measured and calculated bending moment is of the same order, although the predicted distribution is not accurate.

To improve this result the following steps should be taken:

1. *the forces due to the TBM should be more closely monitored*
2. *the subgrade reaction of the hardening grout material in the zone just behind the TBM should be better understood.*

Evaluation of the results of the Second Heinenoord tunnel

Installation inaccuracies appear to cause additional bending moments in the tunnel lining. In this chapter an attempt is made to quantify the effect of

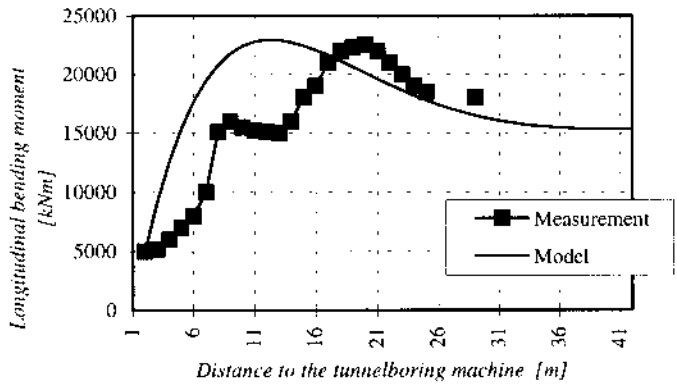

Figure 7.46 Comparison between measurements and analysis for longitudinal bending moments

installation inaccuracies.

The analytic solutions, for soil loading, seem to be reasonably reliable with respect to their ability to describe soil reactions and their effect on the stress distribution in a tunnel lining. Agreement between the model and field measurements is better for the bending moments than for the hoop forces. The latter is attributed to the stress level around a tunnel, whereas the former is related to the variations of stress around the tunnel.

The agreement between measurement and calculation of the soil stresses is improved when finite element analysis is used. It should be noted, however, that the low stress level obtained from the numerical analysis and measured in the pressure gauges, may be influenced by time. The hoop forces in the lining seem to increase with time. A second aspect to consider is the influence of the grouting pressure. At the North bank, a relatively low grouting pressure was used, whereas on the South bank, the grouting pressure was above the K_0 value of the horizontal soil stress. Though the grouting pressure mainly has a local effect, which diminishes after the grout consolidates and hardens, the fact that the back-analysis for the North bank seems to be in better agreement than for the South bank may be influenced by the high back grouting pressure on the South bank.

For the structural design of a tunnel lining the analytical model and the finite element model both seem to be appropriate to predict the stresses due to soil loading. The finite element analysis has the advantage, however, that it may be used to model the volume loss, leading to an improved prediction of soil stresses. For the dimensioning of a tunnel lining segment, the stresses and deformation due to installation should be combined with those due to soil loading. Finally the influence of second order deformations should be added, by using an empirical multiplier as discussed in section 7.4.2.

Finally, to derive a large enough distance between design and practice, a safety factor should be included.

7.6 CONCLUDING REMARKS

In contrast to flexible structures such as sheet pile walls, the derivation of stresses and strain in a tunnel lining is relatively insensitive to soil plasticity. Instead, the elastic parameters of the soil have a substantial influence on the stress level in the structure.

The analysis of tunnel loading was focussed on the bending moments in the tunnel lining. It seems, however, that bending moments in the tunnel lining are only of minor importance for the ultimate limit state. If the lining is strong enough to bear the hoop forces, collapse of the tunnel due to insufficient reinforcement of a tunnel lining under influence of the soil loading alone would be unlikely.

Reinforcement of the tunnel lining is mainly required to resist construction loading. The monitoring of the Second Heinenoord tunnel has shown that the

stress development during assembly and loading by the jacks of the Tunnel Boring machine are of the same order or higher than due to soil loading. If the construction phase could be optimised and the development of peak stresses in this phase limited, a cheaper lining is feasible.

The measurements and observations of tunnel lining behaviour such as described in section 7.5.5 show that some of the problems observed in practice are not related to an inadequate description of mechanics. Instead they are associated with various stochastic processes that occur during construction.

The thickness and strength of the liner should be chosen by considering the hoop forces in the liner and also the allowable deformation. Attention should be given to the accuracy with which tunnel lining segments are assembled into a tunnel ring.

In comparison to a sheet pile retaining wall, the analysis of a tunnel lining for soil loading is relatively easy. This observation might be used to justify a lower partial safety factor with respect to the stresses and strains caused by soil loading.

The methodology of developing models, based on knowledge of the ultimate limit state seems to be useful for tunnels. Although the potential for further development of tunnel design methods is large, the results of back-analysis with different hierarchical models suggests that there would be diminishing returns for further development of the models.

It is emphasised that finite element methods have considerable advantages over analytical models because they include complex features such as non-linear material behaviour, consolidation or creep. In addition, unlike the empirical models, finite element methods can, in principle, be developed to deal with problems of increased complexity.

CHAPTER 8

Conclusions and recommendations

8.1 *Introduction*

In this study it has been tried to formulate the development of models for structural analysis in an objective framework.

In chapter 2 an approach has been taken where the optimisation of a design alternative is placed into to framework of an economic problem. The observations are that both model uncertainty and cost of analysis are important.

In chapter 3 a methodology for the development of models is formulated. Both verification, the testing of the integrity of a model, and evaluation, testing the accuracy of a model are dominant tests for a model. Accuracy and uncertainty are related aspects of a model.

In chapter 4 the toolbox for the analysis of geotechnical problems is put forward. Here the emphasis is put on those principles which are applicable for the development of numerical models based on continuum mechanics fundamentals. The formulation of groundwater flow is given similar to that of equilibrium of stresses, where it is shown that both formulations can be regarded as fitting in the principle of virtual work.

Subsequently in the chapters 5, 6 and 7 several examples of model development are worked out, verified and evaluated. As a spin-off of this approach the conclusions are not limited to those related to model development. Inevitably conclusions with respect to the structure types, and the economical approach of designing these structures come forward. In the chapters dedicated to the structure types, conclusions with respect to structure types are described. Here in chapter 8, only the conclusions with respect to the main objective of this study, model development, are repeated or formulated, conclusions which are of special importance, or conclusions which are general for all structure types.

8.2 *Conclusions*

The finite element method has given us a powerful means for the development of models for structural analysis. Both the development of finite elements for groundwater flow and for equilibrium of stresses, has given us a powerful tool for structural design. The advantage of finite element analysis above other types of models is that thus far there is not a limit to the point that physical observations

can be included in finite element models. For the structural analyst the advantage of finite elements is that it reduces the number of different models in his toolkit. Seen from the point of training, the number of methods the structural analyst has to learn keeps limited.

In order to be able to do structural design, the model being used has to be supported by a design philosophy. There needs to be a frame of reference, a limit state for which the model is dedicated. The design philosophy, gives a frame of reference for the establishment of the necessary distance between the construction behaviour to be established for practice, and the (Ultimate) Limit state. If such a frame of reference is lacking, the model does not have any more significance than as a behavioural model. The necessary (partial) safety factor(s) cannot be established then.

A second demand for a model is that the determinate independent variables for the model need to be available with a small enough margin of uncertainty. If this uncertainty is to large, the model might be good enough as a behavioural model, for back-analysis purposes, but not fit for design purposes. The analytical model for uplift of blocks, such a discussed in section 5.3.2.1, might be regarded as such model. The establishment of the cover-layer permeability, is that uncertain, that it is nearly impossible to make an adequate prediction of the value for this parameter. With this observation the analytical model for block stability becomes unfit for design purposes.

Numerical models can be regarded as a class of analytical models. The only difference with models which are truly called analytical (e.g. closed form solutions), is the solution technique. Analytical models distinguish themselves, in practice, only with respect of the level on which empirical observations are processed. For the models we are looking at, empirical models are used on a level that the structure as a whole is concerned whereas analytical models are based on observations of material behaviour. We have to be aware however that with this a number of relevant aspects, which play a part on the structural level are not implicitly included if an analytical model is adopted. Important aspects such as, consolidation, creep, time dependant behaviour, dynamics, 3D deformations, have to be put into the model explicitly to be analysed. Empirical models are based on observations on the structural level, and therefore implicitly include these effects. Where it is unsafe to apply empirical models outside the range of observations on which it is based, the power of analytical models is beyond that. Provided that the model is verified and validated, according to procedures, the power of an analytical models is beyond the empirical observations on the structural level.

Both the evaluation of the models for the structural analysis of the liner for a bored tunnel has shown that the application of simple models, here the Duddeck model, is not outdated yet. Sometimes a simple model, with a clear display of its physical content might out-rival more complex models, which are sometimes hard to work with and to interpret.

Where the case study on the Karlsruhe sheet pile test has shown that a clear understanding of the physical observations, using a finite element model seems to be possible, the evaluation of the measurements on the bored tunnel makes clear that for other types of structure the unravelling of all the physical processes is sometimes hard work. For a prototype measurement it is sometimes hard to distinguish which process is determinate for the result. The further development of statistical evaluation techniques such as the Maximum Likelihood methods such as used for the sheet pile test might give an objective approach to solve this problem.

The evaluation of damages at the Second Heinenoord tunnel made clear that it is not only the mechanical modelling of the structure that is determinate for an accurate description of the observed stresses. The influence of stochastic processes which in practice determine the geometry of the structure might be of the same importance.

The knowledge of the hierarchical levels enhances the success of further model developments.

Continuity in groundwater flow is discussed within the framework of variations. For small displacements it is shown that continuity in groundwater flow can be conceived in a similar framework as used for equilibrium of stresses, i.e. the principle of virtual work..

8.3 *Recommendations*

In order to improve the establishment of accurate input parameters for models evaluation of laboratory tests and prototype measurements has to be advocated. The application and further development of Maximum Likelihood methods in combination with finite elements might improve the benefit of these.

In order to guide the research on bored tunnels, the formulation and establishment of an accepted design philosophy would be beneficial.

In order to enhance integral weighing of design alternatives, the application of economic principles such as marginal cost-benefit analysis, and in addition to that, weighing of external costs-benefits has to be advocated.

List of symbols

Symbol	*Description*
a	the space of solutions
a	dummy parameter
$\boldsymbol{a}$	vector of nodal displacements
b	dummy parameter
b	filter thickness
b	width
c	cohesion
c_u	undrained cohesion
e	energy density
f	yield function
f_i	distributed load
f_i^c	calculated (model) value
f_i^t	measured (test) value
g	plastic potential
g	acceleration of gravity
h	height, depth
h_i	vector of interpolations
h_1	sheet pile length
h_2	Embedment depth
i,j,k,l,m,n	index
i	hydraulic gradient
k	(Darcy) permeability
k	subgrade reaction modulus (bedding modulus)
k'	Permeability of revetment cover layer
l	length
n	porosity
n	amplification factor for 2nd order effects
n_i	normal (to a surface)
p	pore water pressure
p	isotropic stress
$\Delta\mathbf{p}$	pseudo load vector
q	load
q_i	hydraulic discharge (filter velocity)
$\mathbf{q}$	load vector

r	interest
r	radius
s	entropy
t	time
u	displacement
v	velocity
x	independent variable(s)
x,y,z	co-ordinate
$\langle x \rangle$	a priori estimated value's of parameters
y	dependant variable(s)
w	deflection
z	vertical axis
A	coefficient in the Forchheimer permeability relation
A	(sectional) Area
A	elastic stiffness matrix
$\mathbf{A}$	matrix of partial derivatives
B	coefficient in the Forchheimer permeability relation
$\mathbf{B}$	differential operator
C_i	coefficient with number i
C_a	value per area
C_b	added value for activity
Cv	cash value
C_x^n	covariance matrix of the a priori information
C_f	measurement covariance matrix
D	block thickness
D	diameter of a bored tunnel
D_i	coefficient with number i
$D_{erosion}$	erosion depth
$\mathbf{D}$	material elasticity matrix
$\mathbf{D}$	partition coupling matrix
E	first moment (statistical)
E	Young's modulus
E	energy
Et	the total costs, the Expenditures (including rent)
F_i	force (number)
Fp	the profit as a function within the solution space
$Fv)$	the (functional value)
$\mathbf{F}$	partition matrix
G	shear modulus
G_{50}	secant shear modulus at 50 % strength
H_s	significant wave height
H_b	breaker height
$\mathbf{H}^T$	vector of interpolation functions, (for the geometry)
I	beam moment of Inertia
$\mathbf{J}$	Jacobian matrix

K_0	coefficient of horizontal initial soil stress
K^r	relative permeability
K_{ij}	permeability matrix
K_{ac}	coefficient for active soil failure with respect to cohesion
K_{pc}	coefficient for passive soil failure with respect to cohesion
KP	system matrix for permeability domain
L	span
$L(x)$	likelihood function
L	strain operator
M	(bending) Moment
M	tensor relating input parameters with output
N	normal force
$\mathbf{N}^T$	vector of interpolation functions
O	circumference
P_a	face support pressure
P_f	probability of failure
$P(\ )$	probability
Q	thermal energy
Q	shear force
Q	partition load vector
R	strength (Resistance)
R_d	rundown
S	loading (Solicitation)
S	likelihood function
S	revetment extent (vertical upwards)
S	stiffness matrix
T	transformation matrix
V_s	volume loss
X_i	material co-ordinates
Z	yield function
Z_l	groundwater head in the filter layer
Z_b	revetment extent (vertical downwards)
α	inclination angle
α_i	influence ratio
$\alpha = \frac{E_g D^3}{8 E_b I_b}$	stiffness ratio (in radial direction) for bored tunnel lining
β	breaker angle
β'	compressibility of the pore fluid
$\beta = \frac{E_g D}{2Ed}$	stiffness ratio (in tangential direction) for bored tunnel lining
β_s	stiffness ration in Winkler's subgrade reaction model concept
δ	friction angle (adhesion)
δ_{ij}	Kronecker delta
ε^e	elastic strain

ε^p	plastic strain
ε_{ij}	infinitesimal strain tensor
ε_v	volume strain
ϕ	potential
γ_w	weight of the pore water; $\gamma_w = \rho_w g$
γ_i	partial safety factor
η	local co-ordinate axis
φ	friction angle
κ	curvature
λ	ratio of plastic strain
λ	leakage height
λ	length scale in Winkler's subgrade reaction model
λ_a	coefficient of active soil pressure
λ_n	coefficient of neutral soil pressure
λ_p	coefficient of passive soil pressure
λ_i	Influence length
μ	mean value
ν	Poisson's ratio
θ	rotation
τ_{cr}	critical shear stress
ρ	density
ρ_p	particle density
ρ_w	pore water density
σ'	effective stress (according to Terzaghi)
$\sigma_1, \sigma_2, \sigma_3$	principal stresses
σ_{ij}	Cauchy stress tensor
σ_v	vertical soil stress
σ_h	horizontal soil stress
σ_z	standard deviation of yield function
σ^2	variation
ξ	local co-ordinate axis
ψ	angle of dilatancy
ζ	the arc enclosed by a tunnel lining segment
Λ	leakage length
Δ_h	retained soil height
Δ_w	relative density ratio
$\Delta(P)$	pressure difference
$\Delta\mathbf{P}$	pseudo load vector for plasticity
Φ	groundwater head
Γ_u	stability ratio for block revetment stability
Γ_{si}	stability ratio

References

Adel, H. den, (1987), *Re-analysis of permeability measurements using Forchheimer's equation* (Dutch), Delft Geotechnics Report, Delft, The Netherlands.

Ahrens, H., E. Lindner & K.H. Lux, (1982), Zur dimensionierung von Tunnelausbauten nach den 'Emphelungen zur Berechnung von Tunneln im Lockergestein'. In: *Die Bautechnik 8 und 9* 1982.

Aubry, D. & O. Ozanam, (1988), Free-surface tracking through non-saturated models. In: *Numerical Methods in Geomechanics* (ICONMIG), Innsbruck, Austria.

Barends, F.B.J., (1980), *Non linearity in Groundwater flow.* Doctoral Thesis, Delft University of Technology.

Bakker, K.J. & P.A. Vermeer, (1987), Finite element analyses of sheet-pile walls, In: *Numerical Models in Geomechanics*, Gent 1987, Belgium.

Bakker, K.J. & P. Meijers, (1988), Stability against sliding of flexible revetments. Int. Symp. on Model, *Soil-Water-Structure Interactions*, (SOWAS). Delft, The Netherlands.

Bakker, K.J., (1989), Analysis of groundwater-flow through revetments. In: *III International Symposium on Numerical Models in Geomechanics*, Niagara Falls, Canada.

Bakker, K.J. & R.B.J. Brinkgreve, (1990), The use of hybrid beam elements to model sheet-pile behaviour in two dimensional analysis. 2end ENUMGE, *Numerical models in Geomechanics* Santander, Spain.

Bakker, K.J. & R.B.J. Brinkgreve, (1991), *Deformation analysis for a sheet pile wall using 2 dimensional analysis*, Proc. ECSMFE, Florence, Italy.

Bakker, K.J. & R.C.A Beem (1994), Modelling of the sheet pile wall test in Karlsruhe 1993 In: *Proc. 3th European Conf. on Numerical methods in Geotechnical Engineering*; ECONMIG 94, Manchester/UK/7-9-Sept.

Bakker, K.J., W. van Schelt & J.W. Plekkenpol, (1996), Predictions and a monitoring scheme with respect to the boring of the 2nd Heinenoord tunnel, In: *Underground Construction in soft Ground*, TC28 London, April 1996.

Bakker, K.J., P. v.d. Berg & J. Rots, (1997a), *Monitoring soft soil tunnelling in the Netherlands; an inventory of design aspects*, Proc. ISSMFE, Hamburg.

Bakker, K.J., (1997b), Modelling tunnel lining behaviour for soft soil conditions; an hierarchical overview of design, models, In: II[nd] *Diana conference on Numerical analysis; Amsterdam*, The Netherlands.

Bakker, K.J., (1999a), Modelling tunnel behaviour for soft soil conditions; models for structural analysis and monitoring results, In: *Proc. PLAXIS 2000*, Amsterdam, The Netherlands.

Bakker, K.J., F. de Boer & Kuiper J.C, (1999b), *Extensive independent research programs on Second Heinenoord tunnel and Botlek Rail tunnel, In: XII ECSMGE*, Amsterdam, The Netherlands.

Bakker, K.J., W.L., Leendertse, P.S Jovanovic & van Oosterhout, G.P.C., (1999c), Monitoring; evaluation of stresses in the Lining, of the Second Heinenoord Tunnel, In: *Proc. IS-Tokyo '99, Geotechnical Aspects of Underground Construction in Soft Ground*, Japan, July 1999.

Bathe, K.J., & M.R. Koshgoftaar, (1979), Finite element free surface seepage analysis without mesh iteration, Int. Journal on *Numerical and Analytical Methods in Geomechanics*, 3, 13-22.

Bathe, K.J. (1982), Finite Element Procedures in Engineering Analysis, Prentice-Hall, Inc. Englewood Cliffs, New Jersey.

Becker, E., & W. Burger, (1975), *Kontinuumsmechanik*, Teubner Studienbücher, Stuttgart.

Besseling. J.F. (1975), *Stiffness and strength 2* (in Dutch), Oosthoek, Scheltema & Holkema.

Bezuijen, A., M. Klein Breteler & K.J. Bakker, (1987), Design criteria for placed block revetments and granular filters, In: *II Int. Conf. on Coast and Port Engineering in Developing Countries*, Beijing.

Bezuijen, A. & J.S. van der Schrier, (1994), The influence of a bored tunnel on pile foundations. *Proc. Conf. Centrifuge 94* (Lee and Tan, eds.). Balkema, Rotterdam.

Biarez, J. (1958), Remarques sur la rotation des massifs de fondation. *Proc. Brussels conference '58, on earth pressure problems*. Vol 3, 217-226

Blom, C.B.M., G.P.C. Duurland, G.PC. van Oosterhout & P.S. Jovanovic, (1998), Three-Dimensional Structural Analysis and Design of Segmented Tunnel Lining at Construction Stage, In: *Proc. 4th Europ. Conf. on Numerical Methods in Geotechnical. Engineering*., Udine, Italy, Springer-Wien-NewYork.

Blum H., (1931), *Einspannungsverhaltnisse bei Bohlwerken*, Ph.D. Thesis Braunschweig University. Kruger G.m.b.H. Dortmund.

Blum H., (1932), Wirtschaftliche Dalbenformen und deren Berechnung. *Die Bautechnik 9* (1932), Heft 5, S. 50

Bogaards, P.J. & K.J. Bakker, (1999), Longitudinal bending moments in the tube of a bored tunnel, In: *Numerical Models in Geomechanics*, Numog VII, Graz, Austria, sept 1999.

Borst, R. de, & P.A. Vermeer, (1984), Possibilities and limitations of finite elements for limit analysis, *Geotechnique 34*, No. 2, 199-210.

Bouma, A.L. (1993), *Mechanics of Structures; 'Elasto-statics of slender structures'*. (in Dutch), Delftse Uitgevers Maatschappij, Delft, The Netherlands.

Buisman, J., (1978), *The Netherlands, 'as it was, and like it is today'*, (in Dutch), Sesam, Geographics of the Netherlands.

Caquot A. et Kerisel J., (1948), *Tables de butee, de poussee et de force portante des fondations*. Gauthier-Villars, Paris.

Centre for civil engineering research, codes and specifications (1993), *Manual on the 'Design, construction, management and Maintenance of sheet-pile walls'*. (In Dutch), Report no; 166, CUR, Gouda, The Netherlands.

Craig R.F. (1974, 1978), *Soil Mechanics*, van Nostrand Reinhold, London.

COB-Commission K100, '*Instrumentation and Measuring plan*'; K100-01, (1995), (in Dutch), Centre for Underground Construction, Gouda, The Netherlands,

COB-Commission K100, '*Prediction report on the Second Heinenoord tunnel*'; K100-04, (1997) (in Dutch), Centre for Underground Construction, Gouda, The Netherlands,

COB-Commission K100, (1999), *Monitoring of the Second Heinenoord tunnel, 'Report on a large scale monitoring of bored tunnelling'*, Final report of K100, Centre for Underground Construction, CUR/COB, Gouda, The Netherlands.

COB-Commission L500, (1996), *Inventory of design methods for bored tunnels for road- and rail-transport.* Report of subcommittee L510, Centre for Underground Construction, CUR/COB, Gouda, The Netherlands.

Desai, C.S. & G.C. Li, (1983), *A residual flow procedure and application for free surface flow in porous media*, Int J. Advances in Water Recourses. Vol.6. 1983, pp 27-35.

Duddeck, H., (1980), *Empfehlungen zur Berechnung van Tunneln im Lockergestein,* Die Bautechniek 10/1980.

Duddeck, H., (1984), Analysis of Linings for Shield driven Tunnels, In: *Proc. Int. symp. on tunnelling in soft and water-bearing ground*, Lyon 27-29 Nov 1984, Balkema Rotterdam.

Duddeck, H., (1991), Application of Numerical analysis for Tunnelling. Int. J. for *Num. and Anal. Meth. in Geomechanics*, Vol. 15, 223-239.

Duncan J.M. & C.Y. Chang, (1970), Non-linear Analysis of Stress and Strain in Soil, ASCE *J. of the Soil Mech. and Found.* Div. Vol. 96.

Dupuit, J., (1863), *Etudes Theoretiques et Pratiques sur le Mouvement de Eaux dans les Canaux Decouvertes et a Travers les Terrains Permeables*, 2nd ed. Dunod Paris.

Elementair, Bouwdienst Rijkswaterstaat, (1996), *Elementair version 2.0*; 01/01/96 (in Dutch, private communication).

EAU, *Empfehlungen des Arbeitsausschusses 'Ufereinfassungen' Hafen und Wasserstraßen EAU* 1996, Ernst & Sohn

Field, B.C., (1994), *Environmental Economics; an introduction* McGraw-Hill International Editions; economic series.

Frissen, C.M., (1996), *Numerical modelling of block revetments, effects in the length axis of the dike*, (in Dutch), Rijswijk, 1996, TU Delft rapport 03.21.1.22.26, TNO report (96-NM-R-0994), MSc.Thesis Delft University of Technology, Delft, The Netherlands.

Fujita, K. et al, (1993), *Underground Construction in Soft Ground in Japan*, JSSMFE, 53-63.

Gerressen, B., (1997), *Stability of Block Revetments, 'considerance on dike revettments as a bedded beam model'*, (in Dutch), MSc.Thesis, Delft University of Technology, Delft, The Netherlands.

Groot, M.B. de, A. Bezuijen, A.M. Burger& Konter, J.L.M., (1988), The interaction between soil, water and bed or slope protection, In: *Proc. SOWAS; Modelling Soil-Water-Structure Interactions*, Delft, The Netherlands.

Gudehus, G.(1980), Erddruckermittlung, *Grundbau Tasschenbuch*, Wilhelm Ernst & Sohn, Berlin.

Hartog, J.P. den, (1952), *Advanced Strength of materials*, Dover publications, Inc, New York.

Hernandez, J., (1989), *Block mattresses on the Houtribdijk; analysis of damages*, (in Dutch) WBA-N-89.005, RWS Road and Hydraulic Engineering Division, Public Works Department, Delft, The Netherlands.

Hetenyi, M., (1946), *Beams on elastic Foundation*, The University of Michigan Press.
Hjortnaes-Pedersen, A.G.I., J.A.M. Teunissen & H. Best, (1986), Groundwater flow with a Phreatic line as a non stationary process, In: *ECONMIG '86* Stuttgart, 1986
Horn, M., (1961), *Horizontaler erddruck auf senkrechte abschussflächen von tunnelröhren*, Studiengesellschaft fur unterirdische verkehrsanlagen e.v. Düsseldorf (STUVA), Landeskonferenz der ungarischen Tiefbauindustrie, Referate zum thema 'Unterirdische Bauwerke', November 1961, Budapest, Deutsche Überzetzung von Szoerenyi G.
Hueting, R., (1974), *New scarcity and economic growth*, Agon Elsevier, Amsterdam/Brussel.
Jaky (1944), Talaymechanika (*Bodenmechanik*), Budapest.
Janczecs, S. and W. Steiner, (1994), Face support for a large Mix-shield in heterogenous ground conditions. *Proc. Tunnelling '94*, IMM London 531-550
Kinderen, S. van, (1995), *Risk-analysis for a bored tunnel* (in Dutch), MSc-thesis, Delft University of technology, Delft, The Netherlands.
Kenny, A, (1995), *Frege, an introduction to the founder of modern analytic philosophy*, Penguin Books.
Klein Breteler, M., A.M. Burger, L. Banach & A. Bezuijen, (1988), *Analytical design methods for block revetments*, In: *XXI Int. Conf. Coast. Eng.*, Malaga.
Klein Breteler et/al (1995), *Design manual for pitched slope protection*, CUR/TAW Report 155; Centre for Civil Engineering Research and Codes/Technical Advisory Committee on Water Defences, Balkema, Rotterdam
Lambe, T.W. (1973), Predictions in Soil Engineering, 13th Rankine Lecture, *Geotechnique 23*, 2, pp 149-202
Langen H. van, (1991), *Numerical Analysis of Soil structure Interaction*, Doctoral Thesis, Delft University of Technology, Delft, The Netherlands.
Ledesma, A., A. Gens, A. & E. Alonso E. (1989), Probabilistic back-analysis using a maximum likelihood approach, In: *XII ICSMFE*, Rio de Janeiro, Brasil.
Leendertse, W.L., K.J. Bakker & E.A.H. Teunissen, (1997[a]), TBM-Tunnelling in the Netherlands, In: *Proc. ITA. Vienna*, april 1997. Rotterdam: Balkema.
Leendertse, W.L. et al. (1997[b]) *Analysis of the damage on the tunnel lining due to construction* (in Dutch), Bouwdienst Rijkswaterstaat
Mair, R.J., (1987), Tunnel face support pressure, soft Clay, *Proc. 8th Asian regional conference on SMFE.* 2, 290 JSSMFE, Tokyo
Mathcad user's guide, (1995), *Mathcad 6.0* Mathcad plus 6.0, Cambridge Mathsoft
Méndez Lorenzo, M.G., (1998), *Reliability analysis of a steel fibre reinforced concrete tunnel lining*, ITM report D50000-013, Delft University of Technology, may 1998
Mill. J.S., (1862), *Principles of Political Economy*, London 1862/1876
Müller-Breslau, H. (1947), *Erddruck auf Stützmauer*, Kröner Verlag, Stuttgart.
Nova R., M. Boulon & A. Gens, (1995), Numerical modelling and information technology, Theme Report 6, In: The Interplay between Geotechnical Engineering and Engineering Geology, *Proc. XI European Conf. on Soil Mechanics and foundation Engineering*, Copenhagen
Oosterhout, G.P.C. (1999[a]), *Second order evaluation of the tunnel construction at the Second Heinenoord tunnel, part 4*, Measuring report, K100-W-095, Centre for Underground Construction, CUR/COB, Gouda, The Netherlands.
Oosterhout, G.P.C. (1999[b]), *Development of pressures, forces and moments in the liner of*

the Second Heinenoord tunnel, part 2, Measuring report, K100-W-099. Centre for Underground Construction, CUR/COB, Gouda, The Netherlands.

O'Reilly, M.P., R.J. Mair and G.H. Alderman, Long-term settlements over tunnels: an eleven-year study at Grimsby. *Tunnelling '92*, London.

Peck, R.B., (1969[a]), Deep excavations and Tunnelling in soft Ground, *7th ICSMFE* Mexico.

Peck, R.B., (1969[b]), Advantages and limitations of the Observational Method in Applied Soil Mechanics, Ninth Rankine Lecture, *Geotechnique 19*, No 2, 171-187.

Polak, B.M., (1993), *Functional design; Formulation and solution of design problems*, (in Dutch), Lecture notes, bb25, Faculteit der Civiele Techniek.

Popper, K.R., (1959), *The logic of Scientific Discovery*, London.

Potts, D.M., and Burland, J.B., (1983), *A parameter study of the stability of embedded earth retaining structures*. Transport and Road Research Laboratory (TRRL) Supplementary report 813

Ridder, H.A.J., (1994), *Design and Construct 'of complex civil engineering systems'* PhD Thesis, Delft University of Technology, Delft University Press

Ruitenberg, J. & K.J. Bakker, (1998), Stresses and forces in the lining of a bored tunnel, comparison of models, and probabilistic analysis, In: *XIIIth Int. Conference on prestresses concrete*, Amsterdam, 23-29 mai 1998.

Schmidt, B., (1966), Discussion of 'Earth Pressures at Rest Related to Stress History', *Canadian Geotechnical Journal*, Vol 3, No. 4, Nov. 1966, pp. 239-242

Smith, I.M., (1982), *Programming the Finite Element method, with application to geomechanics*, John Wiley & Sons.

Smith, I.M., (1988), Class A Predictions, (Innsbruck)

Steenhuis, C.M., P.C. van Staalduinen & F.B.J. Gijsbers, (1995), *Inventory of design aspects for Bored tunnels* (in Dutch), BSW/95-28, TNO Building Constructions; 95-CON-R0567

Stuip J., (1980), Methodical approach of Offshore Civil Engineering structures, (in Dutch), *PAO Design method of Civil and Building design problems*, Delft, Nov 1980.

Song, E.X., & P.A. Vermeer, (1993), *Implementation of (Curved) Mindlin Beam elements in PLAXIS*, Report No. 363, Geotechnical Laboratory, Faculty of Civil Engineering Delft University of Technology, Delft, The Netherlands.

Stive, R.J.H, (1986), *Oblique wave impact on embankments for regular waves*, (in Dutch) Delft Hydraulics laboratory, H195.2 may 1986

Tatsuoka, F., R.J. Jardine, D.Lo Presti, H.Di Benedetto & T.Kodaka, (1997), Characterising the Pre-Failure Deformation Properties of Geomaterial, *Proceeding XIV ICSMFE*, Hamburg Germany, Balkema Rotterdam.

Terzaghi, K., & R.B. Peck, (1948), *Soil Mechanics in Engineering Practice*. John Wiley & Sons, Inc. London, Chapman & Hall, Ltd.

Teunissen, J.A.M., (1982), Mechanics of a fluid-gas mixture in a porous medium, *Mechanics of Materials*, Vol. 1, pp 229-237.

Timoshenko, S.P. & J.M. Gere, (1936), *Theory of elastic stability* McGraw-Hill, Kogakushi ltd, 1961.

Tiemersma, L.J., (1977), Research on the application of screw-anchors for bankprotections (in Dutch), *Otar*, 1977, 8 en 9

Tiemersma, L.J. & H.J.A.M. Hergarden, (1984), Research on the design criteria for screw anchors for embankment walls, *Otar*, 1984, 9

Toorn, A. van der (1994), The maintenance of civil engineering structures *Heron 39*, 2, Delft, The Netherlands.

Vermeer, P.A. & R.B.J. Brinkgreve, (1995), *PLAXIS, Finite Element Code for Soil and Rock Analysis*, Balkema, Rotterdam.

Verruijt, A., (1969), Elastic storage of aquifers, in *Flow trough Porous Media*, ed. R.J.M. de Wiest (Academic Press, New York).

Verruijt, A., (1983), Numerical analysis beams on elastic foundation (in Dutch), *Cement (XXXV nr 10)* Dutch concrete association..

Visschedijk, M.A.T. (1996), *Ring behavior of a segmented lining, Predictions for the 2nd Heinenoord tunnel*, Technical report 96-MIT-R713, COB: K100-W-022, Centre for Underground Construction, Gouda

Vollema, N, (1996), *Ring loading in bored tunnel liners, comparison of numerical models*, (in Dutch), Technical report 96-NM-R345, TNO, MSc. Thesis, Delft University of technology

Vrouwenvelder, A.C.W.M. & J.K. Vrijling (1982), *Lecture notes on Probabilistic Design, B3*, Delft University of Technology, Delft, the Netherlands.

Vrijling, J.K., (1998), *Civil engineering Structures, special topics, Lecture notes on immersed and bored tunnels*, Ctwa5305, Delft University of Technology, The Netherlands.

Wittgenstein, L. (1922), *Tractatus logico-philosophicus*, Vertaald door W.F. Hermans, Athenaeum-Polak & Van Gennep, Amsterdam (1989)

Wolffersdorff, P.A. von, (1994), *Workshop Sheet Pile Test Karlsruhe*, Delft University, October 6 and 7, 1994.

Wolffersdorff, P.A. von, (1996), *Vervormungsprognosen von Stutzkonstruktionen*, Habilitationsschrift, Universitat Fridriciania Karlsruhe.

Wolsink G.M., (1985), in. *Placed Block Revetments*, research 1980-1984, summary report (in Dutch). Delft Hydraulics/Delft Geotechnics, Report M1881/XIV, CO-272500/7 Delft, 1984.

Wylie C.R. & L.C. Barrett, (1985), *Advanced Engineering Mathematics*, Mc.Graw-Hill.

Wijnen G., W. Renes & P. Storm, (1984), *Project based workscheme* (in Dutch) Marka, Het spectrum Uitgeverij BV, The Netherlands.

APPENDIX A

Equations of equilibrium for a ring

A-1 DIFFERENTIAL EQUATIONS

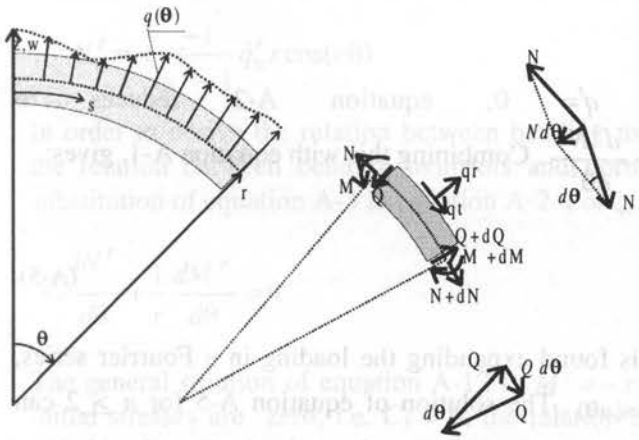

Figure A - 1 Equilibrium of a curve beam

According to Bouma, (1993), the equations for static equilibrium, for a curved beam with a distributed load are given by:
in the radial direction:

$$\sum r \Rightarrow \frac{dQ}{d\theta} d\theta - N\, d\theta + q^r\, r d\theta = 0 \qquad \text{(A-1)}$$

in the tangential direction:

$$\sum t \Rightarrow \frac{dN}{d\theta} d\theta + Q\, d\theta + q^t\, r d\theta = 0 \qquad \text{(A-2)}$$

and for equilibrium of moments:

$$\sum M \Rightarrow \frac{dM}{d\theta} d\theta - Q\, r d\theta = 0 \qquad \text{(A-3)}$$

With respect to deformations, the following relation between radial deformations and bending moments can be derived:

$$M = -\frac{1}{r^2} EI\,(w + \frac{d^2 w}{d\theta^2}) \tag{A-4}$$

In order to derive a relation between the external loading and internal loads, both bending moments and normal (circumferential) forces, a step wise evolution is followed, to begin with only for radial loads. Subsequently a derivation for tangential loads is developed. For the case of loads as actions, and elastic behaviour of the curved beam the result can be added to yield a combined equation.

A-1.1 *Radial loads only*

for the case that $q^t = 0$; equation A-2 reduces to $\frac{dN^r}{d\theta} d\theta = -Q^r\, d\theta \Rightarrow \frac{dQ^r}{d\theta} = -\frac{d^2 N^r}{d\theta^2}$. Combining this with equation A-1, gives:

$$\frac{d^2 N^r}{d\theta^2} + N^r = q^r r \tag{A-5}$$

A solution of this equation is found expanding the loading in a Fourrier series, according to $q^r(\theta) = \sum_{n=1}^{\infty} \hat{q}_n^r \cos(n\theta)$. The solution of equation A-5 for $n \geq 2$ can then be found rewriting equation A-5 according to:

$$\frac{d^2 N_n^r}{d\theta^2} + N_n^r = \hat{q}_n^r r \cos(n\theta) \tag{A-6}$$

the general solution for which is:

$$N = C_1 \cos(\theta) + C_2 \sin(\theta) \tag{A-7}$$

A particular solution is sought of the form:

$$N_n^r = n_n^r \cos(n\theta) \tag{A-8}$$

taking into account that:

$\frac{dN_n^r}{d\theta} = -n_n^r n \sin(n\theta)$, and $\frac{d^2 N_n^r}{d\theta^2} = -n_n^r n^2 \cos(n\theta)$, and substituting these equations in equation A-6 gives;

$$-n^2 n_n^r \cos(n\theta) + n_n^r \cos(n\theta) = q_n^r r \cos(n\theta) \tag{A-9}$$

which gives that $n_n^r = \frac{1}{1-n^2}\hat{q}_n^r r$.

Substituting this in equation A-8 and adding the general solution A-7, the total solution is then found according to:

$$N_n^r = C_1 \cos(\theta) + C_2 \sin(\theta) + \frac{-1}{n^2-1}\hat{q}_n^r r \cos(n\theta) \tag{A-10}$$

As the loading is two times symmetric, the normal force has to be symmetric too, which means that both C_1, and C_2 need to be zero. The final solution for the Normal force will then be:

$$N_n^r = +\frac{-1}{n^2-1}\hat{q}_n^r r \cos(n\theta) \tag{A-11}$$

In order to derive the relation between bending moments and radial loads, first the relation between bending moments and normal forces is derived, by the substitution of equation A-3 in equation A-2. For $q_t = 0$ this will give:

$$\frac{dN^r}{d\theta} + \frac{1}{r}\frac{dM^r}{d\theta} = 0 \tag{A-12}$$

The general solution of equation A-12 is $M^r = -rN^r + C_3$. If. we assume that initial stresses are zero; i.e. $C_3 = 0$, the relation between bending moment and radial loading can be derived according to:

$$M_n^r = +\frac{1}{n^2-1}\hat{q}_n^r r^2 \cos(n\theta) \tag{A-13}$$

A-1.2 *Tangential loads only*

Equation A-1, for $q^r = 0$ can be simplified to give; $N^t d\theta = \frac{dQ^t}{d\theta}d\theta$ and as equation A-3 rewritten reads as: $Q^t = \frac{1}{r}\frac{dM^t}{d\theta}$, this can be combined to give:

$$N^t = \frac{1}{r}\frac{d^2M^t}{d\theta^2} \tag{A-14}$$

If we differentiate this with respect to the inclination angle θ,

$$\frac{dN^t}{d\theta} = \frac{1}{r}\frac{d^3M^t}{d\theta^3} \tag{A-15}$$

and combine this with equation (A-2), we arrive at:

$$\frac{d^3M_n^t}{d\theta^3} + \frac{dM_n^t}{d\theta} = -q_n^t r^2 \tag{A-16}$$

Similar to the solution for radial loading, the tangential loading is expanded in a Fourrier series according to: $q^t(\theta) = \sum_{n=1}^{\infty} \hat{q}_n^t \sin(n\theta)$. For a generic term of the loading series, for $n \geq 2$,

equation A-16 can be rewritten to give:

$$\frac{d^3M_n^t}{d\theta^3} + \frac{dM_n^t}{d\theta} = -\hat{q}_n^t r^2 \sin(n\theta) \tag{A-17}$$

Similar as for the radial loading, for symmetry reasons, the general solution of the equation is of no consequence and therefore we will focus on the particular solution.

Again looking for a particular solution of the form:

$$M_n^t = m_n^t \cos(n\theta) \tag{A-18}$$

and recognising that:

$$\frac{dM_t}{d\theta} = -m_n^t n \sin(n\theta), \quad \frac{d^2M_t}{d\theta^2} = -m_n^t n^2 \cos(n\theta) \quad \text{and} \quad \frac{d^3M_t}{d\theta^3} = m_n^t n^3 \sin(n\theta).$$

These equations are substituted in equation (A-17) which gives:

$$n^3 m_n^t \sin(n\theta) - m_n^t \sin(n\theta) = -\hat{q}_n^t r^2 \sin(n\theta) \tag{A-19}$$

which gives that $m_n^t = \frac{-1}{n(n^2-1)}\hat{q}_n^t r^2$. Substituting this in equation A-18 will give:

$$M_n^t = \frac{-1}{n(n^2-1)}\hat{q}_n^t r^2 \cos(n\theta) \tag{A-20}$$

Using equation A-14, the circumferential normal force can be derived too, to give:

$$N_n^t = \frac{n}{(n^2-1)}\hat{q}_n^t r \cos(n\theta) \tag{A-21}$$

A-1.3 *Combined equations for the stresses*

For a more general loading case, with both radial and tangential loads, for the linear elastic situation, the solutions may be added to give:

for the normal forces:

$$N_n = q_0^r r + \left(\frac{-1}{(n^2-1)} \hat{q}_n^r + \frac{n}{(n^2-1)} \hat{q}_n^t \right) r \cos(n\theta) \tag{A-22}$$

and for the bending moments:

$$M_n = \left(\frac{1}{(n^2-1)} \hat{q}_n^r + \frac{-1}{n(n^2-1)} \hat{q}_n^t \right) r^2 \cos(n\theta) \tag{A-23}$$

A-1.4 *Radial Deformations*

As the tangential deformations are generally of an order smaller, due to the greater stiffness with respect to normal forces than for bending, our main interest goes out for the radial deformations.

The general differential equation for the radial deformations is given by equation A-4, which can be rewritten to give:

$$\frac{d^2 w}{d\theta^2} + w = \frac{-r^2}{EI} M \tag{A-24}$$

Once again we expand the bending moment in the liner, M in a Fourrier series according to:

$$M = m_n \cos(n\theta) \tag{A-25}$$

Similarly to the derivations of stresses for the radial loading, a solution for the radial displacement w is found, expanding w in a Fourrier series, according to

$$w = w_n \cos(n\theta) \tag{A-26}$$

The solution for equation A-26 is found according to:

$$w_n = \frac{1}{(n^2-1)} \frac{r^2}{EI} m_n \tag{A-27}$$

or fully written out, taking into account equation (A-22);

$$w = \frac{1}{(n^2-1)} \left(\frac{1}{(n^2-1)} \hat{q}_n^r + \frac{-1}{n(n^2-1)} \hat{q}_n^t \right) \frac{r^4}{EI} \cos(n\theta) \tag{A-28}$$

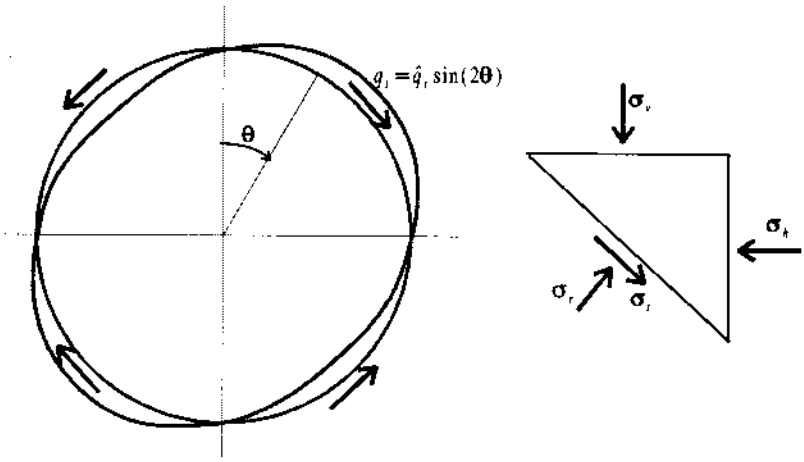

Figure A - 2 Decomposition of radial load

A-2 EXAMPLE, FOR A TUNNEL

According to accepted engineering practice, it is assumed that the liner of a tunnel is loaded by the soil. The soil loading is composed of vertical stresses and horizontal stresses. The vertical stresses in the soil, are mainly caused by the weight of the overlaying soil cover, denoted with σ_v whereas the horizontal stresses in the soil denoted by σ_h, are often related to the vertical soil stresses. For non over-consolidated situations where the geological formation of the soil strata is sedimentary, the horizontal soil stresses are lower than the vertical soil stresses; $\sigma_h \leq \sigma_v$.

The stress difference between horizontal and vertical stresses gives rise to the development of bending moments in the liner. In order to accommodate the solution described in the preceding section to this loading situation, the loading is rewritten as a part which is a function of the angle of inclination, and a part which is constant according to;

$$q = q_0^r + q_2^r = -\left(\frac{\sigma_v + \sigma_h}{2}\right) - \left(\frac{\sigma_v - \sigma_h}{2}\right)\cos(2\theta) \qquad \text{(A-29)}$$

Whether there is a tangential load, depends on the roughness of the outer surface of the tunnel liner. If we assume the initial soil stresses as active loading on the tunnel, assuming a sinusoidal shape of the stress distribution the tangential loading on the tunnel liner can be derived according to:

$$q_2^t = -\hat{q}_2^r \cos(2\theta - \pi/4) = \left(\frac{\sigma_v - \sigma_h}{2}\right)\sin(2\theta) \qquad \text{(A-30)}$$

Assuming a rough wall, and accounting for isotropic loading, related to the q_0^i term which is not included into the aforementioned derivations, but which can be included applying the kettle formula, the Normal forces in the liner can be derived as:

$$N = q_0^r r + \left(-\frac{1}{3}\hat{q}_2^r + \frac{2}{3}\hat{q}_2^t\right) r\cos(2\theta) = q_0^r r - \hat{q}_2^t r\cos(2\theta) = \\ -\left(\frac{\sigma_v + \sigma_h}{2}\right) r + \left(\frac{\sigma_v - \sigma_h}{2}\right) r\cos(2\theta) \tag{A-31}$$

For the bending moments in a similar way we find:

$$M = \left(\frac{1}{3}q_2^r - \frac{1}{6}q_2^t\right) r^2\cos(2\theta) = \\ \left(\frac{1}{3} + \frac{1}{6}\right) q_2^r r^2\cos(2\theta) = -\left(\frac{\sigma_v - \sigma_h}{4}\right) r^2\cos(2\theta) \tag{A-32}$$

Finally, the displacements are composed of a part due to the compressive stresses, and a part related to the stress difference, and are found to be:

$$w = q_0^r \frac{r^2}{EA} + q_2^r \frac{r^4}{EI}\cos(2\theta) = \\ -\left(\frac{\sigma_v + \sigma_h}{2}\right)\frac{r^2}{EA} - \left(\frac{\sigma_v - \sigma_h}{12}\right)\frac{r^4}{EI}\cos(2\theta) \tag{A-33}$$

APPENDIX B

Ultimate limit state for a tunnel lining

B.1 ULTIMATE LIMIT LOAD FOR A TUNNEL LINING RING

In § 7.3 in Fig 7.8 the mechanism of a tunnel lining taking an horizontal oval shape due to the overburden soil load, has been discussed.

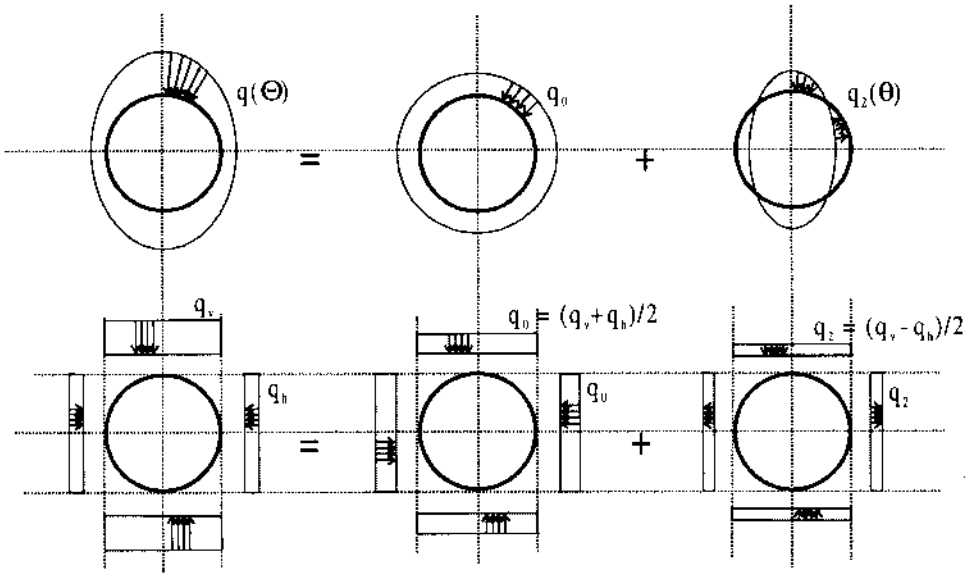

Figure B-1 Soil loading split in a compression part and a distortion part. Above for distributed loads. Under; simplified.

There it was argued that an horizontal ovalisation leads to a stress path in the soil, where the soil besides the soil is compressed, and the soil above and under the tunnel is decompressed. This would mean a decrease in the distortional loading of the tunnel. Even if there is only a compression at the sides of the tunnel, equilibrium would be reached before the soil reaches a limit stress state. If the soil besides the tunnel reaches a neutral stress state; i.e. if $\sigma_h = \sigma_v$, equilibrium is reached far before the deformations that would lead to a passive stress state.

The question is for what deformations the equilibrium state is reached. If the decrease in distortional loading would be less than the increase in 2nd order

effects, the equilibrium state would not be reached, but a collapse, if the capacity of the tunnel to bear the bending moments is exhausted

In order to evaluate this mechanism, a simple model is developed based on equilibrium in the Ultimate Limit State. The basic assumptions are initial stresses related to the K_0 stresses in the soil. An elastic response of the soil, and a plastic response of the tunnel lining with respect to the bending moment in the tunnel lining.

B.2 THE ULTIMATE LIMIT STATE MODEL

Similar to the analytical model discussed in appendix A, the loading of the tunnel is split into a part that is related to compression of the tunnel ring, and a part that is related to the distortion of the tunnel ring, see Fig. B-1

The model is based on an Ultimate limit state situation, such as sketched in Fig. 7.8, in chapter 7.

In Fig B-2, the model is sketched. The circular lining is divided in four parts, four shell elements. The four shells are kept in equilibrium by 2 horizontal springs and forces between the shells. The soil loading is split into a compressive part q_1, which is acting in the direction of the tunnel both from all four directions

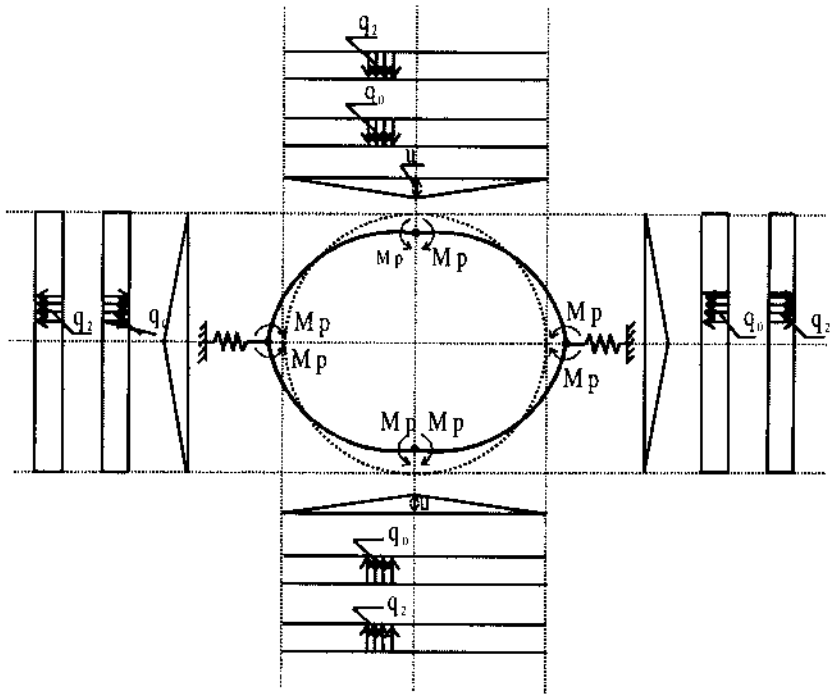

Figure B-2 Simplified model for the ultimate limit state, for the distortion part

of the tunnel and a distortional part q_2 which is acting in the direction of the tunnel on top and underneath the tunnel, and counter-wise in the other direction at the sides of the tunnel, such as indicated in Fig B-2. The loading is associated with a deformation which is triangular shaped; i.e. a deformation which has its largest amplitude at the horizontal and vertical axis going through the tunnel centre, diminishing to zero at the tunnel sides. For the deformation of the tunnel shells, rigid rotations are assumed. At the points where the shells are connected, plastic work is being generated as a plastic spring relation is being assumed.

Due to this deformation, i.e. a vertical displacement, where the top and the floor is displaced u in the vertical direction. The sides of the tunnel moving outward u in the horizontal direction. Simultaneously the plastic springs between the shell elements will show a rotation of

$$\theta_{pl} = \frac{u}{r} \tag{B-1}$$

In the Ultimate limit state equilibrium demands that there is a balance in the virtual work being generated and absorbed by the system. External virtual work is generated by the load, whereas internal virtual work is being generated by 1) elastic springs (the soil support), and 2) by the Plastic energy of the rotation between the shell elements.

The balance of virtual work, guarantees equilibrium;

1) The external work due to the compression part is calculated as:

$$E_c^{ex} = 2q_0(2r+2u)\tfrac{1}{2}u - 2q_0(2r-2u)\tfrac{1}{2}u = 4q_0u^2 \tag{B-2}$$

Which means that the virtual work is:

$$\delta E_c^{ex} = 8q_0u\delta u \tag{B-3}$$

2) External Energy due to the distortional part:

$$E_d^{ex} = 4q_2\,2r\tfrac{1}{2}u = 4q_2ru \tag{B-4}$$

Which means that the virtual work due to the distortional part is given by:

$$\delta E_d^{ex} = 4q_2r\delta u \tag{B-5}$$

3) The internal energy in the soil spring will give:

$$E_1^{in} = 2\tfrac{1}{2}Ku^2 = -Ku^2 \tag{B-6}$$

Which means that the virtual work due to the soil spring is given by:

$$\delta_1^{in} = -2Ku\delta u \tag{B-7}$$

4) Whereas the internal energy in the plastic hinges will give

$$E_2^{in} = 4M_{pl}2\theta_{pl} = 8M_{pl}\frac{u}{r} \tag{B-8}$$

Which means that the virtual work due to the plastic hinges is given by:

$$\delta E_2^{in} = -\frac{8M_{pl}}{r}\delta u \tag{B-9}$$

Balancing the virtual work is given by:

$$8q_0 r\delta u + 4q_2 r\delta u - 2Ku\delta u - \frac{8M_{pl}}{r}\delta u = 0 \tag{B-10}$$

The latter equation has to hold for any virtual displacement δu. If we divide δu and rearrange, the following relation can be obtained:

$$M_{pl} = \frac{1}{2}q_2 r^2 + q_0 ur - \frac{Kur}{4} \tag{B-11}$$

Before equation B.5 is evaluated, first the parameters which are determinate for its outcome will be estimated.

1) The compression part of the tunnel loading; in analogy with the derivation of the analytical model in appendix A, the compression loading is determined by the average; the mean loading on the tunnel ring:

$$q_0 = \frac{(\sigma_v + \sigma_h)}{2} \tag{B-12}$$

2) The distortional part of the tunnel loading is determined by the representative value of the loading difference. Evaluating A-28, this representative value can be distinguished as:

$$q_2 = \frac{(\sigma_v - \sigma_h)}{2} = \frac{(1 - K_0)}{2}\sigma'_v \tag{B-13}$$

3) It is assumed that only the horizontal pre-stressing of the soil gives an elastic response. The vertical movement is assumed to behave plastic and therefore not to contribute to elastic energy and thereby to bearing capacity. The bedding modulus for the horizontal soil response is estimated as:

$$K = k\,D = \frac{2E}{D}D = 2E \tag{B-14}$$

However due to the fact that the largest displacements are at half height, and therefore only half the spring is reacting, in practice the spring constant is not as high as estimated with equation B-13. Here it is assumed that the spring is only half as stiff as for the situation that the tube as a whole is displaced.

$$K \approx \frac{2E}{D} r = E \tag{B-15}$$

If we use the estimations according to the equations B-12, B-13 and B-15 in combination with equation B-11, the following equation is found:

$$M_{pl} = \frac{(1-K_0)}{4} \sigma'_v r^2 + \frac{(\sigma_v + \sigma_h)}{2} ur - \frac{Eur}{4} \tag{B-16}$$

Subsequently we will evaluate this.

1) For the static situation without deformations:

$$M_{pl} = \frac{(1-K_0)}{4} \sigma'_v r^2 \tag{B-17}$$

is found. Comparing this with the analytic solution, according to equation A-32, we see that that the same result is found. This result can be understood if we realise that both in the ultimate limit state as well as in the equilibrium solution of equation A-32 the same distribution of bending moments comes forward; i.e. there is no re-distribution of stresses. The way that the soil loading is being assumed implicitly assumes that there is tangential interaction between soil and liner; i.e. that there is shear stress interaction.

2) For the situation of large displacements, if the soils springs are not in operation:

$$M_{pl} = \frac{(1-K_0)}{4} \sigma'_v r^2 + \frac{(\sigma_v + \sigma_h)}{4} ur \tag{B-18}$$

In the second term of this equation the addition due to 2nd order bending moment can be recognised, similar to the derivation in § 7.4.2 The addition due to the 2nd order effect is only half of what is expected based a direct comparison with column theory.

The fact that the amplification is missing here comes forward because here the deformation in the ultimate limit state is assumed whereas in equation 7.24, the first order deformation is used.

3) For the situation that both soil springs and second order effects, are feasible, all the components in equation B-16 have to be evaluated. According to the Duddeck solution such as described in § 7.4.2, the activation of the soil springs leads to a reduction of the bending moments. The minus sign in equation B-16, for the last term is in balance with that.

The question arises however for which situation the decrease in bending moment due to activation of the soil springs is not surpassed by an increase

of bending moments due to 2nd order bending moments. Such is the case if; $\frac{(\sigma_v+\sigma_h)}{4} u r \geq \frac{E u r}{4}$, or in other words this mechanism can be avoided if:

$$(\sigma_v+\sigma_h) \leq E \quad or \quad E \geq (\sigma_v+\sigma_h).$$

For a Dutch soft soil situation with a tunnel depth of at least 1 diameter of soil-cover, if we assume a wet soil weight of 16 kN/m^3, for a tunnel diameter of 8 m, the Young's modulus of the soil has to be larger than; $E \geq 1.5\ D \cdot (10+(\gamma_w-10)\frac{(1+K_0)}{2}) \geq 1.5*8*(10+(16-10)*\frac{(1+0.5)}{2} \geq 175 kPa$.

If we realise that for the Dutch soft soil conditions, the Young's modulus ranges between $1000 < E_s <= 100000$, such a mechanism is not a high risk. As this derivation is linear in the tunnel diameter, we may extrapolate this conclusion without consequences at least up to a tunnel diameters, of 15 m.

The reduction of the bending moment in the tunnel lining as derived by an activation of the soil stiffness is combined with a deformation of the tunnel lining; the tunnel takes an oval shape with its longest axis in the horizontal direction. Due to the construction method, limits have to be formulated with respect the admissible deformation. Because the lining has to keep in between the air space in the tail of the TBM, which is of the order of 0.1 m. An admissible deformation of e.g. 0.025 m would be feasible. As a function of the tunnel diameter a ratio of *D/300* would be feasible; or in our notation; *r/150.*

If we would include this in equation B-16 this would give a design value for the bending moment of

$$M_{min} = \frac{(1-K_0)}{4}\sigma'_v r^2 + \frac{(\sigma_v+\sigma_h)}{300} r^2 - \frac{E r^2}{600} \qquad \text{(B-19)}$$

Equation B-19 gives a rough estimate for the minimum bending moment to consider for tunnel design. It is advised here that for a practical situation the limit requirement are established with a more elaborate model such as a Finite Element code, which includes both large deformations as well as a plastic analysis of the tunnel lining.

Soil-retaining structures offer the possibility to reduce the necessary space for the development of structures for buildings and for infrastructure. Besides that soil retaining structures enables to build below the soil surface and underground. For the development of infrastructure, for our densely populated cities, it becomes increasingly difficult to realise the necessary infrastructure for transport, water-management and water-defence. On the one hand there is insufficient space for conventional construction methods and on the other hand society enforces restrictions, taking into consideration the need to conserve environmental values.

In order to design the necessary structures, safe and reliable, one needs to have models for structural analysis. In this study the models being evaluated are numerical models, mostly based on finite element techniques. To develop these models a frame of reference for the verification and validation of these models is described and applied.

In the study of block revetments, the modelling of ground-water flow is being described. The model is verified for turbulent flow in coarse filter material. Besides that a simple model to evaluate the stability against sliding of revetments is being evaluated in a field study on block-mattresses.

In the study of flexible retaining wall, the development and verification of a plane strain finite element model is described. The validation of this type of model is described in a field study on a sheet pile wall.

The number of tunnels bored in soft soil is increasing. This type of structure offers large opportunities for our densely-populated cities. In the chapter on bored tunnels, the problems of tunnelling in soft soil is discussed. In a field study on the construction of the Second Heinenoord tunnel, in the Netherlands, both empirical models as well as the finite element models are being evaluated.